The Influence of Heat Transfer Limitations on the Properties of PET Yarn Produced by Melt Spinning

Tyrone Kotze
BScEng(Chemical)

Thesis presented for the degree of:
Masters in Engineering Science
In the Department of Chemical Engineering
University of Cape Town

August 2008

Declaration:

I know the meaning of plagiarism and declare that all the work in this document, save for that which is properly acknowledged, is my own.

Tyrone Kotze

Abstract

The production of synthetic yarns requires a cost efficient process whilst simultaneously incorporating process methods which ultimately lead to a high quality fibre. A critical part of the production process is the spinning of the molten polymer into individual filaments which are brought together to form the filament bundle. During this process a quench air stream is blown across the filament bundle to aid in cooling the molten polymer. Here, heat transfer limitations may cause inter-filament property variations, which will adversely affect the quality of the yarn. This thesis focuses on the development of a model which allows for an *a priori* prediction of the influence of major process variables on the degree of fibre property uniformity.

Fibre quality is characterised by the high degree of uniformity in the properties which affect the structural features of the yarn. Yarn morphology is dictated by the degree of crystallinity and molecular alignment of the polymer macro-molecules parallel to the fibre axis. These properties are strongly influenced by online tensile stress and local temperature which are, in turn, affected by heat transfer effects between the quench air and filament surface. A model that predicts the influence of heat transfer limitations on the uniformity of the as-spun fibre is therefore needed.

Previous research in this field is limited with most work focussed on single filament model development. In this investigation, a monofilament model developed by previous workers (Jarecki *et al.,* 2000) is integrated into a multifilament framework. This model assumes Newtonian behaviour of the polymer with viscosity strongly dependent on local temperature and crystallinity. The development of the multifilament model involves dividing the spinning zone into a number of cells, in which the filament properties are modelled using the monofilament model. The change in quench air temperature is estimated by means of an energy balance incorporating air flow terms and heat transfer through forced convection from the filament surface. A novel iteration approach is proposed in which the temperature of the quench air exiting each cell is iterated for until convergence is met. In simplifying the model, it was found that uniform quench air flow profile could be assumed, since the quench flow channel length was found to fall far short of the length required for

turbulent flow to develop. However, it is known that increased contact time for heat transfer would occur if air were dragged down with the filament. Although modelling this effect is beyond the scope of the project, the heat transfer gradients are worsened by air-dragging and hence the model presented in this thesis reveals whether polymer uniformity is possible even under the best possible flow patterns. A negative result therefore indicates that non-uniformity will definitely occur.

Numerical challenges encountered during this investigation included mathematical singularity of crystallinity dependent viscosity, the selection of initial force values in order to obtain the desired take-up velocity and high crystalline kinetic activity experienced during optimum stress and temperature ranges. The proposed model is verified by comparison of property trends with previous work developed in a similar way (Jarecki *et al.,* 2000, Dutta 1987).

Process conditions investigated include quench air temperature and velocity, polymer extrusion rate and temperature, and take-up velocity. Results showed quench air velocity to have the largest influence on final property uniformity with low variance achieved at higher velocities. However, a trade-off between property variance and magnitude of final orientation achieved forced intermediate quench air velocities to be proposed as the optimum process condition. Quench air temperature had minimal effect on as-spun fibre property variance. Low extrusion rates were deemed the optimum as this resulted in a lower degree of non-uniformity in final fibre properties as well greater levels of molecular orientation being achieved. This leads to a yarn with a greater tensile strength due to the lower elongation at break values. However, careful process control of this property is recommended as a trade off between possible filament breakage and increased levels of final property uniformity and orientation was identified. Extrusion temperature had negligible effect on system performance. However, it was proposed that lower extrusion temperatures would reduce operating costs. Simulations showed increasing take-up speeds to decrease the final product property variance as well as achieving higher levels of orientation and crystallinity. As such, it is recommended to produce fibres at the highest possible take-up velocity.

Ultimately, the model developed in this thesis showed non-uniform quench thermal gradients to have adverse effects on the quality of the as-spun yarn. It is shown that these effects are caused by heat transfer limitations between the quench air and filament surface. Results revealed that reducing these effects required operating at the optimum spinning conditions proposed. Potential Further work may involve coupling CFD code, used to model the air flow profile around the bundle, and resulting effects on heat transfer, with the current model. Further more, a more efficient coding algorithm would significantly reduce the computation time required by the current model by avoiding the large force ranges in which the desired initial force is to be found. This would add significant value and further increase the accuracy of the current model.

Acknowledgements

This thesis is a culmination of two years work which, at times, seemed endless and daunting to say the least. During this time many difficulties were experienced in solving the problem at hand and were overcome with the help of certain people to which I am indebted.

Firstly, I would like to thank my supervisor Dr R Rawatlal for the supreme level of direction and patience with which the supervision of this work was carried out. I have acquired an open yet disciplined frame of mind when approaching difficult problems which can only be attributed to the steadfast guidance of Dr R Rawatlal over the past two years.

The help of Dr L Jarecki in ironing out the numerical difficulties in the single filament model was invaluable and I am extremely grateful to have liaised with such a distinguished contributor in the field of synthetic fibre research.

I would like to thank those whom I‘ve interacted with personally during the past two years. These persons include Alistair Hughes who helped with many programming difficulties encountered along the way, Sarah Dowling for your good humour and support which was always on offer and to all those in the chemical engineering department who offered some form of guidance and advice throughout the course of this work. I thank you deeply.

Lastly, I would like to thank those who are closest to me. I thank my house mates for putting up with my constant niggling about noise levels and for the humorous times around the dinner table. To my sister and brother, Varne` and Desmond van der Smit, who have provided me with endless warmth and support, thank you. The comforting support offered by my father, Nick Kotze, has been a constant throughout the past two years, thank you very much.

Finally, this work is dedicated to my mother, Avril Gail Kotze. You are my light in the darkest of times, and the reason for my success in life thus far.

Table of Contents

Nomenclature

Symbol	Definition	Units
Δh	Heat of crystallisation	cal/g
Δn	Optical birefringence	-
Δp	Tensile stress	dyne/cm^2
A	Stress induced crystallisation coefficient	
A_r	Flux area	m^2/cm^2
B_i	Expansion coefficients	-
C_f	Skin friction factor	-
C_{opt}	Stress optical coefficient	-
C_p	Heat capacity	cal/g K
d	Diameter	m or cm
D_E	Wetted perimeter	m or cm
D_h	Half height of crystallisation rate function	^{o}
E_a	Activation energy	cal/g
F	Force	dyne
f_h	Heat transfer coefficient	cal/m^2 s deg
f_i	Orientation factor	-
G	Gibbs free energy	cal
g	Gravitational constant	m^2/s
H_i	Enthalpy	cal
K_i	Crystallisation rate	1/s
λ_s	Thermal conductivity	Cal/cm^2 s deg
l_0	Characteristic length	m or cm
n	Avrami exponent	-
$\dot{N}_{th}$	Thermal nucleation rate	1/s
$\dot{N}_{ath}$	Athermal nucleation rate	1/s
Δn_a^o	Amorphous birefringence of ideally oriented molecules	-
η_T	Temperature viscosity contribution	poise
η_X	Crystallinity viscosity contribution	poise
η^0	Dynamic viscosity	poise
ρ	Density	kg/m^3
S_i	Entropy	cal/K
θ_i	Angle of molecular alignment to a specific dimension axis	^{o}
T_g	Glass transition temperature	^{o}C
T_m	Melting temperature	^{o}C

Symbol	Definition	Units
T_{max}	Temperature corresponding to maximum crystallisation rate	^{o}C
V	Velocity	m/min
$v*$	Critical cluster size	-
V_0	Initial velocity	m/min
v^0	Kinematic viscosity	stokes
V_a	Quench air speed	m/s or cm/s
V_L	Take-up velocity	m/min
W	Polymer mass flow rate	g/s
w	Distance between filaments	cm or m
X	Crystallisation	-
X^*	Critical crystallisation	-
z	Distance from spinneret	cm or m

Glossary

Anisotropy – difference in a physical property for some material when measured along a different axis.

As-spun – the property state of the fibre directly after the spinning process prior to any drawing or post treatment.

Attenuation – the thinning or stretching of a filament corresponding to a decrease in diameter due to acting tensile forces.

Birefringence – an optical property of the polymer influenced by the alignment of polymer molecules along the spine line, used as a measure of orientation.

Denier – A unit of weight expressing the size or coarseness of a natural or synthetic fibre or yarn.

Elongation at break – Elongation recorded at the moment of rupture of the specimen, expressed as a percentage of the original length. It corresponds to the breaking or maximum load.

Extensibility – a measure of the fibre extension as a percentage of the original length, similar to attenuation and elongation at break.

Mathematical singularity – In mathematics, a singularity is in general a point at which a given mathematical object is not defined, or a point of an exceptional set where it fails to be well-behaved in some particular way, such as differentiability.

Maxwell material – This is a viscoelastic material having the properties both of elasticity and viscosity. It is named for James Clerk Maxwell who proposed the model in 1867. It is also known as a Maxwell solid.

Morphology – the physical structure of matter influenced by the molecular make-up as well as the conditions under which the molecules were set into place.

Tenacity – Numerically it is the breaking force in grams per denier unit of yarn or filament size (grams per denier, g/denier).

Viscoelastic – pertaining to a substance having both viscous and elastic properties.

List of figures

Chapter 1

Chapter 2

Chapter 4

Chapter 5

Chapter 6

Chapter 7

Chapter 8

Appendices

List of tables

Chapter 2

Chapter 4

Chapter 6

Chapter 7

Chapter 8

Chapter 9

Appendices

Part A: Background

1 Introduction

1.1 A summary of past and present technological advances

Mankind has long tried to mimic natural biological processes by engineering processes aimed at producing a product with the same properties as those found naturally. One such example is living organisms producing natural fibres which include silks, threads and wool. However, manmade technology has never been fully able to produce synthetic fibres with the same ideal properties as those produced naturally. These natural fibres consist of regular polymeric structures which are extremely strong and elastic. It has only recently been discovered, with the invention of apparatus allowing man to probe the nano or molecular realm, that it is indeed the molecular structure which ultimately determines the properties of a piece of yarn, be it synthetic or natural (Forbes, 2006).

Major expansion and research in trying to produce synthetic fibres using the most economic process and materials involved in high speed fibre spinning has been carried out as early as the 1930's (Dees and Spruiell, 1974). After the 1950's technological advances were hindered by financial and marketing reasons as well as unreliable high speed spinning equipment, such as godet and windup rolls, restricting the fine tuning of process control as well as the final take up velocity achieved by the yarn. Advances in spinning technology have allowed the previously separate spinning and drawing stages to be reduced to a single *high- speed spin-draw-winding* process for textile fibres. This is achieved by spinning the fibres at high speed and then drawing them (before winding) onto two heated godet rolls with idler rolls for yarn support purposes. The overall production process requires extreme uniformity in terms of the polymer melt with a minimum in heterogeneity by use of the purest raw materials that can be obtained not to mention precise process control and special equipment such as smooth walled pipes and vessels designed to reduce dead spots and improve polymer flow (Beyreuther *et al.*, 1989).

At present, manufacturers of synthetic yarn aim at producing high quality synthetic yarns which are further used as raw materials in the production of safety apparel such as seat belts, parachutes, air bags etc. Thus it is imperative that these yarns have a good balance of properties (e.g. extensibility, shrinkage, high strength, good tenacity).

These properties are strongly dependent on the molecular structure of the synthetic yarns which is, in turn, affected by the applied process conditions during the production of the synthetic yarn particularly during the spinning and drawing stages (Sharpe, 2002). Thus, it is critical to obtain a fundamental understanding of the factors affecting the structural composition of synthetic yarns. Recent advances in industry include the development of melt spinning models which allow one to calculate the most important properties of the spinline. The benefits gained through this advancement include reducing both the time and cost incurred by avoiding the physical process of carrying out the necessary experiments (Beyreuther *et al.*, 1989).

Three major types of spinning processes are used in industry which include wet, dry and melt spinning. The wet and dry spinning processes both entail dissolving the polymer in a solvent to form a viscous medium called the "spin dope". In the case of wet spinning, the filaments are spun in water which removes the solvent from the polymer solvent solution. In contrast, dry spinning relies on the solvent being extremely volatile and simply evaporating from the spin dope as it is extruded from the spinneret and spun. The third process, melt spinning, introduces the molten polymer to a gas phase in which the individual filaments are cooled and solidified. This process allows for high spinning velocities as compared with other production methods. The process equipment (e.g. spinning rigs) are simpler in design and operation and auxiliary materials such as solvents and precipitation agents are not needed (Ziabicki, 1976).

Beyreuther and co-workers (1989) analysed numerous publications and concluded that, at the time, research had focused on three major areas each answering the following questions:

- How to produce highly orientated yarn without additional winding?
- How to increase output by increasing the spinning velocity bearing in mind the increase in orientation and reduced drawability of the yarn?
- How to construct a reliable model linking adjustable input parameters to important yarn characteristics and final as spun properties?

The present thesis focuses research on the hot tube melt spinning process. This process achieves solidification by cooling the polymer melt using a quench air system after which the thread line is reheated in a hot zone followed by being cooled again. Increased molecular orientation of the spun yarn has been found to be an advantage of this technique. However, the degree of structural uniformity within the yarn produced using the hot zone method is still in question (Beyreuther *et al.*, 1989). As such, one of the aims of this thesis is to investigate the structural uniformity of yarn produced using the hot tube spinning process. This will be done by investigating the following parameters:

- uniformity of the quench air temperature profile by altering the quench rate and temperature,
- variation of polymer extrusion rates and temperatures, and

(i) the effects of varying take up speeds on the uniformity of properties throughout the yarn.

1.2 Fundamentals of the synthetic yarn production process

The formation of fibres through the melt spinning process involves many auxiliary sub-processes. These processes control yarn quality and uniformity. The following section gives a general summary of the commonly used auxiliary processes exploited in the melt spinning process. These processes include the following:

- *Preparation of the polymer raw material*

  The process begins with the feed of raw materials needed for the production of the respective polymer e.g. PET, nylon 6.6. Since the spun filaments are very fine (<10 μm) it is essential that the polymer produced be of the purest form to avoid any weak spots in the yarn when it is spun. The polymer has to be conditioned to an appropriate moisture content (approximately 220 ppm) to avoid further polymerisation if too dry and hydrolysis if too wet. Once these purity criteria are met, the polymer chips are then transported to the respective melt units *via.* feed hoppers.

- *Preparation of the polymer fluid to be spun*

  Since the spinning process is continuous, a constant throughput of polymer melt from the melt unit is required. Product quality is maintained by keeping the polymer residence time and temperature constant. The chips are fed from the feed hoppers into the melt unit and onto the melt grid via a screw mechanism. The melt grid consists of a series of steel fins filled with a superheated vapour which serves as the heat source to melt the polymer chips. Due to the excessive heat generated by the melt grid (290-300 ^{o}C) the chips are melted into what is known as the 'polymer melt', which is constantly stirred inside the melt pot. This molten polymer is then booster pumped to a gear pump which, in turn, supplies the filter packs with the relatively high amount of pressure (>19000 kPa) required to filter the molten polymer. The filter packs are generally made of filtering material such as sand or alumina powder. The melt must be cleaned of any foreign particles since the diameter of the filaments is very small (10 µm) and any particles in the same size range could cause the filaments to break. After the polymer melt has been filtered, it is extruded through the spinneret, which is the beginning of the filament formation process.

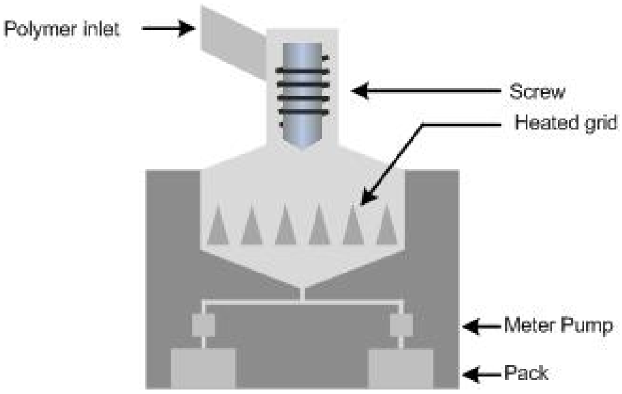

Figure 1-1: A schematic of a screw pressure melter used in preparation of the polymer.

- *Spinning*

  Due to the relatively high force that the polymer melt is subjected to from the gear pump, it is forced through a shower head like device known as the spinneret. The purpose of this device is, firstly, to split the polymer melt into separate filaments and, secondly, to introduce the melt to the gaseous phase. The spinneret is a metal disk which has many small holes varying in number from 200-1000 holes per spinneret. Each hole has a diameter ranging from 200 - 500 µm depending on the specific product properties needed. The layout of the holes in the spinneret is circular, although other geometric shapes have been used (e.g. pentalobal, hexalobal, rectangular). The spinneret structure has to be durable and able to withstand the high pressure subjected to it by the polymer melt.

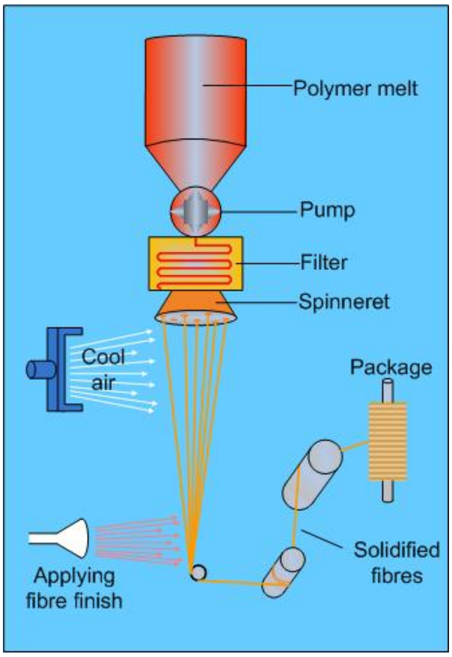

Figure 1-2: A schematic of the melt spinning process.

Once the polymer has been extruded from the spinneret in the form of single filaments it is stretched due to the large difference in initial (5-30m/min) and final take up speed (250-3000m/min). This attenuation has the effect of decreasing the filament diameter as well as resulting in some degree of orientation of the polymer macro-molecules within the filament. This phenomenon is known as molecular orientation and significantly affects yarn morphology and microstructure. This is discussed in great detail in section 2.1. Solidification, also known as crystallisation, occurs within this region of the process. During this extrusion phase the filaments are subjected to a quench air stream introduced perpendicularly to the filament axis. This aims to stabilise the filaments by providing increased tension (see Figure 1-3). The temperature of the quench air stream can vary from 18-25^{o}C and is filtered many times to remove any particles as well as to provide a steady and even flow pattern to the filaments. The individual filaments then enter a convergence line where they are brought together to form thread lines before entering the conditioner tube. The conditioner tube uses steam to reduce any static electricity produced as well as to moisten the thread line allowing for easy application of the spin finish.

We focus this investigation on this section of the process as this is the area during which most of the structural changes of the polymer takes place.

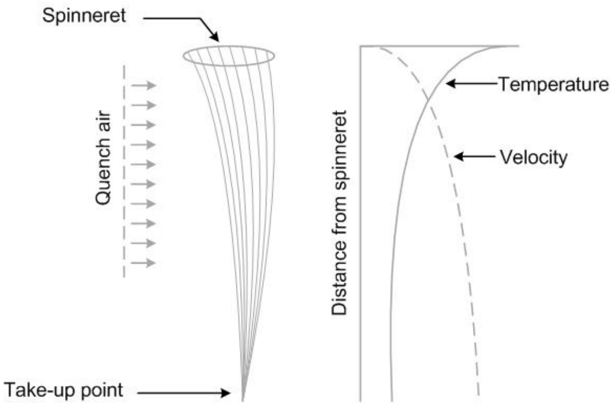

Figure 1-3: The general geometry, temperature and velocity profile experienced by the filaments due to the quench stream.

- *Drawing, relaxing and windup*

  After the spin finish has been applied the yarn is drawn by passing over two godet rolls spinning at the same speed but each having slightly different diameters, thus stretching the yarn. The purpose of drawing is to increase molecular orientation within the yarn and secondly to create the constant tension needed prior to wind up. The yarn is relaxed by over feeding a heated section of yarn between two rollers which run at different speeds which results in the yarn being relaxed. The purpose of relaxing the yarn is to allow a suitable amount of shrinkage to occur to satisfy customer requirements.

  The process of winding-up is done so that the spun yarn can be packaged and unwound wherever it is needed. This process entails careful control of the rotational speed of the package as it increases in diameter during windup. Since yarn tension is to be kept constant, the increase in package diameter has to be accounted for by decreasing the rotational speed accordingly. The build of the yarn is controlled by a traverse guide mechanism which moves back and forth along the roll as the yarn is fed.

Figure 1-4: A flow diagram summarising the fundamental production processes.

- *Conditioning*

  This is done with the aid of heat in the form of steam and serves to increase molecular mobility, whereas if treated with solvent results in the relaxation of internal stress and brings the overall structure closer to thermodynamic equilibrium.

(Ziabicki, 1976 and Sharpe, 2002)

1.3 Critical remarks

Extent of crystallinity, molecular orientation and local filament tensile stress play a major role in determining yarn morphology and microstructure. As a result, these same factors significantly influence the polymer strength, a highly desirable property (Galeski 2003). In the production of synthetic yarns, final product quality is extensively influenced by the uniformity of the above the mentioned properties which affect the structural characteristics (Dutta 1987). As such, maintaining process conditions which result in the highest degree of product uniformity is of significant importance. These parameters include the quench conditions which influence the rate of heat transfer from the polymer ultimately affecting the local temperature. Due to the sensitivity of the above mentioned properties on polymer temperature, a study into the effect of the variation of this measurable throughout the filament bundle on the overall yarn properties will be of significant value. More specifically, the effects of variable thermal gradients in the quench air will be modelled and analysed.

2 Literature Review

The final objective of this study is to develop a melt spinning model that predicts the filament properties across the fibre bundle whilst taking into account the effects of varying quench conditions. Thus, factors such as the influence of crystallisation reaction conditions on fibre morphology, molecular orientation and micro structure must first be established. Previous models proposed in literature should be reviewed in order to ascertain the areas of research which lack focus and understanding (i.e. crystallinity and molecular orientation).

In this chapter the morphology of polymer fibres and the dependence of final mechanical fibre properties on the microstructure of the fibre are first discussed. This chapter also establishes the factors influencing molecular orientation and some of models used to describe this phenomenon. Thereafter the thermodynamic factors, more specifically temperature, influencing the crystallisation kinetics are presented. This section focuses at summarising some of the commonly used kinetic models in current literature. Heat transfer effects are then discussed in some detail. This section summarises some of the more commonly proposed correlations that make up the heat transfer coefficient and the application of these in melt spinning models. Lastly, the historical development of both the single and multifilament models is discussed in depth.

2.1 Morphology, microstructure and molecular orientation

2.1.1 Research and theory

Yarn morphology and microstructure, which significantly affects the behaviour of the material in subsequent processes, is dependant on the melt spinning process conditions (i.e. quench conditions, polymer temperature and online stresses) prior to any drawing operations. Much literature is available in this specific field of fibre spinning, with countless experimental analyses being carried out and models proposed. This section outlines the evolution to the current state of understanding.

Early work focussed on developing a link between the spinning process conditions and the as-spun product properties in the form of empirical equations. Abhiraman and Hagler (1987) investigated the morphological factors associated in providing this link.

The length of the spinline was divided into separate regions according to the type of morphological mechanism occurring there. This scheme, shown in Figure 2-1, illustrates the phase transitions occurring. The melt zone (MZ) is where only molten amorphous material occurs and is the region where the molten polymer is first introduced into the gaseous phase. In crystallisable polymers the melt zone is followed by the crystallisation zone. This is the region where some of the amorphous molten material solidifies and the molecules become ‘frozen’ into place. The static zone is the final zone where negligible morphological change takes place.

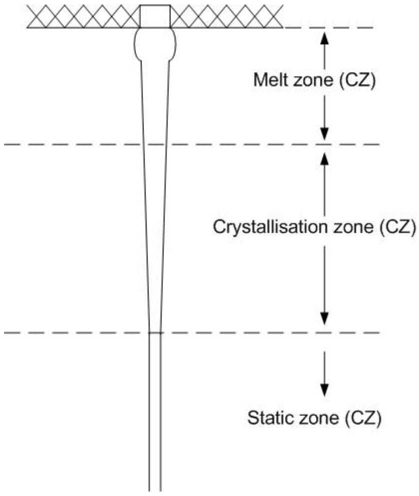

Figure 2-1: A diagram indicating the structure development in the thread line (Abhiraman, 1987).

Clearly the molecular structure within a section of filament may contain two phases, as also supported by the work of Ziabicki (1976), Heuvel *et al.* (1992) and McHugh and Doufas (2001). According to these researchers the first phase consists of an inhomogeneous disordered amorphous structure. The inhomogeneity in this structure results in a distribution of stresses over the molecules on mechanical loading. This lack of molecular cooperation causes weak spots in the overall fibril structure. The molecules in this region have some freedom to move and will, upon heating, pursue configurations of enhanced configurations and hence, begin to coil. The second phase consists of a crystalline structure which can be viewed as stiff homogeneous blocks. Polyethylene crystallises readily from the melt to form an orthorhombic unit cell with dimensions a = 7.41, b = 4.94 and c = 2.54 Å (White and Cakmak 1986). The two phases described above alternate within the filament (see Figure 2-3), the frequency of which determines the coarseness of the yarn. Single macromolecules pass between the two phases several times thus providing the structural coherence with the yarn (Heuvel *et al.* 1992).

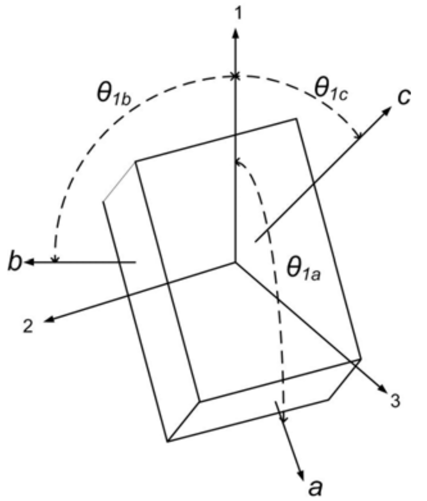

Figure 2-2: Orientation of an orthorhombic unit cell (White and Cakmak, 1986).

The unique properties of a fibre are governed by the formation of the actual fibrillar crystallites of optimal dimensions within the semi-crystalline morphology and, secondly, the presence of polymer chains of optimal orientation and distribution within the intervening amorphous regions (Jaydeep *et al.,* 1998). Many lattice models have been proposed in the literature with a comprehensive review by Jaydeep *et al.* (1998). In the work, the derivation of the statistics describing the property characteristics is developed by using the microscopic fibre properties to predict the macroscopic behaviour for two dimensional systems.

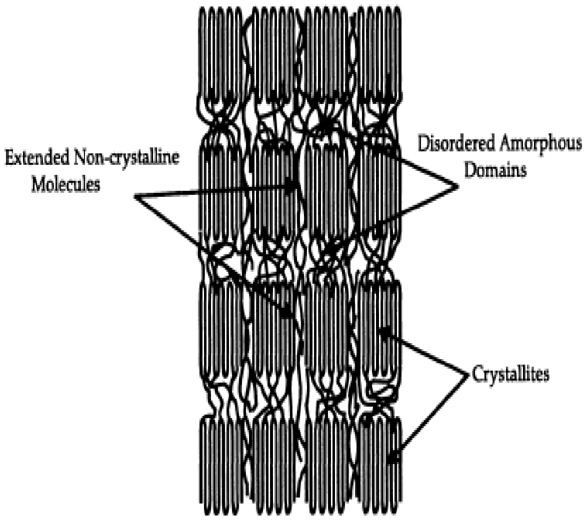

Figure 2-3: A diagram indicating the fibrillar structure of a section of yarn filament (Elsevier, Vol. 82, Jaydeep *et al.*, '*Lattice based simulations of chain confirmations in semi-crystalline polymers with application to flow induced crystallisation*', pg 340, ©1998 with permission from Elsevier).

Original molecular models included the *fringed micelle* model, in which a crystallite is considered to be composed of segments of many different molecules. However, with the discovery of polymer single crystals which could not be explained by the *fringed micelle* model, the *chain-folded crystals* and *extended chains* model were developed which included incorporating entire folded molecules (Ziabicki, 1976).

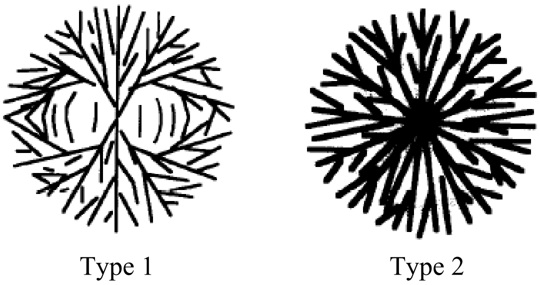

Figure 2-4: The two possible types of spherulitic growth morphologies (Pergamon, Vol. 20, Long *et al.*, '*Kinetics of Polymer Crystallisation'*, pg 658, ©1995 with permission from Elsevier).

Another characteristic of polymer crystallites is the geometry of the crystal lattice. Crystal growth in polymers with an already sufficiently high crystallinity is known to result in the geometry of two basic types of spherulitic microstructure. These structures are depicted in Figure 2-4. Type 1 takes the form of crystalline lamella, nucleated separately and independently from each other, which initiate from a central nucleus growing radially in all directions. This type of spherulite exhibits a spherical symmetry extending to the centre of the spherical structure. Type 2 spherulites originate from a single lamella crystal. The spherical shape is achieved by the continuous fanning out and branching of the crystalline structure which initially had an undirected growth pattern, known as the sheaf stage.

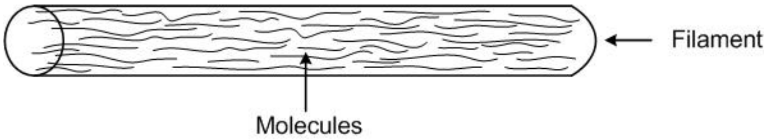

Figure 2-5: A diagram indicating the alignment of molecules in a single filament.

Molecular orientation is the ability of macromolecules to align along the axis of filament. One would expect some orientation to occur within the spinneret, but due to the relaxation in the die swell being so rapid after the extrusion from the spinneret, all orientation that has occurred is lost. A second factor negating this phenomenon is that the residence time (or time of action in the shear field) within the spinneret is too short for any major permanent orientation to occur (Ziabicki 1976). Orientation in the melt zone is weakly influenced by the draw ratio, i.e. V_L/V_0, where V_0 is the initial filament velocity and V_L the take up velocity, and is related more closely to the rate at which the filament is stretched and cooled while the molecules are in their orientated state (Abhiraman and Hagler 1974).

Orientation within the spinline occurs gradually starting from zero in the melt zone, reaching some saturation value at some point in the thread line. In a study by Ziabicki and Kedzierski (1962) it was found that the molecular orientation increases with a decrease in filament diameter and increase in velocity difference i.e. V_L - V_0. Orientation has been shown to increase with average molecular weight of the polymer and decrease with an increase in extrusion temperature. These effects are associated with viscosity and relaxation phenomena (Ziabicki, 1976). In his work, Ziabicki (1976) derived a relationship illustrating the dependence of molecular orientation on local filament velocity (see eq. 2.1). This relationship shows that orientation is almost a linear function of the local velocity and describes the orientation of macromolecular chains in purely amorphous systems.

$$f(x) = \frac{const.F_{ext} \cdot V(x)}{W} = k \cdot \Delta p(x) \qquad \text{eq. 2.1}$$

Where: $f(x)$ = molecular orientation factor, F_{ext} = force, $V(x)$ = local filament velocity, W = mass flow rate, Δp = tensile stress and k = constant.

This relationship is similar to the one proposed by Hamana *et al.* (1969). Here the comparison of local birefringence (the degree of molecular alignment within the polymer influencing the passage of light through the material) and tensile stress characteristics along with the velocity gradient lead to an empirical relationship describing the birefringence as a linear function of the tensile stress (eq. 2.2). The stress optical coefficient is obtained from the gradient of birefringence vs. tensile stress plot and is generally in the order of 10^{-10} cm^2/dyne due to the tensile stress being so large in magnitude.

$$\Delta n = C_{opt} \cdot \Delta p(x) \qquad \text{eq. 2.2}$$

Where Δn = birefringence, C_{opt} = stress optical coefficient.

In the amorphous regions (see Figure 2-3), the molecular segments have a large variety of angles in which they align with respect to the fibre axis. In a study by Heuvel *et al.* (1992), a distribution of these angles was described using the cosine of the respective angles over the entire distribution (i.e. $\cos^2 \theta$, $\cos^4 \theta$, where θ is the angle between the molecule and the fibre axis). Thus for perfectly aligned molecules $\theta = 0$ and $\cos\theta = 1$. For less aligned molecules the value would be between 0 and 1. In the same work it was found that the distribution of orientations in drawn yarns spun at high winding speeds is broader than the distribution obtained at lower winding speeds. The effect of molecular orientation was interpreted as promoting the occurrence of a denser network, the breaking down of which would require a higher force due to there being more strengthening physical cross links.

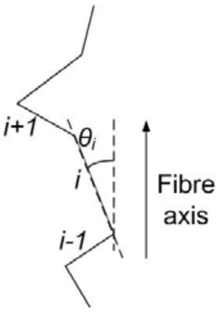

Figure 2-6: Molecular orientation, θ_i is the angle between the tie molecule *i* and the direction of the fibre axis (Heuvel *et al.*, 1992).

The effect of take up velocity on the type of homogeneous crystalline structure (see Figure 2-3) formed was predicted by Dees and Spruiell (1974) in the form of a morphological model. This attempted to explain to some degree the observed morphology in melt-spun Polyester fibres (Figure 2-7). The morphological model was based on the development and type of crystalline orientation observed during the spinning process as well as the observed changes associated with altering the spinning conditions. The following relationship was used in describing the different types of orientation:

$$f_a + f_b + f_c = 0 \qquad \text{eq. 2.3}$$

where the axial orientation factor (f_i) is a characteristic used to describe the macroscopic behaviour of the system in terms of uniaxial orientation. More specifically, f_a, f_b and f_c are the orientation factors associated with each dimension in the crystal unit cell within the yarn (see Figure 2-7). Using eq. 2.3 trends were generated which showed the orientation factors varying as functions of velocity. It was concluded that a rapid change in crystal structure from spherulitic to row nucleated took place as the take-up velocity increased. If the velocity were increased further, the cooling rate increased rapidly enough to suppress the crystallisation temperature sufficiently to overcome any crystallisation due to the increased stress.

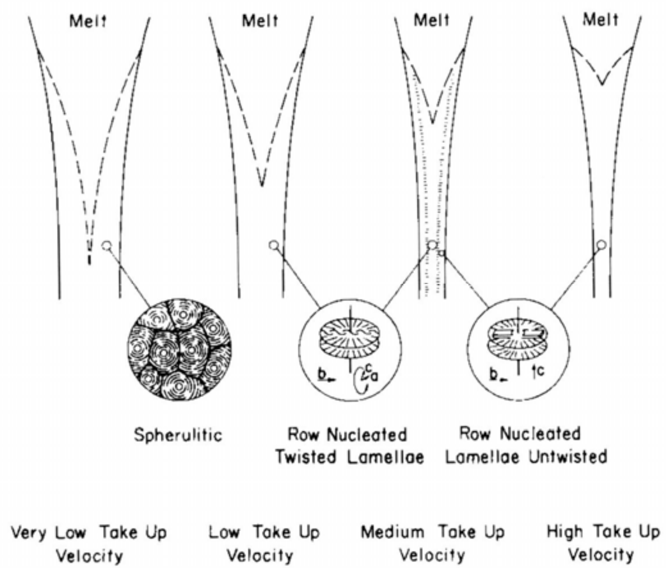

Figure 2-7: Morphological models of PET crystallisation during melt spinning ('*Structural Development During Melt Spinning of Linear Polyethylene Fibers'*, Dees and Spruiell, 1974, © John Wiley & Sons Limited, reproduced with permission).

The potential for different molecular arrangements has a number of effects on the crystallisation kinetics. Jaydeep *et al.* (1999) described the theoretical framework around the microstructure development in a section of filament connected with stress induced crystallisation as being divided into three categories namely:

(i) statistical models describing the development of equilibrium properties of stretched polymer networks,
(ii) statistical mechanical and classical thermodynamic models devoted to describing kinetic properties of the crystallisation phenomena, and
(iii) models connecting the change in morphology with flow and transport phenomena.

Models (i) and (iii) will not be discussed in much detail as they far exceed the scope of this research investigation. Model two is discussed in more detail in section 2.2. The method used to describe and predict molecular orientation in this investigation is covered in detail in section 2.1.

2.1.2 Summary

Generally, a large body of literature supports the occurrence of two phases in a section of filament. These are a disordered inhomogeneous and a homogeneous stiff block like phase which alternate resulting in the physical yarn texture. Together, the two alternating phases comprise the semi-crystalline structure of the fibre, the unique properties of which are governed by fibrillar crystallites of optimal orientation and dimension occurring within the structure. A range of process conditions, namely rate of filament attenuation and cooling, molecular weight, extrusion temperature and tensile stress affect the degree of orientation. Except for extrusion temperature and molecular weight, all the variables listed above are affected to some degree by the take-up velocity. Experimental work suggests that higher spinning speeds lead to higher orientated fibres but, with a greater degree in orientated distribution. The take-up velocity also determines the type, if any, of crystalline structure achieved within the fibre. These observations all suggest that spinning speed plays a significant role in dictating the final yarn morphology and orientation.

Most of the theoretical models predicting the dimension type and degree of molecular orientation are too idealised and specific to a single type of system to be included in the current model. However, work carried out by Jarecki and co-workers (2000) uses a Taylor's series type expansion in defining the orientation factor, f_a, as a function of the tensile stress. This expansion allows one to apply the model to any polymer once the stress optical coefficient and the amorphous birefringence of ideally orientated chains of the respective polymer are known. This expansion is described in more detail in section 4.1.

2.2 Thermodynamics and crystallisation kinetics

2.2.1 Research and theory

The capacity of a polymer to undertake a certain type of phase transition is governed by the thermodynamics of the system. The rate at which the transition takes place is described by the kinetics (Di Lorenzo, 1999). Early research into the kinetic domain generally included the assumptions of idealised process conditions i.e. isothermal conditions and constant cooling rates, and allowed for simple estimations to be made. In practice, crystallisation is more complex than this due to the continuous variation of external conditions resulting in non-isothermal conditions and variable cooling rates. This section first describes the thermodynamic factors associated with crystallisation and, second, the theories proposed in literature which deal with the kinetics of crystallisation in complex external conditions. Finally, the section attempts to highlight the critical factors affecting the occurrence of crystallisation.

Much research has been carried out on the thermodynamic changes taking place during the melt spinning process as well as the kinetics describing the crystallisation rate (Ziabicki 1967, 1996, 2001, Yu Long 1995, Di Lorenzo *et al.,* 1999, Apiwanthanakorn *et al.,* 2004). The onset of crystallisation is a consequence of the change in thermodynamic state of the system. This change could be due to super saturation of a solution, an increase in hydrostatic pressure, or a drop in the temperature below a critical value. Since this thesis investigates the effects of non-uniform quench temperature profiles on the final fibre properties, the theory around the first two factors will not be discussed in much detail, and instead, the effects of temperature changes on thermodynamics and crystallisation kinetics will be dealt with.

Phase transformation can only take place if the change in free energy of the system is negative. However, the initial process starts with the formation of sub-critical nuclei of the new phase by way of positive free energy of cluster formation (Yu Long *et al.,* 1995). For a pure undiluted polymer, the melting temperature (T_m) determines the critical condition for phase transition which, in this case, is melting or solidification. In high molecular weight systems, phase transition is most sensitive to molecular mobility. This molecular mobility becomes practically zero close to the glass transition temperature (T_g). Systems which reach this temperature are considered to be kinetically stable, irrespective of how far the system might be from the true thermodynamic equilibrium. Thus, the occurrence of crystallinity is limited to the temperature ranges between the glass transition and polymer melting temperature. These values vary for PET and nylon polymers (see Table 2-1).

Table 2-1: The kinetically active temperature ranges for PET and Nylon 6.6

	PET	Nylon 6.6
T_g (^oC)	67-70	45
T_{max} (^oC)	190	150
T_m (^oC)	267	264
K_{max} (1/s)	0.016	1.64
D_h	32	40

The only thermodynamic variable causing change in the system is the lowering of the polymer temperature below the equilibrium melting temperature (T_m) of the polymer as it traverses the spinline. Thus the overall change in Gibbs Free Energy can be defined by eq. 2.4.

$$\Delta G = (H_{crystal} - H_{melt}) - T(S_{crystal} - S_{melt}) = \Delta H - T\Delta S \qquad \text{eq. 2.4}$$

As a first approximation to the total free energy, the change in enthalpy is assumed to be equal to the negative of the latent heat of fusion. Since the entropy of the crystal phase has a value much smaller in comparison, the change in entropy can be approximated as being equal to minus entropy of the melt. The rate at which latent heat is released must be less than the heat removal rate in order for crystal growth to continue. At the melting temperature (T_m), the change in enthalpy is $\Delta H = T_m \Delta S$ ($\Delta G = 0$ at phase equilibrium). Below this temperature and provided that the conditions are right for nucleation and crystal growth, in tending to reduce it free energy, the system will undergo crystallisation (Yu Long *et al.,* 1995).

Phase transitions involve two kinetic processes namely i) nucleation and ii) growth of nuclei. The formation of nuclei occurs sporadically and is proportional to the square of the shear rate (Ziabicki, 1976). Three physical mechanisms exist for polymer nucleation: i) spontaneous homogeneous nucleation ii) orientation induced nucleation as a result of the alignment of macromolecules and spontaneous crystallisation, and iii) heterogeneous nucleation which occurs on the surface of a foreign phase. The foreign surfaces concerned with the nucleation are commonly referred to as nucleating agents (Yu Long *et al.,* 1995). Nucleation is necessary as it aids in the process of polymer crystallisation and is promoted by the flow induced phenomena within the polymer melt during the spinning process. This flow induced stress has the effect of altering the type as well as the number of nuclei formed which ultimately dictates the final crystalline structure. In his work, Ziabicki (1968) proposed that the nucleation rate is made of two contributions.

The first contribution, thermal nucleation ($\dot{N}_{th}$), leads to unstable molecular clusters of critical size v^* and is due to the thermal fluctuations across the polymer. This nucleation mechanism is proportional to the flux of clusters passing over a potential barrier at $v = v^*$ on the way to stability. Athermal nucleation ($\dot{N}_{ath}$) is caused by clusters originally in the unstable condition becoming stable as a result of changes in the external conditions. This route of nucleation is proportional to the rate at which critical cluster volume (v^*) changes due to varying external conditions (Ziabicki 2001). Thus it is proportional to the rate of change of the thermodynamics of the system (i.e. temperature and tensile stress fluctuations etc.). Ziabicki (1976) describes the changes in non-isothermal nucleation rates described in eq. 2.7 as a function of the free energy of a cluster as follows:

$$\ln(\dot{N}_{th}(T)) \approx \frac{Const. - [E_a(T) + \Delta F^*_{nucl}(T)]}{kT} \qquad \text{eq. 2.5}$$

$$\dot{N}_{ath} = -\left(\frac{\partial R^*}{\partial T}\right)\left(\frac{dT}{dt}\right)\iint_{S^*} f dS \qquad \text{eq. 2.6}$$

where E_a = activation energy, R^* = vector characteristic for the cluster, S^* = critical boundary over which to integrate, f = distribution function of clusters.

The influence of temperature is mainly through the activation energy and free energy terms as described by eq. 2.5 and eq. 2.6. At high temperatures, due to the activation energy being so small, the dependence of temperature is determined through the ΔF^*_{nucl} term. The activation energy term becomes important at lower temperatures and the nucleation rate passes through some maximum at a temperature corresponding to T_{max}. From eq. 2.6 it is clear that $\dot{N}_{ath}$ is proportional to the cooling rate. It is often believed that athermal nucleation reduces the Avrami exponent which is used in the describing the kinetics of the system (Ziabicki, 1976).

The net result is:

$$\dot{N}(t) = \dot{N}_{th} + \dot{N}_{ath} \qquad \text{eq. 2.7}$$

In later work, Ziabicki (2001) described the crystallisation rate in terms of the two nucleation mechanisms above and showed how this equation could be combined with a single-relaxation-time approximation of the thermal nucleation. It was stated that this equation could be further simplified to a quasi-static result when the product of relaxation time and the rate of change approached zero. In this model, the non-isothermal crystallisation rate simplifies to a function of temperature and stress and is independent of the cooling rate. However, this was proved untrue by experimentation and it was concluded that the crystallisation rate is indeed dependent on the cooling rate.

The most common approach in modelling the overall isothermal crystallisation kinetics seems to be that of the Avrami type approximation (Apiwanthanakorn *et al.,* 2004). This method expresses the Extent of crystallisation as a function of time in the following form:

$$X(t) = 1 - \exp\left[-(K_A t)^n\right] \qquad \text{eq. 2.8}$$

where K_A is the Avrami crystallisation rate constant and n is the Avrami exponent.

The major drawback using the Avrami approximation is that it is only suitable for describing the initial stages of crystallisation with complications arising due to growth site impingement and secondary crystallisation. Ziabicki (1976) proposed an approximation describing the polymer phase transition as a first-order kinetic equation which avoids the use of complicated mathematical models. That is:

$$\frac{dX(t)}{dt} = K(T)[1 - X(t)] \qquad \text{eq. 2.9}$$

where*,* $K(T)$ is the crystallisation rate constant discussed in more detail later and $X(t)$ the fraction of crystalline material. The use of eq. 2.9 holds true for isothermal conditions only. In the case of melt spinning, non-isothermal crystallisation occurs and it is noted that both $X(t)$ and $K(T)$ vary and are dependent on the cooling rate applied. A Gaussian temperature dependent crystallisation rate function, derived by Ziabicki (1976), describes the rate of crystallisation (eq. 2.10 and Figure 2-8). This function includes the parameters T_{max} (described above), D_h, and K_{max}. T_{max} is the temperature corresponding to the maximum crystallisation rate, K_{max}. D_h is the width of the of the $K(T)$ curve at half height. Non-zero crystallisation rates are restricted to temperatures between the glass transition (T_g) and the melting temperature (T_m). The use of eq. 2.10 allows for an estimation of the non-zero crystallinity outside this temperature range. However, the values for D_h are so small when compared with ($T_m - T_{max}$) or ($T_{max} - T_g$) that the relative crystallisation rates do not exceed the values ranging between $2.1\text{x}10^{-5} - 2.1\text{x}10^{-2}\,K_{max}$ for temperatures outside of this range. $K(T)$ is also known as the reciprocal of the crystallisation half time, $t_{1/2}$[s].

$$K(T) = K_{\max} \exp\left[-4\ln 2\frac{(T - T_{\max})^2}{D_h^{\,2}}\right] \qquad \text{eq. 2.10}$$

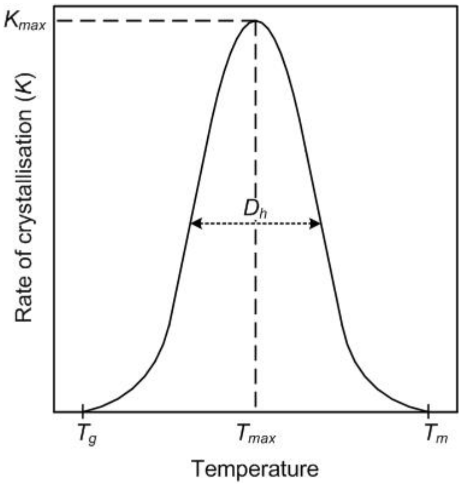

Figure 2-8: A plot of the theoretical crystallisation rate (*K*) vs. temperature.

In recent work carried out by Ziabicki *et al.* (1998), which attempted to model the rheological effects in a melt spinning process using basic dynamic equations for PET, a quasi static or pseudo steady state Avrami approximation was used to model the crystallisation kinetics. This approximation assumes that the variation in some state parameter (e.g. temperature, concentration, orientation factor) is a result of the time dependence of the nucleation and growth rates (Ziabicki 1976). This method approximates the non-isothermal crystallisation rate shown in eq. 2.11.

$$\frac{d}{dt}\left[-\ln(1-X)\right]^{\frac{1}{n}} = K_{st}(T,\Delta p) \qquad \text{eq. 2.11}$$

Where X = degree of crystallinity, K_{st} = crystallisation rate characteristic term (1/s), n = Avrami exponent, Δp = tensile stress (dyne/cm^2).

The exponent n (Avrami exponent) usually varies from 0-4 and is affected by nucleation and growth geometry. Interpreting n is not straight forward and its determination is affected by factors such incomplete crystallisation, annealing or different mechanisms involved during the process (Di Lorenzo, 1999). It has been observed that in the stressed state (orientated) both the crystallisation rate as well as the melting temperature (T_m) increase. The relation between K and K_{st} is discussed in section 4.1.

Molecular orientation has been found to affect the rate of crystallisation to some degree. Orientated polymers crystallise in a selective way according to the amount of orientation: a structure with orientations prevailing in the system will crystallise at higher rates than structures with infrequent orientations (Ziabicki 2001). The effects of average molecular orientation are described by the semi-empirical relationship shown in eq. 2.12.

$$K_{st}(T, \Delta p) = K_0(T)\exp\left[A \cdot f_a(\Delta p)^2\right] \qquad \text{eq. 2.12}$$

where A = stress induced crystallisation coefficient, f_a = amorphous orientation factor.

The orientation factor is a function of the local filament tensile stress through a non-linear relationship derived for non-Gaussian polymer chains (Ziabicki and Jarecki 1986). This method is described in more detail in section 4.1.

2.2.2 Summary

This present investigation focuses on fibre production using melt spinning. Thus, a drop in polymer temperature is the only factor which would result in a phase change. Any change in the degree of molecular mobility and crystallisation kinetics is restricted to temperatures above the glass transition and polymer melt temperature. Hence, it seems that kinetic activity will only take place within this region.

Earlier kinetic models were represented by complex equations describing the system on a microscopic level. This involved empirical equations expressing the athermal and thermal nucleation rates dependant on cooling rates, flow induced stress and local polymer temperature, which in turn affects activation energy. Alternatively, more recent work described the kinetics on a macroscopic level and approximated the phase transition as first order kinetic equation in the form of an Avrami type. However, this was restricted to isothermal systems. This lead to the addition of a Gaussian temperature dependant term which takes into account the varying degree of crystallisation rates, occurring in non-isothermal systems, according to the local polymer temperature (Ziabicki, 1976). Further work established that higher orientated systems readily crystallised more so than less oriented. Hence, a final term describing the average molecular orientation was incorporated into the kinetic equation alongside the Gaussian temperature dependant term (Ziabicki, 2001). Since the orientation factor is solely dependant on the tensile stress of the local filament, the phrase ‘stress induced crystallisation’ (SIC) was coined.

2.3 Heat transfer effects in melt spinning

2.3.1 Historical development

The process of melt spinning exposes the molten polymer to an ambient temperature below the glass transition temperature of the respective polymer. This large temperature gradient results in heat being transferred from the molten polymer to the gaseous phase. Due to the strong dependence of polymer viscosity on the local temperature, the diameter attenuation of the spinline is strongly dependent on the rate of heat transfer. The diameter and temperature of the polymer affect the structural properties of the as-spun polymer, and it is therefore imperative that a good understanding of the heat transfer effects be acquired.

Heat transfer in melt spinning is part of a macroscopic transfer phenomenon of which three mechanisms occur:

(i) Radiation: this mechanism occurs in the spinning of inorganic material (i.e. glasses, metals) where the extrusion temperatures can reach 900-1300 K (Ziabicki 1976). The effect of radiation in melt spinning of organic materials (e.g. PET) is negligible due to the relatively low extrusion temperatures (500-600 K), hence this mechanism is generally ignored in the formulation of equations describing the temperature profile of the polymer in the spinline.

(ii) Free or natural convection: this occurs as a result of the medium surrounding a heat source being heated, moving away due to natural convection and being subsequently replaced by a cooler medium. This is the typical mechanism associated with heat transfer from stationary systems that could be applied to spinning systems at very low take up velocities.

(iii) Forced convection: this is the mechanism generally accepted to apply to melt spinning systems with a transverse quench air system being blown across the spinline. This is due to higher Reynolds numbers which suggest a turbulent air flow resulting in the removal of the natural temperature field around the cooling medium.

For forced convection the Nusselt number ($Nu = f_h d / \lambda^0$), which characterises the heat transfer coefficient, can be defined as a function of the Reynolds and Prandtl numbers as well as the exposed length of filament (x) as follows:

$$Nu = Nu(\mathrm{Pr}, \mathrm{Re}, x / d) \qquad \text{eq. 2.13}$$

where $\mathrm{Pr} = C_p^o \eta^o g / \lambda_s$, $\mathrm{Re} = Vd / v_s$ and C_p^o = specific heat, λ_s = thermal conductivity, η^o = dynamic viscosity, v_s = kinematic viscosity, d = filament diameter, f_h = heat transfer coefficient.

The Biot number describes whether heat transfer is resisted inside the polymer melt or restricted by the air film surrounding the filament and is defined as the ratio of the heat transfer coefficient coupled with the characteristic length (l_o) to the thermal conductivity (λ_0) of the polymer.

$$Bi = \frac{f_h . l_0}{\lambda_s} \qquad \text{eq. 2.14}$$

If the thermal conductivity of the polymer is greater than the product of the heat transfer coefficient and the characteristic length, then temperature gradients within the filament are negligible and heat transfer at the surface is the limiting step. The inverse applies.

Early attempts at modelling the heat transfer from the spinline include those made Andrews (1958), Kase and Matsuo (1965) and Barnett (1967). Andrews (1958) began by deriving equations describing the temperature profile experienced by a thread line during the spinning process. The method involved empirically determining a function relating the forced convection heat loss to the Reynolds number for a moving thread line by comparing the heat lost by a thin wire to that by a polymer thread line. The heat flow equation was derived by considering the filament fixed in space and assuming cylindrical symmetry. Kase and Matsuo (1965) measured the coefficient of heat transfer experimentally by subjecting a heated wire 0.2 mm in diameter to both parallel and transverse air flow and recorded the cooling of the wire. The cooling curves were then converted into Nu-Re relations. From these relations a correlation was derived (see eq. 2.15) based on a coefficient (1+K). The value of K was determined from the angle of the quench air stream to the filament axis and found to be a ratio of V_a/V, where V_a is the quench air flow rate and V is the local filament velocity. Thus K is zero when the flow is parallel and approximately unity when the air flow is at right angles to the filament axis.

$$Nu = 0.42 \cdot \mathrm{Re}^{0.334}(1+K) \qquad \text{eq. 2.15}$$

Where $Re = V_a d/v_s$, v_s = the kinematic viscosity of the air.

This method neglects the attenuation of the spinline and thus its applicability to melt spinning can be questioned. Barnett (1967) used theories based on flow along the surface of thin cylinders derived by Andrews (1958) to describe the required heat transfer coefficients. In the work of Barnett (1967) and Andrews (1958), the magnitude of each of the heat transfer mechanisms (radiation, convective and forced convection) is assessed and compared. It was found that the heat loss due to radiation was small but similar in magnitude to both the forced and free convection mechanisms. Other factors influencing heat transfer which were neglected in the calculations were discussed. These include the filament vibration, the velocity gradient along the filament (only local velocity taken into account) and the turbulence of the surrounding air.

By the mid 1970's, many models for predicting heat transfer coefficients in fibre spinning had been proposed. A complete review of the equations defining the Nusselt number proposed by different workers and the respective ranges in which these can be applied is presented by Ziabicki (pg 164, 1976). It is observed that values computed for f_h for the same spinning conditions range from 1 to 10 which, in turn, greatly affects the calculated temperature distribution.

Kase (1976) improved on earlier heat transfer estimations without the assumption of axis symmetry and used previous data produced on heat transfer variations from cylinders cooled by cross flow air. Intra filament temperature contours were generated and compared to experimental observations, with good agreement being achieved. Chung and Iyer (1992) developed a model incorporating the radial heat conduction inside the fibre and the combined effects of radiation and convection at the boundary of the filament, with results in good comparison to that of Kase and Matsuo (1967). Various values of heat conductivity were investigated with significant variation in the radial temperature being observed. It was found that radiation heat transfer contributed towards 10-15% of the total heat transfer at the initial stage of the filament cooling. Vassilatos *et al.* (1992) used heat transfer correlations developed by Kase and Matsuo (1965) for a thin wire placed in an air stream flowing in parallel, in developing a melt spinning model. Two-dimensional convective heat transfer is analysed through a rigorous macroscopic one dimensional energy balance that differed from the commonly used equation. The results showed that all spinlines exhibit a difference of 9^{o}C or more between the centerline and surface temperatures. Thus it was concluded that the average temperature, as well as the surface temperature, is needed in determining heat transfer coefficients from experimental data. Ramos (2005) found that a greater rate of heat loss decreases the rate of crystallinity and increases the rate of molecular orientation. Thus the initial gradient of the crystallisation is a strong function of the heat losses.

Little research has been carried out recently in deriving more accurate heat transfer correlations. This is most likely due to the current correlations being of a high enough precision to allow sufficiently accurate heat transfer predictions to be made. However, the correlation (eq. 2.15) developed by Kase and Matsuo (1967, 1974) is still the most commonly used form in predicting the heat transfer effects from a spinline (Ziabicki *et al.* 1998, Jarecki *et al.* 2000, Harvey and Doufas 2007). The expanded and simplified version of the correlation in terms of both measurable and predictable variables along the spinline is given by eq. 2.16.

$$f_h = 0.42 \cdot \lambda_s \cdot v_s^{-0.344} \cdot d(z)^{-0.666} \cdot V(z)^{0.344} \cdot \left[1 + 8 \cdot \left(\frac{V_a}{V(z)} \right)^2 \right]^{0.167} \qquad \text{eq. 2.16}$$

Where: λ_s = thermal conductivity [cal/ cm.s.K] and v_s = kinematic viscosity [cm^2/s] of the cooling medium.

2.3.2 Summary

The theory suggests that heat transfer is generally a function of the turbulence of the gas phase around the filament, exposed length and diameter of filament and the cooling medium viscosity. Although radiative heat transfer is commonly neglected in most melt spinning models, it does significantly contribute to the overall heat transfer in the initial spinning stages. However, much evidence supports the theory of the natural temperature profile around the spinline being removed due to turbulent conditions. This certainly suggests that forced convection is the only relevant heat transfer mechanism which should be taken into account in the current melt spinning model. Empirical correlations were developed by comparing the heat transfer of thin wire to that of a polymer thread. Reynolds and Nusselt numbers were correlated with the aid of a constant which took into account the angle of the quench stream to the filament bundle. Empirical models shifted from simple correlations to complex relationships predicting intra-filament temperature profiles. However, more recent models neglected intra-filament temperature variations suggesting that these profiles have a negligible effect on the overall heat transfer. Earlier melt spinning models used various heat transfer correlations. This was most likely due to the innovative stage in which this field of study was in during that time. However, recent models all focus on the simple empirical correlation developed by Kase and Matsuo (1967, 1974) which suggests it being the most accurate.

2.4 The development of a monofilament melt spinning model

2.4.1 Historical development

Since properties such as tensile strength, elongation and shrinkage affect downstream operations such as drawing, texturising and relaxing (Dutta, 1982), the need for a model which predicts the as-spun filament properties is of significant importance. The following section summarises the development of research carried out on single (mono) filament modelling techniques.

The earliest work in attempting to predict the temperature profile of a single filament during the melt spinning process appears to be that of Andrews (1958). Here, steady state heat flow equations were derived based on the differential volume element being fixed in space and solved approximately with the aid of empirical data. Both radial and axial temperature gradients along the filament were predicted. Here the ‘freezing’ phenomenon of the filament diameter corresponding to the polymer temperature dropping to below the glass transition temperature was first observed. The approach was restricted, however, by difficulties in obtaining a numerical solution due to the magnitude difference between the radial and axial step sizes resulting in incremental problems. In a series of papers, Kase and Matsuo (1965, 1967 and 1974) carried out extensive research into the simulation approaches. In their work, the mass, heat and force balances are derived and combined as a set of partial differential equations for both the steady and transient states with the solutions of the steady state equations being in good agreement with experimental data. The work carried out by these authors assumes that the viscosity of the polymer is a function of local temperature alone, and fails to account for the effects of air resistance and surface tension in the force balance based on the take up speed being sufficiently low. Negligible elastic elongation, uniform temperature distribution across the filament and no heat conduction in the axial direction are the other assumptions made in the above authors work. Hamana and co-workers (1969) went one step further and included the effects of air resistance and surface tension, but only applied their simulation to low spinning speeds of around 900 m/min.

The attempt made by Prastaro and Parrini (1975) in developing a sound mathematical model describing the dynamics around melt spinning seems to be the first of its kind with the purpose being to establish critical spinning conditions. Here, the assumptions are that elastic effects, axial asymmetry across the filament, variation in polymer material properties (i.e. heat capacity and density) and the surface tension contributions towards the force balance are all negligible. Both radial and axial effects are taken into consideration in the equations of motion. The model only concerns the thread portion that is in the molten state. The authors classified the parameters influencing the process of melt spinning: i) characteristic material properties (i.e. intrinsic viscosity, density and specific heat) and ii) spinning conditions (i.e. mass flow rate, temperature of extrusion etc.).

Gagon and Denn (1981) used the Phan-Thien and Tanner constitutive equation (Phan-Thien, 1978) in describing the fluid rheology (viscoelastic effects) to construct a melt spinning model. The outputs from the simulations were compared to experimental results with good agreement. Newtonian and viscoelastic models were compared and it was concluded that viscoelastic effects are important at low to intermediate take-up speeds. This work seemed to be the first that considers stress induced crystallisation effects but neglected the phenomena in the actual mathematical model. Work done by George (1982) plotted velocity and temperature profiles for take-up speeds of 1000, 2000 and 3000 m/min with good comparison to experimental data. A more simplified approach is adopted here in comparison to the work carried out by Gagon and Denn (1981). The simplification involved the use of Trouton's Law of temperature dependent viscosity in describing fluid viscosity instead of the Phan-Thien and Tanner constitutive equation. Profiles are calculated for intermediate take-up speeds (750-3500 m/min) where the effects of crystallisation are negligible. This model is restricted to spinning conditions where negligible structural development arises (V_L<3500 m/min). Bragato and Gianotti (1983) included kinetic effects of macromolecular orientation and crystallisation in their model. The model is similar to that of Gagon (1982) but differs in that molecular orientation and crystallinity trends are calculated along the spinning path.

From this point on, it appears that research shifted focus to establishing a link between the spinning process conditions and the as-spun fibre properties in the form of correlations and coefficients, more specifically, in providing a link between the optical birefringence and tensile stress. Dutta and Nadkarni (1984) constructed a monofilament model along with a procedure allowing one to predict critical process variables. Here, it was realised that the molecular orientation is uniquely a function of the spinline stress. Their assumptions include steady state, velocity and temperature profiles independent on radial position and that Trouton's law be used to describe polymer viscosity. An explicit force balance seems to be absent in the approach contrary to an accurate initial force guess being crucial for smooth operation of the numerical solution. However, the fact that inertia, gravity, surface tension and air drag effects are assumed negligible suggests that the force is dependent upon cross sectional surface area and local filament viscosity. Shenoy and Nadkarni (1984) went one step further to include a force balance which took into account force changes due to inertial, gravity and air drag on the filament. Their aim was to produce a complete simulation package allowing one to predict the birefringence based on the local spinline stress through the linear correlation discussed in section 2.1 with a case study illustrating the relevance of the model to industrial application. Dutta (1986) expanded on earlier work done in the hope of illustrating the application of computer simulation in PET melt spinning. The model is almost identical to earlier work except for the dependence of material parameters (i.e. heat capacity, density etc.) on temperature variations being taken into account.

Most of the models at this stage were based on a system of ordinary differential equations solved using the initial value problem with the user having to define or guess an initial force since no knowledge of this value is known *a priori*. The accuracy of this initial force was crucial for the specific model to converge. Papanastasiou *et al.* (1987) developed a viscoelastic model solved using a two-point boundary value problem with the main focus being the type of constitutive equation used in the model. Here, an integral type constitutive equation is adopted with good application to the spinning process being achieved.

As opposed to previous researchers, Chung and Iyer (1992) included surface tension and radiation heat transfer effects in their analysis. Heat transfer effects were compared and it was found that radiation effects are relatively small. Accounting for both axial and radial components in their mathematical model, Vassilatos *et al.* (1992)

were able to show significant centerline to surface temperature differences of 9 ^{o}C or more experienced by the filament and highlighted the importance in using the correct heat transfer correlations. However, the effects of these temperature differences on the rest of the filament characteristics are not shown. Ziabicki *et al.* (1998) compared Newtonian and viscoelastic Maxwell fluid models. In their model the effects of stress induced crystallisation (SIC) is taken into account. The results showed that for values of high enough shear moduli (10^9 dyne/cm^2) both models exhibit almost identical trends for certain characteristic filament properties. The inclusion of Stress Induced Crystallisation effects into the model was shown to have dramatic effects on the dynamics of the system, leading to complete solidification of fluid. SIC effects were investigated in a model developed by Jarecki and co workers (2000). Here, the model includes subjecting the filament to a heating zone with the purpose of increasing the amorphous orientation factor for moderate take-up speeds. A Newtonian type correlation, critically dependent on local filament crystallinity and temperature, describes the change in viscosity. It is shown that at higher take-up velocities, three solutions exist in terms of the type of phase that the filament exhibits. These phases differ in crystallinity and stress level. Further research was needed to determine whether the co-existence of multiple phases in real systems can indeed occur.

Harder (2001) concentrated less on the qualitative aspect of the results but more on the numerical stability of the model, and assumed the cooling of the yarn to be a stationary process, thus allowing the time derivatives to be neglected and that all yarn properties are constant within each differential volume element. The heat of crystallisation was neglected in this model and the filament cross sectional area instead of the radius was calculated. The profile trends from this approach agree with other articles relevant in this field but have yet to be confirmed experimentally. McHugh *et al.* (2001) coupled the polymer microstructure with macroscopic velocity, stress and temperature fields in a novel two phase approach which included the addition of a frame invariant enhancement factor in the energy balance aiming to mimic the effect of flow on crystallisation for both nylon and PET yarns. Results were in excellent quantitative agreement with experimental data.

Ziabicki *et al.*(1999) states that a sound mathematical model is one which is complete, tractable and based on experimentally measurable characteristics of the yarn.

However, after much research, no single mathematical model satisfies the above. As such, it may be said that these models should be used to predict filament behaviour qualitatively rather than a quantitatively.

2.4.2 Summary

Early monofilament models only predicted the behaviour of single variables i.e. filament temperature along the spinline with the aid of experimental data. However, numerical difficulties restricted progress. From the 1960's onwards, systems of ODE's could be solved easily through the use of numerical methods developed as computing power advanced. This enabled many fibre properties to be estimated simultaneously. The major differences among models at this time were the correlations used to describe heat transfer and polymer rheological properties. Approaches of this time assumed negligible viscoelastic effects and applied the models to relatively low spinning speeds.

The 1980's saw the incorporation of viscoelastic, air drag and surface tension effects into melt spinning single filament models focusing on providing a link between process conditions and final as spun product properties. Some models included crystallinity but only to a small degree. In spite of the advances in viscoelastic modelling techniques, recent approaches still assume Newtonian behaviour of the polymer with good experimental agreement. Only at the turn of the century have the effects of stress induced crystallisation been taken into account in some models, with a single Avrami type model being used to estimate the crystallisation kinetics.

2.5 The development of a multifilament melt spinning model

2.5.1 Historical development

Most monofilament models are based on a pre-determined velocity and temperature field of the cooling medium, only predicting the changes of variables inside the filament. The assumptions do not apply to multifilament systems due to the geometry of the spinning rig. Flow and temperature profiles are non-uniform due to the extreme spinning velocities and subsequent heat transfer from the filaments to the cooling medium taking place. Although literature on multifilament model predictions and development is minimal, some attempts have been made at trying to model the dynamics of a multifilament system. This section aims at summarising the past and current developments of multifilament model research.

Early attempts in multifilament simulations include those made by Dutta (1987) for transverse quench air melt spinning in differing system geometries and Ishihara et al. (1989) for air jet melt spinning. In each case, the fundamental system balances differ slightly due to changing air drag coefficients, rheological properties and geometry assumptions. Both these approaches modelled the velocity and temperature profiles of the quench air by applying mass and energy balances across cells. These cells were constructed by dividing the filament bundle into a number of filament rows (radial direction) and segments (axial direction). The technique used in estimating the amount of air being dragged downwards by the filament differs in each approach, but both assume turbulent air flow around a moving cylinder. The work done by the above authors showed that significant differences in the quench air temperature are experienced by the filaments according to their position in the filament bundle and distance from the quench air entry point. Dutta (1989) then went on to estimate the variability of spun fibre properties using the same multifilament model described in earlier work. In the work, a coefficient of variance is defined and used to estimate the variation of the freezeline stress with the aim being to apply the same methodology to calculate the degree of variance in other fibre properties.

Gotz *et al.* (2001) used CFD code to predict the changes in air properties around the filament and subsequently coupled the CFD and filament grid. The quench air flow is modelled as particles using a Generalised Lattice Boltzmann method (GLB) which is specifically suited for fluid flow interactions around flexible structures such as a filament suspended in cooling medium. Here, the fibre's position, cross sectional surface area, velocity and temperature are estimated with inertial force and radiative heat transfer considerations ignored. The experimental and theoretical trends differed slightly with regards to spinline deflection but agreed well with respect to velocity and temperature profiles. The work done by Gotz *et al.* (2001) illustrates the difficulty in modelling all of the filament properties accurately. Zhang *et al.* (2007) used similar correlations to Dutta (1987) and Ishihara *et al.* (1989) in estimating the mass of air being dragged down by the filament, but assumed that the quench air temperature around the filament follows an exponential decrease in magnitude, thus resulting in a more complex heat balance for the described cells. An extra equation describing the change in birefringence with distance from the spinneret was included in the set of overall PDE's describing the system. This allowed for a relation between the birefringence and fibre elongation to be made. The most detailed multifilament approach to date seems to be that of Harvey and Doufas (2007). Here a previous melt spinning model constructed by Doufas (2000) is coupled to a three dimensional Navier-Stokes CFD code. Stress induced crystallisation effects are neglected in the model formulation. Although not clearly stated, this is most likely due to the low spinning speeds that the system is modelled at resulting in negligible crystallisation taking place. In the work, it is shown that for large fibre bundles (72 filaments), large variations in filament cooling and tensile stresses exist across the filament bundle with the conclusion that subsequent variations in fibre tensile properties would be obtained.

2.5.2 Summary

Early work aimed at providing an *a priori* prediction of the fibre properties and the extent of variation across the bundle. In general, the multifilament models proposed in literature differ with respect to the assumptions made around the system geometry (i.e. spinneret length, distance between extrusion points, grid construction) and temperature profile surrounding each filament. These two factors significantly affect the material and heat balances used to describe the behaviour of the system. Up until the early 1990's, techniques used to describe the air flow around each filament was solely based on empirical correlations. Following this era, work was aimed at coupling CFD techniques, used to describe the cooling medium properties, with previously developed multifilament frameworks. However, the accuracy of the results obtained from these attempts lack experimental support. Instead, it seems that the major aim of these attempts was to develop coding algorithms and more efficient computing techniques.

3 Thesis objectives

The primary objective of this work is to develop a multifilament melt spinning model which accurately predicts the complex dynamics between properties inherent in the melt spinning process. In spite of the inherent complexity, the model should still be based on the fundamental understanding of each of the major factors influencing the dynamics of the melt spinning process and account for the relationships that exist between these factors. A model which allows for *a priori* estimate of the as spun fibre properties would be of significant value and would avoid having to carry out both time consuming and expensive experimental tests.

It is a well known fact that due to the system geometry, certain deformations to the quench properties arise which in turn results in some degree of inter-filament property variation. Determining the magnitude of these variations across the bundle and the associated factors causing these variations is a key objective of this work. As such, the final model should be able to predict fibre properties which affect the structure of the final product (i.e. tensile stress, molecular orientation) whilst taking into account the effects of a changing quench air temperature profile on the uniformity these properties. In doing so, optimum conditions which lead to the least amount of variation in product structural properties will be identified. In addition to this, process conditions which adversely affect the melt spinning process will be highlighted and discussed.

Based on the literature review carried out, it is clear that a precise understanding of the melt spinning process is yet to be achieved. Several proposals exist in the literature for modelling the microscopic properties of the fibre. However, a study of the polymer fibre microstructure far exceeds the scope of this investigation, whose primary focus is on the engineering aspects of melt spinning. As such, the first objective of this work is to construct the model which describes the macro properties of the fibre and, hence, resolve the influence of system geometry and process conditions on the spun fibre properties. The model should also be constructed in a general manner for application to any polymer and rigorous enough such that it is numerically stable and provides an output which is realistic when comparing to previous models.

With regard to simulating of the model developed, emphasis is laid on well structured coding algorithms which would be used to solve the system of mathematical equations to a maximum degree of accuracy. Generally speaking, validating the model would require performing experimental runs and comparing this data to the output generated by the model. However, since the focus of the present work is on the model development, validation will be constrained to comparison of the results obtained with the data available in the published literature.

As outlined in the literature review, previous multifilament models focus on the influence of a single process condition on a single polymer property (e.g. polymer intrinsic viscosity and take-up speed). In this work, however, the attempt is to determine the influence of process conditions on all significant polymer product properties for a rigorous understanding of melt spinning dynamics. In particular, the influence of stress induced crystallisation is of key interest to this study as little attention has been paid to this area in previous multifilament models. Identifying secondary effects by factors such as polymer temperature, quench conditions and take-up velocity on the degree of crystallisation is an additional objective in this study as this would further increase the understanding of this phenomena. The final objective of this study is to draw key conclusions based on the results and each of the objectives listed above.

Based on the above discussion the following points summarise the key objectives of this thesis.

(i) To develop a multifilament model which accurately predicts the complex system dynamics and magnitude of the final property variation (molecular orientation, tensile stress) which affect the structural integrity of the fibre,

(ii) to ascertain the degree to which heat transfer between the individual filaments and the cooling medium affects the final fibre property variation of the fibre,

(iii) to determine the influence of key process conditions (i.e. quench conditions, extrusion rate and temperature, take-up speed) on the degree of final property variation of the fibre,

(iv) to establish optimum process conditions leading to the least amount of final property variation, and finally

(v) to draw key conclusions and propose valuable recommendations based on the results generated by the simulations performed.

Part B: Modelling

4 Monofilament model

Constructing a monofilament model allows for an *a priori* prediction of the as-spun filament properties, therefore avoiding costly experimental tests and saving time. The development of a rigorous monofilament model which is numerically stable is of significant importance as the monofilament model is a key building block used to construct the multifilament model which is the primary objective of this study. Crystallinity, temperature, force, filament speed and diameter are the five fibre properties estimated in this simulation. The rates of change of the first four characteristics will each be described by an ordinary differential equation (ODE). These equations are derived using material, energy, force and momentum balances with the filament diameter being related to the velocity and initial mass flow rate of polymer melt through the continuity equation. Each of these equations applies to the behaviour of a single filament. This section illustrates the derivation of these governing equations and describes the auxiliary correlations used in predicting the polymer properties.

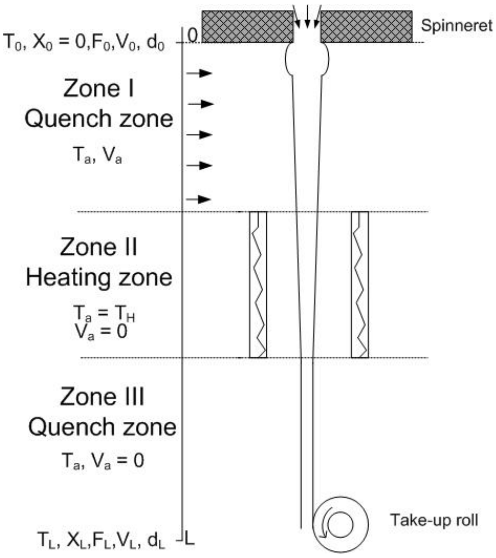

Figure 4-1: The monofilament system and boundary conditions.

The system consists of a filament immersed in a cooling medium as illustrated by Figure 4-1. This cooling medium is generally introduced perpendicular to the filament but in some industrial applications cases radial quenching, in which the quench air is introduced from the spinneret in a co-current direction to that of filament, is the preferred manner. The variables are all modelled as functions of the axial distance from the spinneret (z-dimension) starting from point zero, just after the spinneret, down to the take-up point. One has to take into account the interrelation of variables during the melt spinning process in order to fully understand the dynamics of the system. Figure 4-2 illustrates the relationship between the key variables. The parameters ε_H, R_H and S are the elongation at break (%), breaking force (g/denier) and shrinkage of the yarn (%) respectively and are generally determined through experimental methods and thus are not included in this model. From the figure one can clearly see the level of complexity inherent in the system.

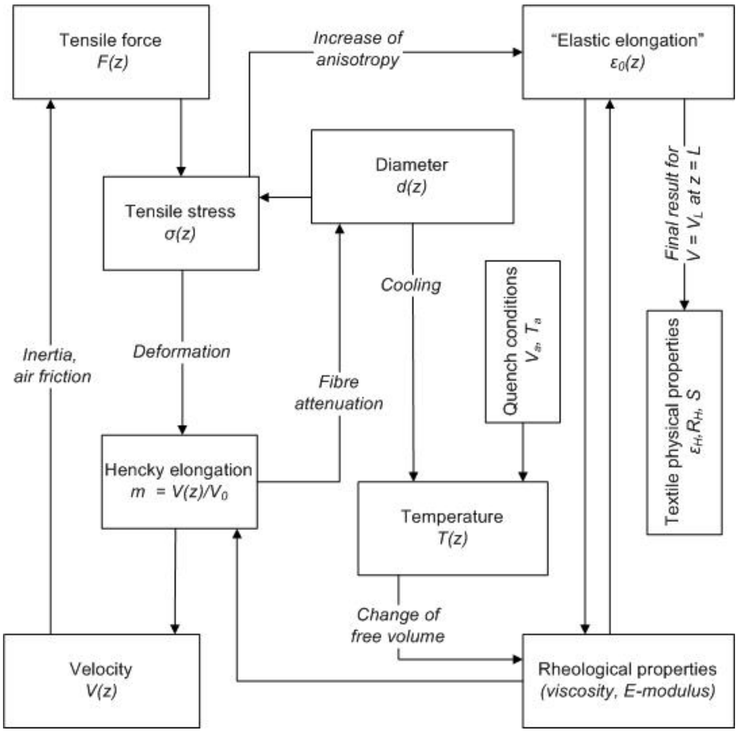

Figure 4-2: A flow chart illustrating the interrelatedness of variables (Beyreuther *et al.,* 1989).

Assumptions enabling the system dimensions and complexity to be simplified consist of the following:

- cylindrical symmetry which reduces the problem to two space variables: axial coordinate z (spinning direction) and radial coordinate r (radial distance from spinneret axis).
- Sufficiently thin filaments: allows one to neglect internal temperature and velocity gradients which are represented by eq. 4.1.

  $$\frac{\partial T}{\partial r} = 0 \; ; \; \frac{\partial V}{\partial r} = 0 \qquad \text{eq. 4.1}$$

  This further reduces the problem to one dimension problem in the z coordinate (spinning direction or distance from spinneret),

- the cooling medium velocity profiles remain unchanged in the radial direction,
- the degree of crystallinity on the polymer heat capacity (C_p, cal/g K) and thermal conductivity (λ_s, cal/s cm K) is negligible, and
- no lag phase which implies that the quench conditions for zone 1 begin as soon as the polymer melt is extruded from the spinneret.

The assumptions listed above greatly reduce the complexity of the system. However, it will be seen later that complications associated with the accuracy and closeness to reality of the model arise when the assumptions based on the cooling medium properties are revisited.

4.1 Crystallisation equation (Avrami type)

A material balance around a differential volume element (DVE) was carried out to derive an equation which describes the change in crystallinity with distance from the spinneret. This is shown in Figure 4-3.

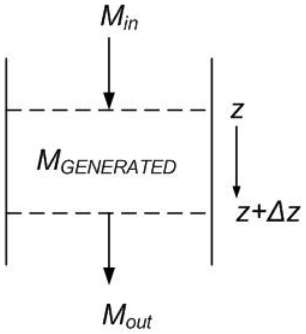

Figure 4-3: The DVE for the material balance.

The material balance is carried out only for the crystalline material. Based on the material flow entering and leaving the system, the conservation of mass at steady state leads to eq. 4.2.

$$\dot{M}_{OUT} = \dot{M}_{IN} + \dot{M}_{GENERATED} \qquad \text{eq. 4.2}$$

The material flow terms in eq. 4.2 represent the amount of material that is crystallised and not the total polymer flow. Thus, the fraction of total polymer material in each DVE that is crystallised, denoted as X_i, must be known. The crystallised mass generated is the result of crystallisation along the spinline due to stress induced effects. The mass flow rate of the polymer (W, g/s) is dependent on the local polymer density, velocity and cross sectional area of the filament (A) as is described eq. 4.3.

$$\dot{W} = \rho(T) \cdot V(z) \cdot A \qquad \text{eq. 4.3}$$

By replacing the mass generated term with the intrinsic reaction rate per unit volume [1/s], eq. 4.2 can be written symbolically as eq. 4.4.

$$\dot{W} \cdot X\big|_{z+\Delta z} = \dot{W} \cdot X\big|_{z} + r' \cdot A \cdot \rho \cdot \Delta z \qquad \text{eq. 4.4}$$

Substituting equation eq. 4.3 into equation eq. 4.4 and rearranging:

$$V \cdot (X\big|_{z+\Delta z} - X\big|_{z}) = r' \cdot \Delta z \qquad \text{eq. 4.5}$$

and taking the limit as Δz tends to zero yields eq. 4.6.

$$\frac{dX}{dz} = \frac{r'}{V(z)} \qquad \text{eq. 4.6}$$

In eq. 4.6 the conventional form of *r'* will be defined by eq. 4.7.

$$r' = \frac{dX}{dt} = n(1-X)[-\ln(1-X)]^{(n-1)/n} K_{st}(T, \Delta p) \qquad \text{eq. 4.7}$$

The equation listed above is the differential form of the Nakamura equation based on the Avrami type approximation (Mubarak *et al.* 2001). The Avrami exponent n in this equation varies from 0 to 4 and is dependent on the whether the nucleation and growth rates take on a linear form, in which case $n = 0$, or the growth is diffusion controlled, where $n = 4$. Doufas *et al.* (2000) assumed that $n = 1$ in order to model the decrease in dimensionality of the crystal growth. However, for this model n is set to 4 as recommended by Jarecki *et al* (2000) for high speed spinning processes. The rate of crystallisation is proportional to the amount of amorphous or non-crystallised material through a crystallisation reaction rate constant *K(T)* or crystallization rate characteristic, $K_{st}(T,\Delta p)$ [1/s], defined as follows:

$$K_{st}(T, \Delta p) = K_{st,0} \cdot \exp(A_s \cdot f_a(\Delta p)^2) \qquad \text{eq. 4.8}$$

where A_s is the stress induced crystallization coefficient.

The amorphous orientation factor, f_a, which accounts for molecular orientation is dependent on the process spinning conditions. The clear dependence of the crystallisation rate on the molecular orientation of the amorphous polymer molecules which is, in turn, a strong function of the tensile stress as described in eq. 4.9. This does seem intuitive as one expects the alignment of molecules to increase with increasing tensile stress in the axial direction. The orientation factor (f_a) is described using a truncated Taylor series type function applicable only to a limited range of tensile stresses (Jarecki *et al.,* 2000). This is shown in eq. 4.9.

$$f_a(\Delta p) = B_1 \cdot \Delta p + B_2 \cdot \Delta p^2 + B_3 \cdot \Delta p^3 \qquad \text{eq. 4.9}$$

where $\Delta p = \dfrac{\rho \cdot F \cdot V}{\dot{W}}$ eq. 4.10

Δp = tensile stress (*dyne/cm²*).

The terms B_i are expansion coefficients and are defined in terms of the stress optical coefficient, C_{opt}, and the amorphous birefringence, Δn_a^0, of ideally orientated chains. These coefficients are defined by eq. 4.11.

$$B_1 = \frac{C_{opt}}{\Delta n_a^0}\ ,\ B_2 = -\frac{3}{7}\left(\frac{C_{opt}}{\Delta n_a^0}\right)^2\ ,\ B_3 = -\frac{1}{7}\left(\frac{C_{opt}}{\Delta n_a^0}\right)^3 \qquad \text{eq. 4.11}$$

(cm^2/dyne, cm^4/dyne^2, cm^6/dyne^3)

From eq. 4.8, the Gaussian temperature dependent term ($K_{st,0}$) is given by the correlation shown in eq. 4.12. This correlation given below shows that crystallization only occurs in the range between the glass transition temperature and the melting point temperature which is discussed fully in section 2.2.

$$K_{st,0} = K_{\max} \exp\left[-4\ln(2)\cdot\frac{(T-T_{\max})^2}{(D_{0.5})^2}\right] \qquad \text{for } T_g<T<T_m$$

$$K_{st,0} = 0 \qquad \text{for } T<T_g \text{ and } T_m<T \qquad \text{eq. 4.12}$$

Where: $D_{0.5}$ = half-width of the Gaussian $K(T)$ curve (see Figure 2-8), T_{max} = maximum crystallisation temperature, K_{max} = maximum crystallisation rate corresponding to the maximum temperature, T_g = glass transition temperature, T_m = melting temperature.

The dependence of crystallisation dynamics on the polymer temperature is evident from the correlations given above. As such, changes in the polymer temperature along the spinline must be predicted accurately. This is the topic of the next section.

4.2 The energy balance

The importance of temperature on the extent of crystallisation has been highlighted above in section 4.1. In addition to the kinetic factors mentioned, the polymer rheological properties of the polymer, such as the modulus and viscosity, are dependent on temperature. Therefore, the axial change in temperature must be accurately predicted if the model is to be used for reliable simulations.

Energy is transported from the melt to the gaseous phase via three mechanisms as discussed in section 2.3. Heat conduction prevails within the fibre whereas convection and radiation are the mechanisms for heat transfer from the surface of the filament to cooling medium. Figure 4-4 illustrates the flow of energy around the DVE.

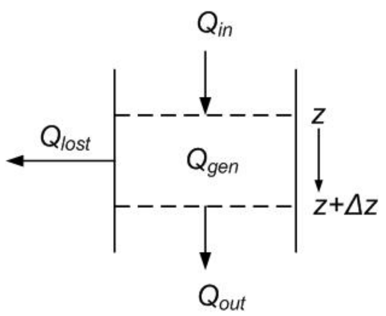

Figure 4-4: The DVE illustrating the flow of energy around a DVE

To begin with, an energy balance around the DVE based on first principles is developed. This is illustrated by eq. 4.13.

$$Q_{ACCUM} = Q_{IN} - Q_{OUT} + Q_{GEN} - Q_{LOST} \qquad \text{eq. 4.13}$$

The in and out terms are the amounts of energy associated with the amount of polymer melt entering and leaving the DVE. As the filament is cooled the temperature drops below the polymer's melting point temperature (T_m) resulting in thermal energy being released due to the exothermic crystallisation taking place. This is accounted for in the Q_{gen} term. Q_{lost} is the term accounting for energy exit flow due to forced convection around the filament as a result of the quench air cooling system. It must be noted that the heat contribution due to viscous dissipation is not incorporated into the model as it does not fall in the scope of this investigation. As discussed in section 2.3, heat loss due to radiation is only significant in the initial stages of the spinning line and thus is assumed to be negligible. When written in terms of standard thermodynamic definitions, eq. 4.13 can be rewritten as:

$$0 = \rho \cdot A \cdot V(z) \cdot C_p \cdot (T\big|_z - T\big|_{z+\Delta z}) + \Delta h \cdot \rho \cdot A \cdot V(z) \cdot (X\big|_z - X\big|_{z+\Delta z}) - f_h \cdot A_R \cdot (T - T_a)$$

where A = cross sectional surface area of the filament [cm^2], A_R = surface area of the filament [cm^2], f_h = heat transfer coefficient [W/cm^2 K]. eq. 4.14

A and A_R are defined as follows:

$$A = \frac{\pi \cdot d^2}{4} \quad \text{and} \quad A_R = 2 \cdot \pi \cdot \frac{d}{2} \cdot \Delta z = \pi \cdot d \cdot \Delta z \qquad \text{eq. 4.15 and eq. 4.16}$$

Dividing through by the ΔV, the volume of the DVE, and taking the limit as $\Delta z \rightarrow 0$ yields eq. 4.17.

$$0 = -\rho \cdot V(z) \cdot C_p \cdot \frac{dT}{dz} + \Delta h \cdot \rho \cdot V(z) \cdot \frac{dX}{dz} - \frac{4 \cdot f_h}{d(z)} \cdot (T(z) - T_a) \qquad \text{eq. 4.17}$$

On arrangement eq. 4.18 is obtained.

$$\frac{dT}{dz}=\left(\frac{\Delta h}{C_p}\right)\cdot\frac{dX}{dz}-\frac{4\cdot f_h}{d(z)\cdot\rho\cdot V(z)\cdot C_p}\cdot(T(z)-T_a) \qquad \text{eq. 4.18}$$

It is shown in section 4.5 that the filament diameter can be represented by equation eq. 4.40. Substituting this into equation eq. 4.18 leads to eq. 4.19.

$$\frac{dT}{dz}=\frac{\Delta h}{C_p}\cdot\frac{dX}{dz}-\frac{2\cdot f_h}{C_p}\cdot\left(\frac{\pi}{\rho\cdot V(z)\cdot\dot{W}}\right)^{\frac{1}{2}}\cdot(T(z)-T_a) \qquad \text{eq. 4.19}$$

The heat capacity and density terms are both linearly dependant on temperature. These are described by eq. 4.20 and eq. 4.21 (Jarecki *et al.*, 2000)

$$C_p(z)=C_{p0}+C_{p1}[T(z)-273] \ \ [\text{cal/gK}] \qquad \text{eq. 4.20}$$

$$\rho(z)=\rho_0-\rho_1[T(z)-273] \ \ [\text{g/cm}^3] \qquad \text{eq. 4.21}$$

The heat transfer coefficient developed by Kase and Matsuo (1967, 1974) is used in this simulation. This correlation seems to be the most commonly used form and is described by eq. 2.16 listed in section 2.3.1. Here, the commonly used heat conduction coefficient (λ_s) and the kinematic viscosity (v_s) of the cooling medium are defined by eq. 4.22 and eq. 4.23 (Jarecki *et al.* 2000).

$$\lambda_s=4.9805\times10^{-6}\frac{T_a^{\ 3/2}}{T_a+114} \ \ [\text{cal cm}^{-1}\ \text{s}^{-1}\ \text{deg}^{-1}] \qquad \text{eq. 4.22}$$

$$v_s=4.1618\times10^{-5}\frac{T_a^{\ 5/2}}{T_a+114} \ \ [\text{cm}^2\ \text{s}^{-1}] \qquad \text{eq. 4.23}$$

where T_a is the temperature of the cooling medium (K).

4.3 The force balance

The net result of the various forces acting on the filament is to influence the distribution of molecular orientation and tensile force along the filament length. As such, a fundamental understanding of the different forces acting on a single filament is required. The continuous extrusion of a viscoelastic fluid undergoing uniaxial elongation and taken up with constant velocity is a typical flow for man-made fibre production processes (Ziabicki 1976). In this model the deformation rates are assumed to be low enough for steady-state elongation flow to dominate. Therefore, the fluid viscosity is assumed to be Newtonian, strongly influenced by crystallisation and temperature. Under this assumption elastic deformation may be ignored, greatly reducing the complexity of model equations and hence the numerical solution used, since no stress tensors need be included in the force balance.

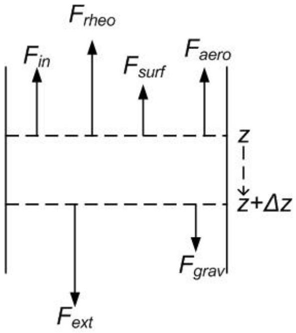

Figure 4-5: The DVE for the force balance

Figure 4-5 shows the forces acting on a filament during the spinning process at steady state. Using this, a force balance is derived which is shown by eq. 4.23.

$$F_{ext} + F_{grav} = F_{inertia} + F_{aero} + F_{surf} + F_{rheo} \qquad \text{eq. 4.24}$$

Rearranging this equation for the change in rheological force causing the flow in the spinline one obtains eq. 4.25.

$$\Delta F_{rheo} = -\Delta F = \left(\Delta F_{ext} + \Delta F_{grav}\right) - \left(\Delta F_{in} + \Delta F_{aero} + \Delta F_{surf}\right) \qquad \text{eq. 4.25}$$

F_{ext} is the force exerted due the external take up tension as a result of the constant winding up of the filament at the take up roll device and is usually constant throughout the filament, thus $\Delta F_{ext} = 0$. F_{grav} is the force exerted on the filament due to gravity, the change of which can be defined by eq. 4.26.

$$\Delta F_{grav} = m \cdot a = \dot{W} \cdot t \cdot g = \dot{W} \cdot \frac{\Delta z}{V(z)} \cdot g \qquad \text{eq. 4.26}$$

$F_{inertia}$ accounts for the inertial force opposing the change in velocity of the filament. The change in the inertial force experienced by the filament is based on the difference in velocity across the DVE. This is represented by eq. 4.27.

$$\Delta F_{in} = \dot{W} \cdot (V|_{z+\Delta z} - V|_{z}) \qquad \text{eq. 4.27}$$

F_{aero} is the force due to skin friction as a result of drag occurring between the filament skin and the cooling medium as the filament travels downwards:

$$\Delta F_{aero} = C_f \cdot \rho_s \cdot V(z)^2 \cdot A_R = C_f \cdot \rho_s \cdot V(z)^2 \cdot \pi \cdot \frac{d(z)}{2} \cdot \Delta z = C_f \cdot \rho_s \cdot V(z)^2 \sqrt{\frac{\dot{W} \cdot \pi}{\rho \cdot V(z)}} \cdot \Delta z$$

where: ρ_s = cooling medium density [g/cm^3], C_f = skin friction factor. eq. 4.28

The skin friction factor can be described in many ways. However, it appears that the selection of a skin friction coefficient depends on the diameter of the filament and type of flow surrounding the filament (Ziabicki, 1976). Based on these criteria, the correlation described by eq. 4.29 will be adopted (Jarecki 2000).

$$C_f = 0.37 \cdot \left(\frac{V(z) \cdot d(z)}{v_s} \right)^{-0.61} \qquad \text{eq. 4.29}$$

A surface tension exists around the exterior of the filament due to the cohesive forces of the molecules present in this region which is represented by F_{surf}. However, this force is negligible and makes up less than 1% of the external take up tension. Substituting eq. 4.26 - eq. 4.28 into eq. 4.25 yields eq. 4.30.

$$\Delta F = \dot{W} \cdot (V|_z - V|_{z+\Delta z}) + C_f \cdot \rho_s \cdot V(z)^2 \sqrt{\frac{\dot{W} \cdot \pi}{\rho \cdot V(z)}} \cdot \Delta z - \dot{W} \cdot \frac{\Delta z}{V(z)} \cdot g \qquad \text{eq. 4.30}$$

Dividing through by Δz and taking the limit as this tends to zero yields eq. 4.31. This balance lacks the stress tensors included in the force balance derived in more recent work (Doufas *et al.* 2000). However, the assumption of the polymer being an inelastic Newtonian fluid allows for the stress tensors to be negated.

$$\frac{dF}{dz} = \dot{W} \cdot (\frac{dV}{dz} - \frac{g}{V(z)}) + C_f \cdot \rho_s \cdot V(z)^2 \sqrt{\frac{\dot{W} \cdot \pi}{\rho \cdot V(z)}} \cdot \qquad \text{eq. 4.31}$$

4.4 The constitutive equation

Viscous behaviour of the filament is used to describe the velocity profile with respect to the axial length. This requires that the rheological behaviour of the fibre forming polymer be taken into consideration in the form of a constitutive equation. Since it is assumed that the deformation rates along the spinline are low enough for elongation flow to dominate, it is possible to describe the polymer viscosity using the Trouton Law. This states that the elongational viscosity of polymer can be assumed to be three times the Newtonian viscosity (Ziabicki 1976).

$$\eta_{app} = 3 \cdot \eta_0(T, X) \qquad \text{eq. 4.32}$$

Figure 4-6 illustrates the shear viscosity behaviour of PET as the shear rate is increased and shows that Newtonian flow is obeyed for shear rates up to 10^2 s^{-1}.

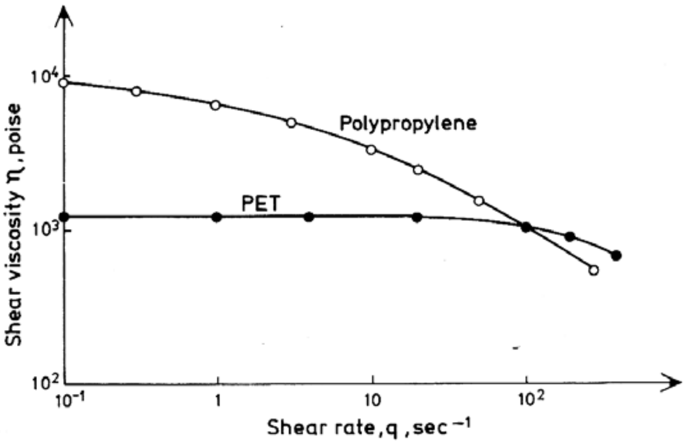

Figure 4-6: The shear viscosity behaviour for PET and Polypropylene (“*Fundamentals of Fibre Formation*”, A. Ziabicki 1976, © John Wiley & Sons Limited, reproduced with permission).

The relationship between axial length and velocity is defined using the rheological constitutive equation based on the definition of shear stress described by eq. 4.33.

$$\Delta p = \eta_{app} \cdot \frac{dV}{dz} = 3 \cdot \eta_0 \cdot \frac{dV}{dz} \qquad \text{eq. 4.33}$$

The shear stress can also be defined by eq. 4.34.

$$\Delta p = \frac{F(z)}{A} = \frac{F(z) \cdot \rho \cdot V(z)}{\dot{W}} \qquad \text{eq. 4.34}$$

Equating eq. 4.33 and eq. 4.34 results in eq. 4.35.

$$\frac{dV}{dz} = \left(\frac{1}{3 \cdot \eta(T,X)} \right) \cdot \frac{\rho \cdot F(z) \cdot V(z)}{\dot{W}} \qquad \text{eq. 4.35}$$

The effect of crystallinity and temperature on the Newtonian viscosity can be defined by the product of the crystallinity and temperature dependent viscosity terms:

$$\eta(T,X) = \eta_T(T) \cdot \eta_X(X) \qquad \text{eq. 4.36}$$

where:

$$\eta_T(T) = \eta_0 \cdot \exp\left(\frac{E_a}{k \cdot T} \right) \text{ and } \eta_X(X) = \frac{1}{\left(1 - \frac{X}{X^*}\right)^{\alpha}} \qquad \text{eq. 4.37 and eq. 4.38}$$

here, η_0 = temperature dependent viscosity coefficient [poise], X^* = critical crystallinity estimated from a range of 0.01 to 0.1, α varies from 1 to 3.4 depending on the molecular weight of the polymer.

The values of X^* and α are 0.1 and 1 respectively as recommended by Jarecki *et al.* (2000). After the critical crystallinity value is reached the filament traverses the rest of spinline as a solid rod due to the extent of crystallinity caused by the viscosity of polymer approaching infinitely large values.

4.5 The mass balance

Since no mass transfer takes place between the cooling medium and the filament and due to the continuous nature of the filament, a useful relationship can be made relating the filament diameter, density and velocity. This is relation is termed the condition of continuity and is defined by eq. 4.39. Once rearranged, this relationship will determine the diameter of the filament in the simulation.

$$\dot{W} = \rho \cdot V(z) \cdot \left(\frac{\pi \cdot d(z)^2}{4} \right) \tag*{eq. 4.39}$$

Rearranging equation eq. 4.39 into eq. 4.40 results in leads to an equation describing the relation between the filament diameter, $d(z)$, velocity and density.

$$d(z) = \sqrt{\frac{4 \cdot \dot{W}}{\rho \cdot V(z) \cdot \pi}} \tag*{eq. 4.40}$$

4.6 Complete system of equations

The overall set of equations used to describe crystallinity, filament velocity, temperature, force and diameter derived in sections 4.1 - 4.5 are shown by eq. 4.41 to eq. 4.45.

$$\frac{dX}{dz} = n(1-X)\left[-\ln(1-X)\right]^{(n-1)/n} \cdot \frac{K_{st}(T,\Delta p)}{V(z)} \tag*{eq. 4.41}$$

$$\frac{dT}{dz} = \frac{\Delta h}{C_p} \cdot \frac{dX}{dz} - \frac{2 \cdot f_h}{C_p} \cdot \left(\frac{\pi}{\rho \cdot V(z) \cdot \dot{W}} \right)^{\frac{1}{2}} \cdot (T(z) - T_a) \tag*{eq. 4.42}$$

$$\frac{dF}{dz} = \dot{W} \cdot \left(\frac{dV}{dz} - \frac{g}{V(z)}\right) + C_f \cdot \rho_s \cdot V(z)^2 \sqrt{\frac{\dot{W} \cdot \pi}{\rho \cdot V(z)}} \cdot \tag*{eq. 4.43}$$

$$\frac{dV}{dz} = \left(\frac{1}{3 \cdot \eta_0} \right) \cdot \frac{\rho \cdot F(z) \cdot V(z)}{\dot{W}} \tag*{eq. 4.44}$$

$$d(z) = \sqrt{\frac{4 \cdot \dot{W}}{\rho \cdot V(z) \cdot \pi}} \tag*{eq. 4.45}$$

The system of equations is solved simultaneously to produce trends describing the characteristic profiles of the system along the filament length. Table 4-1 shows all the constants and parameters used in the model.

Table 4-1: The constants for Polyethylene Terephthalate (PET) used in this model.

$C_{opt} = 5 \cdot 10^{-10}$ cm^2/dyne	$n = 4$
$\Delta n_a^o = 0.275$	$\Delta h = 1.237 \cdot 10^9$ erg/g
$\rho_0 = 1.356$ g/cm^3	$\rho_1 = 5 \cdot 10^{-4}$ g/cm^3
$C_{p0} = 1.356$ cal/g K	$C_{p1} = 5 \cdot 10^{-4}$ cal/g K
$\eta_0 = 0.0976[\eta]^{5.2893}$ poise	$[\eta] = 0.6$ dl/g
$E_a/K = 6923.7$ K	$T_g = 343$ K
$K_{max} = 0.016$ s^{-1}	$T_{max} = 463$ K
$D_{1/2} = 32$	$T_m = 553$ K

The overall structure of the model allows for it to be applied to any polymer by simply altering the parameters listed in Table 4-1 to those specific to the target polymer. The dependence of the individual filament properties to one another is clearly illustrated from the set of equations listed above and results in a system with high level of inherent complexity. This level of complexity necessitates the need for a clear fundamental understanding of the system dynamics and, as such, any attempt in identifying process parameters of significant influence to the final properties of the filament must be performed with this prior knowledge.

5 Multifilament model

5.1 Introduction

Chapter 4 dealt with the development of a monofilament model which would be able to predict the properties of the filament as a function of the filament length alone. This single filament model is based on constant quench conditions. Industrial production of a synthetic fibre involves spinning a large amount of individual filaments, each experiencing unique quench conditions due to the heat transfer between filaments and the passing quench air. Since the key objective of this study is to determine the influence of thermal gradients on the variation of filament properties across a fibre, a method is required which firstly, predicts the change in quench air temperature and secondly, is capable of estimating the effects of this thermal change on the as spun filament properties. The present section deals with the approach used to include the monofilament model as part of a multifilament framework to predict the performance of a filament bundle under varying quench conditions.

In the following chapter certain assumptions are listed to simplify the complexity of the system. The method used to compartmentalise the filament bundle is described. An energy balance is derived for the heat flow from the filament to the cooling medium. This energy balance is unique when compared to previous work carried out as a convection term is incorporated which includes the heat transfer coefficient in the energy transferred term. Two different numerical approaches are used to calculate the change in the quench air temperature across each compartment (see chapter 7). Both these methods are described in detail. Given that the changes in quench air profile and velocity are ignored, it is expected that the two approaches listed above will allow for a conservative estimation to be made in the change in quench air temperature across the filament bundle. In turn, the effects of these changes on the variation of the characteristic yarn properties, governing the structural properties, are estimated using the model.

5.2 System geometry and basic assumptions

Figure 5-1 (a) shows the general system geometry. In order to fully describe the method used to integrate the monofilament model, the following terms need to be defined. Considering the assumption of uniform quench air flow, the quench axis is the direction corresponding to that of the quench air flow direction (*r* direction). The direction in which the filaments travel is termed the filament axis (*z* direction). Lastly, the direction in which zero change in both quench and filament properties occurs is defined as the constant axis (*x* direction).

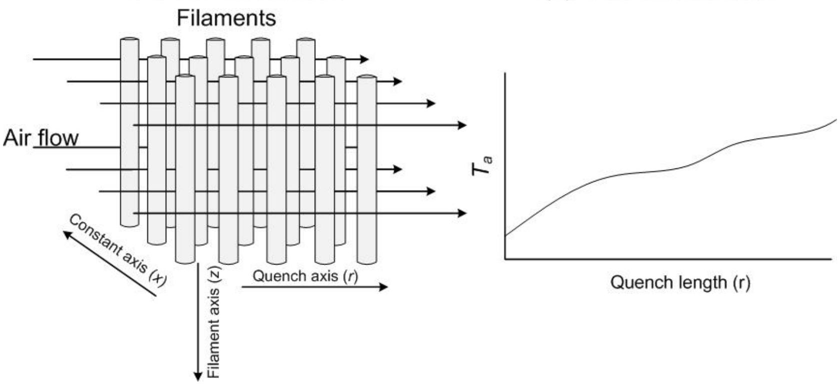

Figure 5-1: (a) A diagram illustrating the system dimension, and (b) idealised quench air behaviour through the filament bundle.

Multifilament melt spinning is significantly more complex than monofilament melt spinning. The single filament model assumes a constant quench temperature and air flow rate surrounding the filament. In the case of multifilament melt spinning, a large number of filaments are spun under varying quench conditions according to their position within the filament bundle. A quench stream, introduced perpendicular to the direction in which the filaments traverse, cools the individual threads. Figure 5-1 (b) illustrates the quench air behaviour through a section of a filament bundle. As the air traverses the filament bundle it is heated due to heat transfer from the individual polymer filaments. As a result, individual filaments experience unique conditions. It is expected that the filaments on windward side of the bundle will be cooler that those on the leeward side due to the heating of the quench stream. It is this variation in filament temperature across the bundle which affects the crystallisation rate, molecular orientation and tensile stress of the filaments. In this model the behaviour of a single row of filaments in the quench direction (r-axis) will be estimated along with the change in quench temperature. The number of filaments in the bundle for this simulation in the direction of the *r*-axis will be taken as ten (Dutta 1987). Increasing this number would significantly increase simulation time.

Industrial melt spinning rigs differ in many ways. In particular, spinneret dimensions can vary significantly depending on the number of filament holes through which the molten polymer is extruded. The layout of the holes affects the degree to which the quench air flow profile is altered. Previous work showed that air profiles for a spinneret with a circular hole layout are significantly more non-uniform when compared to a spinnerets of a rectangular layout (Dutta, 1987). Intuitively, one would expect this as the distance that the quench air has to travel through the bundle varies due to the presence of more filaments at the centre of the spinneret when compared to the extremities of the circular spinneret. The geometry of the rectangular spinneret is more uniform and, as such, affects the air flow profile to a lesser degree.

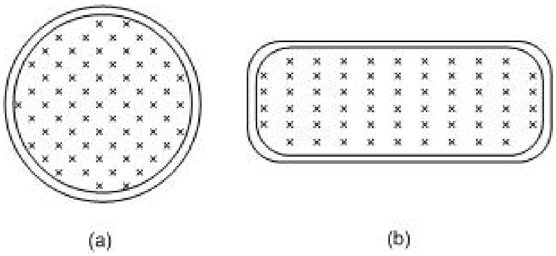

Figure 5-2: Basic spinneret geometry: (a) Circular spinneret (b) Rectangular.

Due to the complexity of the system, a number of assumptions have to be made in order to predict the change in the quench air temperature. These include the following:

- the spinneret type is of a rectangular geometry,
- fixed filament position in the bundle (no curvature of bundle due to aerodynamic or harmonic effects),
- relative to the total spinline length, negligible change in the filament position will occur in the first quench zone. Therefore, it is safe to assume that the distance between each filament, in both the quench and filament direction, is constant.
- Each filament row, along the *x* axis, experiences the exact same quench conditions. Hence, in the x direction, all filaments in the same row have identical properties, and
- an unaltered flow profile of the quench air (i.e. no chimney effect). This assumption has known complications associated with it. It is well known that the flow profile of the quench stream in industrial melt spinning rigs is altered severely due to the excessive speeds with which the filaments are spun (Ziabicki 1976, Harvey and Doufas 2007). The assumption of an unaltered flow profile is made here as predicting the flow profile is not in the scope of this investigation and requires CFD codes and complex numerical techniques to solve. The assumption simplifies the mass and energy balances used to estimate the behaviour of the quench air. Another justification for this assumption is the length required (l_e) for a fully developed flow pattern to develop in a channel (Geankoplis 1993, Perry *et al.* 1997). Assuming that the air flow profile is laminar at the entrance point, the distance needed for fully developed flow is a function of the Reynolds number and the flow pattern upstream of the air upstream. The required length is proportional to the equivalent diameter with the proportionality constant being a function of the Reynolds number. Here, the constant is 40 as recommended by Perry *et al.* (1997). This method is illustrated by eq. 5.1.

$$l_e = 40 \cdot D_e \qquad \text{eq. 5.1}$$

Where, D_e is the equivalent diameter (m).

The equivalent diameter is given by the following equation:

$$D_e = \frac{4 \cdot A_r}{wet \cdot perrimeter} = \frac{4 \cdot l \cdot b}{2 \cdot (l + b)} \qquad \text{eq. 5.2}$$

where A_r is the cross-sectional area [m^2]; l is the length and b is the breadth of the channel [m].

If the flow through the quench unit is assumed to be analogous to flow through a channel with a 20 by 100 cm cross sectional area, then the required length for fully developed flow to occur is calculated as 13.3 cm. Comparing this to the total flow length required by the spinneret (7 cm) it is clear that not enough flow length exists and hence, according to the theory, fully developed turbulent flow will not be achieved. As such, the flow is laminar throughout the bundle. The assumption of an unaltered flow profile is made for a number of reasons. Previous attempts at modelling a multifilament system with incorporated flow profile changes (Dutta 1987, Harvey and Doufas 2007) all show that the air flow is severely altered by the filament bundle with a large portion of the air being dragged downwards with the filaments. This suggests that air passing through the filament bundle has more time for heat transfer than an unaltered flow profile would allow. As such, the approach of modeling for thermal variations is most likely to be true. This model does provide a simple method in obtaining a conservative estimate to investigate whether a more rigorous CFD study is needed. Secondly, correlations describing the change in air velocities across the filament bundle are excluded to simplify the computational process. Determining the value of the initial force required for a desired take-up velocity for each filament would be overly complicated if air drag effects were taken into account. Furthermore, the separation of the spinning path into different zones adds to the complexity of the system.

In light of the discussion and the assumptions listed above, Figure 5-3 illustrates the system along with the position of the boundary conditions and various quench zones.

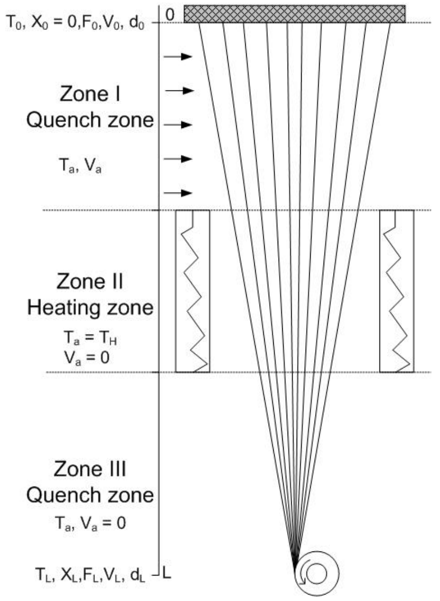

Figure 5-3: A diagram illustrating the multifilament system.

5.3 Model development and energy balance

Figure 5-4 (a) and (b) show the grid layout. This is constructed by splitting the filament bundle into a number of filament rows running in the direction of the quench axis which are then sub-divided in the constant direction as illustrated. This results in the formation of cells in which the filament properties are estimated using the single filament model.

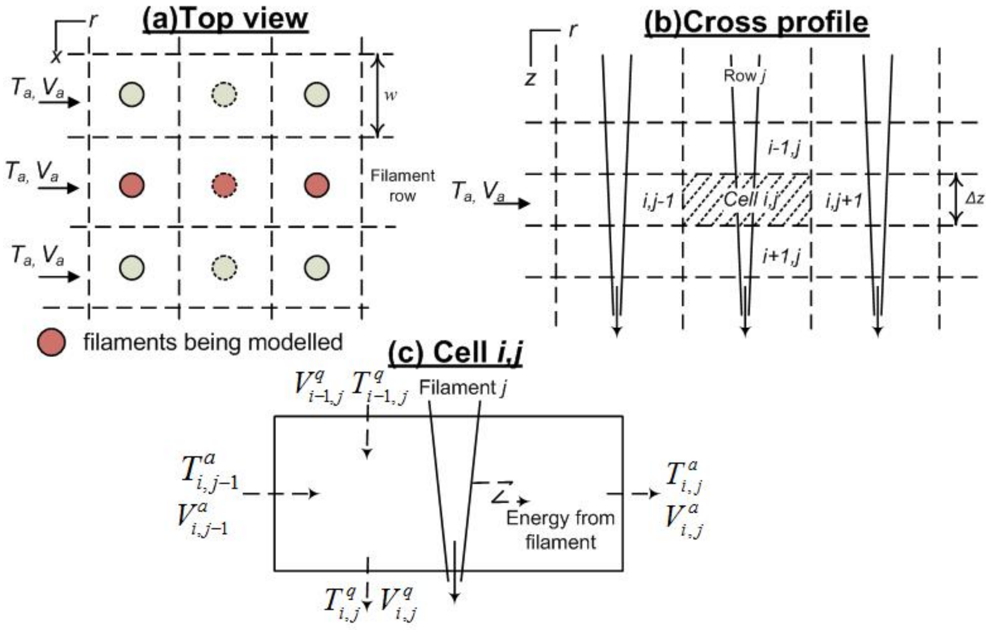

Figure 5-4: (a), (b) A diagram illustrating filament bundle divided into compartments, and (c) an individual cell over which the energy balance is performed.

It must be noted that the energy balance is carried out across the volume of air within the cell and not over the polymer filament section. Figure 5-4 (c) indicates a section of filament within the cell over which the balance is carried. The energy balance carried out across each cell (see Figure 5-4) is described by eq. 5.3.

$$Q_{out} = Q_{in} + Q_{source} \quad \text{eq. 5.3}$$

The Q_{in} and Q_{out} terms are the amounts of energy associated with the air flowing into and out of the compartment. These heat flow terms are described by eq. 5.4 and eq. 5.5.

$$Q_{in} = V_{a,i-1} \cdot C_p^a \cdot (T_{a,i-1} - T_{ref}) \cdot \rho_{air} \cdot \Delta z \cdot w + V_{a,j-1} \cdot C_p^a \cdot (T_{a,j-1} - T_{ref}) \cdot \rho_{air} \cdot \Delta z \cdot w$$

$$Q_{out} = V_{a,i} \cdot C_p^a \cdot (T_{a,i} - T_{ref}) \cdot \rho_{air} \cdot \Delta z \cdot w + V_{a,j} \cdot C_p^a \cdot (T_{a,j} - T_{ref}) \cdot \rho_{air} \cdot \Delta z \cdot w$$

eq. 5.4 and eq. 5.5

Here, w is the spacing between filaments (hole to hole) assumed to be 0.0035 m (Dutta 1987). Based on the assumption of negligible air being dragged down by the filaments, the first terms in eq. 5.4 and eq. 5.5 fall away. Secondly, this assumption implies that the mass of air entering the cell equals the exit flow in the quench direction. The change in density and heat capacity of the cooling medium (air) is assumed negligible over the temperature ranges experienced in the melt spinning system.

The heat source term, Q_{source}, is the amount of heat transferred by convection from the filament to the cooling air and is estimated by the definition of Newton's law of cooling (Thompson, 2000). This law assumes that rate of cooling is proportional to the temperature difference between the bulk fluid (T_a) and filament surface (T) (Winterton 1997). This term includes the heat transfer coefficient taking into account resistance to heat transfer as a result of the boundary layer of the air around the individual filament. Thus the term representing the amount of heat being transferred from the filament to the cooling medium is defined as:

$$Q_{source} = Q_{convection} = f_h \cdot (T_{ave}^{polymer} - T_{bulk}^{a}) \cdot A_s \quad \text{eq. 5.6}$$

where f_h = heat transfer coefficient [J/m^2 s K], A_s = heat transfer area.

Here, the filament surface temperature, $T_{ave}^{polymer}$, will be taken as the average temperature of the polymer entering and leaving the cell. T_{bulk}^{a} is the bulk temperature of the volume of air surrounding the filament. Heat is transferred via forced convection in radial direction from the filament to the surrounding air. The heat transfer area is the cross sectional area normal to the direction in which heat is being transferred. In this case, A_s is defined as the surface area of a cone excluding the top and bottom surface areas. This is described by eq. 5.7.

$$A_s = \frac{\pi}{2} \cdot (R_1 + R_2) \cdot \Delta z \qquad \text{eq. 5.7}$$

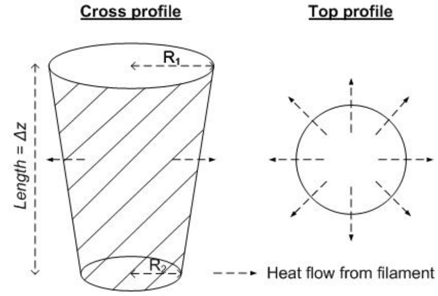

Figure 5-5: The surface area of filament through which heat transfer takes place.

Substituting eq. 5.4 - eq. 5.7 into eq. 5.3 and solving for the exit air temperature we obtain eq. 5.8.

$$T^a_{i,j} = T^a_{i,j-1} + \frac{f_h \cdot (T^{polymer}_{ave} - T^a_{bulk}) \cdot A_s}{V_{air} \cdot \rho_{air} \cdot \Delta z \cdot w \cdot C^a_p} \qquad \text{eq. 5.8}$$

In the z direction, the initial conditions for each cell are taken as the final properties of the filament section from the previous compartment. The approach described above is unique when compared to previous work carried out in this field. In previous work it is generally assumed that the amount of energy lost by the filament is gained by the air. This assumption holds true for approaches neglecting crystallisation effects. However, in this model exothermic crystallisation results in a sudden increase the local filament temperature and as a result, the quench air temperature decreases in this region due to the nature of the previously proposed energy balance. This occurs even though the temperature of the quench air being much lower in magnitude than that of the filament. This is solely due to the reversal of heat flow as a result of the assumption made in previous attempts. This unrealistic and cannot be applied in this simulation. The present approach pre-empts this error from occurring as the amount of heat being transferred is calculated separately using heat transfer coefficients.

From the above discussion, it is clear that a well structured algorithm, which incorporates numerical techniques, is required to solve the system. This is discussed in chapter 7. The layout of boundary conditions and the sensitivity of the system to these conditions are of significant importance. This is the topic of the following chapter.

6 Sensitivity to boundary conditions

One of the novel aspects of this work is the inclusion of stress induced crystallisation (SIC) of the PET polymer as it changes phase from molten to solid along the spinline. Previous work (White and Cakmak 1986, Ziabicki and Jarecki 1986, Ziabicki and Kedzierska 1962) has lead to a well defined link being established between the degree of online crystallisation and tensile stress which, in turn, influences the degree of molecular orientation of the filament. Incorporating SIC effects alters the definition of polymer viscosity as no longer is it just a function of local temperature but, of the degree of crystalline material present as well. This complicates the relation between the initial force and the final take-up velocity. As such, this chapter describes the influence of stress induced crystallisation on the selection of the initial force. The sensitivity of the initial force to the final take-up velocity is first established as this is a crucial step in determining what initial force is needed in order to obtain the desired take-up velocity.

Secondly, process conditions are then varied to investigate the dynamics of the melt spinning process. These process conditions include quench air temperature and velocity, extrusion rate and temperature and finally, take-up velocity. Characteristic diagrams (CD) of the final take-up velocity versus initial tension are constructed which will aid in the justification of choosing to investigate the effects of the above process conditions on final product uniformity. The selection of take-up velocities under which these conditions are going to be applied to the system will be discussed. Here, it is shown that changing quench conditions result in further complications in selecting the initial force required for the desired take-up velocity to be obtained. This complication applies to the multifilament model where heat transfer from the filaments to the quench air results in changing quench conditions throughout the bundle. Following this, a summary of the way in which the above mentioned process conditions affect the system will be given.

6.1 Boundary conditions

Defining precise boundary conditions is crucial in order for accurate and realistic results to be obtained from any mathematical model. In both the mono and multi-filament models, four ordinary differential equations need to be solved simultaneously with the continuity equation. Thus, four boundary conditions are required. Since the solution method is an initial value problem, property values need to be estimated at the spinneret outlet point.

The initial conditions needed to solve the system are easy to control except that of the initial force value. Realistically, the initial force controls the initial velocity gradient of the spun fluid. This value is controlled by the desired take-up velocity. SIC effects complicate the relationship between the final take-up velocity (V_L) and the initial force (F_0). Jarecki and co-workers (2000) generated plots of V_L versus F_0 for constant process conditions. Firstly, these plots showed that the relation is no longer monotonic and, secondly, high take-up velocities had multiple solutions of initial force, the magnitude of which controlled the final phase of the polymer. This is discussed in more detail in section 6.2. The initial conditions for ordinary differential equations can be summarized by equation eq. 6.1.

$$z = 0,\ X = X_0,\ T = T_0, \text{ and } V = V_0 = \frac{4 \cdot W}{\pi \cdot d_0^2 \cdot \rho(T_0)} \qquad \text{eq. 6.1}$$

$$z = L,\ V = V_L$$

The extrusion velocity is dictated by the initial mass flow rate of the polymer and the spinneret hole diameter. The initial filament diameter is assumed to be approximately equal to that of the spinneret hole diameter, d_0. The precise values and selection of the rest of the boundary conditions are discussed in section 6.3.

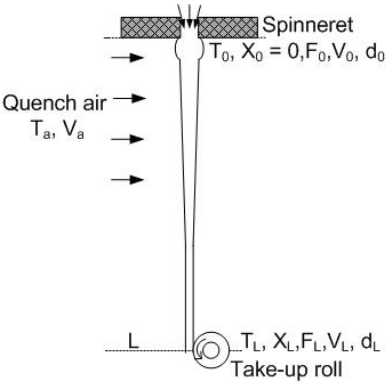

Figure 6-1: A diagram illustrating the monofilament system and boundary conditions.

6.2 Initial force selection and the effects of SIC

As mentioned in the previous section, most of the initial conditions are easy to control except for the initial force. Previously, without the effects of stress induced crystallisation (SIC), the final take-up velocity (V_L) versus initial tension (F_0) relationship was monotonic allowing for the initial tension to be replaced by the take up velocity. However, this is not the case in this study. Due to the effects of SIC on the local viscosity of the polymer and the axial gradient of velocity resulting in the final take-up velocity, the relation between V_L and F_0 is more complicated as shown in Figure 6-2. As a consequence of reduced fluidity when crystallisation occurs, the velocity does not increase with increasing initial tension but starts to decrease at some critical tension. This requires a careful selecting procedure when choosing the initial force required for a specific take-up velocity. This is discussed in more detail in chapter 7.

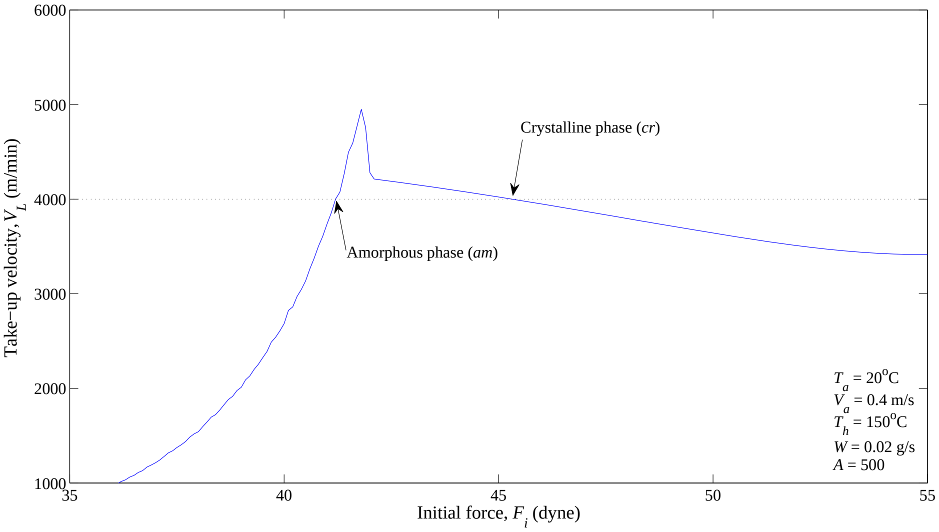

Figure 6-2: A plot of the final take-up velocity versus initial tension relationship.

The sensitivity of the initial force to the final take-up velocity is clearly seen in Figure 6-2 where a steep gradient is observed in the region leading up to the maximum take-up velocity. The maximum velocity is achieved at some critical value of initial tension. This point corresponds with the onset of significant crystallisation. After this point the velocity starts to decrease as described above with a decrease in the sensitivity between the two variables. As a consequence of this non-monotonic relationship, multiple roots of initial tension exist for the same final take-up velocity. The first root leads to an amorphous phase (am) with marginal online crystallinity being achieved. However, the second phase results in the filament being made up of a crystalline phase (cr). It must be noted that the multiple solutions are not due any discontinuities (e.g. eq. 4.38) in the system of mathematical equations used to construct the model. As such, there are no asymptotes in Figure 6-2.

The factors described above illustrate the complex system dynamics associated with the selection of the initial force due to the occurrence of SIC. In this simulation it is the final take-up velocity which controls the initial tension. As such, establishing the relation between the final take-up velocity and initial tension is important in obtaining the desired take-up velocity and phase type. The likelihood of obtaining either one in an industrial process is yet to be understood (Jarecki *et al.,* 2000). However, the physical meaning between the two phases is clear. A definite difference in the amount of kinetic activity and resulting degree of crystallinity is obtained. It will be seen that the phase type selected according to the initial force significantly influences the uniformity of the properties across the bundle.

6.3 Process conditions investigated

6.3.1 Quench air temperature

The focus of this investigation is to determine the effects of changing quench conditions on the variation of the overall as spun fibre properties. A change in the quench air temperature will affect the cooling rate of the polymer as the temperature gradient between the cooling medium and hot polymer is altered. This factor alone justifies investigating the effects of applied quench air temperatures on the as-spun fibre properties. Common quench temperatures used in industry vary from 18-25^{o}C. The selection of a lower quench temperature and the associated effects on the variation of as-spun polymer properties would provide a broader spectrum on the overall effects of the quench temperature. Plots of the final take-up velocity versus initial tension illustrate the effects of varying a certain process condition on the overall system. Hence, from this point onward these diagrams will be referred to as 'characteristic diagrams' (CD).

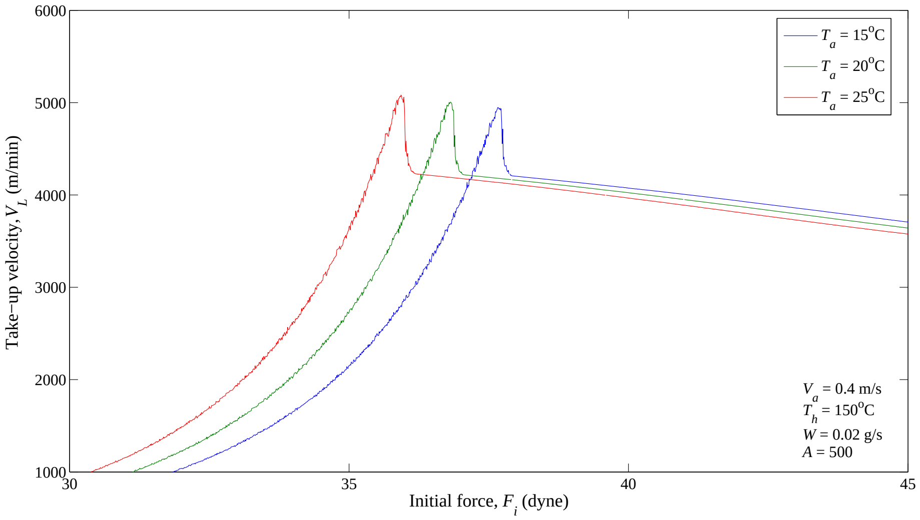

Figure 6-3: The take-up velocity versus initial force plot for a range of quench temperatures (T_a).

Figure 6-3 shows the effects of various quench air temperatures on the system dynamics. Here, it is clear that a change in the applied quench air temperature will affect the system dynamics to some degree. An increase in the quench air temperature results in lower online forces for the same take-up velocity. Considering all of the above, the range of temperatures to be investigated will be from 15 to 25 °C.

6.3.2 Quench air velocity

The magnitude of the quench air velocity dictates the amount of time the passing volume of air has to exchange heat with the polymer. This will affect the amount of heat removed from the filament. Quench air velocities range from 0.4 to 1 m/s in industrial spinning processes. The characteristic diagram for varying quench air velocities is shown in Figure 6-4. Here, it can be seen that quench velocity has a significant affect on the system dynamics. Higher quench air velocities result in the peaks shifting to higher tensions. Here, it is noted that greater online stresses are required for the same take-up velocity. Thus, the range of quench velocities shown in Table 6-1 will provide a sufficient field of investigation. It is important to note the distance between the peaks as this will affect the force range selected for specific set of quench velocities.

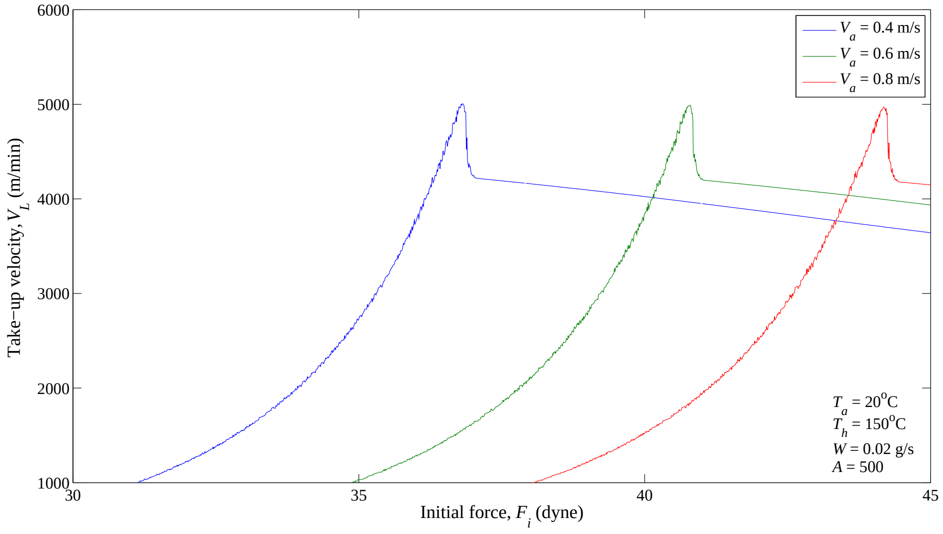

Figure 6-4: The take-up velocity versus initial force plot for a range of quench air velocities (V_a).

6.3.3 Polymer extrusion rate

Another factor which influences the polymer cooling rate is the amount of polymer present at the point of cooling. A large mass of polymer will require more heat to be removed than a smaller mass. Thus, the initial polymer flow rate (*W*) is a further property to be tested in this investigation. Varying the extrusion rate will further affect the velocity profiles due to the relation between the initial velocity, diameter and mass flow rate through equation eq. 6.1. In Figure 6-5 it is shown how varying the initial mass flow rate affects the relation between the take-up velocity and the initial force. Here it is demonstrated that by increasing the polymer extrusion rate from the spinneret, higher initial tensions are required to achieve the same take-up velocity.

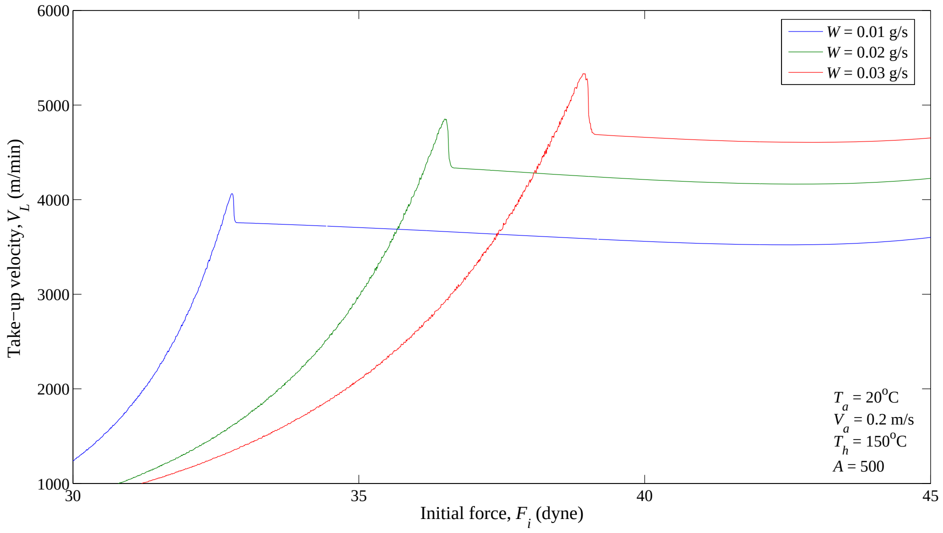

Figure 6-5: The take-up velocity versus initial force plot for a range of polymer extrusion rates (*W*).

Figure 6-5 indicates that varying the initial mass flow rate results in the system being affected to a large degree. This justifies the need for further investigation on the effects of this variable on the uniformity of the as-spun properties of the fibre. Increasing the extrusion rate has the effect of increasing the take-up velocity which in turn has a direct influence on the positioning on the multiple roots described in section 6.3. Thus, if the simulation is run with an extrusion rate of 0.02 g/s for a take-up velocity of 4000 m/min two phases could obtained. However, for an extrusion rate of 0.03 g/s two phases could be obtained at 5000 m/min and not at 4000 m/min. The distance between the peaks decreases as the extrusion rate is increased. As in the previous section, the distance between the peaks will affect the force range selected according to the extrusion rate applied to the system. The extrusion rate of 0.01g/s will not be investigated as this does not allow for high enough take-up velocities to be investigated.

6.3.4 Polymer extrusion temperature

The rate at which heat is exchanged is strongly influence by the temperature gradient between the bulk temperature of the cooling medium and the surface from which the energy is being transferred. As such, varying the extrusion temperature will alter the temperature profile of the filament which, in turn, will change the temperature gradient between the polymer and the bulk air surrounding the filament. This leads one to suggest that the effect of varying the polymer extrusion temperature (T_i) as an initial condition should be investigated. Trials runs showed that varying this parameter had a similar effect to varying the quench air temperature but to a larger degree (see Figure 6-6). Based on this it was decided to investigate the effects of varying polymer extrusion temperatures on the system. Melt extrusion temperatures range from 285-300°C for PET melt spinning processes. Thus, the two extremes of the spectrum will be investigated namely 285 and 300°C. As can be see in Figure 6-6 very different force ranges are required for the range of take-up velocities being investigated. This has complications when applying the method of selecting the initial tension in order for the desired take-up velocity to be achieved. This is discussed in more detail in chapter 7. The trend representing the system with T_0 set to 300°C seems to be tending towards a second peak. However, obtaining a fibre which is made of material in this phase is not realistic. Thus, the operating range extending from F_i equalling to 50 dyne onwards will not be considered when T_0 is set to 300°C.

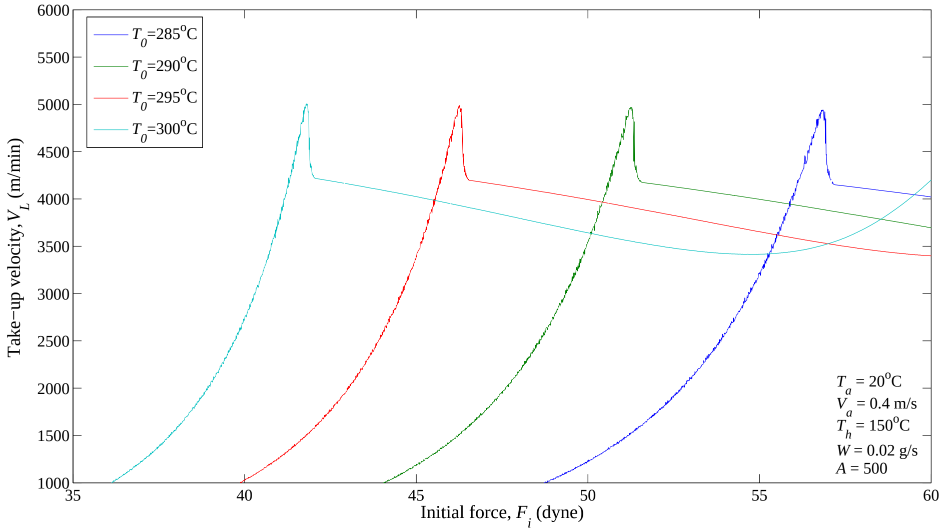

Figure 6-6: The take-up velocity versus initial force plot for a range of extrusion temperatures (T_0).

6.3.5 Take up velocities

The final velocity (V_L) under which the yarn is wound-up greatly influences the dynamics of a melt spinning system. The cooling rate, filament attenuation, online tensile force and, in turn, local molecular orientation are some of the properties affected by the take-up velocity. The selection of the take-up velocity value is influenced by other process variables such as the extrusion rate. This can be seen in Figure 6-5 where greater take-up velocities are possible at higher extrusion rates. Using an extrusion rate of 0.02 g/s allows one to operate at a maximum take-up speed of approximately 4850 m/min. The maximum velocity investigated under this extrusion rate was chosen to be 4000 m/min as this will allow for both phases to be obtained as possible solutions. In comparison, using an extrusion rate of 0.03 g/s results in the maximum attainable velocity to be approximately 5400 m/min. This would allow a take-up velocity of 5000 m/min to be investigated whilst simultaneously achieving both amorphous and crystalline phases. However, only an amorphous phase can be achieved for a take-up velocity of 4000 m/min for an extrusion rate of 0.03 g/s. The lower take-up velocities of 2000 and 3000 m/min will be investigated in all of the simulations.

6.4 Summary

It is clear from the discussion above that a range of process variables influence the dynamics of melt spinning. In work carried out by Dutta and Nadkarni (1984), the aim was to identify critical process variables which strongly affected final product properties. It was concluded that polymer extrusion temperature and rate, melt intrinsic viscosity, quench conditions and take-up velocity affect the as-spun fibre orientation to a large degree. This agrees with the process variables discussed above. Thus, it is felt that the chosen process conditions will result in a broad enough spectrum to investigate the dynamics of the system and, more importantly, the degree of variation in the final product properties. Intrinsic viscosity changes as a result of varying polymer production conditions and the associated effects on the final as-spun polymer properties are not covered in this investigation. However, it can be said that small changes in the intrinsic viscosity from 0.57-0.60 have large effects on the degree of variation on the as-spun fibre properties (Dutta and Nadkarni 1984). Table 6-1 summarises the process variables to be investigated with a polymer extrusion rate of 0.02 g/s.

Table 6-1: Table of parameters to be investigated at W = 0.02 g/s.

V_L (m/min)	2000	3000	4000
T_a (^{o}C)	15	20	25
V_a (m/s)	0.4	0.6	0.8
W (g/s)		0.02	0.03
T_0 (^{o}C)		285	300

Table 6-2 summarises the process conditions to be simulated using an extrusion rate of 0.03 g/s. The extra take-up velocity condition is possible due to the maximum attainable velocity being higher for an extrusion rate of 0.03 g/s when compared to 0.02 g/s. Table 6-2 lists the process conditions tested under an extrusion rate of 0.03 g/s.

Table 6-2: Table of parameters to be investigated at W = 0.03 g/s.

V_L (m/min)	2000	3000	4000	5000
T_a (^{o}C)	-	15	20	25
V_a (m/s)	-	0.4	0.6	0.8
W (g/s)	-	-	0.02	0.03
T_0 (^{o}C)	-	-	285	300

The above discussion highlights the sensitivity of the single filament model to applied process conditions. In the chapter it was shown that the take-up velocity controls the initial force value to be used in the set of boundary conditions. The influence of SIC effects on the characteristic diagrams were discussed. Here it was realised that the maximum take-up velocity is limited by the fluidity of the polymer strongly influenced by SIC. The selection of process conditions to be tested was carried out where it was realised which variables have the largest influence on the system dynamics. These process conditions are varied in this investigation to test whether changing quench conditions and the associated heat transfer effects are influenced to some degree. It is hoped that through this, valuable findings can be made with regards to final product property uniformity and online process conditions.

7 Numerical scheme and model verification

The first part of this section discusses the numerical difficulties encountered during the simulations and the different coding algorithms and numerical methods used to overcome these difficulties. Some of these difficulties include stiff solutions of the system, the careful selection of the initial tension leading to the desired take-up velocity in both the mono and multifilament models and possible singularity of certain terms in the constitutive equation. The characterisation of the different conditioning zones along the spinline is also discussed.

Since the monofilament model is based on earlier work (Jarecki *et al.* 2000), verifying the current model by comparing the output obtained to that of the model proposed by the above authors is necessary to determine whether the current model is adequate in predicting the online properties of a single filament. This is the topic of the second section. Verifying the multifilament model is included in this section. Here, since the proposed multifilament model is novel, profiles are compared to that of closest existing model found in literature (Dutta 1987).

7.1 Numerical difficulties and solutions

7.1.1 Run-away crystallisation rates and solution stiffness

The model is programmed in MATLAB® version R2007a. Initially, a Runge-Kutta based solver (ode45) was used to numerically solve the system. Trials runs showed non-stiff trends for lower initial tensions. However, after some critical initial stress the profiles obtained suggested some solutions were tending to exhibit characteristics of a stiff system. More specifically, the degree of crystallinity was identified as the cause of the 'stiffness' in the solution. This is caused by the sudden increase in kinetic activity at the optimum stress and temperature ranges. This led to a one step solver (ode23s) based on a modified Rosenbrock formula of order 2 being used. This method is applicable to solving some stiff systems and was found adequate for this system.

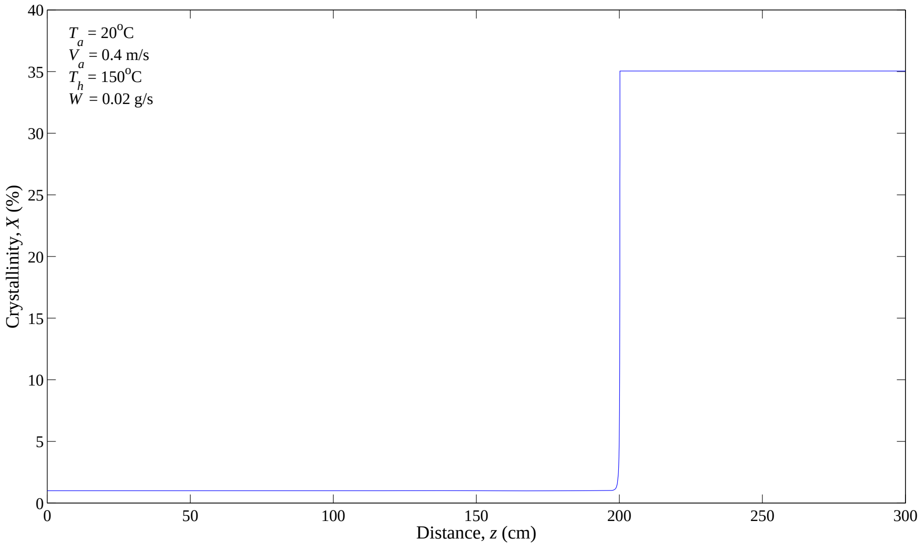

Figure 7-1: A plot illustrating the stiff solution obtained for crystallinity.

Figure 7-1 illustrates the stiff solution obtained for the degree of filament crystallisation under the appropriate conditions. This is caused by very large crystallisation rates at optimum online temperature and tensile stress values. These large crystallisation rates coupled with the stiff solution procedure cause complete solidification to take place of polymer. However, the maximum degree of crystallisation for PET is roughly 35% (Jarecki *et al.* 2000). This forced a further criterion to be added to the coding which sets the crystallisation rate to zero after the maximum crystallinity value is reached. If this criterion is not included in the coding, the solution becomes too stiff for the type of solver used with an error report indicating that integration tolerances are exceeded during the solution attempt.

7.1.2 Mathematical Singularity in some functions

Under conditions near critical crystallinity ($X^* = 0.1$), the structure of certain auxiliary functions used to construct the model results in mathematical singularities causing the simulation to terminate. This occurs specifically in eq. 7.1 where the denominator becomes a very small value as the crystallinity tends towards the critical value resulting in the overall crystallinity viscosity contribution tending toward infinity. Without the singularity occurring the velocity gradient would ultimately tend to zero as the filament is expected to have a rod-like behaviour once the critical crystallinity has been achieved.

$$\eta_X(X) = \frac{1}{\left(1 - \frac{X}{X^*}\right)^{\alpha}} = \frac{1}{D} \qquad \text{eq. 7.1}$$

$$\text{As } X \to X^*,\ D \to 0 \text{ and } \therefore \frac{1}{D} \to \infty \qquad \text{eq. 7.2}$$

To avoid this singularity a criteria is introduced to the coding where the velocity gradient is forced to zero once the crystallinity has reached the critical value. As a result the filament acts as a solid rod after the critical crystallinity with no attenuation of the spinline occurring. Other changes include inverting the crystallinity and temperature dependant terms such that one multiplies by the fluidity of the polymer in the constitutive equation rather than dividing by the viscosity. This further reduces the potential of any singularities occurring. Thus eq. 4.35 becomes:

$$\therefore \frac{dV}{dz} = \frac{1}{3} \cdot \frac{\left(1 - \frac{X}{X^*}\right)^{\alpha}}{\eta_{IV} \cdot \exp\left(\frac{E_a}{k \cdot T}\right)} \cdot \frac{\rho \cdot F(z) \cdot V(z)}{\dot{W}} \qquad \text{eq. 7.3}$$

7.1.3 Initial force selection

As described in chapter 6 the selection of an initial force leading to the desired take-up velocity is crucial if the correct output from the single filament model is to be acquired. The selection of the initial force is simple with respect to the monofilament model. Here, a straightforward plot of the initial force versus take-up velocity, which is obtained from the single filament model (using the initial force as a boundary condition), allows one to determine the initial force required for the desired take-up velocity. This method assumes the quench conditions applied remain constant along the quench zone. Figure 7-2 shows the relation between the initial force and the final velocity obtained from the monofilament model.

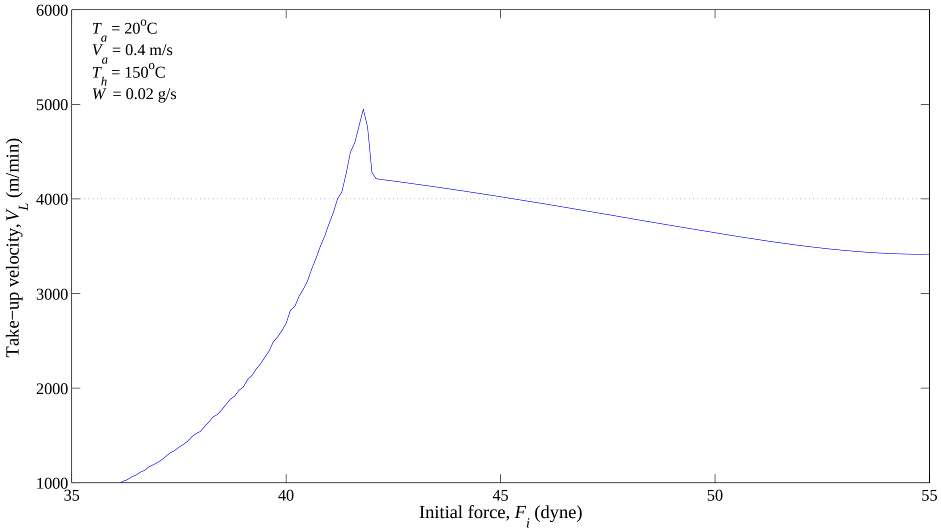

Figure 7-2: A plot illustrating the relation between initial tension and the take-up velocity for the monofilament model.

With respect to the multifilament model, the selection process is somewhat complicated due to the change in quench conditions from one filament to the next. Figure 7-3 illustrates the varying characteristic diagram for each filament according to the quench condition experienced. If the same initial force were applied to each filament across the bundle as an initial condition, varying take-up velocities would be achieved across the filament bundle. This would not simulate a real industrial process. To overcome this difficulty, the relation between the initial force and take-up velocity is determined for each filament as the quench air temperature changes axially along the spinline. This allows the correct initial force to be chosen for the desired take-up velocity to be achieved. As a result, the final velocity of the filaments is uniform throughout the bundle. The exact algorithmic approach to solve this problem is discussed in sections 7.2.2 and 7.2.3 for each of the approaches taken.

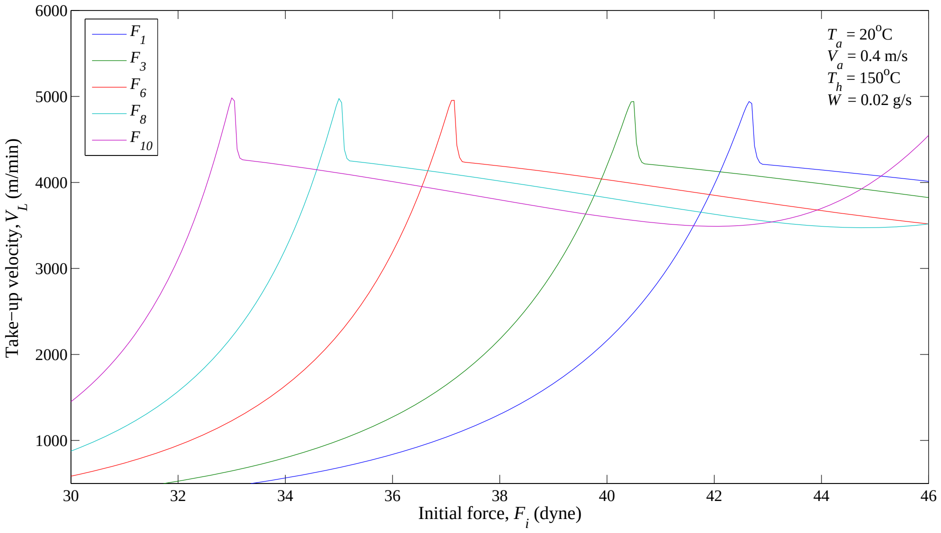

Figure 7-3: A plot illustrating the relation between initial tension and the take-up velocity for multifilament model (F_1 = filament 1 etc.).

7.2 Simulation Algorithms

An Algorithm is a set of step by step instructions following a logical thought process which should finally solve the problem at hand and produce an answer. Important considerations to take into account when constructing an algorithm are computational speed, space and overall code structure. Computation time and the amount of memory required by the solution procedure are the most important factors as these generally lead to expensive hardware being needed. One should design an algorithm which results in a solution procedure which is fast, consumes the least amount of random access memory (RAM) possible and is the easiest and shortest to describe. This section briefly summarises the algorithmic logic behind each solution procedure for each of the models constructed.

7.2.1 Monofilament model

Figure 7-4 shows the basic algorithm constructed to solve the system. Other than the selection of the initial force leading to the desired take-up velocity being achieved, step 4 in the algorithm is the most important step. This is because many calculations are carried out during this step which includes referring to a number of sub-files containing the auxiliary correlations as well as the system of ODE’s. Firstly, the sub-file containing the fundamental ode’s and material balance is called up followed by any auxiliary equations required by the ode’s such (i.e. heat capacity, polymer density

, heat transfer and skin friction coefficient). These auxiliary correlations are defined as sub-files separately in the coding. The selection of the quench air temperature according to the distance from the spinneret is carried out within a separate sub-file which defines the quench air temperature according to the distance from the spinneret. Finally, once all the parameters described by each of the ode's are solved for, the polymer diameter is calculated simultaneously according to the continuity equation. The code can be viewed in Appendix C.1.

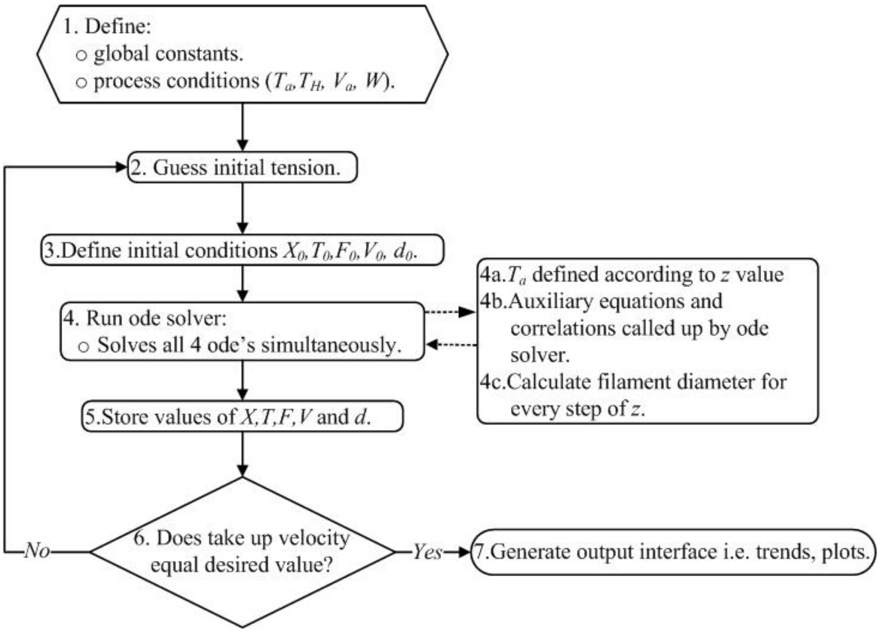

Figure 7-4: The coding algorithm used to simulate the single filament system.

It is realised that this method is unstable when high gradients (towards second peak) are achieved for the characteristic diagrams at high initial forces. However, as stated above, these forces are not included in the operating ranges tested in this investigation. This is because it is highly unlikely to obtain a fibre produced under these conditions. The computation time is relatively fast (1.37s) for the single filament model under low initial tensions. This is due to the lack of stiffness in the system resulting in a greater step size taken by the solver. The computation time taken for tensions resulting in online crystallisation occurring is slightly longer (1.63s) due to the generation of a stiff solution because of the sudden high crystallisation rates resulting in large gradients in the crystallinity profile (Figure 7-1). This may not have any significant effect on the system now but this small time difference has a large influence on the simulation time for the multifilament model. This will be discussed separately in section 7.2.1.

7.2.2 Multifilament model - Conventional approach

The first approach is similar to that of Dutta (1987) and as such, will be termed the ‘conventional approach’. A very important factor to take into account is the change in quench air temperature for a specific cell from one filament to the next. The exiting quench air temperature calculated from a specific cell is taken as the entering quench air temperature for the following cell in the next filament row. Changing quench air temperatures in the filament axial direction affect the initial force versus take-up velocity relationship and thus, influences the selection of the initial force required for a desired take-up velocity.

Figure 7-5 illustrates the coding algorithm constructed to solve the system. Defining global constants and the system dimensions is the first step in the algorithm. In this simulation the spinning length is set to three meters with the first meter after the spinneret being the quench zone. The filament bundle is divided into three hundred cells which run axially for each filament. This results in each cell having an axial length of 1cm. Defining an entering quench air temperature for each cell along the spinline for the first filament is a starting point to the simulation. An initial force range is defined for each filament within which it is known that the initial force value for the required take-up velocity will exist. These ranges are determined from trial runs. Each initial force element is applied as an initial condition to the first cell of the first filament. Using the monofilament model, the final characteristics for that DVE are calculated and used as the initial conditions for the next cell in the axial direction. This process is repeated until the final cell properties are calculated at a distance of 300 cm from the spinneret. The final velocity is stored in a vector under the same element number as the initial force applied to the first cell of that filament. This is done so that once the desired take-up velocity is achieved the element can be defined and used to extract the initial force value from the force range defined initially. This initial force is applied to the monofilament model for the first cell once again except this time the exiting quench air conditions are calculated for each cell. This is done for each cell by firstly calculating all the filament characteristics after which energy balance across is used to calculate the exit quench air temperature.

The Quench air temperatures exiting each of the cells are used to calculate the initial force versus take-up velocity relation for the following filament. The process is then repeated until the final filament's properties along with the exit quench conditions are calculated. This solution procedure takes into account the changes in the quench air temperature across the filament bundle (quench direction) and the effects this phenomenon has on the filaments properties. Statistical calculations are then carried out on the filament properties as they vary across the filament bundle. The final grid layout consists of entire filament length in the *z*-direction of all ten filaments in the *r*-direction. An output interface is then generated in a user friendly way for easy interpretation of the overall results.

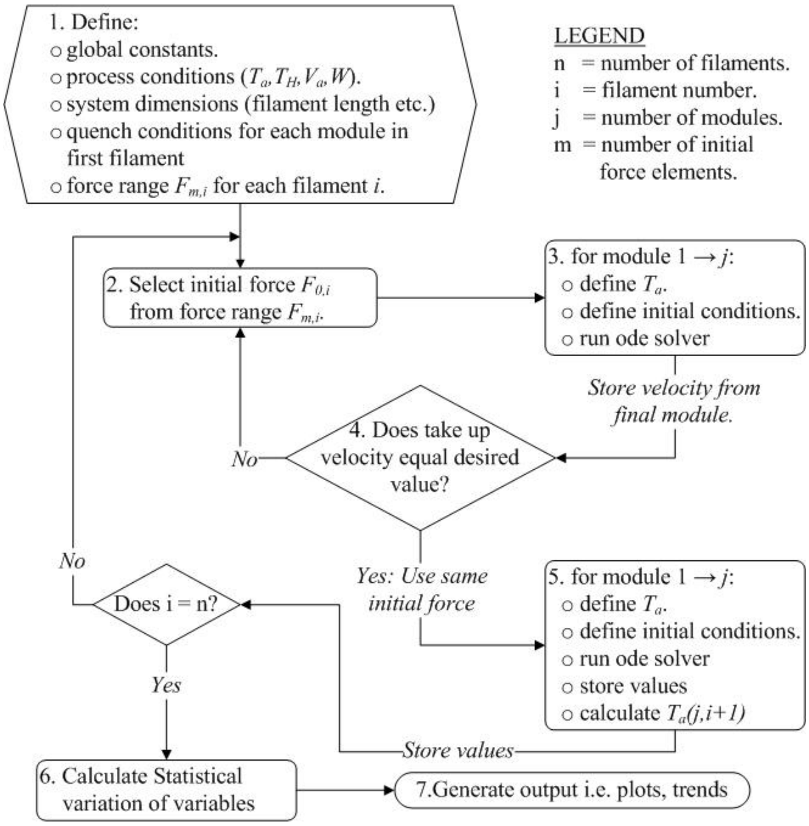

Figure 7-5: The coding algorithm used to simulate the multifilament conventional model.

Areas of the coding that require long periods of time to complete are steps 3 to 5. More specifically, under initial forces which result in crystallisation and a stiff solution, steps 3 and 5 result in the simulation time being in the order of hours. This is due to the ode solver having to reduce the step size for stiff solutions and the thousands of times that the ode solving process is repeated for each cell in every filament. The total simulation time for this approach is approximately 12 hours.

7.2.3 Multifilament model - Cell iteration approach

As described in the construction of the multifilament model, Newton's law of cooling is used to describe the amount of heat transferred from each filament section to the surrounding volume of quench air. This requires that the bulk temperature of the volume of air surrounding each cell is known. In the conventional approach described in the previous section, the bulk air temperature of cell is taken as that of the air which enters the cell in the quench direction. The exit quench air temperature is calculated once from this value and accepted as the final. Intuitively, is expected that as the quench air passes the filament surface it is heated resulting in the quench air temperature increasing as it passes through each cell. This suggests that the bulk air temperature is actually higher than the entering quench air temperature. As such, an iteration approach in calculating the change in quench air temperature across the bundle is proposed here and from this point onward will be referred to as the 'iteration model'. This approach assumes that bulk quench air temperature of each cell is the average of the entering and exiting quench air temperature to that cell. The exit quench air temperature is obtained through an iteration procedure where by the new exit quench air temperature converges to within 0.1% of the preceding value. This leads to a more realistic solution.

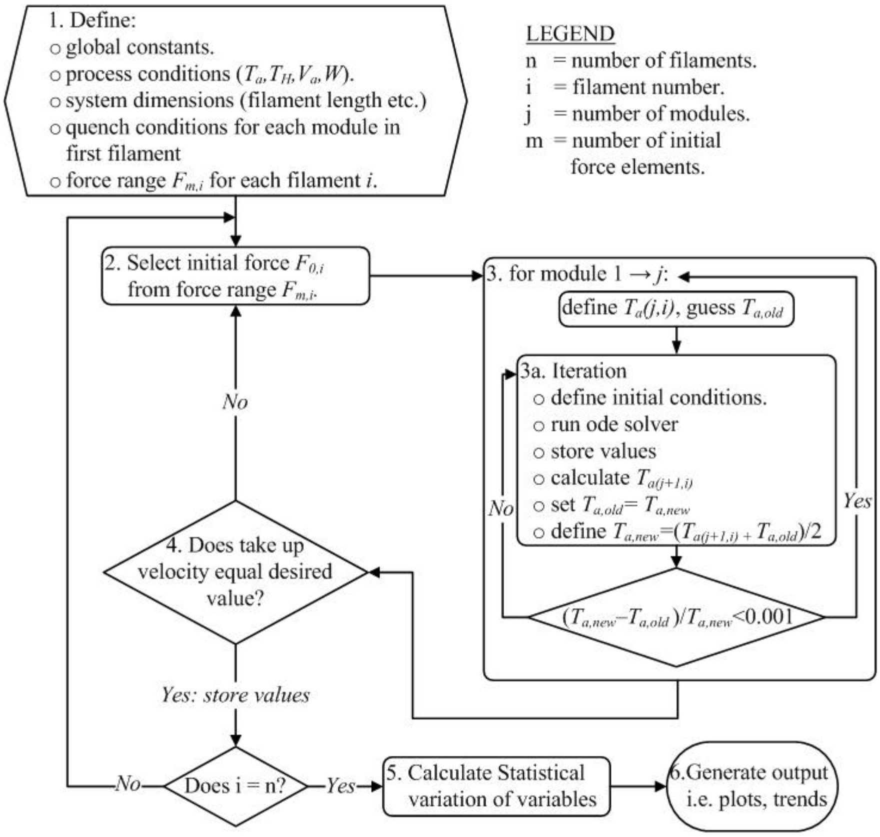

Figure 7-6: The coding algorithm used to simulate the multifilament iteration model.

The algorithm structure is similar to that of the conventional approach except step 3 entails the iteration process and secondly, step 5 of the previous approach is neglected. The exclusion of step 5 is achieved by storing all the filament properties as they are calculated for each initial force and quench air temperature. This results in the overall coding structure being more efficient and, secondly, compensates for the increase in simulation time as a result of the iteration process in step 3 requiring more computation time. However, the approach requires the use of more RAM due to the entire set of filament properties calculated being stored according to each initial force and set of quench conditions applied. The algorithm used for the iteration code is illustrated in Figure 7-6.

The iteration procedure entails the following: two constant are created namely $T_{a,new}$ and $T_{a,old}$. The first value of $T_{a,new}$ is defined from the predefined matrix set up in step 1 and that of $T_{a,old}$ is guessed as double that of $T_{a,new}$ as a first approximation. Using $T_{a,new}$ in the energy balance across the cell the first estimate of the exit temperature is calculated. The value $T_{a,old}$ is then redefined as that of $T_{a,new}$. The value of $T_{a,new}$ is defined as the average of the newly calculated exit temperature and $T_{a,old}$. The iteration criteria is set as the difference between $T_{a,new}$ and $T_{a,old}$ defined as a percentage of $T_{a,old}$. The tolerance is set to 0.001. If the criterion is not met the procedure is repeated using a loop which can only be exited once the criterion is met. This is done for each cell along the spinline. The final converged value calculated for the exit quench air temperature is used as the entering temperature value for same cell in the following filament.

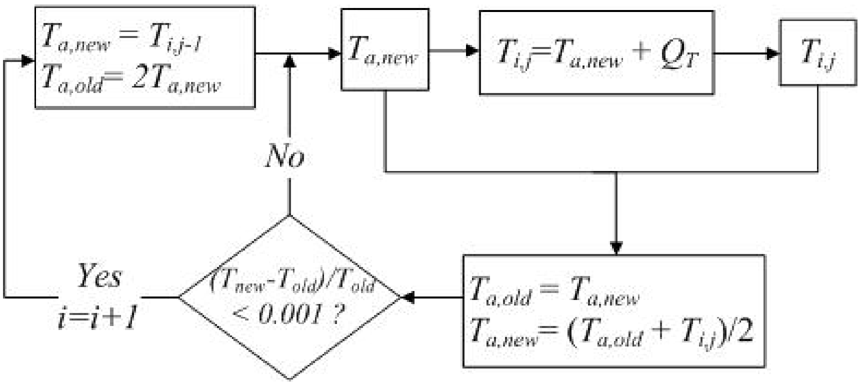

Figure 7-7: A simple block diagram showing the multifilament iteration step process.

The simulation time for this approach is approximately 15 hrs. The extended simulation time when comparing to the conventional approach is directly a consequence of the number of iterations having to be carried out for each cell.

7.2.4 Conventional versus iteration approach

As discussed above, the multifilament model estimates the amount of heat transferred using Newton's law of cooling which requires that the bulk air temperature of each cell is known. In the conventional approach this value is assumed to be the entering quench air temperature to each cell. In the iteration model, the bulk air temperature of the cell is taken to be the average of the entering and exiting quench air temperatures. The new bulk air temperature is applied to the energy balance to obtain the new exit quench air temperature which is repeated until convergence is met. The output from these two approaches are significantly different with regards to the amount of heat transfer estimated between the filaments and quench air as well the difference in degree of property variation across the fibre bundle as a result.

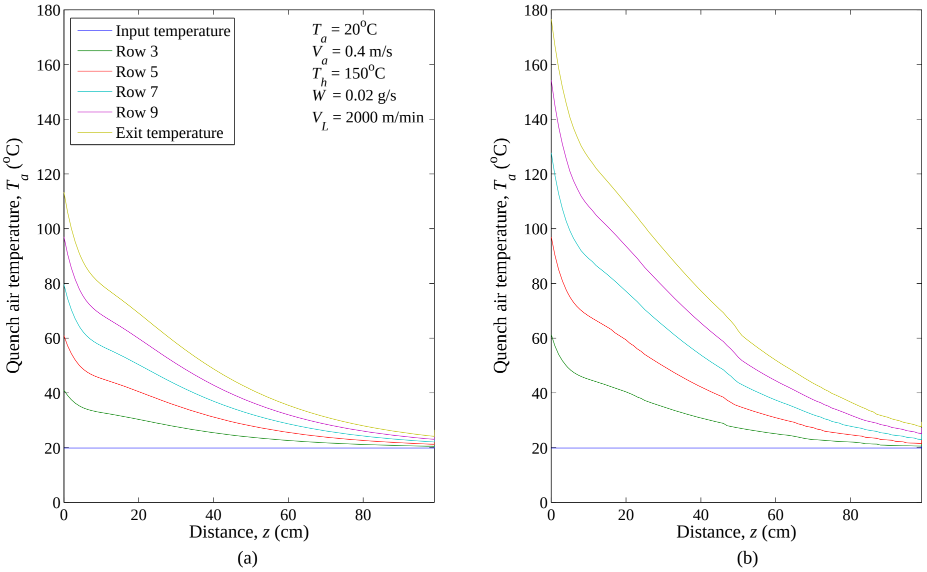

(a) (b)

Figure 7-8: A diagram indicating the different output obtained for the quench air temperature (T_a, ^{o}C) using (a) the conventional, and (c) the iteration multifilament models.

Figure 7-8 illustrates the difference in the amount of heat transfer obtained between the conventional and iteration approaches. Clearly, the iteration approach estimates a greater degree of heat transfer between the filaments and quench air temperature. This is directly attributed to the definition of the bulk air temperature term in the iteration approach. Here, this term is greater in magnitude when compared to the conventional approach leading to the quench air in the iteration approach having a greater temperature for the same point in the filament bundle when compared to the conventional approach. The iteration approach coincides to a greater extent with data published in literature (Ziabicki 1976). Figure 7-9 shows the difference in inter-filament temperature variation estimated by the conventional and iteration approaches. Here, it is clear that a greater variation in inter-filament properties is predicted by the iteration model. This is the case for all process conditions tested. As such, the degree of property variation estimated by the iteration model is greater in all of the applied process conditions when compared to the conventional approach (see appendices A and B).

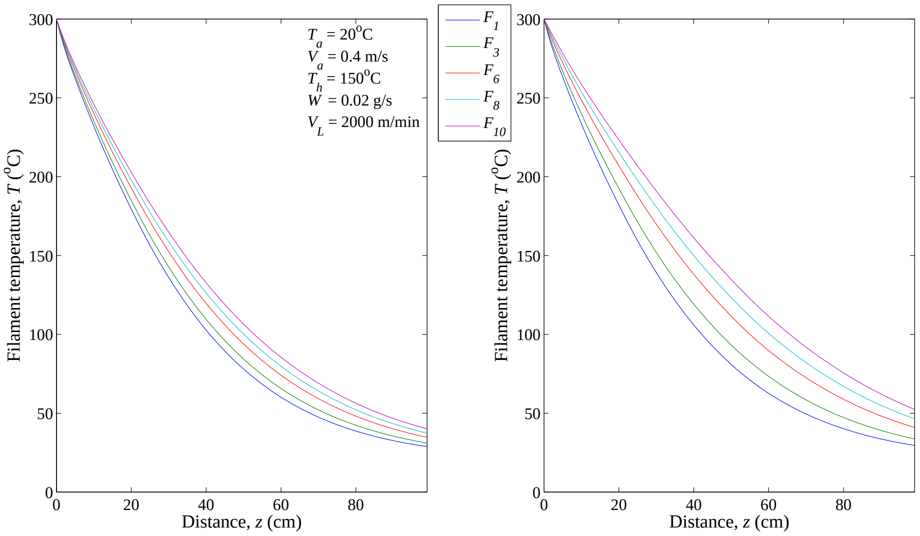

(a) (b)

Figure 7-9: A diagram indicating the different output obtained for the inter-filament temperature (*T*, °C) using (a) the conventional, and (c) the iteration multifilament models.

From the discussion above, it is clear that the iteration approach simulates a real industrial process more accurately when compared to the conventional approach. As such, when considering the output obtained from the two different approaches for discussion, only the iteration model output will be evaluated and conclusions drawn based on the findings.

7.3 Model verification

This chapter discusses the method used to verify if both the mono and multifilament models are predicting system behaviour correctly. The monofilament model is verified simply by simulating a system already described in literature (Jarecki *et al.*, 2000) and comparing the results obtained. On the other hand, since the multifilament model proposed in this thesis is novel, verification is by comparing against the closest model existing in the literature, namely that proposed by Dutta (1987).

In the work of the Jarecki *et al.* (2002) property profiles, such as filament temperature and velocity versus axial distance are shown. These trends will be compared with that generated using the same conditions in the simulator used in this thesis.

7.3.1 Monofilament model

The monofilament model verified in this discussion is that which is described in chapter 4 in this thesis. The monofilament model is based on that constructed by Jarecki and co-workers (2000) which is designed around a melt spinning rig containing a heating zone (see Figure 4-1). As such, the conditions under which the current simulation will be tested are those which shown in the work of Jarecki and co-workers (2000). These are described in Table 7-1.

Table 7-1: The process conditions simulated.

T_0 (°C)	300
d_0 (um)	300
V_L (m/min)	3850
T_h (°C)	150
V_a (cm/s)	40
T_a(°C)	20
W (g/s)	0.02

The temperature profile is shown in the work of Jarecki *et al.* (2000) is compared with results of the simulator used in this thesis and the results are shown in Figure 7-10. It is clear that the current model fits the data generated by the previous work carried out with a R^2 value of 0.99. Subtle differences in the trends exist directly after the spinneret. This is due to the larger difference in the velocity profiles, discussed in the proceeding paragraph resulting in different cooling rates.

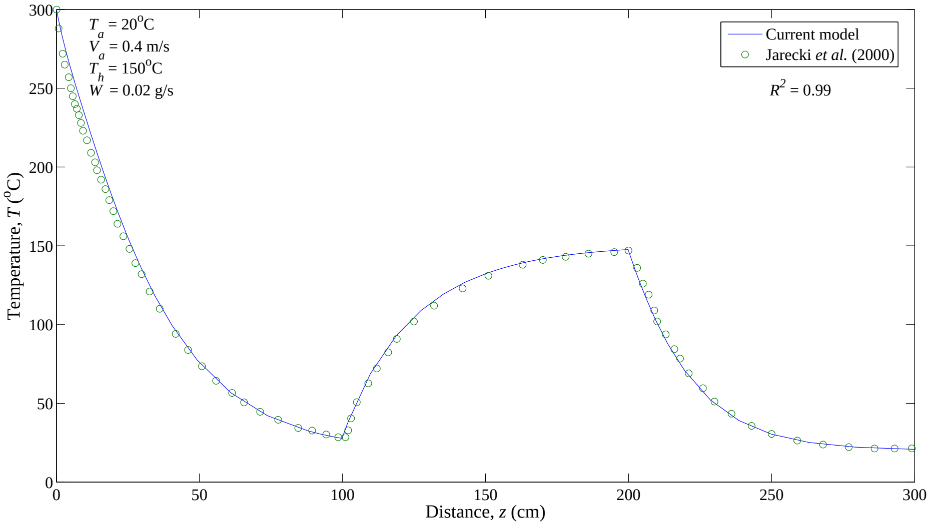

Figure 7-10: A plot illustrating the filament temperature (*T*, °C) versus distance (*z*, cm) relationship from both the work of Jarecki *et al.* (2000) and the current monofilament model.

Figure 7-11 illustrates the velocity profiles for each simulation. Clearly, the simulation fits the data generated from the previous work carried out to a sufficient degree of accuracy (R^2 = 0.99). The small differences that exist between the profiles at the first plateau are attributed to the various coding conditions added to the current model to aid in simulation convergence. The exact differences cannot be determined as the numerical techniques used in the previous work are not stated explicitly. However, it can be said that because the velocity is affected by the polymer viscosity which is, in turn, critically dependent on the degree of crystallinity, very small differences in crystallinity are propagated due to the structure of eq. 7.1. Such is the sensitivity that even small rounding off errors could be the cause of the subtle difference in the trends.

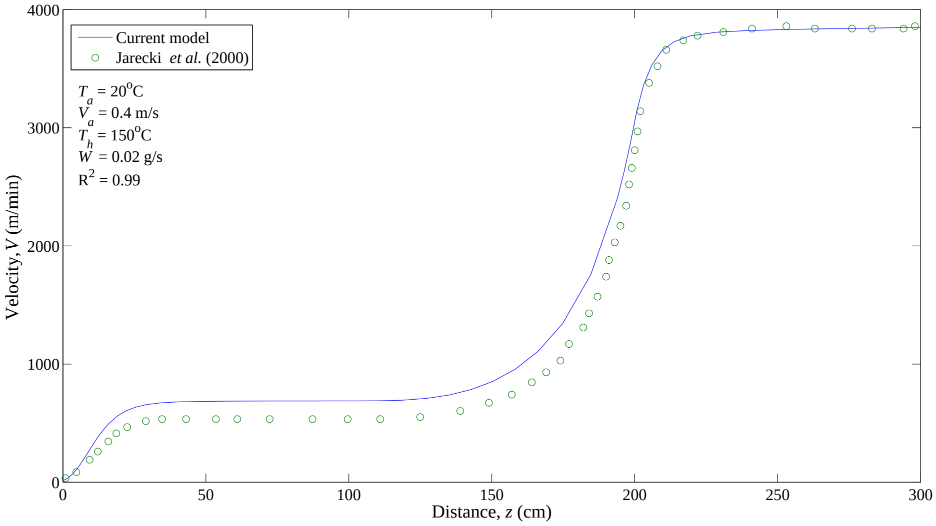

Figure 7-11: A plot illustrating the filament velocity (*V*, m/min) versus distance (*z*, cm) relationship from both the work of Jarecki *et al.* (2000) and the current monofilament model.

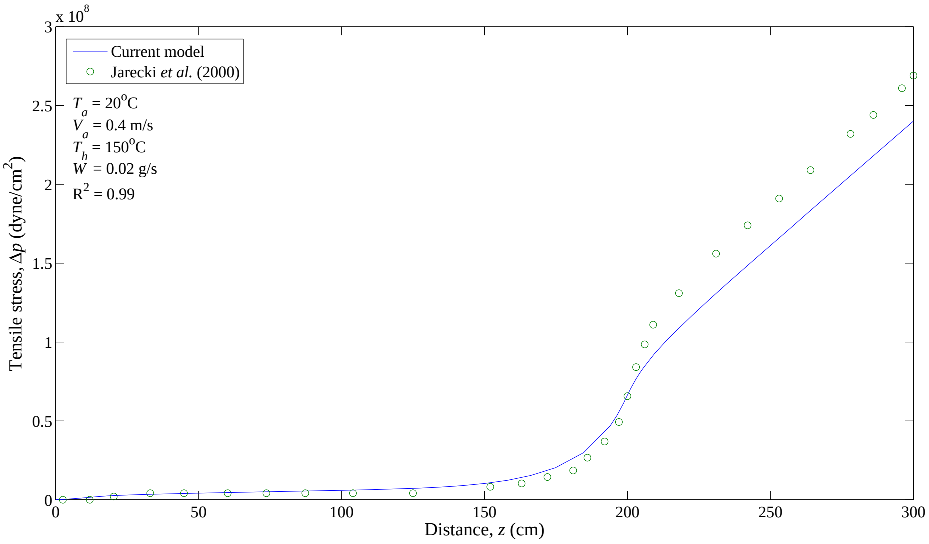

Figure 7-12: A plot illustrating the filament tensile stress (Δ*p*, m/min) versus distance (*z*, cm) relationship from both the work of Jarecki *et al.* (2000) and the current monofilament model.

Figure 7-12 compares the tensile stress profiles of the current model to that of Jarecki *et al.* (2002). Here, it is seen that differences in the profiles exist in the region further down the spinline. This is attributed to the small difference in the velocity gradient between 150 and 200 cm resulting in varying degrees of tensile stress. However, the data fits with a coefficient of determination (R^2) value of 0.99 which indicates that the output obtained from the current model can be considered accurate enough for the purposes of this study. As such, the current model is considered verified.

7.3.2 Multifilament model

Verifying the multifilament model is more complex than simply comparing trends as it seems from literature that no multifilament model based on the work of Jarecki *et al.* (2002) has ever been attempted. Multifilament model results shown in literature all have different input parameters and are constructed using assumptions differing to those applied in the current approach. However, since some attempts at modelling a multifilament system have been made, some information and results do exist allowing basic comparisons between the results shown in literature and that produced by the current model to be made. These basic comparisons consist of comparing quench air temperature profiles and filament to filament variation in polymer temperature.

With respect to quench air temperature profiles, one expects the temperature to increase due to the exchange of heat from the polymer to the gas phase. This trend is observed in all of the work aimed at multifilament modelling found in literature (Dutta 1987, Harvey and Doufas 2007) as well as in the multifilament model used in the current thesis. Figure 7-8 (b) illustrates the trends obtained for estimated quench air temperatures across the filament bundle using the iteration approach. Ziabicki (1976) shows experimental work illustrating that the quench air temperature can increase as much as 180^{o}C between the windward and leeward side of the filament bundle. This magnitude is similar to the one predicted by the iteration model.

To verify that the current model correctly describes the heat transfer phenomena between the quench air temperature and polymer, a plot of the filament temperature versus distance for various row numbers should show an increase in polymer temperature since the quench temperature increases. As the quench air temperature rises, the driving force for heat transfer is reduced, resulting in a decrease in the filament temperature gradient as illustrated in Figure 7-9 (b). This is indeed observed in the present simulation. When compared to literature this trend is the norm.

Figure 7-13 illustrates the velocity profiles of the individual filaments obtained under the applied process conditions shown. In industrial spinning processes all of the filaments in the fibre bundle are wound up on the same godet roll and, as a result, reach the same final take-up velocity. As such, another method to verify the multifilament model is to determine if all of the filaments reach the same take-up velocity for the initial force applied.

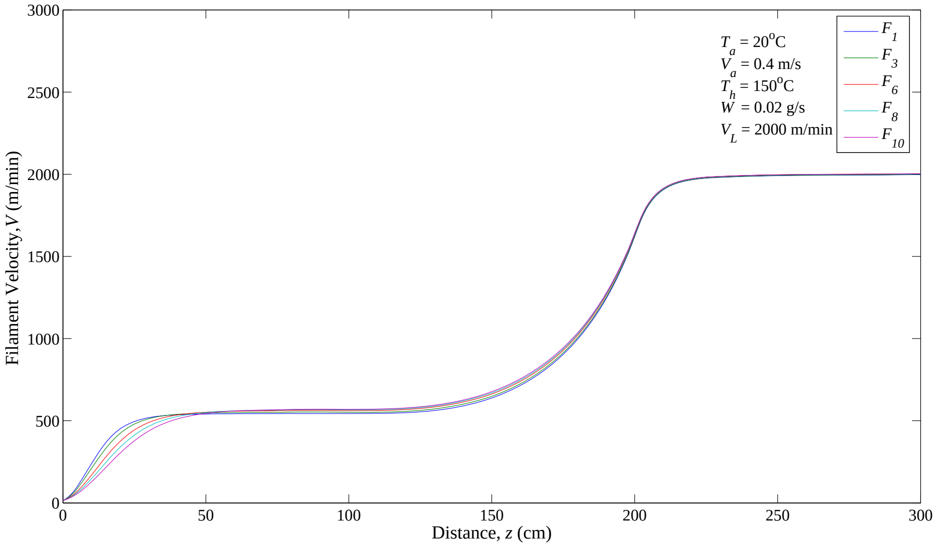

Figure 7-13: Filament velocity profiles varying in spatial position from windward side using the iteration model.

A uniform final velocity profile, shown Figure 7-13, indicates that the model estimates the velocity profiles correctly. From the trends presented here it is clear that the multifilament model estimates the dynamics of a real filament bundle system to a sufficient degree for a quantitative analysis to be carried out.

Part C: Simulation results and discussion

8 Results and discussion

It is well known that varying quench conditions influence the degree of property uniformity of the as-spun product (Dutta 1987). This chapter aims at identifying which process conditions significantly impact the behaviour of the quench stream and, in turn, determine the to which the physical factors such as heat transfer effects influence the degree of non-uniformity of as-spun product properties. If these factors can indeed be realised, recommendations for improving the melt spinning process can be proposed.

8.1 Statistical techniques and method of analysis

Whereas previous work described development of the multifilament model, the present work describes the use of the model to investigate inter-filament property sensitivity to process conditions with the ultimate goal of process optimisation. As discussed in chapter 6, five process parameters will be investigated. In order to thoroughly investigate the effect of process conditions on the variation on the as-spun fibre properties a range of process conditions and the respective operating values are tested. These include the quench air speed and temperature, polymer extrusion rate and temperature and the fibre take-up speed. Consequently, a large number of simulations were required (one hundred and seventeen) resulting in a large quantity of data being generated. The output from each simulation included temperature (T, K), crystallinity (X, %), force (F, dyne), velocity (V, m/min) and diameter (d, um) profiles of each filament within the bundle as a function of spinline distance (z, m). The orientation factor (f_a) was calculated from the tensile stress (Δp, dyne/cm^2). Due to the large amount of output data, a method is required which summarises each simulation in terms of a single quantitative value. This will allow for easy comparison between the various simulations. Property variation across the filament bundle, as a result of spatial changes in the quench conditions, is the primary focus of this investigation. As such, three statistical coefficients of variation will be calculated to aid in the overall data analysis. These three definitions allow the number of dimensions to be reduced when attempting to understand the effects that a given process condition will have on a specific as-spun yarn property.

The first of the three coefficients to be used is the average variation across the bundle. Although, final property variation significantly influences the strength of the as-spun yarn and, as such, forms a significant part of the results analysis, the variance along the spinline is important, since it indicates where sources of reduced property uniformity across the bundle originate. This is represented by the average variance and defined by eq. 8.1.

$$AV_p = \frac{1}{z} \cdot \int_o^z f(z)dz \qquad \text{eq. 8.1}$$

Where, p is characteristic property and z the spinline distance (cm).

Here, $f(z)$ is the function which describes the coefficient of variation (CV) along the spinline. The coefficient of variation of a property at a specific point along the spinline is defined as follows:

$$CV_j = 100 \cdot \frac{S_j^X}{\overline{X}_j} \qquad \text{eq. 8.2}$$

here, S_j^X is the standard deviation and $\overline{X}_j$ the mean at the specific point.

The second coefficient to aid in the data analysis is the freeze point variation. The freeze point is defined as the point along the spinline where the polymer temperature drops below the glass transition temperature. It is thought that this is where properties are ‘frozen’ into place when the polymer solidifies (Dutta 1987). As such, an important investigative parameter would be the coefficient of variation of the properties at the ‘freezeline’ point which affect the final product quality i.e. molecular orientation. This is defined by eq. 8.2 at the freeze point. It will be seen that this method has some drawbacks as certain properties do still vary, even after the polymer temperature has dropped below the glass transition temperature. The last technique used in the data analysis is the final property variation at the take-up point. Significant variables which affect structural properties of the as-spun yarn include final orientation, crystallinity and tensile force. Final variation of the listed properties is a decisive factor in determining final product quality. Final variation will be defined as the CV value at the take-up point and is calculated using eq. 8.2.

In summary, the results analysis technique used here involves determining the average variation (AV), final property variation (FPV) and freeze-line variation (FLV) and then scrutinising individual simulations that exhibit the greatest variance. Indirect effects of quench conditions on these three properties, through the manipulation of the temperature and force profiles, will be key aspects in determining the influence of the process parameters on the final yarn quality.

8.2 Quench air temperature and velocity

8.2.1 Effects of varying quench temperature and velocity

The effects of non-uniform quench conditions on the system dynamics are analysed by plotting the average filament property trends for fibres under varying process conditions. This would display general trends allowing key observations to be highlighted and discussed. The average coefficient of variation (AV) is shown in the legend bar to illustrate the magnitude of variance for the specific property across the entire spinline.

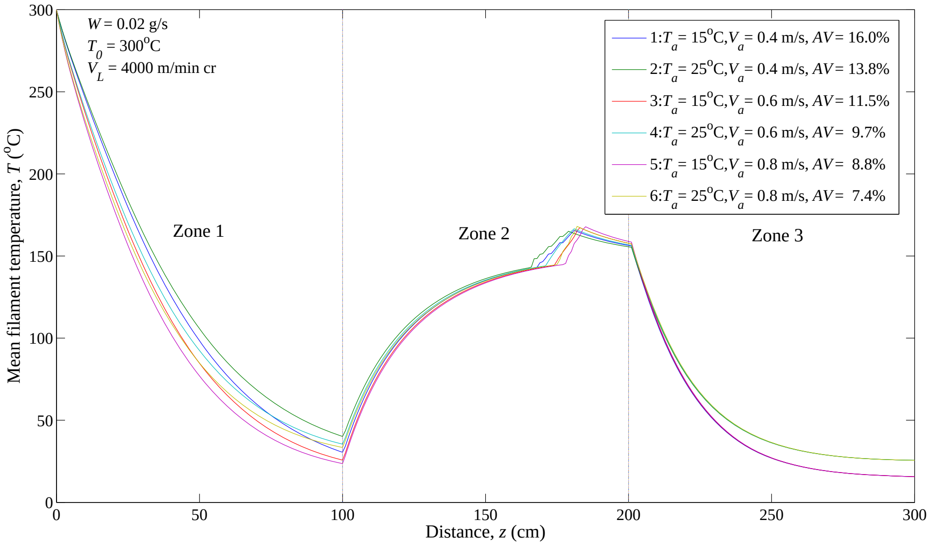

Figure 8-1: A plot of the average fibre temperature (T, °C) for different quench conditions.

Figure 8-1 shows average temperature profiles for fibres under varying quench conditions. Here, the average of the polymer temperature is calculated across the entire filament bundle and displayed as the average fibre temperature. Obviously, greater cooling rates are experienced for lower quench temperatures and higher quench velocities. This is evident from curve 5 which, due to the quench conditions applied, cools down the fastest in the zone 1 (0-100cm). The inverse occurs in curve 2 which experiences the slowest cooling rate at high quench temperatures and low quench velocities. As such, quench velocity significantly affects the rate of heat transfer. The greatest average variation (AV) for the intra-filament temperatures is obtained from the quench conditions experienced by curve 1, T_a = 15°C and V_a = 0.4 m/s. This is shown in more detail in Figure 8-2 where online CV values are plotted for quench zone 1. The CV values are only plotted for zone 1 as this is the region of maximum filament temperature variation. In zones 2 and 3 no quench stream exists.

As a result, filament temperatures within the bundle ultimately converge to the same value after zone 1.

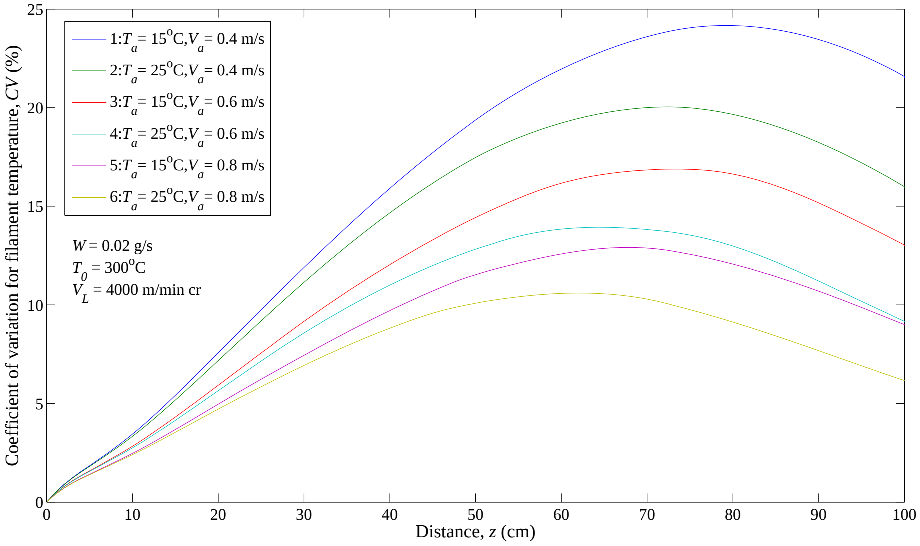

Figure 8-2: A plot of the coefficient of variation (*CV*, %) for inter-filament temperature under varying quench conditions.

In Figure 8-2 it is clear that more inter filament temperature variation occurs at low quench velocities irrespective of the quench temperature. This is to be expected as lower quench velocities result in a higher contact time between the quench air and the filament section. The greater variance obtained in trend 1 indicates that a large temperature difference between first and final filament exists under the applied quench conditions. This most likely due to less heat being transferred from the filaments to the quench air on the leeward compared to the windward side of the bundle. This would cause the filaments situated towards the leeward side of the bundle to be cooled to a lesser degree than the windward situated filaments. This result is expected since filaments situated on the leeward side of the bundle are in contact with quench air that has been heated from preceding filaments. This results in the windward filaments being cooled to a lower temperature that the leeward positioned filaments which is the origin for the large variation. An increase in the quench air speed results in a higher rate of heat transfer and less inter-filament temperature variation. This is because the quench air has less contact time for heat transfer to take place resulting in temperature difference between the air and the filaments being more uniform. Figure 8-2 reveals that the difference in *CV* values for average filament temperature at the same quench speed but different quench temperature increases with axial distance. It will be seen that this has a significant effect on the variation of final fibre properties obtained.

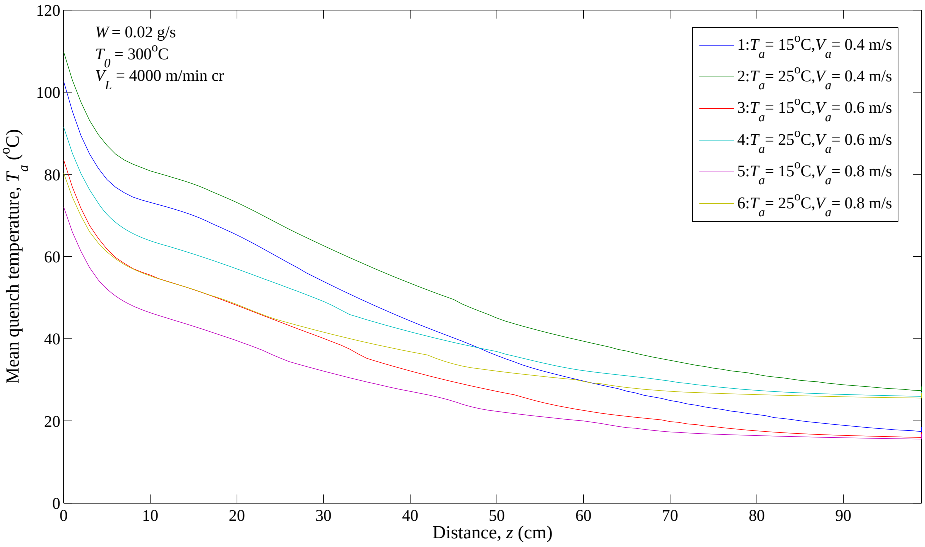

Figure 8-3: A plot of the mean quench air temperature (T_a, °C) across the filament bundle.

Another observation is that the *CV* values for fibres spun under the same quench velocity but varying quench temperatures decrease as the quench velocity is increased. This suggests that at high quench velocities a change in the quench temperature affects the variation of inter-filament temperature to lesser degree than at lower quench air velocities. This is plausible since the quench air velocity dictates the contact time for heat transfer to take place. When the trends for Figure 8-1 and Figure 8-2 are compared, it is clear that, at constant quench air velocity but varying quench temperature, larger cooling rates coincide with a greater variation in filament temperature being achieved. This suggests that, at lower quench air speeds, as the quench air passes the filaments, more heat is transferred resulting in a greater increase in temperature of the quench air. This is plausible since the volume of air travelling across the filament has more time to gain heat from the polymer section in contact. This results in less heat transfer for the following filament and so forth due to the smaller temperature gradient. A plot of the mean quench air temperature applied to each of the fibres illustrated in Figure 8-2 confirms this statement and is further supported by Figure 8-3. Here, it can be noted that for the same initial quench air temperature, a greater increase in the overall quench air temperature is obtained for lower quench air speeds. This confirms that more heat is transferred at lower quench air speeds.

Figure 8-1 reveals a sharp rise in temperature at a distance of approximately 165 cm. This is due to exothermic heat given off during online crystallisation. A plot of the mean filament crystallisation as function of spinline distance is shown in Figure 8-4. Here, it can be seen that even though the axial position at which crystallisation occurs may vary somewhat, the same maximum crystallisation (35% for PET) is always achieved. The overall trend is an increase in the onset distance as both quench temperature and velocity are increased. Once again, it is noted that quench velocity has a larger influence on the onset point than does quench temperature. Trends 1 and 2 correspond to quench conditions which result in the slowest filament cooling rate and largest *CV* values for filament temperature as determined from Figure 8-1 and Figure 8-2 respectively. This indicates that fibres spun under these quench conditions remain in the kinetically active zone for a longer period of time since the filaments are cooled at a slower rate. Secondly, a large variation in the inter-filament temperature results in correspondingly larger *CV* values for crystallinity.

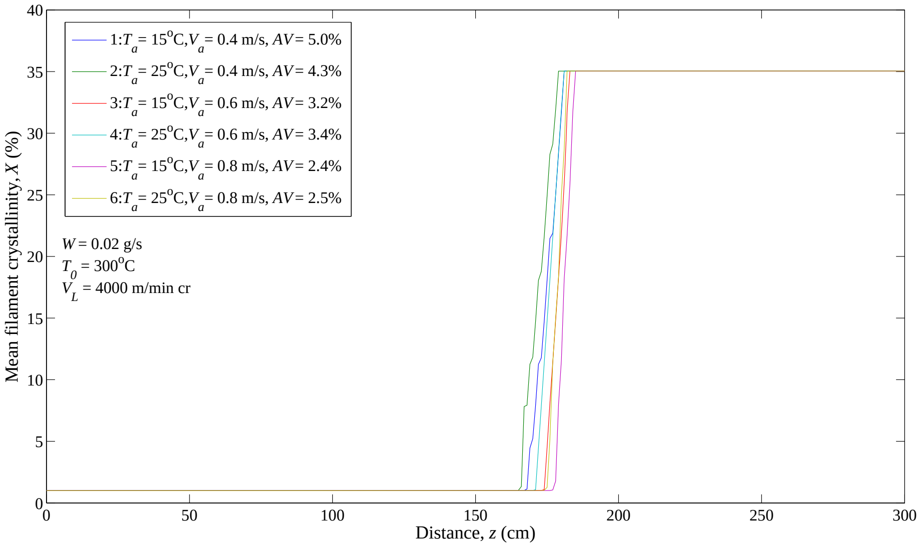

Figure 8-4: A plot of the mean filament crystallinity (*X*, %) across the filament bundle.

The onset of crystallisation is sudden and occurs only in zone 2, the heating zone. In this zone the filaments are reheated to a temperature of 150°C at much higher tensile stresses than at the same temperature in zone 1. At this point some critical stress value is reached which brings about the sudden onset of crystallinity. The mean tensile stress and orientation profiles achieved under the applied process conditions are shown in Figure 8-5.

Figure 8-5 clearly indicates the effects of quench conditions on the average tensile stresses of the filaments. Filaments spun at low quench velocities and high quench temperatures increase in magnitude to a greater degree when compared to other trends. This results in the shorter distance at which the onset of crystallinity occurs as depicted in Figure 8-4. This illustrates the dependence of crystallinity on the local tensile stress of the filament. At the point of crystallisation onset, a marked change in the slope of the tensile stress profiles is observed. This is due to filament crystallinity reaching a critical value which results in the viscosity of the partly crystalline material in the crystalline mode of spinning tending to infinity. After this point no more attenuation of the spinline occurs. Consequently, the filaments behave as a rigid rod.

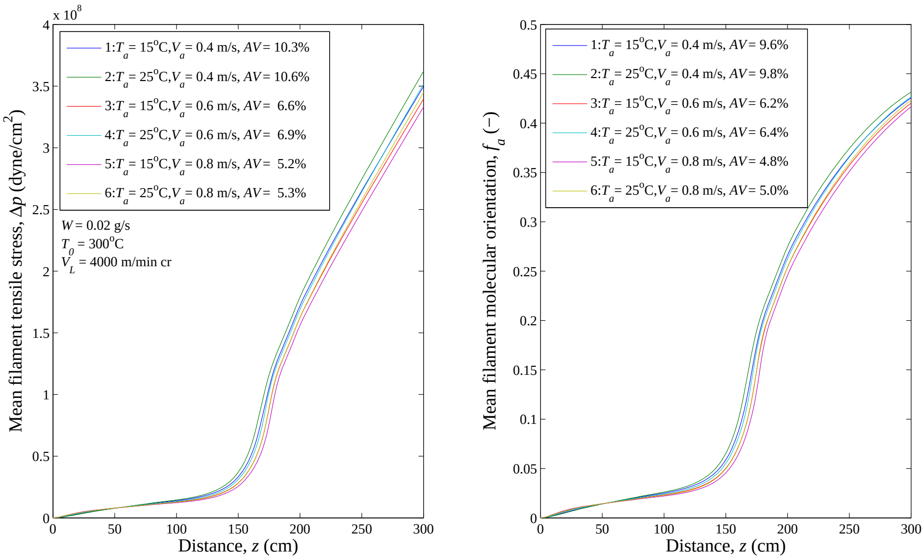

(a) (b)

Figure 8-5: A plot of the (a) mean filament tensile stress (Δp, dyne/cm^2), (b) mean filament molecular orientation (f_a, -) across the filament bundle.

The distance at which the filaments become rigid will be further referred to as the ‘point of rigidity’. Although the filaments traverse the rest of the spinline in a rod-like manner, it is not to say that all the fibre properties are set into place at this point as the overall polymer temperature is still well above the glass transition temperature. As can be seen in Figure 8-5, properties such as molecular orientation still vary as the tensile stress changes. The influence of the rod-like behaviour of the filament on the velocity profile is shown in Figure 8-6 where the mean local velocity is plotted as a function of distance. Here, the point of rigidity can clearly be noted by the final value at which the velocity profiles plateau. The influence of quench conditions on the point of rigidity can be noted by the variation in axial distance at which the velocity profiles reaches its final value. Lower quench velocities result in the point of rigidity being closer to the spinneret. As observed in previous discussion, these variables are more sensitive to quench air velocity than quench temperature on the point of rigidity. High quench temperatures and low quench air speed lead to the filaments reaching the point of rigidity earlier when compared to the other trends. Filaments spun under these quench conditions experience the slowest cooling rates but have the greatest amount of heat transfer. This is as a result of the low quench air speeds allowing more time for heat transfer to take place.

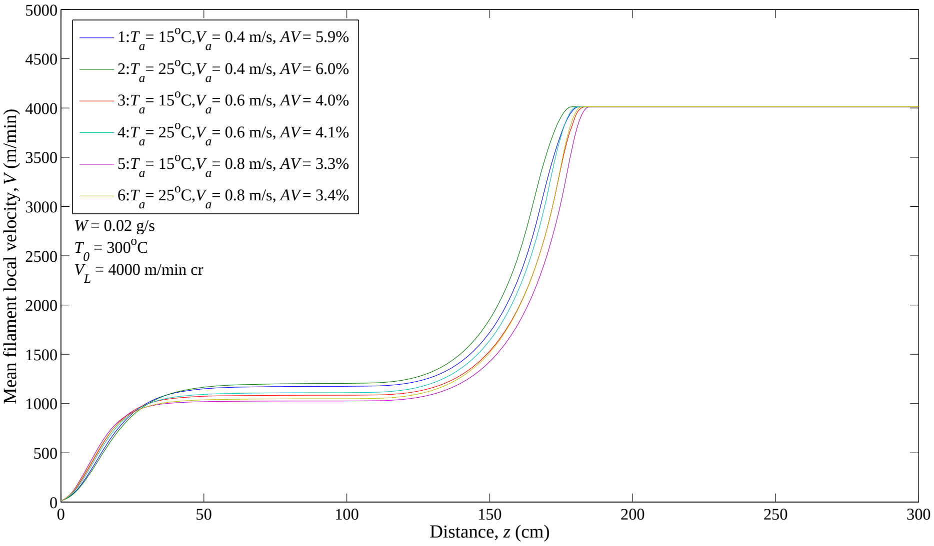

Figure 8-6: A plot of the mean filament local velocity (*V*, m/min) across the filament bundle.

The observations discussed above illustrate the effects of variable quench conditions on the cooling rates of filaments. In Figure 8-6 the effects of variable cooling rates on the velocity profile along the spinline are illustrated. Fibres which exhibit lower cooling rates at low quench air speeds in Figure 8-1 plateau sooner than fibers which are cooled at a higher rate due to greater quench air speeds. As a result of the lower cooling rates at low quench air velocities, filaments which experience higher temperatures attenuate for a longer period of time due to the lower viscosity values when compared to filaments at lower temperatures. This leads one to expect that just after the spinneret, higher tensile stresses are experienced by filaments which have higher cooling rates. The results shown in Figure 8-7 confirm this expectation where filaments spun at high quench speeds exhibit greater levels of tensile stress in the region just after the spinneret. However, after some point, as a result of longer attenuation times in zone 1 leading to higher velocities, intersection points occur.

Filaments spun under high quench air speeds, with initially higher tensile stress values, invert and exhibit lower tensile stresses as a result of the velocity levelling off at a lower value when compared filaments spun at low quench speeds. This causes lower tensile stresses in trends 5 and 6 after the inflection point. This is shown more clearly in Figure 8-7.

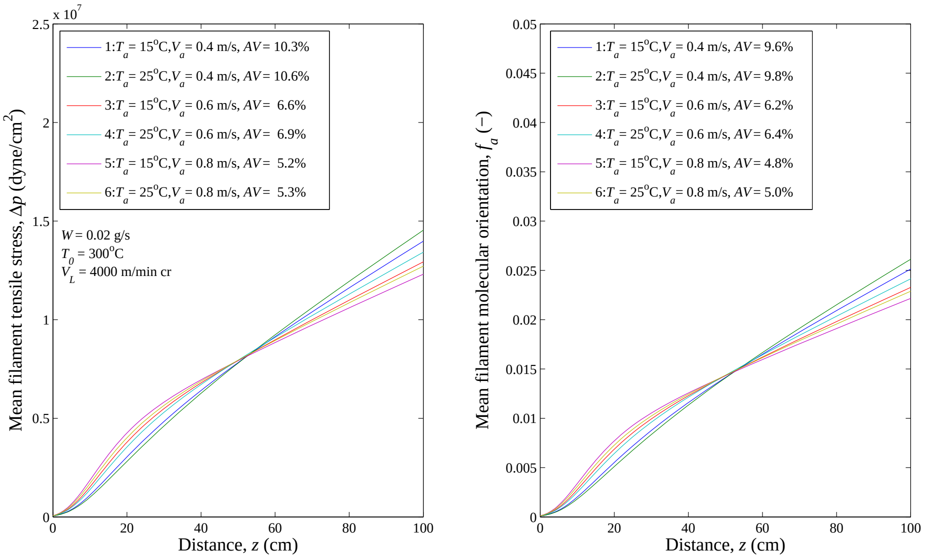

(a) (b)

Figure 8-7: A finer plot indicating the intersection points in (a) the mean filament tensile stress (Δ*p*, dyne/cm^2), and (b) mean filament molecular orientation (f_a, -) across the filament bundle.

The above discussion clarifies the effects of the quench conditions on the online behaviour of the average filament properties which ultimately make up the fibre. More specifically, the effects of varying cooling rates as a result of changing quench conditions throughout the bundle are brought to attention. The next section focuses on the effects of quench conditions on the variation of final yarn properties.

8.2.2 Effects of quench conditions on final fibre property variation

The importance of final property uniformity has been discussed in some detail in previous chapters. In this section intra-filament behaviour within the bundle is examined more closely by analysing individual simulation outputs. This will allow the magnitude of variance of certain filament properties such crystallisation and molecular orientation to be rigorously scrutinised. Final product property variation will then be analysed and interpreted.

Previous definitions used in literature to interpret when final yarn properties are ‘frozen’ into place include the Freeze-line definition. This method uses the glass transition temperature as the point where the filament properties are 'frozen' into place (Dutta 1987). Trial runs showed continuous change in certain properties after the polymer temperature dropped below the glass transition temperature. As such, a more rigorous way of determining the product qualities is through the properties of the individual filaments at the take-up point. This assumes that the final properties of the product take on those of the individual filaments at the take up point. The definition of final product properties as being those of the filaments at the take-up point is thus the preferred method for interpreting the uniformity of the final product properties. This is because the product properties are made up of the individual filaments at the take-up point after which these properties cannot change.

Table 8-1 shows the freezeline *CV* values for properties affecting yarn morphology and micro structure. These were obtained from simulations carried out under various quench conditions for a take-up velocity of 4000 m/min (crystalline phase) and an extrusion rate and temperature of 0.02 g/s and 285°C respectively. These results are discussed as they reflect the effects of process conditions which result in the largest property variation.

Table 8-1: Orientation, local force and crystallinity *CV* values at the freeze point (W = 0.02 g/s, T_0 = 285°C and V_L = 4000 m/min cr).

V_a (m/s)	T_a (°C)	f_a, *CV* (%)	F, *CV* (%)	X, *CV* (%)
0.40	15	4.48	5.87	0.04
	20	4.33	5.75	0.06
	25	4.21	5.68	0.05
0.60	15	3.40	4.34	0.04
	20	3.29	4.25	0.06
	25	3.42	4.46	0.02
0.80	15	2.19	2.39	0.03
	20	2.15	2.39	0.05
	25	2.80	3.61	0.05

Table 8-1 indicates that of all properties analysed, the largest variation is found to exist within the freezeline force (F), followed by the molecular orientation (f_a). The variance in the freezeline crystallinity is negligible in all of the outputs obtained under the applied conditions. This is a positive result as the degree of uniformity in crystalline material throughout the filament bundle significantly affects the structural uniformity. In particular, since the intra-filament uniformity of crystalline material in the above simulation is highly uniform, the occurrence of weak spots in the fibre as a result of inhomogeneous material is negated.

Since the molecular orientation is dependent on the local force, significant variance in the local force may result in similar variance value for orientation. A higher tensile force would result in a higher degree of orientation, the direction of which would be parallel to the applied force. In general, a higher variation in molecular orientation is achieved for low quench velocities irrespective of quench temperature applied. The greatest variation in molecular orientation of 4.5% is achieved at a quench air velocity and temperature of 0.4 m/s and 15°C respectively. The higher dependence of the variation magnitude of molecular orientation on quench air speed rather than quench air temperature could is attributed to the change in initial cooling rate being larger with a change in quench air speed than quench air temperature (refer to Figure 8-3). This influences the variation in the tensile stress across the bundle which results in the change variation for molecular orientation being greater with a change in the quench air speed.

As mentioned in section 8.2.1, the degree of variation in filament temperature is affected by the cooling rate. This initial variation in temperature and velocity, in turn, affects the degree of variation in fibre tensile stress which consequently has an effect on the orientation. The varying cooling rates, as a result of varying quench conditions, influences the magnitude of the online tensile stresses experienced by the individual filaments. As such, the amount of molecular orientation will be influenced accordingly. One way of determining the cooling effects involves analysing intra-filament behaviour obtained from a single simulation run. Analysing the temperature and velocity profiles would give some idea of the magnitude in which heat transfer takes place and secondly, tensile stress and orientation profiles would indicate the associated effects.

Figure 8-8 (a) shows the temperature profiles for each of the filaments as a function of distance obtained from a simulation. It was found that conditions indicated in the figure lead to the greatest variation in orientation and, as such, the property profiles obtained from this simulation will be used for illustration purposes. Other simulation results are shown in the Appendix A. The sharp rise in the temperature profile in zone

2 (100-200 cm) is due to exothermic crystallisation taking place. The temperature profiles reveal that the polymer temperature drops below the glass transition temperature on two occasions. The first varies from 50-75 cm and the second occurs at approximately 220 cm from the spinneret. However, any properties frozen into place by the polymer temperature dropping below T_g in the first zone are changed due to the filaments being reheated in zone 2. As such, only the second freezeline point will be considered. This being said, variation in the distance at which freezeline point occurs is minimal. However, a large variation of the initial cooling rates of the filaments is noted which, as determined in section 8.2.1, significantly influences the local stress experienced by the individual filaments. Figure 8-8 (b) illustrates changes in the velocity profiles. The final take-up velocity is achieved a significant distance before the take-up point. This leads one to suggest that a shortening of the spinning zone would save capital investment by reducing the rig size. However, even though the velocity is constant throughout the bundle, other properties such as tensile stress and orientation will still vary (see Figure 8-9).

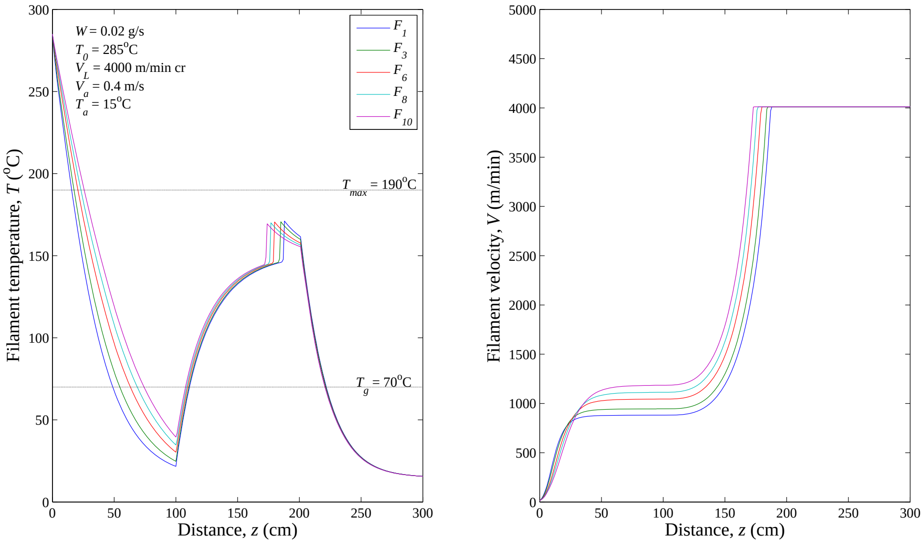

Figure 8-8: Plots of inter-filament (a) temperature, T (°C), and (b) velocity, V (m/min), versus distance.

In Figure 8-9 the influence of variable initial cooling rate on the variation and magnitude of individual filament tensile stress is shown. Filaments that experienced lower cooling rates (e.g. F_1) initially tend to have lower tensile stress values as a result. This is closely related to the viscosity of the polymer which, in turn, affects the velocity gradient of the filament. In both Figure 8-8 and Figure 8-9, a marked increase in the velocity, tensile stress and orientation occurs within the same axial distance (150-180 cm). As such, the small differences in the tensile stress and, as a result, orientation, are magnified by the effects of the hot tube zone.

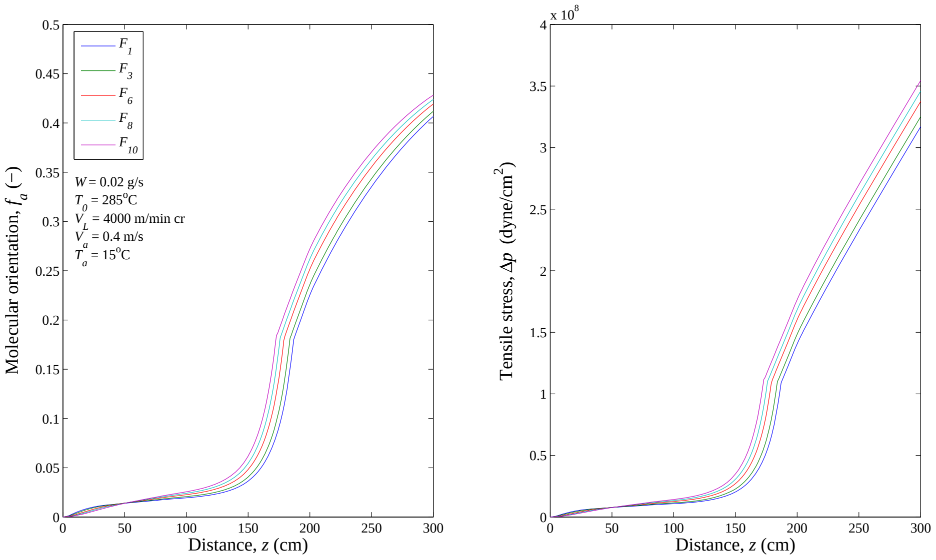

(a) (b)

Figure 8-9: Plots of inter-filament (a) molecular orientation, f_a (-), and (b) tensile stress, Δp (dyne/cm^2), versus distance.

The variation of final yarn orientation, local force and crystallinity are shown in Table 8-2. Here, a significant decrease in the *CV* values is clear when compared to the freezeline *CV* values reported in Table 8-1. This is also visible in Figure 8-9, where the variation in the molecular orientation is greater at the freezeline compared to the take up point. This decrease in variation is attributed to the temperature of the individual filaments tending towards the same final value in zone 3. Since this variation becomes smaller, the only other property which shows a significant degree of variation is the tensile force. Figure 8-9 indicates an increase in the deviation of tensile force. However, the coefficient of variation is smaller (compare Table 8-2 with Table 8-1).

Table 8-2: Final yarn orientation, local force and crystallinity CV values (W = 0.02 g/s, T_0 = 285°C and V_L = 4000 m/min cr).

V_a (m/s)	T_a (°C)	f_a, CV (%)	F, CV (%)	X, CV (%)
0.40	15	1.74	3.75	0.04
	20	1.66	3.75	0.06
	25	1.59	3.74	0.05
0.60	15	1.40	2.80	0.04
	20	1.32	2.75	0.06
	25	1.26	2.72	0.02
0.80	15	0.99	1.54	0.03
	20	0.95	1.55	0.05
	25	1.13	2.32	0.05

The decrease in orientation gradient in zone 3 is as a result of increased tensile stress which tends to some critical value where maximum orientation is achieved after which it decreases. This critical value is approximately 5x10^8 dyne/cm^2. The decrease in variation of the molecular orientation is confirmed by the theoretical definition used to calculate the value. The theoretical definition of the orientation factor is shown in eq. 8.3.

$$f_a(\Delta p) = B_1 \cdot \Delta p + B_2 \cdot \Delta p^2 + B_3 \cdot \Delta p^3 \qquad \text{eq. 8.3}$$

Here, the B_i terms are expansion coefficients and Δp the tensile stress. This phenomenon is illustrated more clearly in Figure 8-10 where a plot of the contribution of each term in the Taylor series describing non-linear orientation is shown.

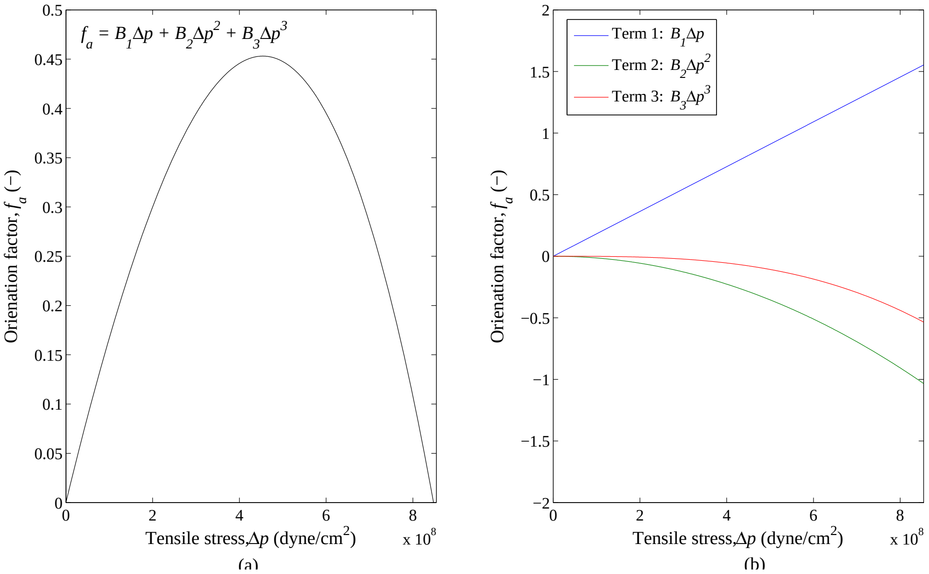

(a)

(b)

Figure 8-10: A breakdown plot of the orientation behaviour as a function of the tensile stress behaviour.

Figure 8-10 shows that at relatively low tensile stress term 1 dominates. However, after a critical value, terms 2 and 3 dominate additively which results in an overall decrease in the orientation factor. This observation agrees with the theoretical study carried out by Ziabicki and Jarecki (1986). In the work it is shown that at low stress ranges the molecular orientation is a linear function of the tensile stress. However, at higher stresses the orientation factor levels of at some critical asymptotic value. Physical properties such as birefringence and anisotropy are limited and approach some constant value when then stress filed increases towards infinity. However, no limitation is placed on the stress. Intuitively, the decrease in orientation could be due to the breaking down of the molecular framework after some critical stress as a result of large forces experienced by the polymer macro-molecules. This could be compared to the early stages of filament breakage indicating that present operating conditions are bordering on unrealistic spinning conditions.

8.2.3 Summary

The following points summarise the above findings of this section:

(i) a change in the quench air speed (V_a) has an dominant effect on the cooling rates of the filaments when compared to the effects of a change in quench air temperature (T_a). This is due to increased levels of forced convection at higher quench air velocities,

(ii) an increase in the quench air temperature whilst applying the same quench speed results in a decrease in the cooling rates of the filaments. This is caused by a decrease in the temperature gradient between the filaments and the quench air which is a significant driving force for heat transfer,

(iii) the largest average variation in quench air temperature is experienced at low quench speeds due to increased contact times which results in a greater degree of heat transfer,

(iv) an increase in the cooling rates results in a decrease in the average variation (AV) of the inter-filament temperatures. This variation directly influences the variation on other properties such as orientation and tensile stress,

(v) Cooling rates in zone 1 of the spinline play a significant role in determining the tensile stresses further down the spinline as differences in property trends in this zone are magnified by the hot tube zone,

(vi) higher orientation factors are achieved for fibres which experienced slower cooling rates initially. This is a result of increased attenuation times leading to higher local velocities which increases tensile stress,

(vii) the highest final property variation is achieved at quench conditions corresponding to low quench air speeds and temperatures. These are conditions under which the largest amount heat transfer takes place between the filaments and the quench air as a result of increased contact times,

(viii) negligible variation in the degree of crystallisation is achieved due to the sudden increase and magnitude of kinetic activity,

(ix) final yarn property variation decreases when compared to the freezeline point variation, specifically regarding the variation in orientation. This is attributed to the physical properties (i.e. molecular orientation) of the filaments being limited to a certain asymptotic value dependent on the tensile stresses experienced along the spinline, and

(x) the initial cooling rate of the individual filaments influences the magnitude of the tensile stress achieved through initial velocity gradients and viscosity. This, in turn, affects the degree of orientation further down the spinline.

This section only investigated changes in the degree of property variation as a result of changing initial quench conditions. The following section deals with changing extrusions rates and the effects of this process parameter on the variation of fibre properties.

8.3 Polymer extrusion rate

The polymer extrusion rate is defined as the mass of polymer melt flowing through a single filament hole per second. The sensitivity of the tensile stress and degree of orientation achieved on this parameter has been determined in previous work by Ziabicki (1976). In the work, it is shown that an increase in the extrusion rate would result in a decrease in the optical birefringence of the fibre. This indicates an associated decrease in the calculated molecular orientation factor. As yet, no literature has been published on the influence of extrusion rate on the degree of inter-filament property variation, which is the subject of the following section.

8.3.1 Effects of initial mass flow rate on system

Figure 8-11 shows the average filament temperature and crystallinity profiles for two different extrusion rates. The average temperature profiles show that a higher extrusion rate leads to lower cooling rates and higher filament temperatures in zone 1. This is plausible since, because the initial quench conditions are identical, more polymer melt requires cooling at a higher extrusion rate resulting in the elevated filament temperatures. This trend is shown again in zone 2 where the filaments spun under a lower extrusion rate are subjected to higher heat transfer rates and, as a result, are heated to higher temperatures.

Figure 8-11 (b) shows the average crystallinity achieved is negligible under the applied process conditions. However, the trend observed is for filaments exposed to higher temperatures for a longer period of time to achieve higher degrees of crystallinity. In zone 1, trend 2 achieves a higher degree of crystallinity due to the lower heat transfer rates experienced by these filaments. The opposite is observed in zone 2, where trend 1 achieves a higher degree of crystallinity as a result of trend 1 being heated to higher temperatures. The differences in the *AV* values for both plots, in terms of absolute numbers, are marginal.

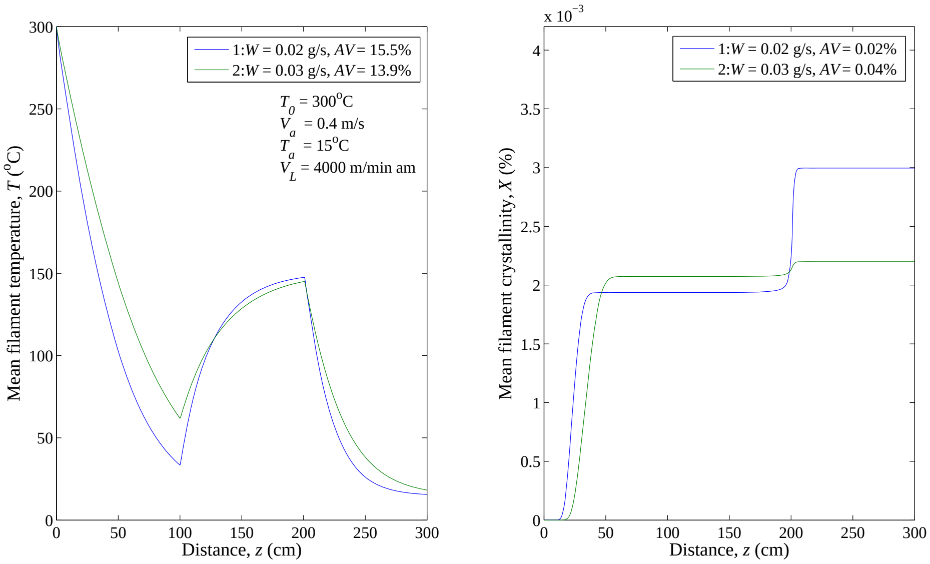

(a) (b)

Figure 8-11: A plot of (a) the average filament temperature (*T*, K), and (b) the average degree of filament crystallinity (*X*, %) for two different extrusion rates.

The difference in heat transfer rates experienced in the various zones is attributed to the difference in the average diameter of the filaments as a result of different initial melt extrusion rate. Figure 8-12 (a) and (b) shows the average filament velocity and diameter profiles. In Figure 8-12 (b), it is clear that filaments spun under conditions represented by trend 1 attenuate to a smaller diameter which, in turn, is the cause for the higher heat transfer rates observed in Figure 8-11. Filaments represented by trend 2 attenuate for a longer distance than those represented by trend 1. This is observed in Figure 8-12 (b) where the velocity profile for trend 2 plateaus at a higher level further down the spinline. The higher extrusion rate causes the increase in attenuation distance indirectly through the difference in the heat transfer rates. The higher temperature for trend 2 allows for a longer attenuation time when compared to trend 1.

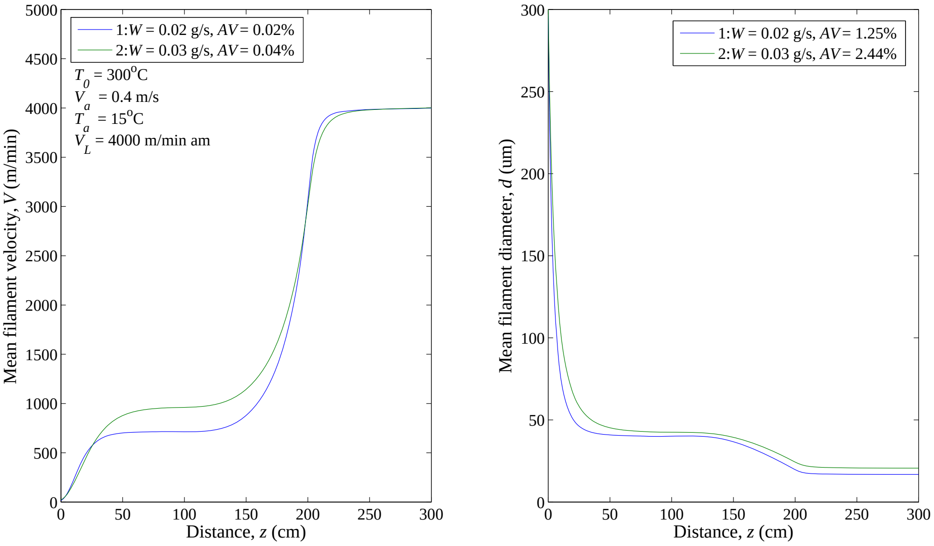

(a) (b)

Figure 8-12: A plot of (a) the average filament velocity profile (*V*, m/min), and (b) the average filament diameter (*d*, um) for two different extrusion rates.

The influence of the different heat transfer rates on online stress experienced by the filaments is depicted in Figure 8-13, which illustrates the tensile stress and orientation profiles. Here, it can be seen that many inflection points occur. In the first 50 cm after the spinneret, trend 1 shows higher tensile stresses. This corresponds to a higher velocity for trend 1 in the same range. The first inflection point occurs at approximately 75 cm at which point the tensile stress applied to filaments represented by trend 2 dominates. Again, this corresponds closely to the velocity profiles in Figure 8-12 (a). Zone 3 shows maximum deviation between the two trends. This is most likely due to a combination of higher heat transfer rates in trend 1 resulting in a lower average filament temperature when compared to trend 2. This lower temperature results in a greater viscosity. Together, the increased viscosity and disappearance of attenuation in zone 3 leads to the sudden increase in the tensile stress. The corresponding changes are noticed for the orientation factor. Filaments spun under the conditions represented by trend 1, as predicted, achieve a greater degree of online orientation than those represented by trend 2. This observation suggests a trade off exists between the degree of online orientation and extreme tensile stress levels which could lead to filament breakage.

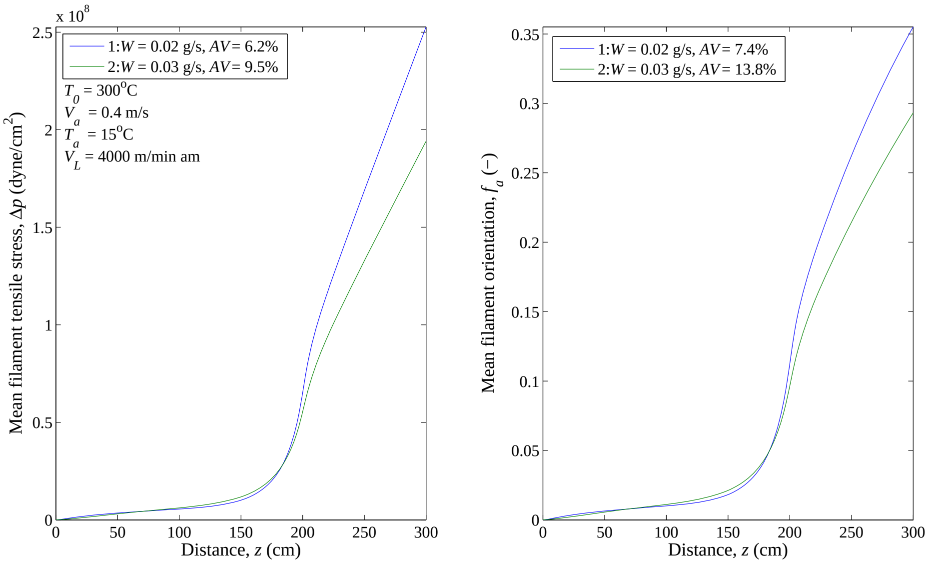

(a) (b)

Figure 8-13: A plot of (a) the average tensile stress (Δp, dyne/cm^2), and (b) the average molecular orientation (f_a, -) for two different flow rates.

The degree in average inter-filament property variation is greater for all filaments spun at higher extrusion rates. This does suggest that a higher extrusion rate leads to higher final product property variation and further discussed in the following section.

8.3.2 Variation of final fibre properties

Table 8-3 and 8-4 list the variation in final product properties using the freezeline and take-up point definitions. In Table 8-3 the difference in freezeline orientation variation between the two extrusion rates is approximately a 1.5% and is considered minimal. Negligible variation in freezeline crystallisation is obtained. Comparing the variation in the take-up orientation to that of the freezeline it is clear that the variation decreases. The crystallinity variation remains the same. This is due the final value being achieved before the glass transition point.

Table 8-3: Freeze line variation (*CV*, %).

W(g/s)	f_a, *CV* (%)	*F*, *CV* (%)	*X*, *CV* (%)
0.02	1.07	1.19	0.01
0.03	2.53	2.84	0.04

Table 8-4: Take-up point variation (*CV*, %).

W(g/s)	f_a, *CV* (%)	*F*, *CV* (%)	*X*, *CV* (%)
0.02	0.43	0.58	0.01
0.03	0.76	1.55	0.04

Although the magnitude of variation is relatively small, the overall influence of the extrusion rate is clearly seen. An increase in the extrusion rate results in an increase in the degree of final product property variation. This does suggest that extrusion rate has some degree of influence on final product property variation.

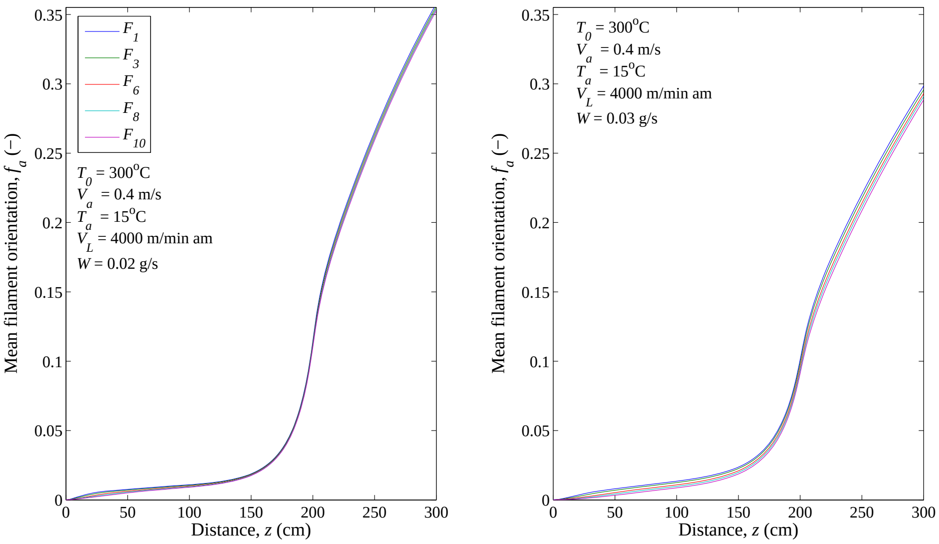

(a) (b)

Figure 8-14: A plot of the inter-filament orientation for (a) *W* = 0.02 g/s, and (b) *W* = 0.03 g/s.

Figure 8-14 illustrates the difference in freezeline (225 cm) and final orientation variation. In Figure 8-14 (a) the degree of orientation is relatively uniform throughout the bundle. However, Figure 8-14 (b) shows a much larger degree of non-uniformity throughout the spinline which carries through to both the freezeline and the take-up point. This illustrates that operating at higher extrusion rates increases final product property variance. However, higher extrusion rates result in lower tensile stress values implying that a more stable spinning regime exists under these conditions. As such, a trade-off exists between achieving higher degrees of orientation and product uniformity and increasing tensile stress values to levels which border on filament breakage.

8.3.3 Summary

We summarise the sensitivity analysis of this section as follows:

(i) lower extrusion rates increase the average attenuation rate resulting in a decrease in the average filament diameter. This is due to lower tensile stresses as a result of increased viscosity along the spinline.

(ii) lower extrusion rates increase the rate of heat transfer from the filaments as a consequence of decreased diameters and increased velocity gradients. This, in turn, increases the degree of stress induced crystallisation, and

(iii) increasing the extrusion rate results in a decrease in orientation levels due to reduced tensile stresses as a result of lower heat transfer rates.

Secondly, the influences of extrusion rate on the freezeline and take-up point property variations were discussed. The following points summarise the findings:

(i) the freezeline variation is higher than the take-up variation which, as discussed before is attributed to physical properties such orientation being limited to a asymptotic value,

(ii) an increase in the extrusion rate results in a higher degree of non-uniformity for both the freezeline and take-up variation which is attributed to lower amounts of heat transfer under these conditions,

(iii) an increase in the extrusion rate increased the distance at which the glass transition point is reached. This is a consequence of decreased heat transfer rates resulting in the filaments reaching this temperature at a later stage along the spinline,

(iv) higher extrusion rates suggest higher degrees of online instability due to the increased amount of variance observed along the spinline. The root cause for the increased variance is explained in the above points, and

(v) there exists a trade-off between increased levels of orientation and product uniformity and increased stress levels which may lead to online filament breakage.

Although the magnitude of final variation achieved is relatively small, the overall effects of the extrusion rate are significant. The low degree of variation could be attributed to other process conditions not investigated in this section. However, as the extrusion rate is increased, freezeline and take-up variations increased accordingly. As such, it can be said that the extrusion rate has a significant effect on the degree of non-uniformity achieved throughout the filament bundle.

8.4 Extrusion temperature

The extrusion temperature (T_0) is the temperature of the molten polymer as it exits the spinneret. It must be said that altering the extrusion temperature must be done with the knowledge of thermal limitations of the polymer in mind in order to avoid unwanted degradation of the polymer. Intuitively, one expects the extrusion temperature to influence the viscosity of the polymer which, in turn, affects the online tension and attenuation rates experienced by the filaments. The aim of the following section is to distinguish the major effects of the initial melt temperature on melt pinning dynamics. More importantly, the influence of the extrusion temperature on the uniformity of final filament properties will be determined.

8.4.1 Effects of extrusion temperature on the system

Figure 8-15 illustrates the average filament temperature and cooling rate profiles for fibres spun at various extrusion rates. Trend 2 describes cooling under higher heat transfer rates as illustrated by Figure 8-15 (b). This is a result of the greater temperature gradient between the cooling medium and the filaments at greater extrusion temperatures when compared to filaments spun at lower values. A significant decrease in the heat transfer rate is observed in the region directly after the spinneret. This suggests that the velocity gradients in this region vary to some degree which, in turn, influence the amount of heat transfer.

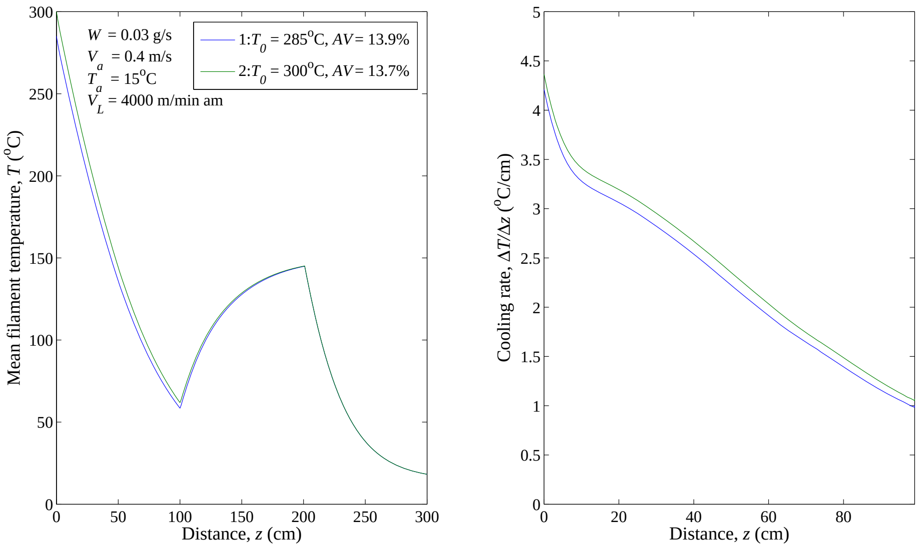

(a) (b)

Figure 8-15: A plot of (a) the average filament temperature (*T*, K), and (b) the cooling rate ($\Delta T/\Delta z$, °C/cm) for two extrusion temperatures.

The difference in the degree of crystallinity achieved is minimal as illustrated by Figure 8-16 (a).The velocity profiles also exhibit negligible differences as depicted by Figure 8-16 (b). On closer inspection, a change in the velocity gradient directly after the spinneret coincides with the change in the rate of cooling as illustrated in the 0-20 cm distance range in Figure 8-15 (b). This indicates the close dependence of filament cooling on the velocity gradient. A decrease in local filament velocity gradient corresponds to a decrease in the cooling rate of the filament.

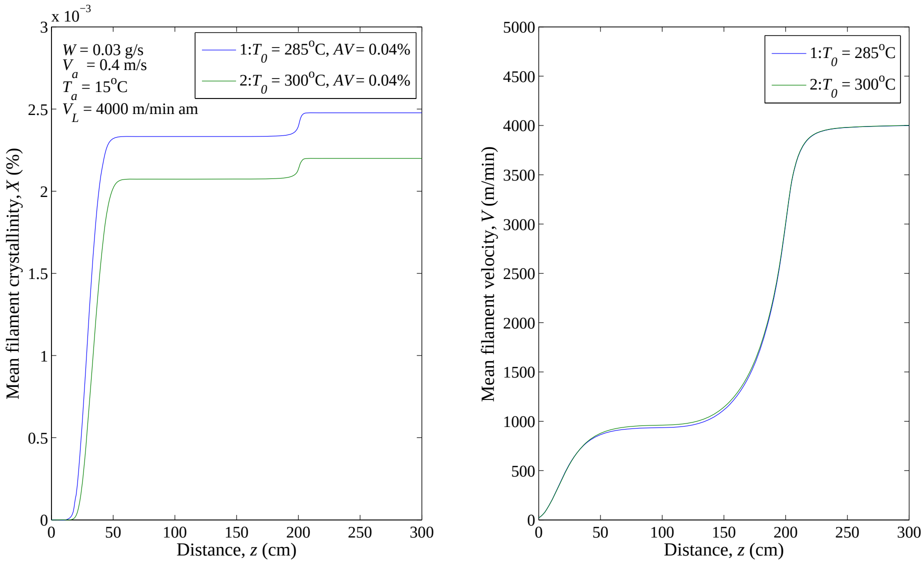

(a) (b)

Figure 8-16: A plot of (a) the average filament crystallinity (*X*, %), and (b) the average filament velocity (*V*, m/min) for two extrusion temperatures.

Figure 8-17 (a) illustrates a plot of the average tensile stress as a function of distance from the spinneret. Trend 1 shows a small degree of greater online tension as a result of the lower average filament temperature shown in Figure 8-15 (a). Lower temperatures reduce the fluidity of the polymer due to increased viscosity. The greater tensions experienced at lower extrusion temperatures results in the difference in degree of crystallinity achieved (Figure 8-16 (a)).

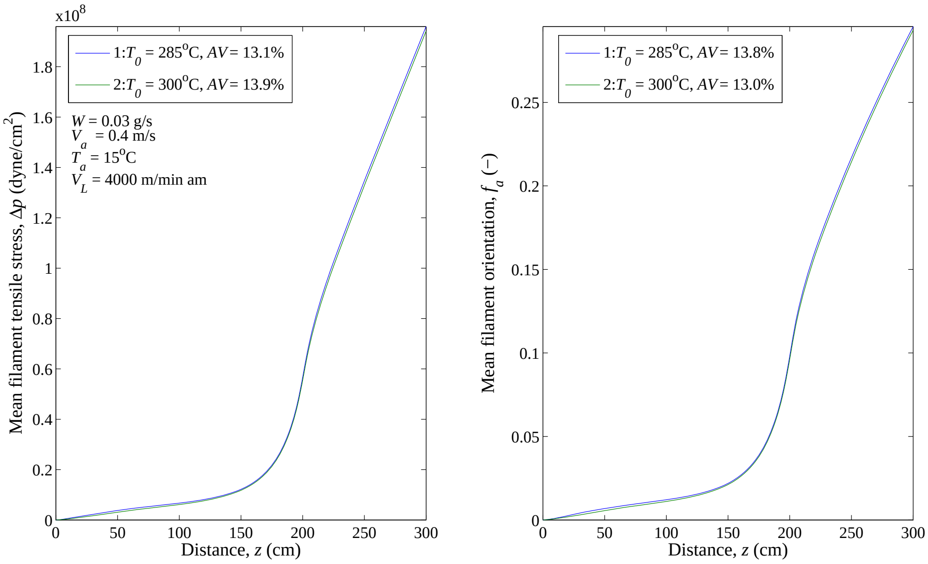

(a) (b)

Figure 8-17: A plot of (a) the average filament tensile stress (Δp, dyne/cm^2), and (b) the average filament orientation factor (f_a, -) for two extrusion temperatures.

Orientation profiles exhibit minimal differences as shown in Figure 8-17 (b). This is directly attributed to the small variance in the tensile stress profiles. However, a relatively large deviation between the two trends is observed in zone 1. The difference in average temperatures influences the tensile stress through the velocity gradient and magnitude of viscosity. These factors result in the initial difference in the tensile stress and orientation profiles.

8.4.2 Variation of final fibre properties

Table 8-5 and 8-6 list the variation of molecular orientation and force at the freeze point and take-up point respectively. Table 8-5 shows negligible change in property uniformity as a consequence of changes in the extrusion temperature. The same can be said for the change in take-up point variation between the different extrusion temperatures illustrated by Table 8-6. The degree of property non-uniformity decreases when the freeze to take-up point variations are compared. This is attributed to the temperature and velocity profiles converging to the same final value as shown in Figure 8-15 (a) and Figure 8-16 (b). The differences in tensile stress between fibres spun at various extrusion temperatures in the initial regions is not large enough to result in a significant amount of variation in properties such as molecular orientation further down the spinline.

Table 8-5: Freeze line variation (*CV*, %).

T_0 (°C)	f_a, *CV* (%)	*F, CV* (%)	*X, CV* (%)
285	2.53	2.84	0.04
300	2.45	2.76	0.04

Table 8-6: Take-up point variation (*CV*, %).

T_0 (°C)	f_a, *CV* (%)	*F, CV* (%)	*X, CV* (%)
285	0.76	1.55	0.04
300	0.62	1.62	0.05

8.4.3 Summary

In light of the above discussion, the following points summarise the findings with respect to changes in the extrusion temperature and the associated effects on the system dynamics.

(i) Larger extrusion temperatures result in larger filament cooling rates. This is a characteristic of increased temperature gradients between the filaments and the passing quench air. However, the overall changes in heat transfer is minimal,

(ii) changes in the extrusion temperature results in minimal affect on the degree of crystallinity obtained. This is attributed to the minimal change in cooling rates associated with a change in the extrusion temperatures which results in the temperature and stress profiles being similar under the various process conditions,

(iii) tensile stress and orientation profiles exhibit negligible change as a result of applying various extrusion temperatures which corresponds to the above point, and

(iv) changes in the degree of property uniformity as a result of applying various extrusion temperatures are negligible as a result of similar heat transfer conditions experienced by the filaments under the various extrusion temperatures.

Although extrusion temperature is an easy controlled process variable, the system is relatively insensitive to changes in this variable and so it cannot be used help optimise the operation further. However, careful consideration in the thermal limitations of the polymer is required as thermal degradation of the polymer occurs at excessive temperatures.

8.5 Take-up velocity

The take-up velocity is the speed at which the yarn is spun at, and is an important process variable in industrial spinning processes. This is due to the rate of product output being directly related to the speed at which the yarn is produced. It is also known that this variable strongly affects the structural properties of the fibre (i.e. tensile stress, molecular orientation) (Jarecki 1976). In the work, it was shown that increasing the take-up velocity had the effect of increasing tensile stress as well as the measured optical birefringence. Other properties that are affected by an increase the take-up velocity include the final filament diameter. It was shown that a decrease in the final filament diameter was obtained for increased take-up velocities. Although this is constraint inherent in the mass balance, the observation is plausible since higher velocities result in the attenuation of the fibre causing the diameter to decrease. These observations do suggest that changes in the final take-up velocity will affect the dynamics of a multifilament system to some degree. In this section the influence of take-up velocity on the system dynamics as well as the final property uniformity will be investigated.

8.5.1 Effects of take-up velocity on the system dynamics

Figure 8-18 illustrates the local filament temperature and the cooling rate. High take-up velocities correspond to filaments achieving slightly lower temperatures in zone 1 as well as a greater degree of crystallinity. A sharp rise in the temperature profile is observed for filaments spun at a take-up velocity of 5000 m/min in the process of online crystallisation. This is attributed to exothermic heat generated from a large amount of polymer material crystallising. The final temperature achieved by the various fibres varies as the final take-up velocity is changed. Fibres spun at lower take-up speeds achieve higher final temperatures. The greatest degree in the average variation of the intra-filament temperature coincides with the greatest take-up speed. This corresponds to greater cooling rates, defined here as the change in temperature per cm of spinline, as a result of an increased temperature gradient caused by lower contact times between the quench air and filament sections as illustrated in Figure 8-18 (b).

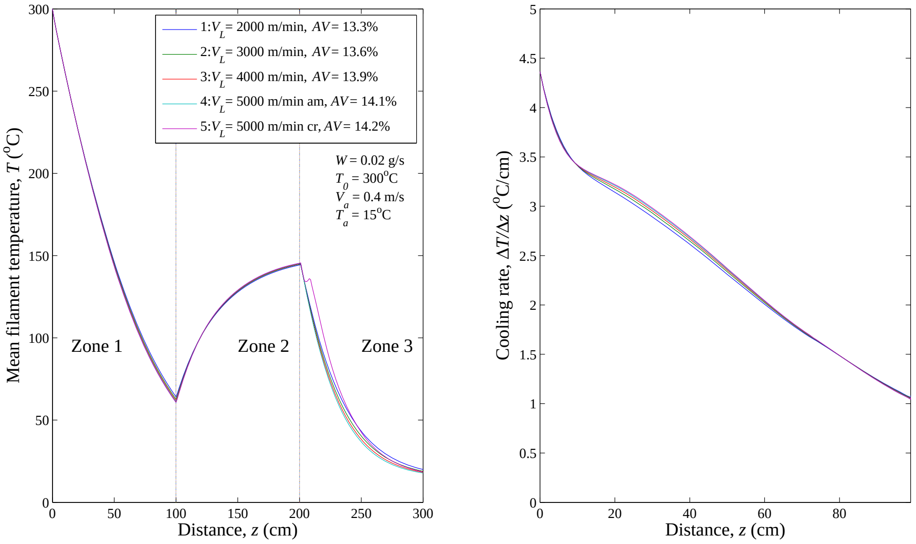

(a) (b)

Figure 8-18: A plot of (a) the average filament temperature (T, K), and (b) the cooling rate ($\Delta T/\Delta z$, ^{o}C/m) for various take-up velocities.

Figure 8-19 illustrates the average velocity and crystallinity profiles. The velocity profiles differ slightly with respect to the various plateau values. As observed in section 8.2.1, this is directly related to the cooling rate of the filaments. Comparing Figure 8-18 (b) and Figure 8-19 (a), more heat transfer occurs at lower take-up velocities in the region just after the spinneret as a result of the increased contact times and lower velocity gradients. This causes filaments spun at lower speeds to attenuate for shorter time intervals. Figure 8-19 (a) confirms this observation where lower plateau values are achieved for filaments spun at slower take-up speeds.

Figure 8-19 (b) illustrates significant changes in the crystallinity profiles obtained as a result of increased take-up velocities. The final degree of crystallinity decreases as the take-up velocity is increased. However, spinning speeds of 5000 m/min result in increased levels of crystallinity. This is attributed to an increase in the tensile stress along the spinline above some critical value which results in a highly orientated molecular structure. Together, the tensile stress and orientated structure induce crystallisation. The magnitude of the initial and online tensile stress is greater for the yarn spun at 5000 m/min which induces a product with a crystalline phase. Figure 8-20 (a) illustrates the increasing level of tensile stress for increased take-up velocities. The influence of crystallisation on the tensile stress profile can be seen for the crystalline phase of yarn spun at 5000 m/min where an abrupt change in the gradient is observed. This is due to the rod-like behaviour of the filaments once critical crystallinity is achieved ($X = 10\%$). Figure 8-19 (a) illustrates this observation by the sudden rate at which the velocity plateaus.

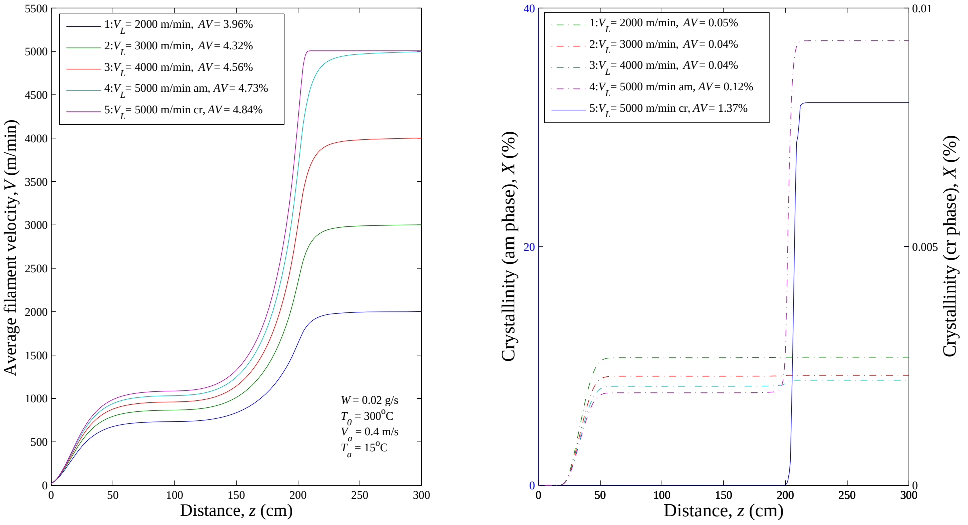

(a) (b)

Figure 8-19: A plot of (a) the average filament velocity (*V*, m/min), and (b) average filament crystallinity (*X*, %) for various take-up velocities.

The orientation profiles depicted by Figure 8-20 (b) exhibit similar trends to the tensile stress profiles with increasing levels of orientation with take-up velocity clearly shown. The sharp increase in both the tensile stress and consequently, the molecular orientation in the region of 150-200 cm are caused by an increase in the polymer fluidity as a result of the heating zone. The increased fluidity results in greater velocity gradients which increase tensile stress levels significantly due to higher air drag forces being balanced by the take-up device.

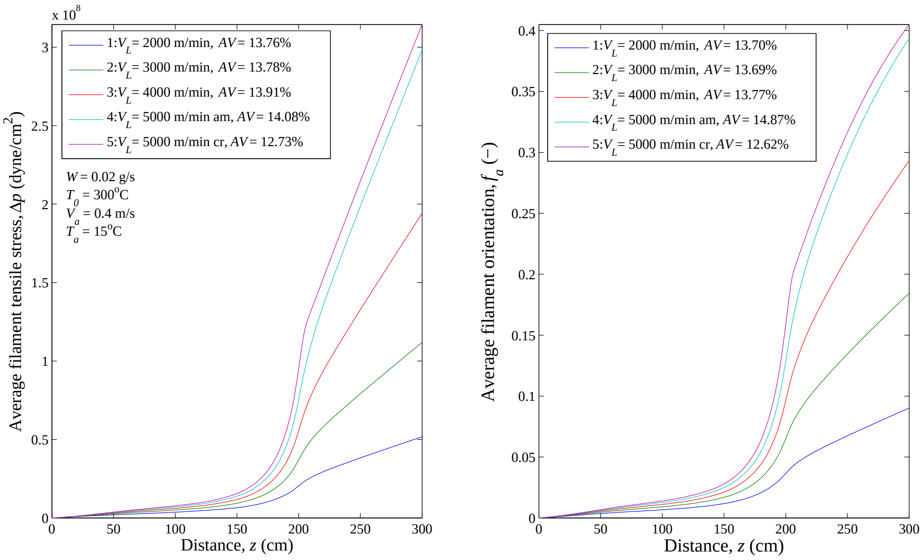

(a) (b)

Figure 8-20: A plot of (a) the average filament tensile stress (Δp, dyne/cm^2), and (b) average filament orientation (f_a, -) for various take-up velocities.

Lastly, an important observation is the absence of the previously observed inversion point in the profiles in the region after the spinneret. This is attributed to the relatively uniform cooling rates experienced by each filament under the given conditions. This leads one to suggest that a change in the take-up velocity has little influence on the uniformity of quench conditions.

8.5.2 Variation of final fibre properties

Table 8-7 and 8-8 indicate the variance of various properties for a change in the take-up velocity. The freezeline variance decreases for an increase in the take-up velocity. This is the general trend except for crystallinity where the values appear to be increasing. This increase in variance is attributed to the sensitivity of the final crystallinity value on the online force experienced by the individual filaments. This sensitivity originates is a result of the sudden kinetic activity which only occurs under certain conditions. This will be dealt with in more detail in the following paragraph.

The take-up point variance shown in Table 8-8 is smaller for all take-up velocities up to 4000 m/min when compared the freeze line variances at the same take-up velocities. The reason for the crystallinity variance remaining unchanged will be dealt with in the following paragraph.

Table 8-7: Freeze line variation (*CV*, %).

V_L (m/min)	f_a, *CV* (%)	*F*, *CV* (%)	*X*, *CV* (%)
2000	3.29	3.39	0.05
3000	2.92	3.15	0.05
4000	2.53	2.84	0.04
5000 am	2.30	2.66	0.31
5000 cr	1.01	1.35	18.79

Table 8-8: Take-up point variation (*CV*, %).

V_L (m/min)	f_a, *CV* (%)	*F*, *CV* (%)	*X*, *CV* (%)
2000	1.17	2.43	0.05
3000	0.81	1.84	0.05
4000	0.76	1.55	0.04
5000 am	0.84	1.42	0.31
5000 cr	0.30	0.65	18.79

Figure 8-21 (a) and (b) illustrate the variation in the temperature profiles for fibres spun at 2000 m/min and 5000 m/min crystalline phase. Filaments spun at 2000 m/min remain at slightly higher temperatures throughout the spinline but converge to the same final temperature as that obtained by filaments spun at greater take-up velocities. However, the degree of variance between the intra-filament temperatures profiles spun at the various take-up speeds is minimal. The effects of exothermic heat of crystallisation are clear as seen in Figure 8-21 (b) where a sharp rise in temperature is experienced in the region just after the heating zone (zone 2). All of the profiles exhibit this rise in temperature except the filament situated on the windward side of the bundle. This is due to the temperature and tensile force being too low for significant crystallisation to occur.

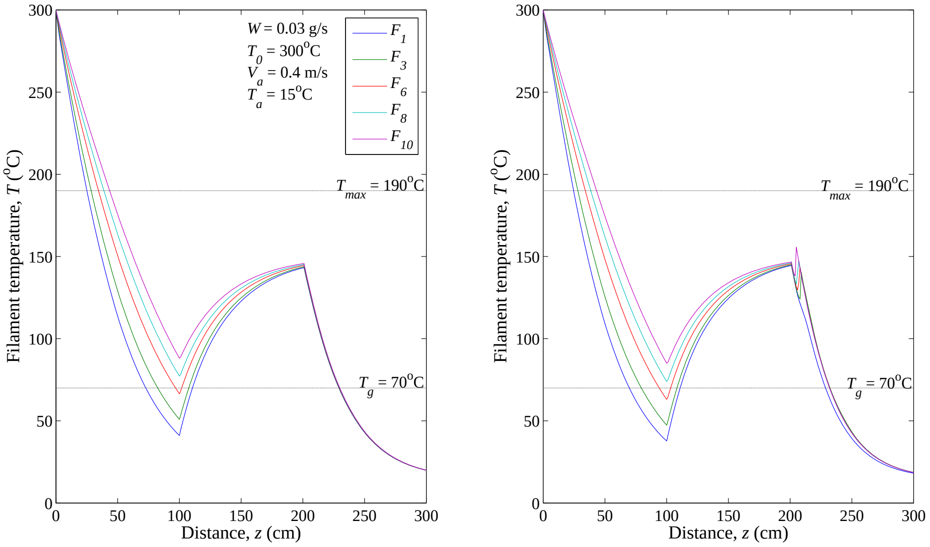

(a) (b)

Figure 8-21: A plot of the filament temperature at (a) at V_L= 2000m/min, and (b) at V_L= 5000m/min crystalline phase.

Figure 8-22 (a) and (b) show inter-filament crystallinity profiles for fibres spun at 2000 m/min and 5000 m/min (cr). Although the overall magnitude of crystallisation is low, some degree of variance still occurs for fibres spun at 2000 m/min as illustrated by Figure 8-22 (a). Fibres spun at this wind-up speed have increasing levels of crystallinity achieved by filaments situated on the leeward side of the bundle. A plausible reason for this occurrence is the increase in temperature associated with filaments situated on the leeward side. This leads to these filaments remaining in the temperature zone corresponding to increased levels of crystallisation kinetics for a longer period of time. This is evident from Figure 8-21 (a) where the filaments on the leeward side of the bundle (F_{10}) are at greater temperatures for longer periods of time. An interesting observation is the distance at which the onset of crystallisation occurs in Figure 8-22 (a). Filaments situated on the windward side of the bundle begin kinetic activity sooner than filaments situated towards the leeward side of the bundle. This is a result of increased initial stresses for windward rather than leeward positioned filaments. This illustrates the effects of tensile stress and cooling rates on the kinetic activity of filaments.

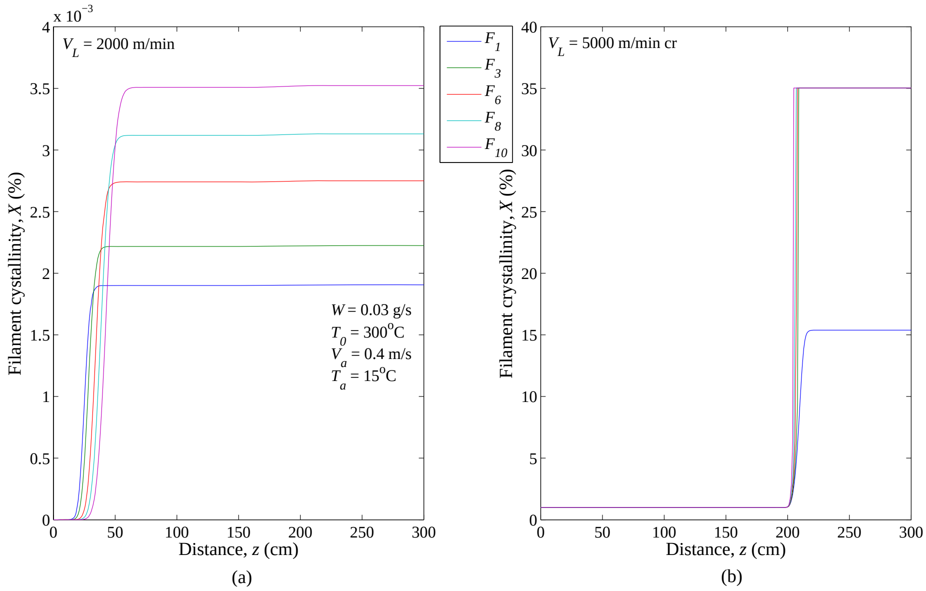

(a) (b)

Figure 8-22: A plot of inter-filament crystallinity (X, %) at (a) V_L= 2000 m/min and (b) at V_L= 5000 m/min crystalline phase.

In Figure 8-22 (b) a clear variance in the degree of crystallinity is obtained for the first filament (F_1) when compared to the other filaments which achieve the maximum degree of crystallinity. Here, F_1 only achieves just over 16% crystallinity. If one considers Figure 8-21 (b), it is clear that this filament remains in the kinetically active zone for the shortest period of time due to greater heat transfer effects as a result of the windward most position in which the filament is situated in. In Figure 8-23 (b) stress profiles illustrate no obvious cause for the decrease in crystalline material achieved for F_1 in Figure 8-22 (b). This confirms that filament temperature plays a significant role in crystallisation kinetics. As such, this suggests that any non-uniformity in the inter-filament temperature along the spinline could result in a large crystallinity variance which adversely affects the strength and quality of the final product.

In Figure 8-23 it is clear that a greater variance in tensile stress is achieved for low take-up velocities. This corresponds to a greater variance in the inter-filament temperature profiles for low wind-up speeds. The magnitude of online filament stress is much larger at a greater take-up speed which is as a result of reduced filament temperature and diameter along the spinline. This, in turn, is caused by the increased take-up velocity.

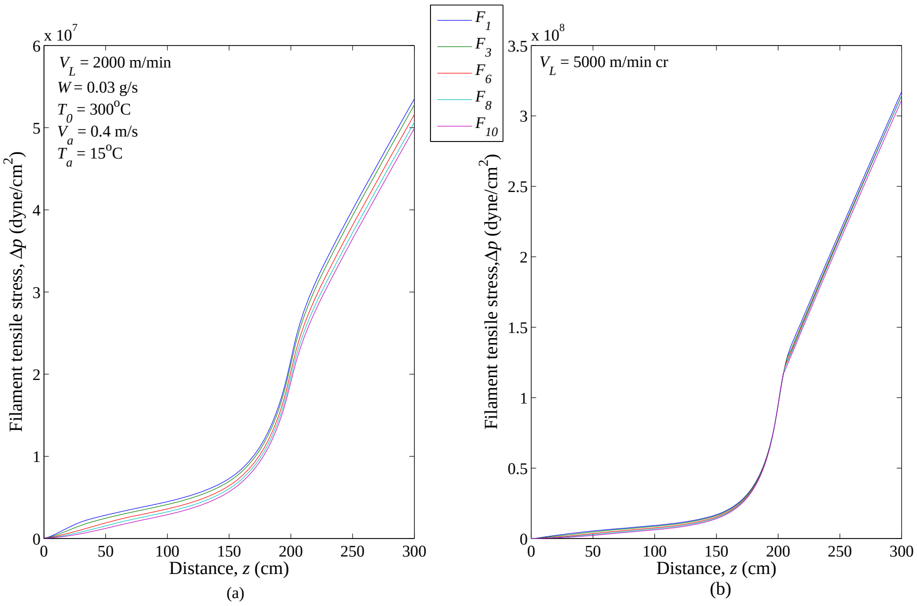

(a)

(b)

Figure 8-23: A plot of inter-filament tensile stress (Δp, dyne/cm^2) at (a) V_L= 2000 m/min and (b) at V_L= 5000 m/min crystalline phase.

Figure 8-24 illustrates the online orientation achieved by the individual filaments spun at different wind-up speeds. A clear increase in variance is distinguished between the inter-filament orientations at low compared to greater take-up speeds. As discussed before, this corresponds to the greater variance in tensile stress at low take-up speeds. Ultimately, the root cause for the increased variance in properties at low take-up speeds is consequence of the small increase in variance of the quench conditions. The increase in quench temperature variance is caused by increased heat transfer at low take-up speeds due to increased contact time between the filament and passing cooling medium.

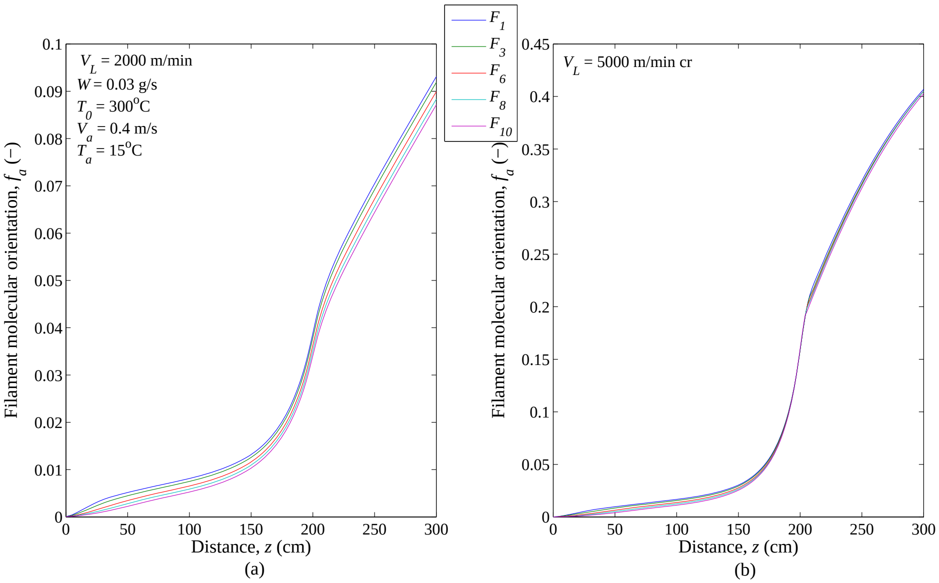

Figure 8-24: A plot of inter-filament tensile stress (Δ*p*, dyne/cm^2) at (a) V_L= 2000 m/min and (b) at V_L= 5000 m/min crystalline phase.

Velocity profiles of filaments spun at various take-ups speeds are shown in Figure 8-25. Here it can be seen that greatest variance occurs in the region from 0-100 cm (quench zone) for both take-up velocities. This is the region where filaments experiences the greatest variation in cooling rates which results in windward filaments being cooled faster than leeward positioned filaments. As such, these filaments experience increased attenuation rates when compared leeward situated filaments. This occurs to a greater extent at increased take-up speeds as depicted in Figure 8-25 (b). The increased attenuation rate for windward situated filaments is confirmed by the diameter profiles illustrated in Figure 8-25 (c) and (d) where filaments with increased attenuation rates are stretched and reduced in diameter. The positions at which changes in the filament diameter are observed correspond to the significant changes in the velocity gradient, illustrating the close relationship between filament velocity and diameter.

Regions of significant property changes in Figure 8-22, Figure 8-23 and Figure 8-24 correspond to regions in Figure 8-25 (a) and (b) where high velocity gradients are obtained. The region in which this occurs to the largest degree is towards the exit of hot tube zone. Here, the filaments are heated at increased tensile stress values which results in the sudden increase in velocity, as a consequence of decreased viscosity and increased tensile stresses, and greater degrees of molecular orientation. This occurs to a greater degree for filaments spun at higher wind-up speeds. Figure 8-25 shows that an increased take-up velocity corresponds to filaments achieving smaller diameters at the take-up point. This is most likely why filaments which experienced a sudden rise in temperature at the exit of the hot tube due to exothermic crystallisation cool fast enough to converge to the same final value as filaments spun at a slower take-up speed.

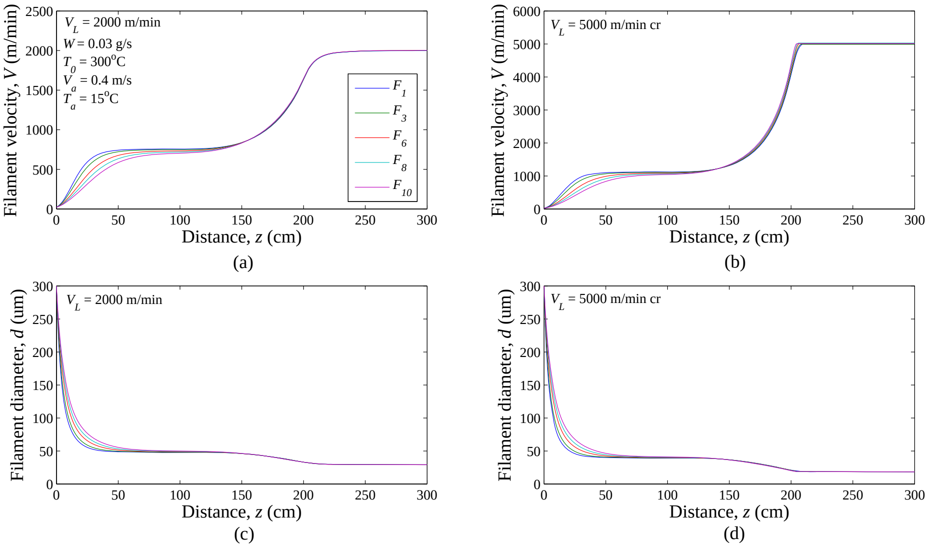

(a) (b) (c) (d)

Figure 8-25: A plot of (a),(b) inter-filament velocity (*V*, m/min), and (c),(d) a plot of inter-filament diameter (*d*, um) at V_L= 2000 m/min and V_L= 5000 m/min crystalline phase.

Figure 8-25 shows that, for the same take-up speed, both the diameter and velocity the profiles plateau at approximately the same value. This influences the tensile stress and orientation profiles. It can be said that since the velocity and diameter profiles remain constant, only the decreasing temperature profiles have the effect of increasing the tensile stress and, consequently, molecular orientation even though the temperature drops below the glass transition temperature.

8.5.3 Summary

In the first part of this section, average property trends were plotted for various take-up speeds and observations made. The following points summarise the finding of this section:

(i) increased take-up velocities result in a small decrease in the amount of heat transferred as well as an increased variance in the inter filament temperature.

This is attributed to lower contact times between the filament and cooling medium at high wind-up speeds,

(ii) take-up velocity greatly affects the final degree of crystallinity. Increased levels of crystallinity are obtained at greater wind-up speeds as a result of increased tensile stress, and

(iii) increased levels of molecular orientation are achieved for faster take-up speeds. This is directly related to the increased levels of tensile stress associated with greater wind-up speeds.

The second part of this section discussed the freezeline and take-up point variances. Secondly, simulations for take-up speeds at 2000 m/min and 5000 m/min (cr) were compared and scrutinised more closely. The following points summarise this section.

(iv) A decrease in the tensile stress and orientation variance is obtained for increasing take-up velocities. This is as result of increased contact times between the filament and passing quench air at lower wind-up speeds,

(v) property variance decreases from the freezeline to the take-up point. This is attributed to the constant velocity and diameter profiles leaving the temperature profiles as the only changing variable in zone 3. Thus, the overall effect is a decrease in the orientation variance,

(vi) increased variance in crystallinity is observed for higher take-up velocities. This is caused by the difference in variance between the filament temperature profiles and, as such, can be related to the difference in amount heat transfer as a result in varying contact times between the filament and passing quench air,

(vii) the velocity and diameter profiles correspond to a significant degree with increased take-up speeds resulting in decreased final filament diameters. This is caused by increased attenuation rates at higher take-up speeds.

The above findings illustrate the effects of various take-up speeds on final product property uniformity. In summary in can be said that take-up velocity does influence the degree of property uniformity to some degree and, as such, is a critical process parameter which should be carefully controlled in industrial spinning rigs.

Part D: Closure

9 Conclusion

The previous chapter illustrates the influence of various process conditions (i.e. quench air temperature and velocity, polymer extrusion rate and temperature and take-up velocity) on the general dynamics of the melt spinning system in question and, specifically, which process variable impacts the system dynamics to the largest extent. The effects of changing these process conditions on the degree of property uniformity of the as-spun product is also established. As highlighted in previous chapters, the major focus of this thesis is to determine the effects of non-uniform quench thermal gradients across the bundle on the degree of property variation of the as-spun product. This is well documented in the previous chapter.

The following section seeks to draw conclusions based on the findings in chapter 8. Firstly, conclusions are drawn based on the effects of the above mentioned process conditions on the general dynamics of the hot tube melt spinning system and degree of as-spun property variation. Secondly, optimum process conditions are proposed based on the degree of product property uniformity. Lastly, recommendations for future work based on the scope of the present investigation are suggested.

9.1 Results

Simulation results showed that quench conditions significantly affect system dynamics. Large differences in the magnitude of thermal gradients were obtained for the various quench conditions applied. The variation in quench air temperature is as a result of heat transfer limitations between the quench air and the fibres. Fibres simulated under high quench velocities exhibited higher cooling rates when compared to low quench velocities. However, low quench velocities yield higher contact times between the filaments and the quench air resulting in a larger amount of heat transfer taking place and, in turn greater quench air temperature variation across the bundle. It was found that the degree of property variance is directly related to the magnitude of temperature variation of the quench air across the bundle. The degree of variance in structural properties such as orientation and tensile force were significantly influenced by quench conditions as a result of the varying cooling rates. Although higher orientation factors were achieved under conditions of increased heat transfer between the filaments and the quench air, a greater degree in variance in these properties was obtained. This suggests that a trade off exists in the maximum degree of orientation achieved to the magnitude of non-uniformity across the bundle. It was found that higher cooling rates corresponded to the lowest variance in tensile stress and orientation. The results showed that altering initial quench conditions does not influence the final magnitude of orientation achieved to a significant degree but affects the degree of property uniformity to a large extent.

The influence of extrusion rate is less evident when compared with altering quench conditions. However, it was found that higher extrusion rates decreased heat transfer rates through decreased filament attenuation. These factors caused higher online temperatures and, in turn, lower tensile stresses and molecular orientation factors. Although elongation at break was not predicted in this simulation, it can be said that increased degrees of orientation result in a decrease in the elongation at break of the fibre (Ziabicki 1976). This indicates an increase in the tensile strength of the yarn under these conditions. Increasing the extrusion rate had the result of increased variance in structural properties as a result of increased variance in the quench thermal gradients. Increased final property uniformity and orientation is limited by online tensile stress levels tending toward conditions which could lead to filament breakage.

Simulation results showed extrusion temperature to have the least impact on the melt spinning dynamics. However, it was shown that heat transfer rates between the filaments and the quench air are influenced by the changing the extrusion temperature. This is as a result of altered temperature gradients influencing the heat transfer driving force between the two phases. Negligible change in the final magnitude of property values as well property variance across the bundle occurred as a result of altering the extrusion rate.

Results indicated that fibre take-up velocity had a significant influence on system dynamics whereas the effects on property uniformity are relatively less significant when compared to other process conditions. An increase in take-up velocity resulted in elevated cooling rates and greater levels of tensile stress and, in turn, final increased orientation and crystallisation being achieved. This corresponds to a yarn with a lower elongation at break and higher tensile strength. The degree of property variance increased to a small extent with increased take-up speeds. With this being said, the inter-filament variance in final crystallinity showed a marked increase of 17%. This is as a consequence of the sensitivity of crystallisation kinetic activity to online tensile stress and temperature. It was shown that at higher take-up velocities, SIC effects influence online property behaviour. Specifically, tensile stress and orientation increased significantly with the occurrence of crystallisation. This coincided with a decrease in final property variance.

It was shown that final property variance is always lower when compared to the freezeline variance. This was firstly attributed to the limitation of physical properties such as molecular orientation to an asymptotic value. Secondly, results showed that after the freezeline point, only temperature and tensile stress still vary whilst local filament velocity and diameter converged to a single value. This contributed to the decrease in final property variation.

In light of the results obtained and the findings listed above, Table 9-1 summarises the influence of the tested process variables on both system dynamics and final property variation.

Table 9-1: Effects of process variables on final structural properties and variance

Process variable	d (um)	X (%)	Δp (dyne/cm^2)	f_a (-)	FPV* (%)
↑ V_a	-	-	↓	↓	↓
↑ T_a	-	-	↑	↑	↓
↑ W	↑	↓	↓	↓	↑
↑ T_0	-	↓	-	-	-
↑ V_L	↓	↓	↑	↑	↓

*Final property variance

9.2 Optimum process conditions

Optimum process conditions lead to a stable spinning process and a product which is of good quality. In this simulation this is characterised by high uniformity of the as-spun fibre properties. Added to this, a fibre which has high molecular orientation has a lower elongation at break and therefore has a greater tensile strength than lower orientated fibres. The following process conditions are deemed as the optimum:

- intermediate quench air temperature and speeds (18-22^{o}C and 0.5-0.7 m/s). This is due to the trade-off between increased property variance and decreased orientation. As such, in order to obtain a yarn which has a good tensile strength and quality, intermediate quench air speeds should be applied, and

- low extrusion rates. This does limit final product output rate however, considering the costs of high quality synthetic yarns with good tensile strength used in the safety apparel industry, the profit obtained in producing this kind of yarn would most likely out way lower quality yarn produced at higher outputs. Added to this, many rigs running in parallel would compensate for the lower product output rate at reduced extrusion rates. However, the trade off between possible filament breakage and increased levels of final product uniformity and orientation must be established in order to determine system stability limits.
- Low extrusion temperatures: the extrusion temperature has negligible effect on both orientation and final property variance. However, it is restricted by the thermal limitations of the polymer. On the other hand, lower extrusion temperatures would result in lower energy requirements and hence lower operating costs and reduce the risk of thermal degradation of the polymer, and lastly
- high take-up velocities are recommended. This results in increased orientation and, as a result, a yarn with a higher degree of tensile stress. Low as-spun property variances are predicted as these conditions. As such, a good quality yarn will be produced at high production rates.

It is predicted that the above conditions will result in a good quality yarn with a high tensile strength. Many process variables induce trade-offs between final property variance and magnitude of orientation achieved. Highly orientated as-spun yarn is desired as this negates further drawing of the yarn. This would further reduce process costs.

9.3 Recommendations for future work

Much experimental work in the field of synthetic fibre dynamics has been carried out in the past. In light of this, a multifilament model was developed which estimates the online properties of the filaments which make up the final fibre. Since this model captures all of the observed effects, experimental work can be carried out to confirm that the optimisations recommended in this work will improve productivity.

The results presented in chapter 8 show that even with the assumption of idealised quench air flow, significant inter-filament property variance still occurs. As such, it is safe to say that should filament bundle air drag effects be taken into account, the observed heat transfer effects would be magnified. With this being said, it is suggested that the CFD work developed by Harvey and Doufas (2007) be coupled with the approach proposed here. By coupling the two models accurate predictions of the quench properties (velocity and temperature) as well as the key fibre properties (crystallinity, orientation) could be made. It must be noted here that all previous multifilament work focussed on the model development and estimated either fibre properties or quench properties. One aspect that could lend some degree of novelty to this investigation is the attempt to combine both these aspects into a single model which predicts the final properties of the final as-spun yarn.

In order for this model to be run in real time, the simulation time must be reduced from 15 hrs to in the order of minutes. This could be carried out by incorporating an algorithm which reduces the force range over which the initial value must be found in order to achieve the final take-up velocity. This work would be restricted by assumptions based on the harmonic effect of filaments cause by the quench air stream. This would affect mesh generation due the moving boundary of the filament surface.

This investigation only tested the influence of process conditions on the uniformity of as-spun fibre properties. An investigation into the effects of other system variables such as the positioning of the quench and hot-tube zones, spinneret geometry and the possible addition of baffles to the system in order reduce quench air flow alterations would provide valuable process design insight.

All in all, the science behind the production of synthetic fibres through melt spinning is a broad field of study. This thesis has shown the complexity inherent in any melt spinning system due to heat transfer effects between the quench air and the filament bundle. The current investigation highlights the effects of non-uniform quench air conditions on the final properties of the as-spun yarn. Based on this, the results obtained from the performed investigation gives good insight into further modelling directions.

References

1. Abhiraman A.S., Hagler G.E., *'Melt spinning of polymers I. An elementary framework for analysing the development of orientation'*, Journal of Applied Polymer Science, **33**, 809-823 (1987).

2. Andreassen E., Myhre O.J., Oldervoll F., Hinrichsen E.L., Grostad K. and Braathen M.D., "*Non-uniform Cooling in Multifilament Melt Spinning of Polypropylene Fibers: Cooling Air speed Limits and Fiber-to-Fiber Variations* ", Journal of Applied Polymer Science, **58**, 1619-1632 (1995).

3. Andrews E.H., '*Cooling of a spinning thread-line'*, British journal of applied physics, **10**, 39-43 (1958).

4. Apiwanthanakorn N., Supaphol P., Nithitanakul M., '*Non-isothermal melt-crystallisation kinetics of polymer(trimethylene Terephthalate)*', Polymer Testing, **23**, 817-826 (2004).

5. Barnette T.R., "*Calculation of the Temperature of Filaments in Melt Spinning*", Applied Polymer Symposia, No. 6, 51-65 (1965).

6. Beyreuther R., "*Modeling and use of Models for Describing Processes in Spinning of Fibres from Melt*", Fibre chemistry, **26**, 231-242 (1994).

7. Beyreuther R., Schauer C. and Schoene A., *'History, present state and future of high speed spinning'*, Acta polymerica, **40**, 695-702 (1989).

8. Bragato G., and Gianotti G., "*High Speed Spinning of PET I: Steady State Equations Fundamental Analysis. Structural Property measurement along the Spinning path*", *Eur. Polym. J.*, **19**, 795-802 (1983).

9. Chung B.T.F. and Iyer V., "*Heat Transfer from Moving Fibers in Melt Spinning Process*", Journal of Applied Polymer Science, **44**, 663-670 (1992).

10. Dees J.R. and Spruiell J.E., '*Structure development during melt spinning of PET fibers'*, Journal of Applied Polymer Science, **18**, 1053-1078 (1974).

11. Di Lorenzo M.L and Silvestre C, *"Non-isothermal crystallisation of polymers"*, Progress in Polymer Science, **24**, 917-950 (1999).

12. Doufas A.K., McHugh A.J., Miller C., '*Simulation of melt spinning including flow induced crystallisation Part I: Model development and predictions'*, *J. Non-Newtonian Fluid Mech.*, **92**, 27-66 (2000).

13. Doufas A.K., McHugh A.J., Miller C., '*Simulation of melt spinning including flow induced crystallisation Part II: Quantitative comparisons with industrial spinline data'*, *J. Non-Newtonian Fluid Mech.*, **92**, 81-103 (2000).

14. Dutta A., "*Application of Computer Simulation in PET Melt Spinning"*, America's Textiles, April, 78-88 (1986).

15. Dutta A., "*Estimating the Variability of PET Spun Fiber Properties Using Computer Simulation*", Textile Research Journal, 411-415, July (1989).

16. Dutta A., "*Melt Spinning of (Multifilament) Poly(Ethylene Terephthalate) Fibers: A simulations Approach"*, Polymer Engineering and Research, **27**, 1050-1058 (1987).

17. Dutta A. and Nadkarni, V.M., "*Identifying Critical Process Variables In Poly(Ethylene Terephthalate) Melt Spinning*", *Textile Res. J,* **54**, 35-42 (1982).

18. Forbes P, "*The Gecko's foot"*, pg 9-11, Harper Perennial, Great Britain (2006).

19. Gagon D.K. and Denn M.M., "*Computer Simulation of Steady Polymer Melt Spinning*", Polymer Engineering and Science, **21**, No. 13, 844-855 (1981).

20. Galeski. A., "*Strength and toughness of crystalline polymer systems*", Prog. Polym. Sci., **28**, 1643-1699 (2003).

21. George H.H., "*Model of Steady State Melt Spinning at Intermediate Take-Up Speeds*", *Polym. Eng. Sci,* **22**, 292-299 (1982).

22. George H.H., Holt A. and Buckley A., "*A Study of the Structural Development in High Speed Spinning of Poly(Ethylene Terephthalate)* ", Polymer Engineering and Science, **23**, 95-99 (1983).

23. Gotz T., Rave H., Reinel-Bitzer D., Steiner K. and Tiemeier H., " *Simulation of the fiber spinning process*", Berichte des Fraunhofer ITWM, No. 26, 1-12 (2001).

24. Hahn B.D., *'Essential MATLAB® for Scientists and Engineers'*, Third Edition, Pearson Education South Africa, Forest Drive, Pinelands, Cape Town (2002).

25. Hamana I., Matsui M. and Kato S., "*Der Veluaf der Fadenbildung beim Schmelzspinnene*" Melliand Textilberichte, **4**, 382-392, (1969).

26. Harder C., "*Finite element analysis",* Journal of materials processing technology, **118,** 454-459 (2001).

27. Harvey A.D. and Doufas K.D., "*Coupled Computational Fluid Dynamics and Multifilament Fiber-Spinning Model*", American Institute of Chemical Engineers, **53**, 78-90 (2007).

28. Heuvel H.M, Lucas L.J, van den Heuvel C.J, De Weijer, "*Experimental relations between physical structure and mechanical properties of a huge number of drawn poly(Ethylene Terephthalate) yarns",* Journal of Applied Polymer Science, (1992).

29. http://www.engineeringtoolbox.com/air-properties-d_156.html, 23 April 2008, 15:49.

30. Ishihara H., Hayashi S. and Ikeuchi H., "*Computer Simulation of Melt filament Air Jet Melt Spinning*", Intern. Polymer Processing, **2**, 91-95 (1989).

31. Jarecki L., Ziabicki A. and Blim A., "*Dynamics of hot tube spinning from crystallizing polymer melts*", Computational and Theoretical Polymer Science, **10**, 63-72 (2000).

32. Jaydeep A., Kulkarny A. and N. Beris, "*Lattice-based simulations of chain conformations in semi-crystalline polymers with application to flow-induced crystallisation",* Journal Non-Newtonian Fluid Mechanics, **82**, 331-366 (1999).

33. Kase S. and Matsuo T., "*Studies on melt spinning. I. Fundamental Equations on the dynamics of melt spinning*", *J. Polym. Sci*, **3**, 2541-2554 (1965).

34. Kase S. and Matsuo T., "*Studies on melt spinning. II. Steady-State and Transient Solutions of the Fundamental Equations Compared with Experimental Results*", *J. Polym. Sci*, **11**, 251-287 (1967).

35. Kase S. and Matsuo T., "*Studies on melt spinning. IV. On the Stability of Melt Spinning*", *J. Polym. Sci*, **18**, 3279-3304 (1974).

36. Lee J.S, Shin D.M, Jung H.J. and Hyun J.C, "*Transient solutions of the dynamics in low-speed fibre spinning process accompanied by flow-induced crystallization*", J. Non-Newtonian Fluid Mech., **130**, 110–116 (2005).

37. Yu Long, Roberts A.S. and Stachurski Z.H., "*Kinetics of Polymer Crystallisation"*, *Prog. Polym. Sci.*, **20**, 651-671 (1995).

38. Matsuo T., "*Air drag on a Continuous Filament in Melt Spinning*", Transaction of the Society of Rheology, **20**, 465-473 (1976).

39. McHugh A.J. and Doufas A.K., *'Modelling flow induced crystallisation in fiber spinning*', Composites: Part A, **32**, 1059-1066 (2001).

40. Mubarak Y., Harkin-Jones E.M.A., Martin P.J. and Ahmad M., "*Modeling of non-isothermal crystallization kinetics of isotactic polypropylene*", Polymer, **42**, 3171-3182 (2001).

41. Papanastatiou T.C., Macosko C.W., Scriven L.E. and Chen Z., "*Fiber spinning of viscoelastic fluid"*, **33**, 834-842 (1987).

42. Phan-Thien, N., *"A Nonlinear Network Viscoelastic Model"*, *J. Rheology,* **22**, 259-283 (1978).

43. Prastaro A., Parrini P., "*A Mathematical Model for Spinning Molten Polymers and Conditions of Spinning",* Textile Research journal, **45**, 118-127 (1975).

44. Ramos J.I., "*Modelling of liquid crystalline compound fibres"*, Polymer, **46,** 12612–12625 (2005).

45. Sharpe J.R.T, "*The basics of yarn making for students",* July 2002, South African Nylon Spinners, Bellville, Cape Town.

46. Shenoy A.V. and Nadkarni V.M., "*Using Poly(Ethylene Terephthalate) Melt Spinning Simulation for Process optimisation*", Textile Research Journal, November, 778-782 (1984).

47. Thompson W.J., '*Introduction to Transport Phenomena*', Prentice Hall PTR, New Jersey, pg. 54-55 (2000).

48. Vassilatos G., Schmelzer E.R. and Denn M.M., "*Issues concerning the rate of heat transfer from a spinline*", Intern. Polymer Processing VII, **2**, 144-150 (1992).

49. White J.L., Cakmak M., "*Orientation development and crystallisation in melt spinning of fibers"*, Advances in Polymer Technology, **6**, 295-338 (1986).

50. Winterton R.H.S., "*Heat Transfer*", Oxford University Press, Great Claredon Street, New York (1997).

51. Zang C., Wang C., Wang H. and Zhang Y., "*Multifilament Model PET Melt Spinning and Prediction of As-spun Fiber's Quality*", Journal of Macromolecular Science Part B: Physics, **46**, 793-806 (2007).

52. Ziabicki A., "Crystallisation *of polymers in variable external conditions*", Colloid Polymer Science, **274**, 209-217 (1996).

53. Ziabicki A., *"Fundamentals of Fiber Formation: the science of fiber spinning and drawing"*, John Wiley & Sons, London (1976).

54. Ziabicki A., "*Kinetics of polymer crystallisation and molecular orientation in the course of melt spinning*", Applied Polymer Symposia, **6**, 1-18 (1967)

55. Ziabicki A., *"Polymer crystallisation in complex conditions. Towards a more realistic modelling of industrial processes"*, *Macromol. Symp.*, **175**, 225-238 (2001).

56. Ziabicki A., Jarecki L., "*The theory of non-linear molecular orientation and stress in polymer fluids",* Colloid and Polymer Science, **264**, 343-351 (1986).

57. Ziabicki A., Jarecki L., Wasiak A., "*Dynamic modelling of melt spinning"*, Computational and Theoretical Polymer Science Vol. **8**, 143-157 (1998).

58. Ziabicki A., Kedzierski K., *'Studies on the Orientation Phenomena by Fiber Formation from Polymer Melts. III. Effect of Structure Orientation. Condensation polymers"*, Journal of Applied Polymer Science, **6**, 111-119 (1962).

Appendix A: Property profiles

A.1 Conventional model

The following profiles were obtained for simulations run at the extreme values of the process variable ranges that were tested. This was done to save space and unnecessary reproductions of profiles.

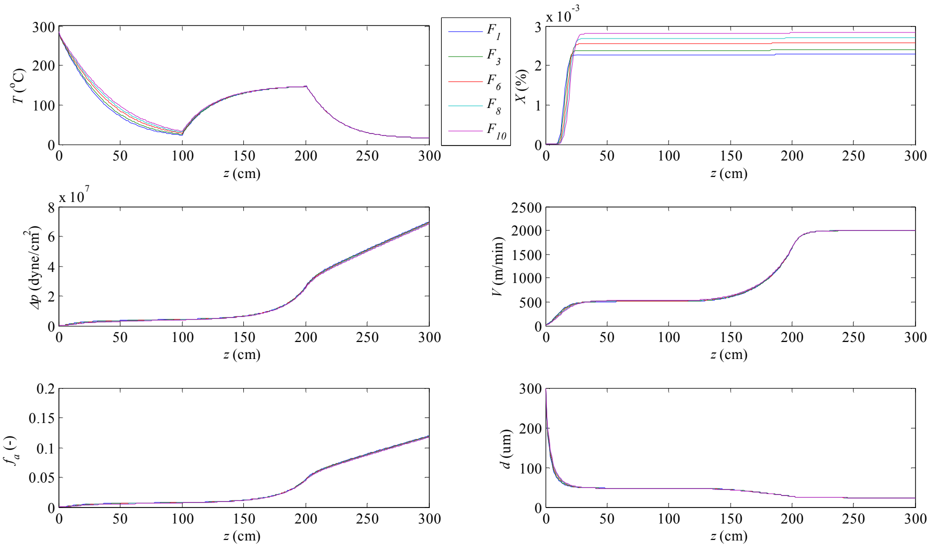

Figure A-1: Property profiles for W=0.02 g/s, T_a=15^{0}C, V_a=0.4m/s, T_0=285^{0}C and V_L=2000m/min obtained using the conventional model.

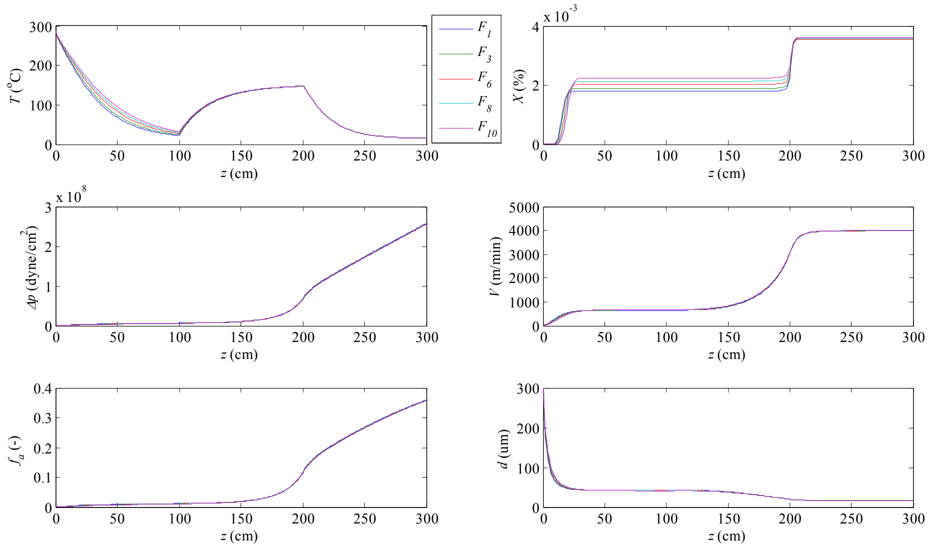

Figure A-2: Property profiles for W=0.02 g/s, T_a=15^{0}C, V_a=0.4m/s, T_0=285^{0}C and V_L=4000m/min (cr) obtained using the conventional model.

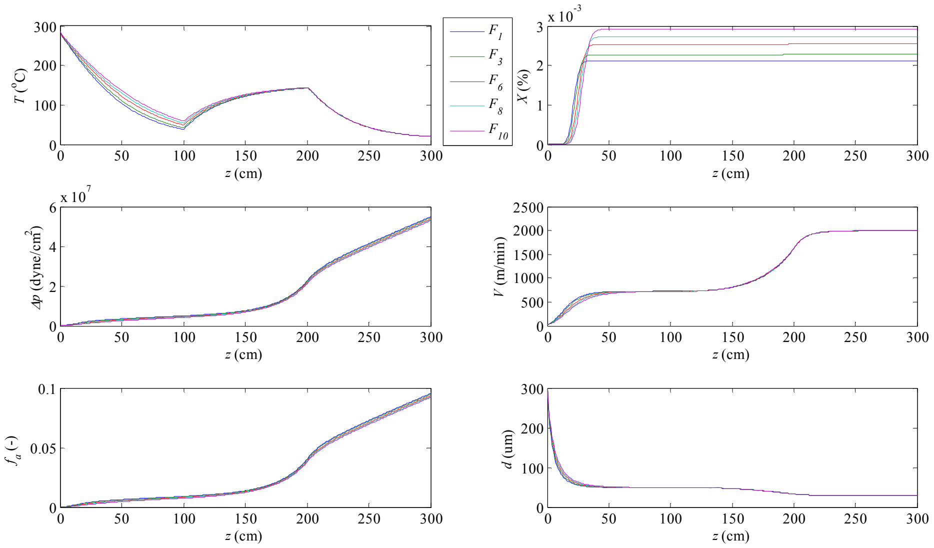

Figure A-3: Property profiles for W=0.03 g/s, T_a=15^{0}C, V_a=0.4m/s, T_0=285^{0}C and V_L=2000m/min obtained using the conventional model.

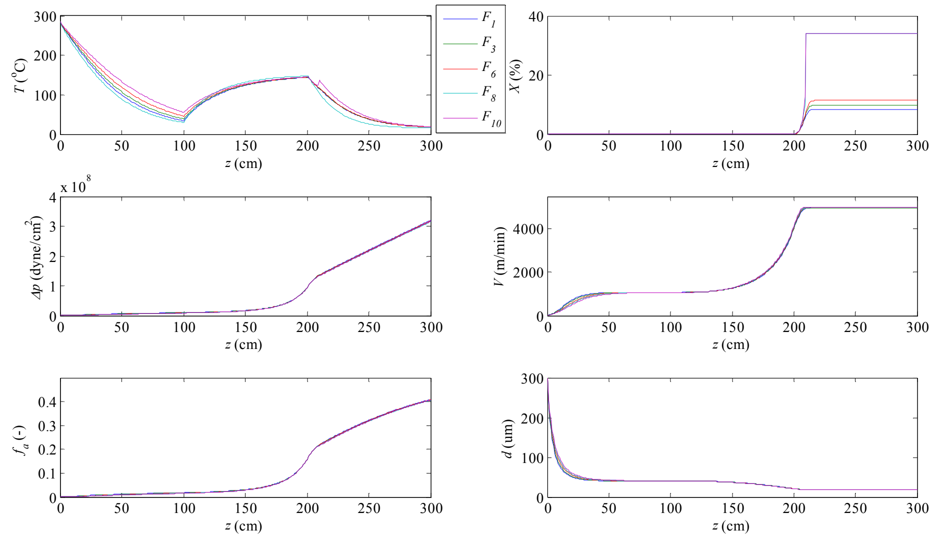

Figure A-4: Property profiles for W=0.03 g/s, T_a=15^{0}C, V_a=0.4m/s, T_0=285^{0}C and V_L=5000m/min (cr) obtained using the conventional model.

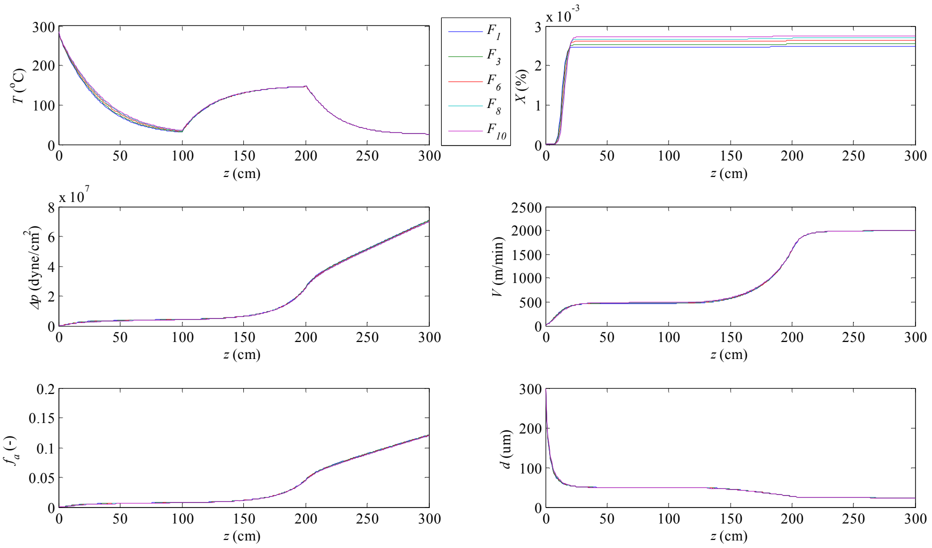

Figure A-5: Property profiles for W=0.02 g/s, T_a=25^{0}C, V_a=0.8m/s, T_0=285^{0}C and V_L=2000m/min obtained using the conventional model.

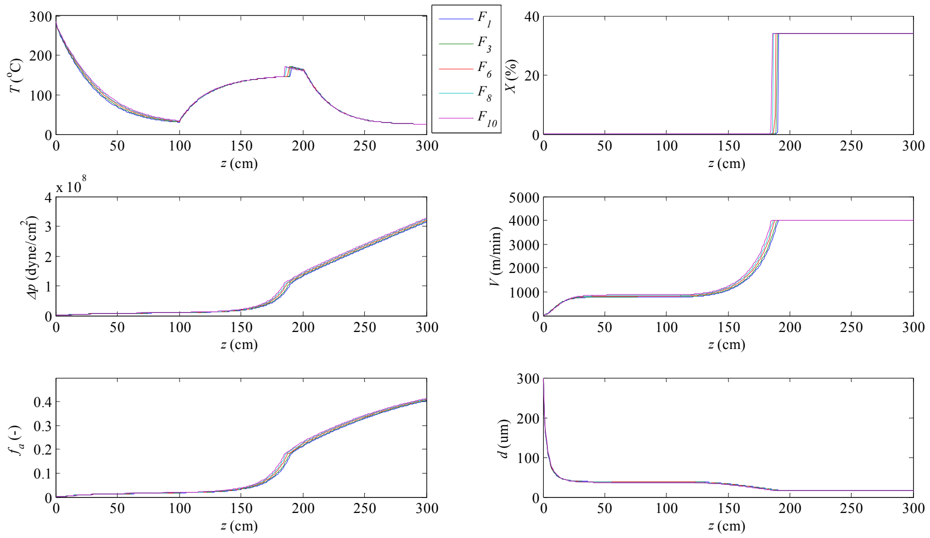

Figure A-6: Property profiles for W=0.02 g/s, T_a=25^{0}C, V_a=0.8m/s, T_0=285^{0}C and V_L=4000m/min (cr) obtained using the conventional model.

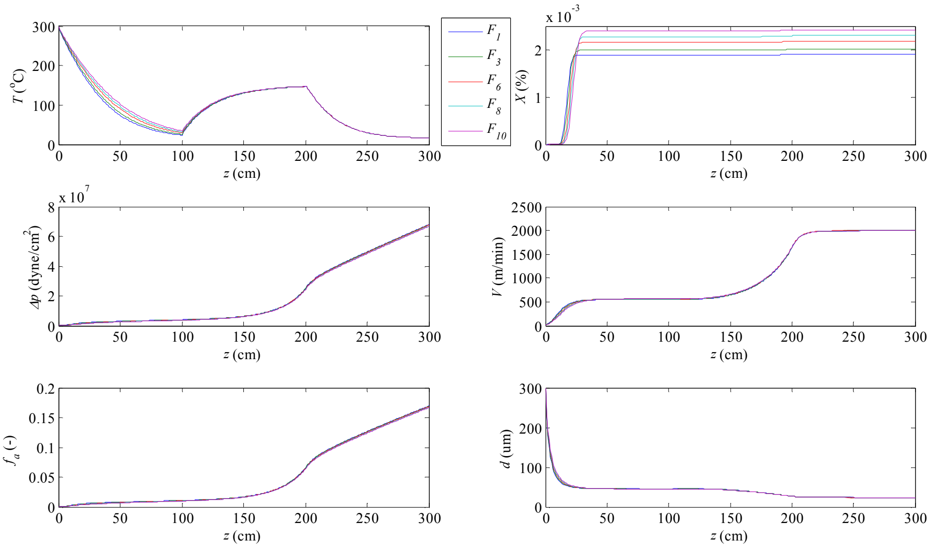

Figure A-7: Property profiles for W=0.02 g/s, T_a=15^{0}C, V_a=0.4m/s, T_0=300^{0}C and V_L=2000m/min obtained using the conventional model.

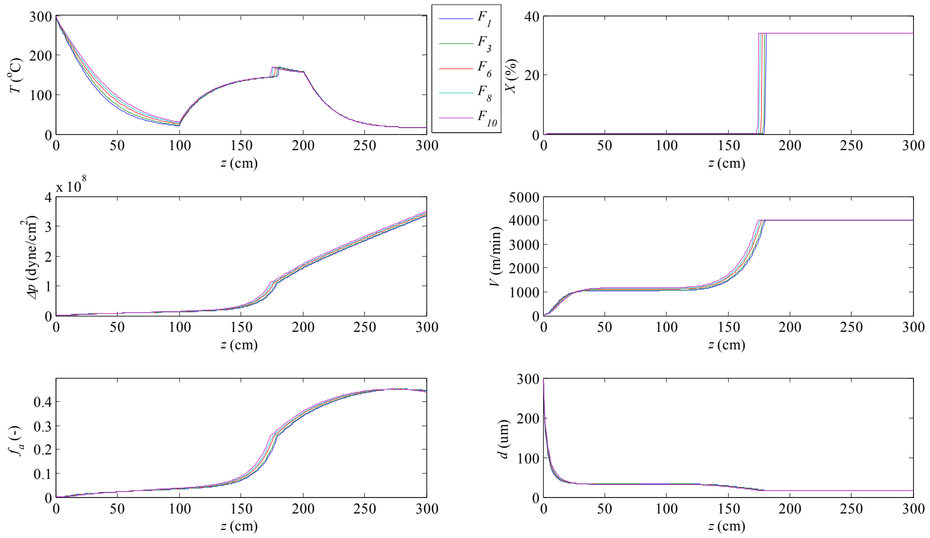

Figure A-8: Property profiles for W=0.02 g/s, T_a=15^{0}C, V_a=0.4m/s, T_0=300^{0}C and V_L=4000m/min (cr) obtained using the conventional model.

A.2 Iteration model

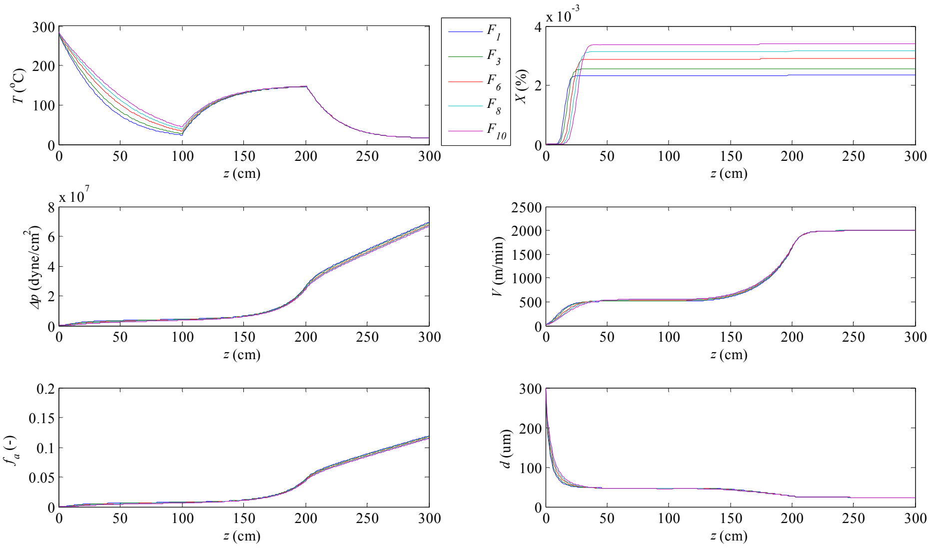

Figure A-9: Property profiles for W=0.02 g/s, T_a=15^{0}C, V_a=0.4m/s, T_0=285^{0}C and V_L=2000m/min obtained using the iteration model.

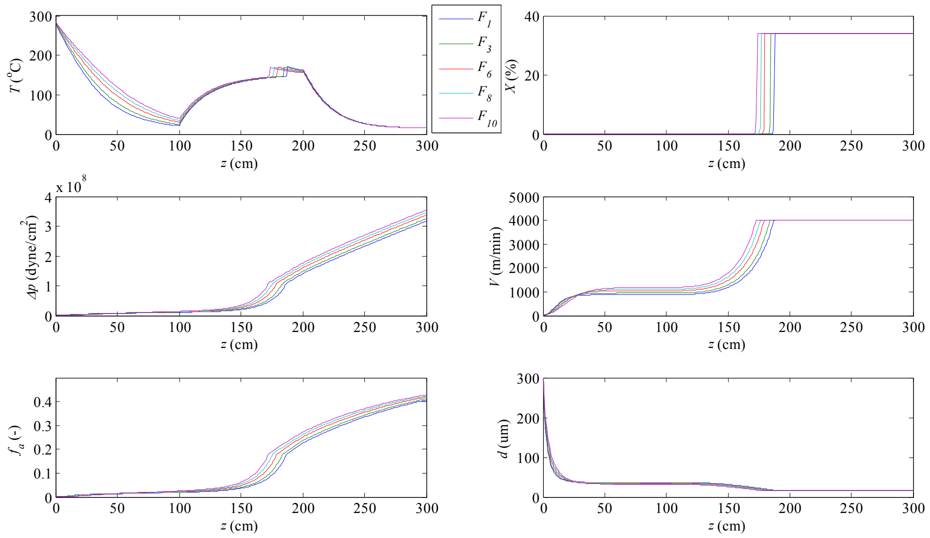

Figure A-10: Property profiles for W=0.02 g/s, T_a=15^{0}C, V_a=0.4m/s, T_0=285^{0}C and V_L=4000m/min (cr) obtained using the iteration model.

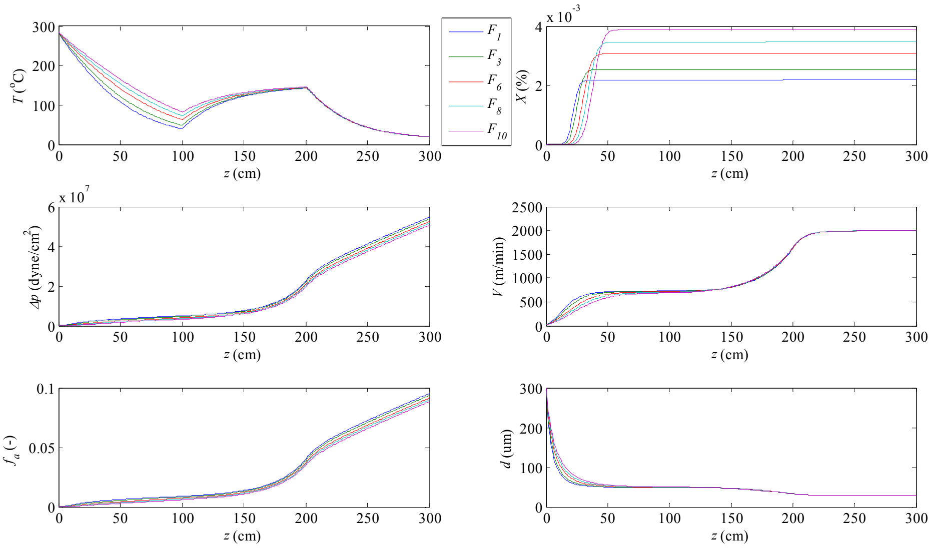

Figure A-11: Property profiles for W=0.03 g/s, T_a=15^{0}C, V_a=0.4m/s, T_0=285^{0}C and V_L=2000m/min obtained using the iteration model.

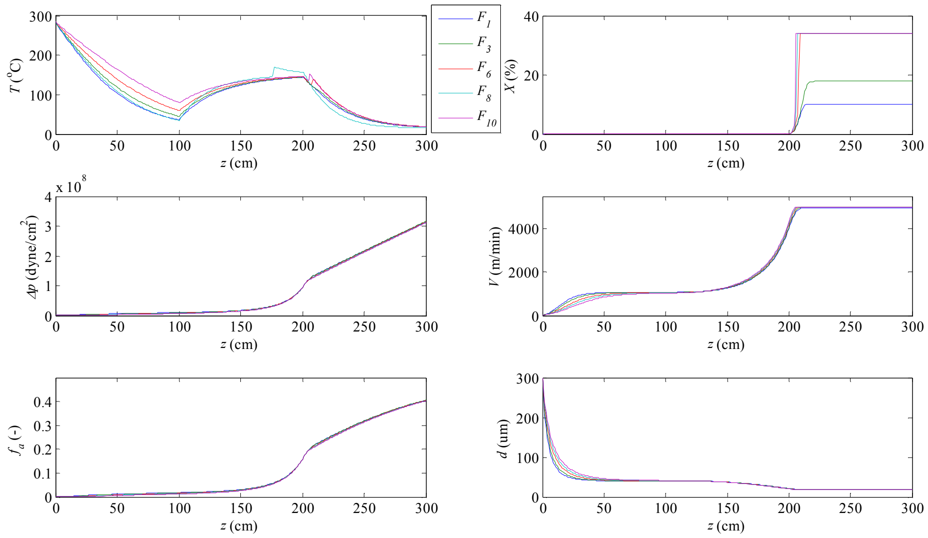

Figure A-12: Property profiles for W=0.03 g/s, T_a=15^{0}C, V_a=0.4m/s, T_0=285^{0}C and V_L=5000m/min (cr) obtained using the iteration model.

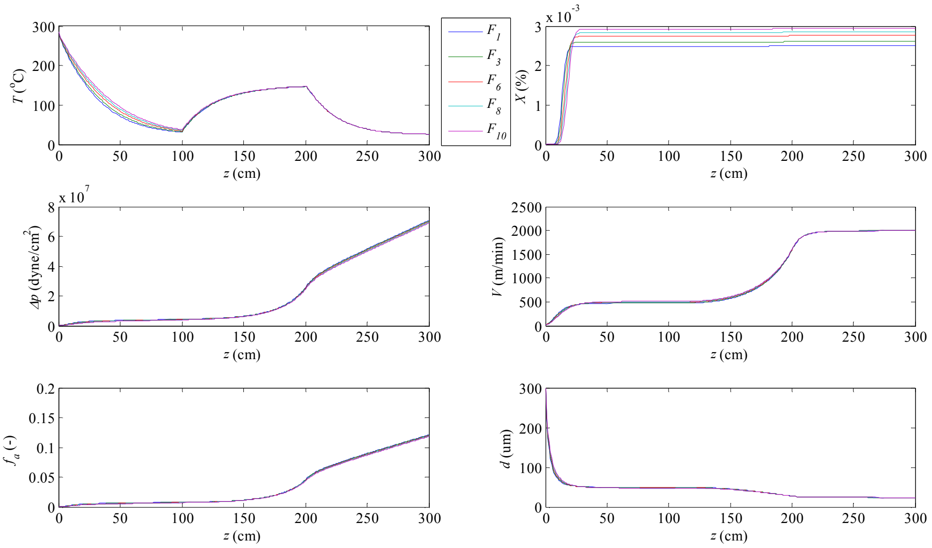

Figure A-13: Property profiles for W=0.02 g/s, T_a=25^{0}C, V_a=0.8m/s, T_0=285^{0}C and V_L=2000m/min obtained using the iteration model.

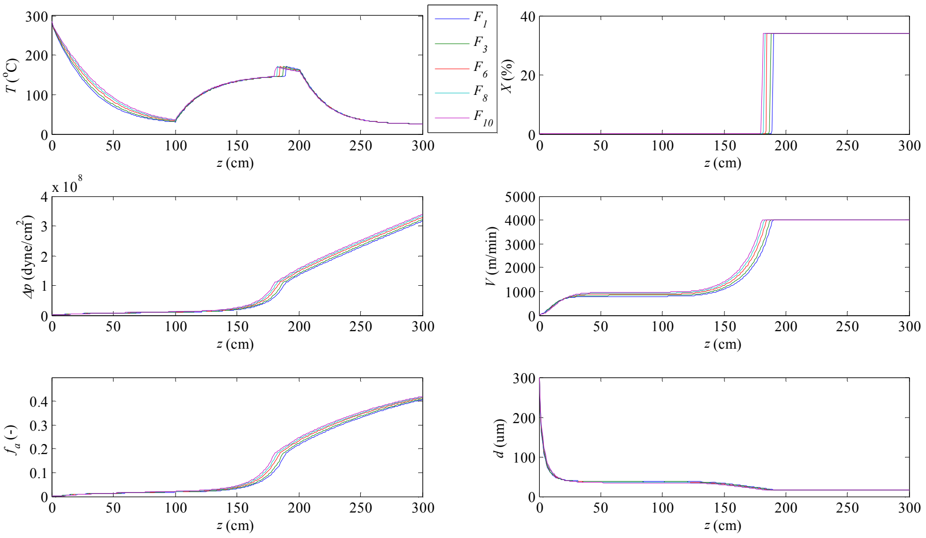

Figure A-14: Property profiles for W=0.02 g/s, T_a=25^{0}C, V_a=0.8m/s, T_0=285^{0}C and V_L=4000m/min (cr) obtained using the iteration model.

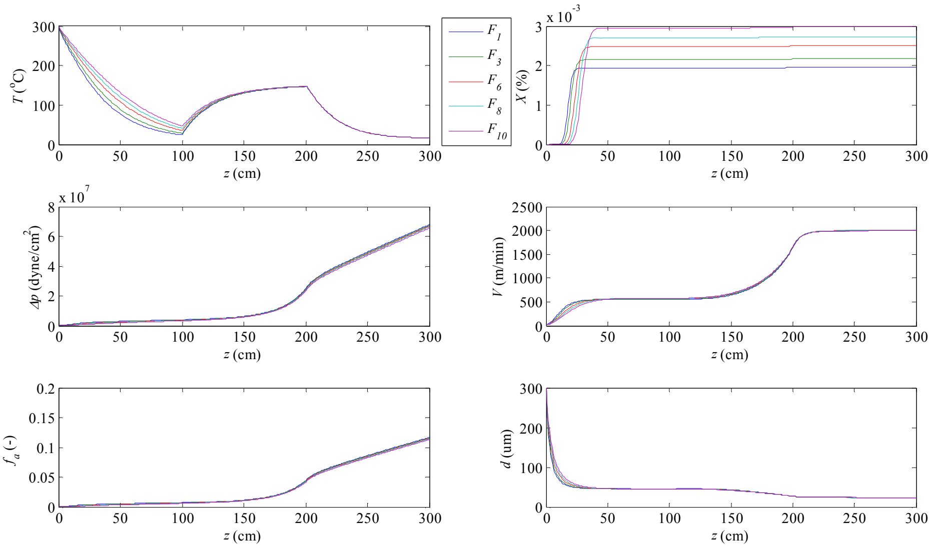

Figure A-15: Property profiles for W=0.02 g/s, T_a=15^{0}C, V_a=0.4m/s, T_0=300^{0}C and V_L=2000m/min obtained using the iteration model.

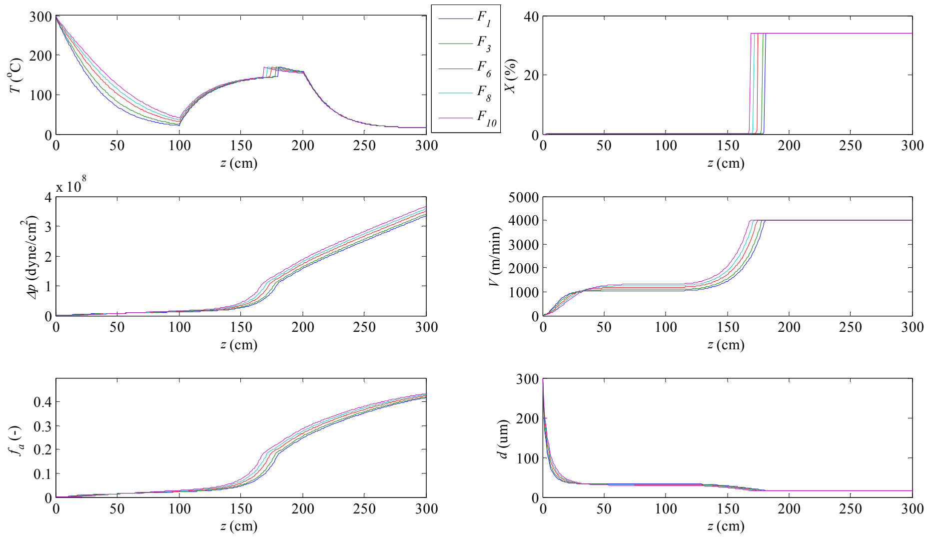

Figure A-16: Property profiles for W=0.02 g/s, T_a=15^{0}C, V_a=0.4m/s, T_0=300^{0}C and V_L=4000m/min (cr) obtained using the iteration model.

Appendix B: Property variances

B.1 Average property variance

B.1.1 Average quench temperature variance

Table B-1: AV (%) predicted by Iteration model (W=0.02 g/s, T0 = 300oC)

V_a	T_a	V_L (m/min)			
(m/s)	(°C)	2000	3000	4000 am	4000 cr
0.4	15	37.56	37.56	37.55	37.49
	20	33.13	33.13	33.13	33.10
	25	29.65	29.65	29.66	29.65
0.6	15	29.42	29.40	29.40	29.31
	20	25.38	25.38	25.38	25.33
	25	22.32	22.32	22.32	22.32
0.8	15	24.15	24.17	24.17	24.17
	20	20.54	20.55	20.55	20.57
	25	17.85	17.86	17.87	17.89

Table B-2: *AV* (%) predicted by Iteration model (*W*=0.03 g/s, T_0 =300°C)

V_a	T_a	V_L (m/min)				
(m/s)	(°C)	2000	3000	4000	5000 am	5000 cr
0.4	15	44.60	44.65	44.68	44.70	44.73
	20	40.30	40.35	40.37	40.40	40.43
	25	36.72	36.77	36.80	36.82	36.84
0.6	15	37.96	37.98	38.01	38.02	38.04
	20	33.40	33.43	33.45	33.47	33.48
	25	29.78	29.81	29.84	29.86	29.88
0.8	15	32.75	32.78	32.80	32.82	32.83
	20	28.27	28.30	28.33	28.34	28.35
	25	24.84	24.86	24.88	24.91	24.92

Table B-4: *AV* (%) predicted by Iteration model (*W*=0.02 g/s, T_0=285°C)

V_a	T_a	V_L (m/min)			
(m/s)	(°C)	2000	3000	4000 am	4000 cr
0.4	15	36.42	36.42	36.42	36.37
	20	31.98	31.99	31.98	31.96
	25	28.50	28.51	28.51	28.52
0.6	15	28.29	28.28	28.28	28.24
	20	24.30	24.30	24.30	24.29
	25	21.28	21.29	21.30	21.31
0.8	15	23.15	23.16	23.17	23.17
	20	19.60	19.61	19.61	19.63
	25	16.96	16.97	16.98	17.01

Table B-3: *AV* (%) predicted by Iteration model (*W*=0.03 g/s, T_0=285°C)

V_a	T_a	V_L (m/min)				
(m/s)	(°C)	2000	3000	4000	5000 am	5000 cr
0.4	15	43.63	43.68	43.72	43.74	43.76
	20	39.23	39.28	39.32	39.34	39.36
	25	35.58	35.63	35.67	35.69	35.71
0.6	15	36.82	36.86	36.89	36.90	36.91
	20	32.23	32.27	32.30	32.32	32.33
	25	28.61	28.66	28.69	28.71	28.72
0.8	15	31.58	31.61	31.62	31.64	31.65
	20	27.12	27.14	27.18	27.18	27.19
	25	23.71	23.74	23.77	23.79	23.80

Table B-5: *AV* (%) predicted by Conventional model (*W*=0.02 g/s, T_0=300°C)

V_a	T_a	V_L (m/min)			
(m/s)	(°C)	2000	3000	4000 am	4000 cr
0.4	15	28.08	28.04	28.01	27.82
	20	23.96	23.94	23.92	23.78
	25	20.89	20.88	20.87	20.77
0.6	15	22.12	22.11	22.10	22.00
	20	18.48	18.47	18.47	18.41
	25	15.84	15.85	15.84	15.81
0.8	15	18.34	18.35	18.35	18.31
	20	15.10	15.11	15.11	15.10
	25	12.81	12.82	12.82	12.82

Table B-6: *AV* (%) predicted by Conventional model (*W*=0.03 g/s, T_0=300°C)

V_a	T_a	V_L (m/min)				
(m/s)	(°C)	2000	3000	4000	5000 am	5000 cr
0.4	15	35.16	35.19	35.20	35.21	35.21
	20	30.58	30.61	30.62	30.63	30.64
	25	27.01	27.04	27.06	27.08	27.09
0.6	15	28.82	28.84	28.85	28.86	28.87
	20	24.45	24.48	24.50	24.51	24.51
	25	21.20	21.23	21.24	21.25	21.26
0.8	15	24.49	24.51	24.53	24.53	24.54
	20	20.44	20.46	20.48	20.49	20.49
	25	17.50	17.52	17.53	17.54	17.55

Table B-7: *AV* (%) predicted by Conventional model (*W*=0.02 g/s, T_0=285°C)

V_a	T_a	V_L (m/min)			
(m/s)	(°C)	2000	3000	4000 am	4000 cr
0.4	15	27.00	26.97	26.95	26.95
	20	22.95	22.94	22.93	22.93
	25	19.95	19.94	19.93	19.93
0.6	15	21.15	21.14	21.14	21.09
	20	17.60	17.60	17.60	17.58
	25	15.05	15.06	15.06	15.04
0.8	15	17.46	17.47	17.47	17.47
	20	14.34	14.35	14.35	14.35
	25	12.14	12.14	12.14	12.15

Table B-8: *AV* (%) predicted by Conventional model (*W*=0.03 g/s, T_0=285°C)

V_a	T_a	V_L (m/min)				
(m/s)	(°C)	2000	3000	4000	5000 am	5000 cr
0.4	15	34.13	34.16	34.17	34.18	34.18
	20	29.55	29.58	29.59	29.60	29.61
	25	26.00	26.03	26.05	26.06	26.07
0.6	15	27.82	27.84	27.86	27.86	27.87
	20	23.50	23.52	23.54	23.55	23.56
	25	20.29	20.32	20.34	20.35	20.36
0.8	15	23.55	23.57	23.59	23.60	23.60
	20	19.57	19.59	19.60	19.61	19.62
	25	16.69	16.71	16.72	16.74	16.74

B.1.2 Average filament temperature variance

Table B-9: *AV* (%) predicted by Iteration model (*W*=0.02 g/s, T_0 = 300°C)

V_a	T_a	V_L (m/min)			
(m/s)	(°C)	2000	3000	4000 am	4000 cr
0.4	15	15.02	15.30	15.48	16.00
	20	13.95	14.19	14.34	14.81
	25	13.00	13.21	13.34	13.76
0.6	15	11.09	11.21	11.30	11.47
	20	10.18	10.28	10.36	10.49
	25	9.42	9.50	9.56	9.68
0.8	15	8.77	8.80	8.84	8.83
	20	8.00	8.02	8.04	8.03
	25	7.36	7.37	7.39	7.36

Table B-10: *AV* (%) predicted by Iteration model (*W*=0.03 g/s, T_0 =300°C)

V_a	T_a	V_L (m/min)				
(m/s)	(°C)	2000	3000	4000	5000 am	5000 cr
0.4	15	13.26	13.64	13.89	14.07	14.15
	20	12.60	12.94	13.16	13.33	13.42
	25	11.99	12.30	12.50	12.65	12.74
0.6	15	10.21	10.46	10.64	10.77	10.83
	20	9.64	9.86	10.02	10.14	10.20
	25	9.11	9.32	9.46	9.56	9.62
0.8	15	8.31	8.47	8.59	8.69	8.73
	20	7.81	7.95	8.05	8.13	8.17
	25	7.36	7.47	7.56	7.64	7.67

Table B-11: *AV* (%) predicted by Iteration model (*W*=0.02 g/s, T_0=285°C)

V_a	T_a	V_L (m/min)			
(m/s)	(°C)	2000	3000	4000 am	4000 cr
0.4	15	14.65	14.90	15.07	15.26
	20	13.55	13.77	13.91	14.08
	25	12.59	12.78	12.90	13.06
0.6	15	10.79	10.89	10.96	10.87
	20	9.88	9.95	10.01	9.93
	25	9.11	9.17	9.22	9.14
0.8	15	8.57	8.56	8.58	8.53
	20	7.79	7.78	7.79	7.74
	25	7.14	7.12	7.13	6.98

Table B-12: *AV* (%) predicted by Iteration model (*W*=0.03 g/s, T_0=285°C)

V_a	T_a	V_L (m/min)				
(m/s)	(°C)	2000	3000	4000	5000 am	5000 cr
0.4	15	13.10	13.47	13.72	13.90	13.97
	20	12.41	12.74	12.96	13.12	13.20
	25	11.77	12.07	12.26	12.41	12.48
0.6	15	10.06	10.30	10.47	10.60	10.65
	20	9.47	9.68	9.83	9.94	9.99
	25	8.92	9.11	9.24	9.34	9.39
0.8	15	8.19	8.33	8.44	8.53	8.56
	20	7.67	7.79	7.88	7.95	7.98
	25	7.20	7.30	7.38	7.45	7.48

Table B-13: *AV* (%) predicted by Conventional model (*W*=0.02 g/s, T_0=300°C)

V_a	T_a	V_L (m/min)			
(m/s)	(°C)	2000	3000	4000 am	4000 cr
0.4	15	9.22	9.40	9.53	9.84
	20	8.47	8.62	8.72	8.98
	25	7.73	7.96	8.05	8.27
0.6	15	6.74	6.82	6.88	6.99
	20	6.15	6.21	6.26	6.34
	25	5.66	5.71	5.75	5.81
0.8	15	5.42	5.45	5.47	5.48
	20	4.92	4.94	4.95	4.95
	25	4.51	4.52	4.54	4.52

Table B-14: *AV* (%) predicted by Conventional model (*W*=0.03 g/s, T_0=300°C)

V_a	T_a	V_L (m/min)				
(m/s)	(°C)	2000	3000	4000	5000 am	5000 cr
0.4	15	8.40	8.69	8.88	9.02	9.08
	20	7.92	8.17	8.35	8.47	8.53
	25	7.48	7.71	7.86	7.97	8.03
0.6	15	6.20	6.38	6.50	6.59	6.63
	20	5.82	5.97	6.08	6.16	6.20
	25	5.48	5.62	5.71	5.78	5.82
0.8	15	5.00	5.11	5.19	5.25	5.28
	20	4.68	4.77	4.84	4.90	4.92
	25	4.40	4.48	4.54	4.58	4.61

Table B-15: *AV* (%) predicted by Conventional model (*W*=0.02 g/s, T_0=285°C)

V_a	T_a	V_L (m/min)			
(m/s)	(°C)	2000	3000	4000 am	4000 cr
0.4	15	8.98	9.15	9.26	9.26
	20	8.23	8.36	8.46	8.46
	25	7.59	7.70	7.78	7.78
0.6	15	6.59	6.65	6.70	6.62
	20	6.00	6.04	6.08	6.01
	25	5.50	5.54	5.57	5.51
0.8	15	5.34	5.34	5.35	5.25
	20	4.83	4.82	4.83	4.75
	25	4.41	4.41	4.41	4.32

Table B-16: *AV* (%) predicted by Conventional model (*W*=0.03 g/s, T_0=285°C)

V_a	T_a	V_L (m/min)				
(m/s)	(°C)	2000	3000	4000	5000 am	5000 cr
0.4	15	8.29	8.57	8.75	8.89	8.94
	20	7.79	8.03	8.20	8.32	8.37
	25	7.33	7.55	7.70	7.81	7.86
0.6	15	6.12	6.28	6.40	6.49	6.52
	20	5.73	5.87	5.97	6.05	6.08
	25	5.38	5.50	5.59	5.66	5.69
0.8	15	4.95	5.04	5.11	5.17	5.19
	20	4.60	4.70	4.76	4.81	4.82
	25	4.31	4.39	4.45	4.49	4.50

B.1.3 Average filament crystallinity variance

Table B-17: *AV* (%) predicted by Iteration model (*W*=0.02 g/s, T_0 = 300°C)

V_a	T_a	V_L (m/min)			
(m/s)	(°C)	2000	3000	4000 am	4000 cr
0.4	15	0.03	0.03	0.02	4.94
	20	0.03	0.03	0.03	4.76
	25	0.04	0.03	0.03	4.36
0.6	15	0.02	0.02	0.01	3.24
	20	0.02	0.02	0.01	3.16
	25	0.02	0.02	0.02	3.46
0.8	15	0.01	0.01	0.01	2.41
	20	0.01	0.01	0.01	2.68
	25	0.01	0.01	0.01	2.48

Table B-18: *AV* (%) predicted by Iteration model (*W*=0.03 g/s, T_0 =300°C)

V_a	T_a	V_L (m/min)				
(m/s)	(°C)	2000	3000	4000	5000 am	5000 cr
0.4	15	0.05	0.04	0.04	0.12	7.37
	20	0.05	0.05	0.04	0.08	1.75
	25	0.05	0.05	0.05	0.05	1.55
0.6	15	0.03	0.03	0.02	0.11	11.03
	20	0.03	0.03	0.03	0.07	1.14
	25	0.03	0.03	0.03	0.04	1.18
0.8	15	0.02	0.02	0.02	0.10	9.96
	20	0.02	0.02	0.02	0.06	1.10
	25	0.02	0.02	0.02	0.04	0.80

Table B-19: *AV* (%) predicted by Iteration model (*W*=0.02 g/s, T_0=285°C)

V_a	T_a	V_L (m/min)			
(m/s)	(°C)	2000	3000	4000 am	4000 cr
0.4	15	0.03	0.03	0.02	5.45
	20	0.04	0.03	0.02	5.67
	25	0.04	0.03	0.03	5.91
0.6	15	0.02	0.02	0.01	4.15
	20	0.02	0.02	0.01	3.83
	25	0.02	0.02	0.01	4.13
0.8	15	0.01	0.01	0.01	1.48
	20	0.01	0.01	0.01	1.33
	25	0.01	0.01	0.01	3.34

Table B-20: *AV* (%) predicted by Iteration model (*W*=0.03 g/s, T_0=285°C)

V_a	T_a	V_L (m/min)				
(m/s)	(°C)	2000	3000	4000	5000 am	5000 cr
0.4	15	0.05	0.05	0.04	0.19	12.41
	20	0.06	0.05	0.05	0.11	1.80
	25	0.06	0.05	0.05	0.07	1.84
0.6	15	0.03	0.03	0.03	0.18	17.27
	20	0.03	0.03	0.03	0.11	7.80
	25	0.03	0.03	0.03	0.06	1.40
0.8	15	0.02	0.02	0.02	0.18	17.51
	20	0.02	0.02	0.02	0.10	12.94
	25	0.02	0.02	0.02	0.06	1.12

Table B-21: *AV* (%) predicted by Conventional model (*W*=0.02 g/s, T_0=300°C)

V_a	T_a	V_L (m/min)			
(m/s)	(°C)	2000	3000	4000 am	4000 cr
0.4	15	0.02	0.01	0.01	2.43
	20	0.02	0.02	0.01	2.29
	25	0.02	0.02	0.01	2.53
0.6	15	0.01	0.01	0.01	1.62
	20	0.01	0.01	0.01	1.82
	25	0.01	0.01	0.01	1.58
0.8	15	0.01	0.01	0.01	1.30
	20	0.01	0.01	0.01	1.73
	25	0.01	0.01	0.01	1.39

Table B-22: *AV* (%) predicted by Conventional model (*W*=0.03 g/s, T_0=300°C)

V_a	T_a	V_L (m/min)				
(m/s)	(°C)	2000	3000	4000	5000 am	5000 cr
0.4	15	0.02	0.02	0.02	0.09	10.57
	20	0.02	0.02	0.02	0.05	0.99
	25	0.03	0.02	0.02	0.03	0.82
0.6	15	0.01	0.01	0.01	0.07	10.68
	20	0.02	0.01	0.01	0.04	0.54
	25	0.02	0.01	0.01	0.03	0.64
0.8	15	0.01	0.01	0.01	0.07	16.73
	20	0.01	0.01	0.01	0.04	0.61
	25	0.01	0.01	0.01	0.02	0.56

Table B-23: *AV* (%) predicted by Conventional model (*W*=0.02 g/s, T_0=285°C)

V_a	T_a	V_L (m/min)			
(m/s)	(°C)	2000	3000	4000 am	4000 cr
0.4	15	0.02	0.02	0.01	0.01
	20	0.02	0.02	0.01	0.01
	25	0.02	0.02	0.01	0.01
0.6	15	0.01	0.01	0.01	2.42
	20	0.01	0.01	0.01	2.15
	25	0.01	0.01	0.01	2.44
0.8	15	0.01	0.01	0.01	1.83
	20	0.01	0.01	0.01	1.96
	25	0.01	0.01	0.01	2.16

Table B-24: *AV* (%) predicted by Conventional model (*W*=0.03 g/s, T_0=285°C)

V_a	T_a	V_L (m/min)				
(m/s)	(°C)	2000	3000	4000	5000 am	5000 cr
0.4	15	0.03	0.02	0.02	0.13	18.19
	20	0.03	0.02	0.02	0.08	7.00
	25	0.03	0.02	0.02	0.05	1.12
0.6	15	0.02	0.01	0.01	0.12	5.20
	20	0.02	0.01	0.01	0.07	13.40
	25	0.02	0.02	0.01	0.04	0.83
0.8	15	0.01	0.01	0.01	0.12	2.30
	20	0.01	0.01	0.01	0.07	15.90
	25	0.01	0.01	0.01	0.04	0.77

B.1.4 Average filament force variance

Table B-25: *AV* (%) predicted by Iteration model (*W*=0.02 g/s, T_0 = 300°C)

V_a (m/s)	T_a (°C)	V_L (m/min)			
		2000	3000	4000 am	4000 cr
0.4	15	6.79	6.42	6.19	5.96
	20	6.85	6.50	6.24	6.02
	25	6.90	6.60	6.37	6.11
0.6	15	4.86	4.52	4.30	3.95
	20	4.88	4.55	4.37	4.01
	25	4.96	4.59	4.44	4.09
0.8	15	3.90	3.60	3.45	3.13
	20	3.92	3.64	3.45	3.16
	25	3.93	3.68	3.51	3.21

Table B-26: *AV* (%) predicted by Iteration model (*W*=0.03 g/s, T_0 =300°C)

V_a (m/s)	T_a (°C)	V_L (m/min)				
		2000	3000	4000	5000 am	5000 cr
0.4	15	9.84	9.59	9.50	9.48	8.68
	20	9.98	9.79	9.64	9.65	8.81
	25	10.11	9.98	9.84	9.80	8.94
0.6	15	6.29	6.12	6.01	5.90	5.46
	20	6.44	6.20	6.10	6.00	5.55
	25	6.53	6.34	6.21	6.14	5.63
0.8	15	4.57	4.58	4.43	4.34	4.01
	20	4.86	4.64	4.51	4.45	4.10
	25	4.95	4.70	4.59	4.51	4.15

Table B-27: *AV* (%) predicted by Iteration model (*W*=0.02 g/s, T_0=285°C)

V_a (m/s)	T_a (°C)	V_L (m/min)			
		2000	3000	4000 am	4000 cr
0.4	15	7.32	6.82	6.56	6.34
	20	7.36	6.90	6.61	6.43
	25	7.38	6.96	6.67	6.52
0.6	15	5.35	4.94	4.68	4.49
	20	5.34	4.97	4.75	4.51
	25	5.39	4.99	4.77	4.55
0.8	15	4.35	3.98	3.79	3.26
	20	4.34	4.01	3.81	3.29
	25	4.38	4.04	3.85	3.69

Table B-28: *AV* (%) predicted by Iteration model (*W*=0.03 g/s, T_0=285°C)

V_a (m/s)	T_a (°C)	V_L (m/min)				
		2000	3000	4000	5000 am	5000 cr
0.4	15	9.86	9.52	9.36	9.24	8.49
	20	9.97	9.66	9.51	9.38	8.60
	25	10.07	9.80	9.61	9.52	8.68
0.6	15	6.47	6.27	6.09	5.98	5.52
	20	6.67	6.34	6.19	6.06	5.58
	25	6.74	6.41	6.27	6.16	5.64
0.8	15	5.08	4.78	4.60	4.49	4.17
	20	5.13	4.83	4.65	4.56	4.21
	25	5.18	4.90	4.72	4.60	4.24

Table B-29: *AV* (%) predicted by Conventional model (*W*=0.02 g/s, T_0=300°C)

V_a (m/s)	T_a (°C)	V_L (m/min)			
		2000	3000	4000 am	4000 cr
0.4	15	3.43	3.17	3.04	2.84
	20	3.50	3.26	3.07	2.91
	25	3.41	3.29	3.19	2.97
0.6	15	2.51	2.36	2.22	2.01
	20	2.57	2.32	2.25	2.08
	25	2.61	2.40	2.31	2.11
0.8	15	2.05	1.93	1.82	1.64
	20	2.06	1.92	1.83	1.69
	25	2.06	1.96	1.88	1.73

Table B-30: *AV* (%) predicted by Conventional model (*W*=0.03 g/s, T_0=300°C)

V_a (m/s)	T_a (°C)	V_L (m/min)				
		2000	3000	4000	5000 am	5000 cr
0.4	15	4.61	4.47	4.39	4.33	3.99
	20	4.72	4.57	4.49	4.45	4.07
	25	4.83	4.68	4.63	4.55	4.16
0.6	15	3.17	3.03	2.94	2.89	2.66
	20	3.23	3.08	3.01	2.95	2.72
	25	3.30	3.15	3.10	3.04	2.78
0.8	15	2.46	2.33	2.26	2.22	2.04
	20	2.53	2.39	2.32	2.27	2.09
	25	2.57	2.44	2.37	2.33	2.14

Table B-31: *AV* (%) predicted by Conventional model (*W*=0.02 g/s, T_0=285°C)

V_a (m/s)	T_a (°C)	V_L (m/min)			
		2000	3000	4000 am	4000 cr
0.4	15	3.74	3.51	3.33	3.33
	20	3.80	3.54	3.39	3.39
	25	3.84	3.57	3.42	3.42
0.6	15	2.82	2.58	2.47	2.38
	20	2.83	2.62	2.49	2.40
	25	2.87	2.65	2.53	2.42
0.8	15	2.29	2.13	2.03	1.98
	20	2.33	2.16	2.03	1.94
	25	2.36	2.17	2.06	2.09

Table B-32: *AV* (%) predicted by Conventional model (*W*=0.03 g/s, T_0=285°C)

V_a (m/s)	T_a (°C)	V_L (m/min)				
		2000	3000	4000	5000 am	5000 cr
0.4	15	4.79	4.58	4.46	4.37	4.04
	20	4.88	4.66	4.55	4.47	4.11
	25	4.96	4.76	4.64	4.57	4.18
0.6	15	3.36	3.17	3.06	2.98	2.78
	20	3.42	3.23	3.13	3.05	2.81
	25	3.48	3.30	3.20	3.13	2.86
0.8	15	2.67	2.49	2.39	2.33	2.17
	20	2.33	2.53	2.44	2.38	2.19
	25	2.32	2.58	2.49	2.43	2.23

B.1.5 Average filament orientation variance

Table B-33: *AV* (%) predicted by Iteration model (*W*=0.02 g/s, T_0 = 300°C)

V_a	T_a	V_L (m/min)			
(m/s)	(°C)	2000	3000	4000 am	4000 cr
0.4	15	7.70	7.52	7.35	9.60
	20	7.80	7.62	7.42	9.66
	25	7.83	7.78	7.60	9.83
0.6	15	5.02	4.78	4.61	6.19
	20	5.04	4.82	4.71	6.31
	25	5.17	4.87	4.82	6.44
0.8	15	3.73	3.51	3.44	4.82
	20	3.74	3.56	3.42	4.88
	25	3.75	3.64	3.52	4.97

Table B-34: *AV* (%) predicted by Iteration model (*W*=0.03 g/s, T_0 =300°C)

V_a	T_a	V_L (m/min)				
(m/s)	(°C)	2000	3000	4000	5000 am	5000 cr
0.4	15	13.70	13.69	13.77	13.87	12.62
	20	13.86	13.96	13.93	14.10	12.79
	25	13.99	14.22	14.21	14.26	12.96
0.6	15	8.32	8.41	8.41	8.33	7.70
	20	8.56	8.48	8.51	8.44	7.75
	25	8.65	8.69	8.64	8.63	7.88
0.8	15	5.59	6.03	5.94	5.89	5.41
	20	6.18	6.11	6.05	6.03	5.52
	25	6.30	6.16	6.14	6.09	5.56

Table B-35: *AV* (%) predicted by Iteration model (*W*=0.02 g/s, T_0=285°C)

V_a	T_a	V_L (m/min)			
(m/s)	(°C)	2000	3000	4000 am	4000 cr
0.4	15	7.56	7.18	7.02	10.22
	20	7.62	7.31	7.09	10.37
	25	7.63	7.41	7.18	10.53
0.6	15	4.95	4.64	4.41	7.19
	20	4.90	4.69	4.54	7.21
	25	5.00	4.70	4.57	7.27
0.8	15	3.71	3.40	3.27	4.20
	20	3.68	3.45	3.31	4.31
	25	3.73	3.49	3.36	5.93

Table B-36: *AV* (%) predicted by Iteration model (*W*=0.03 g/s, T_0=285°C)

V_a	T_a	V_L (m/min)				
(m/s)	(°C)	2000	3000	4000	5000 am	5000 cr
0.4	15	13.06	12.97	12.97	12.93	11.75
	20	13.19	13.17	13.18	13.11	11.89
	25	13.31	13.36	13.29	13.29	12.01
0.6	15	7.95	8.07	7.99	7.93	7.25
	20	8.32	8.16	8.12	8.02	7.29
	25	8.40	8.23	8.23	8.18	7.37
0.8	15	6.00	5.83	5.72	5.64	5.21
	20	6.06	5.89	5.77	5.73	5.22
	25	6.13	5.98	5.86	5.78	5.24

Table B-37: *AV* (%) predicted by Conventional model (*W*=0.02 g/s, T_0=300°C)

V_a	T_a	V_L (m/min)			
(m/s)	(°C)	2000	3000	4000 am	4000 cr
0.4	15	3.77	3.55	3.43	4.28
	20	3.87	3.69	3.47	4.41
	25	4.28	3.69	3.66	4.50
0.6	15	2.52	2.48	2.32	2.94
	20	2.62	2.34	2.36	3.09
	25	2.67	2.48	2.45	3.14
0.8	15	1.96	1.91	1.79	2.38
	20	1.92	1.87	1.79	2.47
	25	1.90	1.92	1.87	2.55

Table B-38: *AV* (%) predicted by Conventional model (*W*=0.03 g/s, T_0=300°C)

V_a	T_a	V_L (m/min)				
(m/s)	(°C)	2000	3000	4000	5000 am	5000 cr
0.4	15	6.36	6.38	6.37	6.35	5.85
	20	6.50	6.50	6.50	6.50	5.91
	25	6.65	6.62	6.69	6.62	6.02
0.6	15	4.19	4.15	4.11	4.08	3.76
	20	4.25	4.20	4.19	4.15	3.80
	25	4.35	4.29	4.31	4.26	3.88
0.8	15	3.12	3.07	3.05	3.02	2.79
	20	3.23	3.14	3.12	3.08	2.82
	25	3.26	3.20	3.18	3.16	2.88

Table B-39: *AV* (%) predicted by Conventional model (*W*=0.02 g/s, T_0=285°C)

V_a	T_a	V_L (m/min)			
(m/s)	(°C)	2000	3000	4000 am	4000 cr
0.4	15	3.61	3.52	3.35	3.35
	20	3.73	3.55	3.45	3.45
	25	3.78	3.58	3.50	3.50
0.6	15	2.52	2.33	2.28	3.87
	20	2.53	2.38	2.30	3.90
	25	2.58	2.42	2.35	3.94
0.8	15	1.87	1.80	1.73	3.27
	20	1.93	1.85	1.73	3.11
	25	1.99	1.85	1.77	3.51

Table B-40: *AV* (%) predicted by Conventional model (*W*=0.03 g/s, T_0=285°C)

V_a	T_a	V_L (m/min)				
(m/s)	(°C)	2000	3000	4000	5000 am	5000 cr
0.4	15	6.21	6.13	6.08	6.02	5.52
	20	6.33	6.24	6.21	6.16	5.60
	25	6.42	6.37	6.31	6.29	5.68
0.6	15	4.13	4.04	3.96	3.91	3.61
	20	4.20	4.10	4.06	4.00	3.64
	25	4.28	4.20	4.15	4.10	3.69
0.8	15	3.14	3.01	2.95	2.92	2.72
	20	3.02	3.07	3.02	2.99	2.72
	25	2.91	3.14	3.08	3.05	2.74

B.2 Freeze-line property variance tables

B.2.1 Freeze-line crystallisation variance

Table B-41: *FLV* (%) predicted by Iteration model (*W*=0.02 g/s, T_0 = 300°C)

V_a	T_a	V_L (m/min)			
(m/s)	(°C)	2000	3000	4000 am	4000 cr
0.4	15	0.03	0.03	0.01	0.04
	20	0.04	0.03	0.02	0.05
	25	0.04	0.03	0.02	0.03
0.6	15	0.02	0.02	0.00	0.03
	20	0.02	0.02	0.01	0.08
	25	0.02	0.02	0.01	0.06
0.8	15	0.01	0.01	0.00	0.04
	20	0.01	0.01	0.00	0.04
	25	0.01	0.01	0.01	0.06

Table B-42: *FLV* (%) predicted by Iteration model (*W*=0.03 g/s, T_0 =300°C)

V_a	T_a	V_L (m/min)				
(m/s)	(°C)	2000	3000	4000	5000 am	5000 cr
0.4	15	0.05	0.05	0.04	0.31	18.79
	20	0.06	0.05	0.05	0.17	0.05
	25	0.06	0.05	0.05	0.07	0.06
0.6	15	0.03	0.03	0.03	0.29	32.81
	20	0.03	0.03	0.03	0.16	0.02
	25	0.04	0.03	0.03	0.08	0.03
0.8	15	0.02	0.02	0.02	0.28	30.95
	20	0.02	0.02	0.02	0.17	0.04
	25	0.02	0.02	0.02	0.08	0.05

Table B-43: *FLV* (%) predicted by Iteration model (*W*=0.02 g/s, T_0=285°C)

V_a	T_a	V_L (m/min)			
(m/s)	(°C)	2000	3000	4000 am	4000 cr
0.4	15	0.04	0.03	0.01	0.04
	20	0.04	0.03	0.01	0.06
	25	0.04	0.03	0.02	0.05
0.6	15	0.02	0.02	0.01	0.04
	20	0.02	0.02	0.00	0.06
	25	0.02	0.02	0.01	0.02
0.8	15	0.01	0.01	0.01	0.03
	20	0.01	0.01	0.01	0.05
	25	0.01	0.01	0.00	0.05

Table B-44: *FLV* (%) predicted by Iteration model (*W*=0.03 g/s, T_0=285°C)

V_a	T_a	V_L (m/min)				
(m/s)	(°C)	2000	3000	4000	5000 am	5000 cr
0.4	15	0.06	0.05	0.05	0.49	35.82
	20	0.06	0.05	0.05	0.26	0.03
	25	0.06	0.06	0.05	0.12	0.06
0.6	15	0.03	0.03	0.03	0.53	54.73
	20	0.04	0.03	0.03	0.28	22.00
	25	0.04	0.03	0.03	0.14	0.03
0.8	15	0.02	0.02	0.02	0.52	58.21
	20	0.02	0.02	0.02	0.29	40.59
	25	0.02	0.02	0.02	0.14	0.03

Table B-45: *FLV* (%) predicted by Conventional model (*W*=0.02 g/s, T_0=300°C)

V_a	T_a	V_L (m/min)			
(m/s)	(°C)	2000	3000	4000 am	4000 cr
0.4	15	0.02	0.02	0.01	0.04
	20	0.02	0.02	0.01	0.05
	25	0.02	0.02	0.01	0.05
0.6	15	0.01	0.01	0.00	0.06
	20	0.01	0.01	0.00	0.03
	25	0.01	0.01	0.01	0.03
0.8	15	0.01	0.01	0.00	0.05
	20	0.01	0.01	0.00	0.07
	25	0.01	0.01	0.00	0.03

Table B-46: *FLV* (%) predicted by Conventional model (*W*=0.03 g/s, T_0=300°C)

V_a	T_a	V_L (m/min)				
(m/s)	(°C)	2000	3000	4000	5000 am	5000 cr
0.4	15	0.03	0.02	0.02	0.24	32.17
	20	0.03	0.02	0.02	0.13	0.04
	25	0.03	0.03	0.02	0.06	0.03
0.6	15	0.02	0.01	0.01	0.21	33.65
	20	0.02	0.01	0.01	0.11	0.04
	25	0.02	0.02	0.01	0.06	0.04
0.8	15	0.01	0.01	0.01	0.20	56.36
	20	0.01	0.01	0.01	0.11	0.03
	25	0.01	0.01	0.01	0.06	0.05

Table B-47: *FLV* (%) predicted by Conventional model (*W*=0.02 g/s, T_0=285°C)

V_a	T_a	V_L (m/min)			
(m/s)	(°C)	2000	3000	4000 am	4000 cr
0.4	15	0.02	0.02	0.00	0.00
	20	0.02	0.02	0.00	0.00
	25	0.02	0.02	0.01	0.01
0.6	15	0.01	0.01	0.01	0.05
	20	0.01	0.01	0.00	0.03
	25	0.01	0.01	0.00	0.06
0.8	15	0.01	0.01	0.01	0.06
	20	0.01	0.01	0.00	0.04
	25	0.01	0.01	0.00	0.05

Table B-48: *FLV* (%) predicted by Conventional model (*W*=0.03 g/s, T_0=285°C)

V_a	T_a	V_L (m/min)				
(m/s)	(°C)	2000	3000	4000	5000 am	5000 cr
0.4	15	0.03	0.02	0.02	0.38	59.10
	20	0.03	0.03	0.02	0.21	19.94
	25	0.03	0.03	0.02	0.11	0.05
0.6	15	0.02	0.01	0.01	0.36	17.20
	20	0.02	0.02	0.01	0.20	43.47
	25	0.02	0.02	0.01	0.10	0.03
0.8	15	0.01	0.01	0.01	0.37	7.49
	20	0.01	0.01	0.01	0.20	52.90
	25	0.01	0.01	0.01	0.10	0.03

B.2.2 Freeze-line force variance

Table B-49: *FLV* (%) predicted by Iteration model (*W*=0.02 g/s, T_0 = 300°C)

V_a	T_a	V_L (m/min)			
(m/s)	(°C)	2000	3000	4000 am	4000 cr
0.4	15	1.17	1.49	1.19	5.01
	20	1.22	1.47	1.14	4.85
	25	1.38	1.49	1.18	4.59
0.6	15	1.41	1.08	0.84	3.41
	20	1.55	1.04	0.85	3.27
	25	1.61	1.02	0.87	3.04
0.8	15	1.74	0.87	0.72	2.60
	20	1.81	0.86	0.65	2.48
	25	1.95	0.87	0.68	2.62

Table B-50: *FLV* (%) predicted by Iteration model (*W*=0.03 g/s, T_0 =300°C)

V_a	T_a	V_L (m/min)				
(m/s)	(°C)	2000	3000	4000	5000 am	5000 cr
0.4	15	3.39	3.15	2.84	2.66	1.35
	20	3.33	2.81	2.35	2.11	1.15
	25	3.23	2.75	2.45	2.21	1.05
0.6	15	2.02	2.01	1.65	1.58	1.65
	20	2.35	1.56	1.75	1.38	0.98
	25	2.09	1.63	1.71	1.55	0.72
0.8	15	1.45	1.49	1.01	1.14	1.80
	20	1.76	1.34	1.27	1.16	0.95
	25	1.77	1.43	1.25	1.10	0.51

Table B-51: *FLV* (%) predicted by Iteration model (*W*=0.02 g/s, T_0=285°C)

V_a	T_a	V_L (m/min)			
(m/s)	(°C)	2000	3000	4000 am	4000 cr
0.4	15	2.39	1.75	1.42	5.87
	20	2.35	1.75	1.37	5.75
	25	2.24	1.73	1.34	5.68
0.6	15	1.87	1.37	1.04	4.34
	20	1.78	1.34	1.07	4.25
	25	1.76	1.28	1.02	4.46
0.8	15	1.60	1.14	0.91	2.39
	20	1.53	1.12	0.88	2.39
	25	1.50	1.10	0.87	3.61

Table B-52: *FLV* (%) predicted by Iteration model (*W*=0.03 g/s, T_0=285°C)

V_a	T_a	V_L (m/min)				
(m/s)	(°C)	2000	3000	4000	5000 am	5000 cr
0.4	15	3.59	3.29	2.76	2.65	1.35
	20	3.58	2.87	2.61	2.09	1.58
	25	3.44	2.83	2.64	2.37	1.14
0.6	15	2.37	2.17	1.62	1.70	2.13
	20	2.61	1.81	1.88	1.66	1.44
	25	2.46	1.83	1.84	1.65	1.00
0.8	15	2.06	1.66	0.99	1.25	1.54
	20	2.02	1.63	1.37	1.24	2.19
	25	1.99	1.61	1.36	1.19	1.03

Table B-53: *FLV* (%) predicted by Conventional model (*W*=0.02 g/s, T_0=300°C)

V_a	T_a	V_L (m/min)			
(m/s)	(°C)	2000	3000	4000 am	4000 cr
0.4	15	1.06	0.75	0.60	2.49
	20	1.07	0.80	0.55	2.51
	25	1.06	0.75	0.65	2.13
0.6	15	0.78	0.64	0.47	1.82
	20	0.80	0.50	0.45	1.76
	25	0.80	0.56	0.48	1.74
0.8	15	0.66	0.54	0.41	1.43
	20	0.62	0.48	0.37	1.21
	25	0.57	0.49	0.41	1.58

Table B-54: *FLV* (%) predicted by Conventional model (*W*=0.03 g/s, T_0=300°C)

V_a	T_a	V_L (m/min)				
(m/s)	(°C)	2000	3000	4000	5000 am	5000 cr
0.4	15	1.57	1.53	1.23	1.24	1.70
	20	1.78	1.19	1.35	1.24	0.60
	25	1.67	1.16	1.37	1.20	0.55
0.6	15	1.23	1.04	0.68	0.81	1.96
	20	1.21	1.01	0.90	0.79	0.39
	25	1.22	1.00	0.90	0.79	0.38
0.8	15	0.94	0.78	0.37	0.62	2.34
	20	0.97	0.79	0.69	0.61	0.56
	25	0.95	0.78	0.68	0.61	0.31

Table B-55: *FLV* (%) predicted by Conventional model (*W*=0.02 g/s, T_0=285°C)

V_a	T_a	V_L (m/min)			
(m/s)	(°C)	2000	3000	4000 am	4000 cr
0.4	15	1.27	0.99	0.76	0.76
	20	1.29	0.96	0.77	0.77
	25	1.26	0.93	0.75	0.75
0.6	15	1.04	0.74	0.62	2.70
	20	1.01	0.74	0.59	2.63
	25	0.99	0.73	0.59	2.58
0.8	15	0.85	0.65	0.53	2.36
	20	0.86	0.66	0.49	2.18
	25	0.86	0.63	0.49	2.05

Table B-56: *FLV* (%) predicted by Conventional model (*W*=0.03 g/s, T_0=285°C)

V_a	T_a	V_L (m/min)				
(m/s)	(°C)	2000	3000	4000	5000 am	5000 cr
0.4	15	1.86	1.64	1.18	1.28	2.33
	20	1.97	1.39	1.43	1.28	1.52
	25	1.94	1.49	1.40	1.27	0.96
0.6	15	1.40	1.15	0.60	0.87	0.43
	20	1.39	1.14	0.99	0.87	2.43
	25	1.38	1.14	0.99	0.87	0.88
0.8	15	1.13	0.89	0.47	0.68	0.32
	20	0.59	0.89	0.76	0.69	2.78
	25	0.44	0.89	0.76	0.67	0.85

B.2.3 Freeze-line orientation variance

Table B-57: *FLV* (%) predicted by Iteration model (W=0.02 g/s, T_0 = 300°C)

V_a	T_a	V_L (m/min)			
(m/s)	(°C)	2000	3000	4000 am	4000 cr
0.4	15	1.07	1.44	1.07	3.72
	20	1.08	1.41	0.98	3.60
	25	1.31	1.48	1.07	3.33
0.6	15	1.27	1.05	0.73	2.61
	20	1.44	0.99	0.78	2.45
	25	1.44	0.96	0.84	2.22
0.8	15	1.62	0.81	0.68	1.99
	20	1.64	0.81	0.56	1.87
	25	1.86	0.84	0.63	1.96

Table B-58: *FLV* (%) predicted by Iteration model (W=0.03 g/s, T_0 =300°C)

V_a	T_a	V_L (m/min)				
(m/s)	(°C)	2000	3000	4000	5000 am	5000 cr
0.4	15	3.29	2.92	2.53	2.30	1.01
	20	3.20	2.61	1.98	1.75	0.86
	25	3.04	2.59	2.14	1.82	0.80
0.6	15	1.80	1.90	1.52	1.31	1.26
	20	2.26	1.35	1.57	1.09	0.75
	25	1.94	1.49	1.51	1.28	0.61
0.8	15	0.96	1.43	0.87	0.93	1.59
	20	1.69	1.25	1.14	0.99	0.85
	25	1.74	1.32	1.11	0.90	0.38

Table B-59: *FLV* (%) predicted by Iteration model (W=0.02 g/s, T_0=285°C)

V_a	T_a	V_L (m/min)			
(m/s)	(°C)	2000	3000	4000 am	4000 cr
0.4	15	2.33	1.59	1.21	4.48
	20	2.27	1.63	1.14	4.33
	25	2.09	1.62	1.11	4.21
0.6	15	1.86	1.29	0.85	3.40
	20	1.67	1.26	0.97	3.29
	25	1.70	1.16	0.88	3.42
0.8	15	1.58	1.04	0.79	2.19
	20	1.46	1.04	0.76	2.15
	25	1.44	1.01	0.75	2.80

Table B-60: *FLV* (%) predicted by Iteration model (W=0.03 g/s, T_0=285°C)

V_a	T_a	V_L (m/min)				
(m/s)	(°C)	2000	3000	4000	5000 am	5000 cr
0.4	15	3.42	3.06	2.45	2.20	1.18
	20	3.40	2.62	2.31	1.66	1.22
	25	3.24	2.62	2.30	1.94	0.96
0.6	15	2.08	2.04	1.42	1.42	1.88
	20	2.53	1.63	1.70	1.36	1.09
	25	2.35	1.63	1.65	1.39	0.83
0.8	15	1.99	1.56	0.82	1.03	1.28
	20	1.95	1.52	1.20	1.03	1.75
	25	1.93	1.52	1.20	0.96	0.82

Table B-61: *FLV* (%) predicted by Conventional model (W=0.02 g/s, T_0=300°C)

V_a	T_a	V_L (m/min)			
(m/s)	(°C)	2000	3000	4000 am	4000 cr
0.4	15	1.06	0.68	0.46	1.33
	20	1.11	0.79	0.38	1.29
	25	1.09	0.67	0.58	1.02
0.6	15	0.74	0.66	0.39	1.04
	20	0.81	0.35	0.37	0.94
	25	0.81	0.50	0.44	0.89
0.8	15	0.66	0.57	0.37	0.83
	20	0.54	0.44	0.31	0.65
	25	0.44	0.47	0.39	0.84

Table B-62: *FLV* (%) predicted by Conventional model (W=0.03 g/s, $\mathrm{T_0}$=300°C)

V_a	T_a	V_L (m/min)				
(m/s)	(°C)	2000	3000	4000	5000 am	5000 cr
0.4	15	1.47	1.46	1.11	1.05	1.26
	20	1.72	1.07	1.21	1.05	0.46
	25	1.62	1.03	1.27	0.98	0.43
0.6	15	1.20	1.00	0.60	0.69	1.52
	20	1.16	0.93	0.81	0.64	0.25
	25	1.18	0.92	0.82	0.64	0.31
0.8	15	0.90	0.73	0.35	0.53	1.93
	20	0.97	0.74	0.63	0.51	0.46
	25	0.91	0.72	0.61	0.51	0.34

Table B-63: *FLV* (%) predicted by Conventional model (W=0.02 g/s, T_0=285°C)

V_a	T_a	V_L (m/min)			
(m/s)	(°C)	2000	3000	4000 am	4000 cr
0.4	15	1.17	0.96	0.64	0.64
	20	1.24	0.91	0.68	0.68
	25	1.21	0.83	0.64	0.64
0.6	15	1.01	0.67	0.56	2.16
	20	0.95	0.68	0.52	2.08
	25	0.95	0.67	0.52	2.01
0.8	15	0.76	0.61	0.48	1.91
	20	0.81	0.64	0.41	1.77
	25	0.83	0.59	0.41	1.57

Table B-64: *FLV* (%) predicted by Conventional model (W=0.03 g/s, T_0=285°C)

V_a	T_a	V_L (m/min)				
(m/s)	(°C)	2000	3000	4000	5000 am	5000 cr
0.4	15	1.77	1.54	1.03	1.04	1.92
	20	1.90	1.26	1.28	1.06	1.24
	25	1.86	1.37	1.22	1.04	0.73
0.6	15	1.35	1.08	0.50	0.70	0.41
	20	1.35	1.06	0.89	0.71	2.00
	25	1.34	1.07	0.90	0.73	0.73
0.8	15	1.11	0.82	0.40	0.57	0.39
	20	1.89	0.82	0.67	0.58	2.27
	25	1.57	0.82	0.67	0.56	0.72

B.3 Final property variance tables

B.3.1 Final force variance

Table B-65: *FPV* (%) predicted by Iteration model (W=0.02 g/s, T_0 = 300°C)

V_a (m/s)	T_a (°C)	V_L (m/min)			
		2000	3000	4000 am	4000 cr
0.4	15	1.12	0.81	0.58	3.11
	20	1.10	0.80	0.53	3.06
	25	1.02	0.84	0.59	3.11
0.6	15	0.88	0.60	0.40	2.09
	20	0.83	0.56	0.44	2.10
	25	0.88	0.54	0.47	2.11
0.8	15	0.71	0.46	0.38	1.71
	20	0.67	0.46	0.31	1.70
	25	0.63	0.48	0.35	1.69

Table B-66: *FPV* (%) predicted by Iteration model (W=0.03 g/s, T_0 =300°C)

V_a (m/s)	T_a (°C)	V_L (m/min)				
		2000	3000	4000	5000 am	5000 cr
0.4	15	2.43	1.84	1.55	1.42	0.65
	20	2.39	1.89	1.48	1.41	0.65
	25	2.32	1.92	1.53	1.33	0.61
0.6	15	1.44	1.21	1.03	0.81	0.53
	20	1.53	1.14	0.97	0.77	0.40
	25	1.49	1.20	0.95	0.82	0.46
0.8	15	0.76	0.91	0.71	0.59	0.19
	20	1.15	0.89	0.71	0.63	0.40
	25	1.18	0.86	0.70	0.58	0.30

Table B-67: *FPV* (%) predicted by Iteration model (W=0.02 g/s, T_0=285°C)

V_a (m/s)	T_a (°C)	V_L (m/min)			
		2000	3000	4000 am	4000 cr
0.4	15	1.42	0.90	0.66	3.75
	20	1.38	0.93	0.62	3.75
	25	1.29	0.92	0.61	3.74
0.6	15	1.14	0.74	0.47	2.80
	20	1.03	0.73	0.54	2.75
	25	1.06	0.67	0.49	2.72
0.8	15	0.98	0.60	0.44	1.54
	20	0.91	0.60	0.43	1.55
	25	0.90	0.59	0.42	2.32

Table B-68: *FPV* (%) predicted by Iteration model (W=0.03 g/s, T_0=285°C)

V_a (m/s)	T_a (°C)	V_L (m/min)				
		2000	3000	4000	5000 am	5000 cr
0.4	15	2.56	1.95	1.62	1.37	0.67
	20	2.53	1.95	1.64	1.35	0.70
	25	2.48	1.97	1.56	1.34	0.73
0.6	15	1.53	1.31	1.07	0.90	0.54
	20	1.73	1.29	1.07	0.86	0.47
	25	1.71	1.24	1.05	0.89	0.49
0.8	15	1.36	1.01	0.80	0.66	0.45
	20	1.34	0.99	0.76	0.66	0.40
	25	1.34	0.99	0.77	0.62	0.38

Table B-69: *FPV* (%) predicted by Conventional model (W=0.02 g/s, T_0=300°C)

V_a (m/s)	T_a (°C)	V_L (m/min)			
		2000	3000	4000 am	4000 cr
0.4	15	0.65	0.40	0.28	1.52
	20	0.67	0.47	0.22	1.55
	25	0.67	0.40	0.36	1.56
0.6	15	0.46	0.40	0.24	1.10
	20	0.50	0.20	0.23	1.14
	25	0.50	0.30	0.28	1.15
0.8	15	0.41	0.34	0.23	0.93
	20	0.34	0.27	0.20	0.95
	25	0.29	0.28	0.25	0.97

Table B-70: *FPV* (%) predicted by Conventional model (W=0.03 g/s, T_0=300°C)

V_a (m/s)	T_a (°C)	V_L (m/min)				
		2000	3000	4000	5000 am	5000 cr
0.4	15	1.15	0.93	0.77	0.66	0.44
	20	1.16	0.91	0.75	0.66	0.35
	25	1.18	0.90	0.80	0.62	0.33
0.6	15	0.81	0.64	0.51	0.43	0.25
	20	0.79	0.60	0.50	0.41	0.20
	25	0.80	0.59	0.52	0.41	0.24
0.8	15	0.61	0.47	0.39	0.34	0.16
	20	0.65	0.47	0.40	0.32	0.20
	25	0.63	0.47	0.39	0.33	0.25

Table B-71: *FPV* (%) predicted by Conventional model (W=0.02 g/s, T_0=285°C)

V_a (m/s)	T_a (°C)	V_L (m/min)			
		2000	3000	4000 am	4000 cr
0.4	15	0.72	0.55	0.35	0.35
	20	0.76	0.52	0.38	0.38
	25	0.75	0.48	0.36	0.36
0.6	15	0.63	0.39	0.31	1.59
	20	0.59	0.40	0.29	1.57
	25	0.60	0.39	0.29	1.55
0.8	15	0.48	0.36	0.27	1.38
	20	0.51	0.37	0.23	1.29
	25	0.52	0.34	0.23	1.44

Table B-72: *FPV* (%) predicted by Conventional model (W=0.03 g/s, T_0=285°C)

V_a (m/s)	T_a (°C)	V_L (m/min)				
		2000	3000	4000	5000 am	5000 cr
0.4	15	1.29	0.99	0.81	0.66	0.36
	20	1.30	0.98	0.81	0.67	0.37
	25	1.28	0.98	0.78	0.67	0.34
0.6	15	0.92	0.70	0.55	0.45	0.38
	20	0.93	0.69	0.56	0.45	0.20
	25	0.93	0.70	0.57	0.47	0.27
0.8	15	0.76	0.54	0.42	0.37	0.36
	20	0.88	0.54	0.43	0.37	0.19
	25	0.69	0.54	0.43	0.36	0.23

B.3.2 Final orientation variance

Table B-73: *FPV* (%) predicted by Iteration model (*W*=0.02 g/s, T_0 = 300°C)

V_a	T_a	V_L (m/min)			
(m/s)	(°C)	2000	3000	4000 am	4000 cr
0.4	15	1.06	0.76	0.43	3.23
	20	1.06	0.73	0.38	3.37
	25	0.91	0.81	0.43	3.68
0.6	15	0.88	0.56	0.27	3.78
	20	0.82	0.52	0.34	4.01
	25	0.91	0.50	0.38	4.25
0.8	15	0.68	0.42	0.30	4.34
	20	0.62	0.41	0.23	4.80
	25	0.56	0.47	0.27	5.17

Table B-74: *FPV* (%) predicted by Iteration model (*W*=0.03 g/s, T_0 =300°C)

V_a	T_a	V_L (m/min)				
(m/s)	(°C)	2000	3000	4000	5000 am	5000 cr
0.4	15	1.17	0.81	0.76	0.84	0.30
	20	1.22	0.88	0.82	0.84	0.34
	25	1.38	0.88	0.91	0.76	0.33
0.6	15	1.41	1.04	0.97	0.44	0.41
	20	1.55	1.08	1.00	0.40	0.22
	25	1.61	1.14	1.04	0.46	0.30
0.8	15	1.74	1.30	1.09	0.32	0.22
	20	1.81	1.41	1.22	0.37	0.32
	25	1.95	1.44	1.25	0.31	0.18

Table B-75: *FPV* (%) predicted by Iteration model (*W*=0.02 g/s, T_0=285°C)

V_a	T_a	V_L (m/min)			
(m/s)	(°C)	2000	3000	4000 am	4000 cr
0.4	15	1.37	0.75	0.42	1.74
	20	1.32	0.80	0.39	1.66
	25	1.17	0.81	0.36	1.59
0.6	15	1.13	0.66	0.28	1.40
	20	0.94	0.65	0.40	1.32
	25	1.01	0.56	0.32	1.26
0.8	15	0.96	0.50	0.29	0.99
	20	0.84	0.51	0.29	0.95
	25	0.86	0.50	0.28	1.13

Table B-76: *FPV* (%) predicted by Iteration model (*W*=0.03 g/s, T_0=285°C)

V_a	T_a	V_L (m/min)				
(m/s)	(°C)	2000	3000	4000	5000 am	5000 cr
0.4	15	1.09	0.84	0.62	0.75	0.30
	20	1.10	0.81	0.59	0.75	0.35
	25	1.14	0.79	0.65	0.75	0.42
0.6	15	0.78	0.59	0.41	0.50	0.42
	20	0.75	0.52	0.40	0.47	0.25
	25	0.77	0.51	0.42	0.51	0.31
0.8	15	0.57	0.42	0.32	0.36	0.49
	20	0.65	0.42	0.32	0.36	0.26
	25	0.60	0.42	0.30	0.33	0.23

Table B-77: *FPV* (%) predicted by Conventional model (*W*=0.02 g/s, T_0=300°C)

V_a	T_a	V_L (m/min)			
(m/s)	(°C)	2000	3000	4000 am	4000 cr
0.4	15	0.65	0.33	0.09	0.53
	20	0.71	0.43	0.06	0.64
	25	0.70	0.32	0.14	0.75
0.6	15	0.42	0.39	0.08	0.31
	20	0.52	0.11	0.09	0.39
	25	0.52	0.24	0.13	0.46
0.8	15	0.47	0.33	0.10	0.22
	20	0.29	0.24	0.09	0.27
	25	0.22	0.26	0.11	0.33

Table B-78: *FPV* (%) predicted by Conventional model (*W*=0.03 g/s, T_0=300°C)

V_a	T_a	V_L (m/min)				
(m/s)	(°C)	2000	3000	4000	5000 am	5000 cr
0.4	15	1.17	0.81	0.76	0.37	0.32
	20	1.22	0.88	0.82	0.38	0.19
	25	1.38	0.88	0.91	0.34	0.18
0.6	15	1.41	1.04	0.97	0.25	0.21
	20	1.55	1.08	1.00	0.21	0.13
	25	1.61	1.14	1.04	0.22	0.16
0.8	15	1.74	1.30	1.09	0.20	0.19
	20	1.81	1.41	1.22	0.18	0.15
	25	1.95	1.44	1.25	0.18	0.20

Table B-79: *FPV* (%) predicted by Conventional model (*W*=0.02 g/s, T_0=285°C)

V_a	T_a	V_L (m/min)			
(m/s)	(°C)	2000	3000	4000 am	4000 cr
0.4	15	0.64	0.51	0.23	0.23
	20	0.72	0.46	0.27	0.27
	25	0.71	0.39	0.23	0.23
0.6	15	0.61	0.32	0.23	0.82
	20	0.54	0.34	0.21	0.78
	25	0.57	0.33	0.21	0.75
0.8	15	0.41	0.31	0.20	0.73
	20	0.47	0.34	0.15	0.69
	25	0.50	0.31	0.17	0.71

Table B-80: *FPV* (%) predicted by Conventional model (*W*=0.03 g/s, T_0=285°C)

V_a	T_a	V_L (m/min)				
(m/s)	(°C)	2000	3000	4000	5000 am	5000 cr
0.4	15	1.22	0.88	0.63	0.35	0.25
	20	1.24	0.86	0.62	0.37	0.19
	25	1.21	0.88	0.59	0.37	0.16
0.6	15	0.87	0.63	0.42	0.23	0.32
	20	0.88	0.60	0.44	0.24	0.12
	25	0.89	0.64	0.46	0.27	0.16
0.8	15	0.74	0.47	0.32	0.20	0.42
	20	2.40	0.47	0.33	0.21	0.16
	25	2.07	0.48	0.33	0.20	0.15

B.3.3 Final crystallinity variance

The variance in crystallinity at the take-up point is identical to the freezeline variance (see appendices B.2.1 for these results).

Appendix C: Program coding

C.1 Monofilament model

C.1.1 Main file

```
Close all;clear all;clc;
tic%starts timer
global type;type = 1; %type 1 selects the monofilament setup in
localAT(z)

%defining global constants
global W; W = 0.02;% mass flow rate (g/s)
global Va; Va = 40; %velocity of cooling medium cm/s
global Ta; Ta = 20 + 273.15; %Cooling medium temp (oC)
global g, g = 9.81*100; %gravitational constant (cm/s^2)
global dh, dh = 1.237*10^2/4.184;%(J/g --> cal/g) Heat of
crystallisation
global ps; ps = 1.2022/1000;% density of air (kg/m^3 --> g/cm^3)
global n; n = 4;%avrami exponent
global Tg; Tg = 70 + 273; %Glass transition temp for PET (343 K)
global Tmax; Tmax = 190 + 273; %Temp corresponding to Kmax for PET
(463 K)
global Km; Km = 0.016; %Max crystallisation rate for PET (1/s)
global Tm; Tm = 280 + 273; %Melting temp for PET (553 K)
global Dh; Dh = 32; %half width of K(T) curve
global A; A = 500; % stress induced crystallisation factor (DKW-ave)
global Co; Co = 5.0*10^(-10); %stress optical co-efficient
(cm^2/dyne*10=m^2/N)
global dn; dn = 0.275; %amorphous birefringence (-)
global Th; Th = 150 + 273; %degrees C
global Eak; Eak = 6923.7; %(K)
global alpha; alpha = 1; %unity for low molecular weights
global X_s; X_s = 0.1; %critical crystallinity
global IV; IV = 0.6;%intrinsic viscosity (poise)
global Xmax;Xmax = 0.35;%Max crystallisation rate set in this
simulation.

%Initial conditions
global di; di = 300e-4;% (cm)
global Ti; Ti = 300 + 273.15; %K
Xi = 1e-2;% 1% needed for nucleation/first guess
Vi = (4*W)/(pi*di^2*density(Ti)); %(cm/s)
Fi = 42; %dyne


x1 = [Xi Ti Fi Vi];%Initial value vector

[z,x] = ode23s('M',[0 300],x1);%ode build in command function, this
solves the system of equations which are in the sub-file 'M' based on
the boundary conditions in x1

%The mass balance equation______________________
x(:,5) = sqrt((4*W)./(density(x(:,2)).*x(:,4)*pi));
x(1,5) = di;

%Setting variable values to logical letters for easy reference.
```

```
X = x(:,1);
T = x(:,2);
F = x(:,3);
V = x(:,4);
d = x(:,5);

%Output generation: Plots X,T,F,V,d as a function of distance
figure(1)
subplot(3,2,1);
plot(z,X.*100)
title('A plot of Crystallinity vs distance');xlabel('Distance z
[cm]');ylabel('Crystallinity [%]')
subplot(3,2,2);
plot(z,T-273,z,Tg-273,'r',z,Tmax-273,'r',z,Tm-273,'r')
title('A plot of Temperature vs distance');xlabel('Distance z
[cm]');ylabel('Temperature [^0C]')
subplot(3,2,3);
plot(z,F)
title('A plot of Tension vs distance');xlabel('Distance z
[cm]');ylabel('Tension [Dyne]')
subplot(3,2,4);
plot(z,V.*60/100)
title('A plot of Velocity vs distance');xlabel('Distance z
[cm]');ylabel('Velocity [m/min]')
subplot(3,2,5);
plot(z,d.*10^4)
title('A plot of diameter vs distance');xlabel('Distance z
[cm]');ylabel('diameter  [microns]')
subplot(3,2,6);

toc%stop timer and displays simulation time
```

C.1.2 Sub-files

The ‘M’ file: This contains the system of ode’s.

```
function f = M(z,x)

global W Vm ps g dh n Eak alpha X_s IV;% calls needed variables
previously defined

[Taz,Vm] = localAT(z);%Quench temperature set according to distance
from spinneret in sub-file localAT(z).
f = zeros(4,1);%set place holder for values to be calculated.

%Mass balance equation____________________________________________
d = sqrt((4*W)/(density(x(2))*x(4)*pi));

%Crystallinity equation___________________________________________
Kstval = Kst(x(1),x(2),x(3),x(4),W);
r = n*(1-x(1))*(-log(1-x(1)))^((n-1)/n)*Kstval;
f(1) = r/(x(4));


%Temperature balance______________________________________________
Hcryst = (dh)/Cp(x(2))*f(1);
Hconvec = (-
2*al(d,x(4),Vm,z))/(Cp(x(2)))*(pi/(density(x(2))*x(4)*W))^(0.5)*(x(2)
-(Taz));
f(2) = Hconvec + Hcryst;
```

```
%Force Balance___________________________________________________
Fdrag =
ps*Cf(x(4),d,Taz,z)*x(4)^2*((pi*W)/(density(x(2))*x(4)))^(1/2); %
Finertia = W*f(4);
Fgravity = W*g/x(4);
f(3) = Finertia - Fgravity + Fdrag;

%Constitutive
equation________________________________________________________
no = 0.0976*IV^5.2893;
inversnT = (1/no).*exp(-Eak./x(2));
inversenX = abs((1-x(1)./X_s)).^alpha;%polymer fluidity, avoids
singularity when X tends to X*.

if  x(1) <= 0.1 %below X*
    f(4) =
((inversnT*inversenX)/3)*((density(x(2))*x(3)*x(4))/(W));%normal
velocity description
else
    f(4) = ((0)/3)*((density(x(2))*x(3)*x(4))/(W)); % sets dV/dx = 0
above X*.
end
```

The ‘localAT’ sub-file: this defines the quench air temperature according to the distance from the spinneret.

```
function [Taz,Vm] = localAT(z)

global Ta Th Va type Ta2;%calls required values.

if type < 2 %for the monofilament model
    if ((z<100)||(z==100))%quench zone (zone 1)
        Taz = Ta;
        Vm = Va;
    else
        if((z<200)||(z==200))%hot tube zone (zone 2)
            Taz = Th;
            Vm = 0;
        else
            Taz = Ta; %the final zone (zone 3)
            Vm = 0;
        end;
    end;
else if type > 1 %for the multifilament model
        if ((z<100)||(z==100))%quench zone (zone 1)
            Taz = Ta2;
            Vm = Va;
        else
            if((z<200)||(z==200))%hot tube zone (zone 2)
                Taz = Ta2;
                Vm = 0;
            else
                Taz = Ta2;%the final zone (zone 3)
                Vm = 0;
            end;
        end;
    end;
end;
```

The Characteristic crystallisation rate sub-file 'Kst': This calculates the crystallisation rate based on the tensile stress and molecular orientation.

```
function K = Kst(X,T,F,V,W)

global Dh Tg Tmax Km Tm A Co dn Xmax; %calls required variables
previously defined.

%Set crystallisation rate to zero if X>0.35.
if (X <= Xmax)
    if T < Tm & T > Tg
        Kpo =  Km*exp(-4*log(2)*((T-Tmax)^2)/Dh^2);
    else
        Kpo = 0;
    end
    dp = ((density(T)*F*V)/(W));
    B1 = Co/dn;
    B2 = (-3/7)*(Co/dn)^2;
    B3 = (-1/7)*(Co/dn)^3;

    fa = B1*dp+B2*dp^2+B3*dp^3;
    K  = Kpo*exp(A*(fa)^2);
else
    dp = ((density(T)*F*V)/(W));
    B1 = Co/dn;
    B2 = (-3/7)*(Co/dn)^2;
    B3 = (-1/7)*(Co/dn)^3;

    fa = B1*dp+B2*dp^2+B3*dp^3;
    K = 0;
end
```

The sub-file 'al' which calculates the heat transfer coefficient (f_h).

```
function a = al(d,V,Vm,z)

[Taz,Vm] = localAT(z);

hcc = 4.9805*10^-6*[Taz^(3/2)/(Taz+114)];%heat conduction coefficient
(cal/cm s deg)
kv = 4.1618*10^-5*[Taz^(5/2)/(Taz+114)];%kinematic viscosity (cm^2/s)

a = 0.42*hcc*kv^(-0.334)*d^(-0.666)*V^(0.334)*[1+(8*Vm/V)^2]^0.167;
%(cal/cm2 s deg)
```

The sub-file 'Cf': this calculates the drag coefficient (C_f).

```
function cf = Cf(V,d,Taz,z)

[Taz,Vm] = localAT(z);%calls the correct quench conditions set by
sub-file localAT.

kv = 4.1618*10^-5*[Taz^(5/2)/(Taz+114)];%kinematic viscosity (cm^2/s)
cf = 0.37*((V*d)/kv)^(-0.61); %dimensionless (Reynolds number
included) Cf = 0.37*Re^(-0.61)
```

The density and heat capacity sub-files 'density' and 'Cp'.

```
function D = density(T)
po = 1.356; % (g/cm^3)
p1 = 5.0*10^(-4); % g/(cm^3 K)

D = (po - p1*(T - 273)); %(g/cm^3)

function C = Cp(T)

%for PET
 Cpo = 0.3; %(cal/(gK))
 Cp1 = 6.0*10^-4; %cal/(gK^2)

 C = (Cpo+Cp1*[T - 273]); %cal/g K
```

C.2 Multifilament – Conventional approach

The sub files used in this programme are identical to those used in the monofilament model. These can be found in Appendix C.1.

C.2.1 Main file

```
%multi filament code
clc;close all;clear all;
tic
global type;type = 2;
dir = 'C:\Documents and Settings\HGHALI004\My Documents\Ty\Iteration
model data 33 285\'; % Sets directory to save data in
%Constants____________________________________________
global W; W = 0.03;% mass flow rate (g/s)
global Va; Va = input('Quench air speed (cm/s):'); %velocity of
cooling medium cm/s
global Ta1;Ta1 = input('Quench air temp in (^oC):') + 273; %Cooling
medium temp (oC)
global g, g = 9.81*100; %gravitational constant (cm/s^2)
global dh, dh = 1.237*10^2/4.184;%(J/g --> cal/g) Heat of
crystallisation (erg/g*10^-7= J/g)
global ps; ps = 1.2022/1000;% density of air (g/cm^3)
global n; n = 4;%Avrami exponent
global Tg; Tg = 70 + 273; %Glass transition temp for PET (343 K)
global Tmax; Tmax = 190 + 273; %Temp corresponding to Kmax for PET
(463 K)
global Km; Km = 0.016; %Max crystallisation rate for PET (1/s)
global Tm; Tm = 280 + 273; %Melting temp for PET (553 K)
global Dh; Dh = 32; %half width of K(T) curve
global A; A = 500; % stress induced crystallisation factor (DKW-ave)
global Co; Co = 5.0*10^(-10); %stress optical co-efficient
(cm^2/dyne*10=m^2/N)
global dn; dn = 0.275; % amorphous birefringence (-)
global Th; Th = 150 + 273; %degrees C
global Eak; Eak = 6923.7; %(K)
global alpha; alpha = 1; %unity for low molecular weights
global X_s; X_s = 0.1; %critical crystallinity
global IV; IV = 0.6;%Intrinsic viscosity

Cp_air = 1.012/4.318; %cal/g deg

%Initial
conditions____________________________________________________
Xi= 0.01;
```

```
Ti= 285 + 273.15;%K
di = 300*10^(-4);% (m)
Vi = (4*W)/(pi*di^2*density(Ti));%cm/s

%System
Dimensions_____________________________________________________
fila_length = 300; %cm
num_filaments = 10; %filaments in R direction
nu_modules = 300; %in z direction
mod_length = (fila_length)/(nu_modules); %length of a cell (cm)
Spinspace = 0.325; %The distance between filaments (cm)
hl = round(100/mod_length);%dummy variable for space vector

%dummy variables used to calculate least error later in code
V1 = 2000*100/60;
V2 = 3000*100/60;
V3 = 4000*100/60;
V4 = 5000*100/60;

%Initial force ranges (guessed from trial
runs)____________________________
F_d1 = 65.0;
F_d2 = F_d1-1.15;
F_d3 = F_d2-1.14;
F_d4 = F_d3-1.13;
F_d5 = F_d4-1.11;
F_d6 = F_d5-1.10;
F_d7 = F_d6-1.09;
F_d8 = F_d7-1.07;
F_d9 = F_d8-1.05;
F_d10 = F_d9-1.03;
diffF_d = 7;
delta = 0.005;

%generates an array of initial force
values__________________________________
F_do = zeros(diffF_d/delta+1,num_filaments);% sets place holders for
elements
F_do(1,:) = [F_d1 F_d2 F_d3 F_d4 F_d5 F_d6 F_d7 F_d8 F_d9 F_d10];

for sa = 1:num_filaments
    for s = 2:(diffF_d/delta+1)
        F_do(s,sa) = F_do(s-1,sa)+delta;
    end
end

%Air mass flow
rate_____________________________________________________
W_air = ps*Va*Spinspace*mod_length;

%Setting up quench air temperature values for first
filament____________
Ta = zeros(nu_modules+1,num_filaments+1,diffF_d/delta+1);
Tan = zeros(hl,num_filaments+1,diffF_d/delta+1);

dd = zeros(1,nu_modules);

for j = 1:nu_modules %space variable
    dd(1) = 0;
```

```
    dd(j+1) = (j-1)*mod_length+mod_length;
end

for j = 1:nu_modules+1 %arranging Ta/Tan(plot) matrix
    if (((dd(j))<100))
        Ta(j,1,:) = Ta1;
        Tan(j,1,:) = Ta1;
    else
        if (((dd(j))<200)||((dd(j))==200))
            Ta(j,1,:) = Th;

        else if (((dd(j))<300)||((dd(j))==300))
                Ta(j,1,:) = Ta1;
            end
        end
    end
end

%Generates place holders to store property values later
X_pp = zeros(nu_modules+1,num_filaments,diffF_d/delta+1); X_pp(1,:,:)
= Xi;
T_pp = zeros(nu_modules+1,num_filaments,diffF_d/delta+1); T_pp(1,:,:)
= Ti;
F_pp = zeros(nu_modules+1,num_filaments,diffF_d/delta+1); %F_pp(1,:)
= Fi id defined below according to take up velocity;
V_pp = zeros(nu_modules+1,num_filaments,diffF_d/delta+1); V_pp(1,:,:)
= Vi;
d_pp = zeros(nu_modules+1,num_filaments,diffF_d/delta+1); d_pp(1,:,:)
= di;

XF = zeros(nu_modules+1,num_filaments,5);
TF = zeros(nu_modules+1,num_filaments,5);
FF = zeros(nu_modules+1,num_filaments,5);
VF = zeros(nu_modules+1,num_filaments,5);
dF = zeros(nu_modules+1,num_filaments,5);
TaF = zeros(nu_modules+1,num_filaments+1,5);

VL_pp = zeros(length(F_d1:delta:F_d1+diffF_d),num_filaments);
DT = zeros(nu_modules+1,num_filaments,diffF_d/delta+1);
As = zeros(nu_modules+1,num_filaments,diffF_d/delta+1);
Q = zeros(nu_modules+1,num_filaments,diffF_d/delta+1);
amax = zeros(1,num_filaments);

%Start of multifilament
coding_____________________________________________
for i =5:num_filaments%:num_filaments

    for m  =1:size(F_do,1) %loop to determine the initial force
required for required take up speed.

        F_pp(1,i,m) = F_do(m,i);%sets initial force to value from
retrieved from array.

        for j = 1:nu_modules%Loop to run through each cell

            x0 = [X_pp(j,i,m) T_pp(j,i,m) F_pp(j,i,m)
V_pp(j,i,m)];%inital value vector
```

```
            global Ta2; Ta2 = Ta(j,i,m);%sets value of quench air
temperature to calculated value from cell in the previous filament
row

            [z,x] = ode23s('M',[(j-1)*(mod_length) (j-
1)*(mod_length)+mod_length],x0,[]);%calculates polymer properties
based on initial conditions from previous cell.
            %stores calculated values
            X_pp(j+1,i,m) = x(size(x,1),1);
            T_pp(j+1,i,m) = x(size(x,1),2);
            F_pp(j+1,i,m) = x(size(x,1),3);
            V_pp(j+1,i,m) = x(size(x,1),4);
            d_pp(j+1,i,m) =
sqrt((4*W)/(density(T_pp(j+1,i,m))*V_pp(j+1,i,m)*pi));

            Tavg = (sum(x(:,2)))/size(x(:,2),1);%average filament
temperature in cell
            DT(j,i,m) = (x(1,2) - x(size(x,1),2));%change in
temperature across cell

            %Conditions for calculating change in air temperature
            if (dd(j)<100)||(dd(j)==100)
                As(j,i,m) =
pi()/4*(d_pp(j,i,m)+d_pp(j+1,i,m))*mod_length;
                Q(j,i,m) =
al(d_pp(j,i,m),V_pp(j,i,m),Va,z(end))*(Tavg-
Ta(j,i,m))*As(j,i,m);%heat transferred

                Ta(j,i+1,m) = Ta(j,i,m)
+(Q(j,i,m))/(W_air*Cp_air);%energy balance, calculates exit quench
air temperature from the cell.

            else if (dd(j)<200)||(dd(j)==200) %set quench temperature
in zone 2.
                    Ta(j,i+1,m) = Th;
                else
                    Ta(j,i+1,m) = Ta1;  %set quench temperature in
zone 3.
                end
            end

        end
        VL_pp(m,i) = V_pp(end,i,m); %stores final cell velocity value
for further use
        c = V_pp(end,i,m);
        %if statement to stop coding once the final desired velocity
is achieved.
        if m < 2
            continue
        else
            if  (VL_pp(m,i)- VL_pp(m-1,i))/(F_do(m,i) - F_do(m-1,i))
< 0 && abs(c - V4)/(V4) < 0.006
                break
            end
        end
    end
end

%Coding to find elements of least error with respect to velocity.
This
```

```
%identifies which initial force to use.
V_error = zeros(size(VL_pp,1),num_filaments,4);
a_element = zeros(5,num_filaments);
a_max = zeros(num_filaments,1);

for i = 1:num_filaments
    for m = 1:size(F_do,1)

        a_max(i) = find(VL_pp(:,i) >= max(VL_pp(:,i))); %finding
maximum velocity element

        V_error(m,i,1) = abs(VL_pp(m,i) - V1); %2000 m/min
        V_error(m,i,2) = abs(VL_pp(m,i) - V2); %3000 m/min
        V_error(m,i,3) = abs(VL_pp(m,i) - V3); %4000 m/min
        V_error(m,i,4) = abs(VL_pp(m,i) - V4); %4000 m/min
    end
    a_element(1,i) =find(V_error(1:a_max(i),i,1) <= min(
V_error(1:a_max(i),i,1))); %2000
    a_element(2,i) =find(V_error(1:a_max(i),i,2) <= min(
V_error(1:a_max(i),i,2))); %3000
    a_element(3,i) =find(V_error(1:a_max(i),i,3) <= min(
V_error(1:a_max(i),i,3))); %4000
    a_element(4,i) =find(V_error(1:a_max(i),i,4) <= min(
V_error(1:a_max(i),i,4))); %5000
    a_element(5,i) =a_max(i) + find(V_error(a_max(i):end,i,4) <= min(
V_error(a_max(i):end,i,4)))-1; %5000ph2
end

%Stores property values according to element with least error.
for j = 1:size(a_element,1)
    for i = 1:size(a_element,2)
        XF(:,i,j) = X_pp(:,i,a_element(j,i))*100;
        TF(:,i,j) = T_pp(:,i,a_element(j,i))-273.15;
        FF(:,i,j) = F_pp(:,i,a_element(j,i));
        VF(:,i,j) = V_pp(:,i,a_element(j,i))*60/100;
        dF(:,i,j) = d_pp(:,i,a_element(j,i))*10^4;
        TaF(:,i,j) = Ta(:,i,a_element(j,i));
    end
end

for j = 1:size(a_element,1)
    TaF(:,11,j) = Ta(:,11,a_element(j,10));
end

%Coding to calculate orientation
Kpo = zeros(size(XF,1),num_filaments,size(a_element,1));
dp = zeros(size(XF,1),num_filaments,size(a_element,1));
fa = zeros(size(XF,1),num_filaments,size(a_element,1));
K = zeros(size(XF,1),num_filaments,size(a_element,1));
TS = zeros(size(XF,1),num_filaments,size(a_element,1));

for j = 1:size(a_element,1)
    for i = 1:num_filaments
        for m = 1:size(XF,1)
            TS(m,i,j) = FF(m,i,j)/(pi*(dF(m,i,j)/10^4/2)^2);%*10^-5;
            if TF(m,i,j)+273.15 < Tm && TF(m,i,j)+ 273.15 > Tg
                Kpo(m,i,j) =  Km*exp(-4*log(2)*(((TF(m,i,j)+ 273.15 -
Tmax)^2)/Dh^2));
            else
                Kpo(m,i,j) = 0;
```

```
            end

            dp(m,i,j) = (density(TF(m,i,j)+
273.15)*FF(m,i,j)*VF(m,i,j)*100/60)/W;
            B1 = Co/dn;
            B2 = (-3/7)*(Co/dn)^2;
            B3 = (-1/7)*(Co/dn)^3;

            fa(m,i,j) = B1*dp(m,i,j)+B2*dp(m,i,j)^2+B3.*dp(m,i,j)^3;
            K(m,i,j)  = Kpo(m,i,j)*exp(A*(fa(m,i,j))^2);
        end
    end
end

%Stores values in logical order.
AX1 = XF(:,:,1);AX2 = XF(:,:,2);AX3 = XF(:,:,3);AX4 = XF(:,:,4);AX5 =
XF(:,:,5);
AT1 = TF(:,:,1);AT2 = TF(:,:,2);AT3 = TF(:,:,3);AT4 = TF(:,:,4);AT5 =
TF(:,:,5);
AF1 = FF(:,:,1);AF2 = FF(:,:,2);AF3 = FF(:,:,3);AF4 = FF(:,:,4);AF5 =
FF(:,:,5);
AV1 = VF(:,:,1);AV2 = VF(:,:,2);AV3 = VF(:,:,3);AV4 = VF(:,:,4);AV5 =
VF(:,:,5);
Ad1 = dF(:,:,1);Ad2 = dF(:,:,2);Ad3 = dF(:,:,3);Ad4 = dF(:,:,4);Ad5 =
dF(:,:,5);
Afa1 = fa(:,:,1);Afa2 = fa(:,:,2);Afa3 = fa(:,:,3);Afa4 =
fa(:,:,4);Afa5 = fa(:,:,5);
ATa1 = TaF(:,:,1);ATa2 = TaF(:,:,2);ATa3 = TaF(:,:,3);ATa4 =
TaF(:,:,4);ATa5 = TaF(:,:,5);
ATS1 = TS(:,:,1);ATS2 = TS(:,:,2);ATS3 = TS(:,:,3);ATS4 =
TS(:,:,4);ATS5 = TS(:,:,5);



%Stats
coding_____________________________________________________________
num = num_filaments;
X_mean = zeros(nu_modules+1,size(a_element,1));
T_mean = zeros(nu_modules+1,size(a_element,1));
F_mean = zeros(nu_modules+1,size(a_element,1));
V_mean = zeros(nu_modules+1,size(a_element,1));
d_mean = zeros(nu_modules+1,size(a_element,1));
fa_mean = zeros(nu_modules+1,size(a_element,1));

for a = 1:size(a_element,1)
    for j = 1:nu_modules+1 %Calculating the mean for each module
throughout filament bundle

        X_mean(j,a) = mean(XF(j,:,a));
        T_mean(j,a) = mean(TF(j,:,a));
        F_mean(j,a) = mean(FF(j,:,a));
        V_mean(j,a) = mean(VF(j,:,a));
        d_mean(j,a) = mean(dF(j,:,a));
        fa_mean(j,a) = mean(fa(j,:,a));

    end
end

X_var = zeros(nu_modules+1,size(a_element,1));
```

```
T_var = zeros(nu_modules+1,size(a_element,1));
F_var = zeros(nu_modules+1,size(a_element,1));
V_var = zeros(nu_modules+1,size(a_element,1));
d_var = zeros(nu_modules+1,size(a_element,1));
fa_var = zeros(nu_modules+1,size(a_element,1));

for a = 1:size(a_element,1)
    X_var(:,a) = var(XF(:,:,a)')';
    T_var(:,a) = var(TF(:,:,a)')';
    F_var(:,a) = var(FF(:,:,a)')';
    V_var(:,a) = var(VF(:,:,a)')';
    d_var(:,a) = var(dF(:,:,a)')';
    fa_var(:,a) = var(fa(:,:,a)')';
end

X_CV = zeros(nu_modules+1,size(a_element,1));
T_CV = zeros(nu_modules+1,size(a_element,1));
F_CV = zeros(nu_modules+1,size(a_element,1));
V_CV = zeros(nu_modules+1,size(a_element,1));
d_CV = zeros(nu_modules+1,size(a_element,1));
fa_CV = zeros(nu_modules+1,size(a_element,1));

for a = 1:size(a_element,1)
    for j = 1:nu_modules+1 %calculating the std deviation for each
module set.
        X_CV(j,a) = 100*sqrt(X_var(j,a))/X_mean(j,a);
        T_CV(j,a) = 100*sqrt(T_var(j,a))/T_mean(j,a);
        F_CV(j,a) = 100*sqrt(F_var(j,a))/F_mean(j,a);
        V_CV(j,a) = 100*sqrt(V_var(j,a))/V_mean(j,a);
        d_CV(j,a) = 100*sqrt(d_var(j,a))/d_mean(j,a);
        fa_CV(j,a) = 100*sqrt(fa_var(j,a))/fa_mean(j,a);
    end
end

CV_2000 = [X_CV(:,1) T_CV(:,1) F_CV(:,1) V_CV(:,1) d_CV(:,1)
fa_CV(:,1)];
CV_3000 = [X_CV(:,2) T_CV(:,2) F_CV(:,2) V_CV(:,2) d_CV(:,2)
fa_CV(:,2)];
CV_4000 = [X_CV(:,3) T_CV(:,3) F_CV(:,3) V_CV(:,3) d_CV(:,3)
fa_CV(:,3)];
CV_5000ph1 = [X_CV(:,4) T_CV(:,4) F_CV(:,4) V_CV(:,4) d_CV(:,4)
fa_CV(:,4)];
CV_5000ph2 = [X_CV(:,5) T_CV(:,5) F_CV(:,5) V_CV(:,5) d_CV(:,5)
fa_CV(:,5)];

%Integration of dimensionless standard deviation plots
A_int = zeros(6,size(a_element,1));
for a = 1:size(a_element,1)

    A_int(1,a) = trapz(dd,X_CV(:,a))/(dd(size(X_CV,1)));
    A_int(2,a) = trapz(dd(1:hl),T_CV(1:hl,a))/(dd(hl));
    A_int(3,a) = trapz(dd,F_CV(:,a))/(dd(size(F_CV,1)));
    A_int(4,a) = trapz(dd,V_CV(:,a))/(dd(size(V_CV,1)));
    A_int(5,a) = trapz(dd,d_CV(:,a))/(dd(size(d_CV,1)));
    A_int(6,a) = trapz(dd,fa_CV(:,a))/(dd(size(fa_CV,1)));

end

%Output generation
figure(2)
```

```
subplot(3,2,1),plot(dd,XF(:,:,1)),title('Crystallinity vs distance'),xlabel('distance [cm]'),ylabel('Crystallinity [%]')
subplot(3,2,2),plot(dd,TF(:,:,1)),title('Temperature vs distance'),xlabel('distance [cm]'),ylabel('Temprature [^oC]')
subplot(3,2,3),plot(dd,FF(:,:,1)),title('Force vs distance'),xlabel('distance [cm]'),ylabel('Force [dyne]')
subplot(3,2,4),plot(dd,VF(:,:,1)),title('Velocity vs distance'),xlabel('distance [cm]'),ylabel('Velocity [m/min]')
subplot(3,2,5),plot(dd,dF(:,:,1)),title('Diameter vs distance'),xlabel('distance [cm]'),ylabel('Diameter [microns]')
subplot(3,2,6),plot(dd,fa(:,:,1)),title('Orientation vs distance'),xlabel('distance [cm]'),ylabel('Orientation [-]')

figure(3)
subplot(3,2,1),plot(dd,XF(:,:,2)),title('Crystallinity vs distance'),xlabel('distance [cm]'),ylabel('Crystallinity [%]')
subplot(3,2,2),plot(dd,TF(:,:,2)),title('Temperature vs distance'),xlabel('distance [cm]'),ylabel('Temprature [^oC]')
subplot(3,2,3),plot(dd,FF(:,:,2)),title('Force vs distance'),xlabel('distance [cm]'),ylabel('Force [dyne]')
subplot(3,2,4),plot(dd,VF(:,:,2)),title('Velocity vs distance'),xlabel('distance [cm]'),ylabel('Velocity [m/min]')
subplot(3,2,5),plot(dd,dF(:,:,2)),title('Diameter vs distance'),xlabel('distance [cm]'),ylabel('Diameter [microns]')
subplot(3,2,6),plot(dd,fa(:,:,2)),title('Orientation vs distance'),xlabel('distance [cm]'),ylabel('Orientation [-]')

figure(4)
subplot(3,2,1),plot(dd,XF(:,:,3)),title('Crystallinity vs distance'),xlabel('distance [cm]'),ylabel('Crystallinity [%]')
subplot(3,2,2),plot(dd,TF(:,:,3)),title('Temperature vs distance'),xlabel('distance [cm]'),ylabel('Temprature [^oC]')
subplot(3,2,3),plot(dd,FF(:,:,3)),title('Force vs distance'),xlabel('distance [cm]'),ylabel('Force [dyne]')
subplot(3,2,4),plot(dd,VF(:,:,3)),title('Velocity vs distance'),xlabel('distance [cm]'),ylabel('Velocity [m/min]')
subplot(3,2,5),plot(dd,dF(:,:,3)),title('Diameter vs distance'),xlabel('distance [cm]'),ylabel('Diameter [microns]')
subplot(3,2,6),plot(dd,fa(:,:,3)),title('Orientation vs distance'),xlabel('distance [cm]'),ylabel('Orientation [-]')

figure(5)
subplot(3,2,1),plot(dd,XF(:,:,4)),title('Crystallinity vs distance'),xlabel('distance [cm]'),ylabel('Crystallinity [%]')
subplot(3,2,2),plot(dd,TF(:,:,4)),title('Temperature vs distance'),xlabel('distance [cm]'),ylabel('Temprature [^oC]')
subplot(3,2,3),plot(dd,FF(:,:,4)),title('Force vs distance'),xlabel('distance [cm]'),ylabel('Force [dyne]')
subplot(3,2,4),plot(dd,VF(:,:,4)),title('Velocity vs distance'),xlabel('distance [cm]'),ylabel('Velocity [m/min]')
subplot(3,2,5),plot(dd,dF(:,:,4)),title('Diameter vs distance'),xlabel('distance [cm]'),ylabel('Diameter [microns]')
subplot(3,2,6),plot(dd,fa(:,:,4)),title('Orientation vs distance'),xlabel('distance [cm]'),ylabel('Orientation [-]')

figure(6)
subplot(3,2,1),plot(dd,XF(:,:,5)),title('Crystallinity vs distance'),xlabel('distance [cm]'),ylabel('Crystallinity [%]')
subplot(3,2,2),plot(dd,TF(:,:,5)),title('Temperature vs distance'),xlabel('distance [cm]'),ylabel('Temprature [^oC]')
```

```
subplot(3,2,3),plot(dd,FF(:,:,5)),title('Force vs
distance'),xlabel('distance [cm]'),ylabel('Force [dyne]')
subplot(3,2,4),plot(dd,VF(:,:,5)),title('Velocity vs
distance'),xlabel('distance [cm]'),ylabel('Velocity [m/min]')
subplot(3,2,5),plot(dd,dF(:,:,5)),title('Diameter vs
distance'),xlabel('distance [cm]'),ylabel('Diameter [microns]')
subplot(3,2,6),plot(dd,fa(:,:,5)),title('Orientation vs
distance'),xlabel('distance [cm]'),ylabel('Orientation [-]')

figure(7)
subplot(3,2,1),plot(dd,TaF(:,:,1)),title('Quench Temperature vs
distance V_L=2000m/min'),xlabel('distance [cm]'),ylabel('Quench
Temp[^oC]')
axis([0 99 300 max(TaF(:,11,1))])
subplot(3,2,2),plot(dd,TaF(:,:,2)),title('Quench Temperature vs
distance V_L=3000m/min'),xlabel('distance [cm]'),ylabel('Quench
Temp[^oC]')
axis([0 99 300 max(TaF(:,11,2))])
subplot(3,2,3),plot(dd,TaF(:,:,3)),title('Quench Temperature vs
distance V_L=4000m/min'),xlabel('distance [cm]'),ylabel('Quench
Temp[^oC]')
axis([0 99 300 max(TaF(:,11,3))])
subplot(3,2,4),plot(dd,TaF(:,:,4)),title('Quench Temperature vs
distance V_L=4000m/min ph2'),xlabel('distance [cm]'),ylabel('Quench
Temp[^oC]')
axis([0 99 300 max(TaF(:,11,4))])
subplot(3,2,5),plot(dd,TaF(:,:,5)),title('Quench Temperature vs
distance V_L=4000m/min ph2'),xlabel('distance [cm]'),ylabel('Quench
Temp[^oC]')
axis([0 99 300 max(TaF(:,11,5))])

figure(8)
subplot(3,2,1)
plot(dd,X_CV),xlabel('distance from spinneret
[cm]'),ylabel('Crystallisation CV [%]')
subplot(3,2,2)
plot(dd,T_CV),xlabel('distance from spinneret
[cm]'),ylabel('Temperature CV [%]')
axis([0 100 min(T_CV(:,size(a_element,1)))
max(T_CV(:,size(a_element,1)))+1])
subplot(3,2,3)
plot(dd,F_CV),xlabel('distance from spinneret [cm]'),ylabel('Force CV
[%]')
subplot(3,2,4)
plot(dd,V_CV),xlabel('distance from spinneret [cm]'),ylabel('Velocity
CV [%]')
subplot(3,2,5)
plot(dd,d_CV),xlabel('distance from spinneret [cm]'),ylabel('Diameter
CV [%]')
subplot(3,2,6)
plot(dd,fa_CV),xlabel('distance from spinneret
[cm]'),ylabel('Orientation CV [%]')

figure(9)
subplot(3,2,1)
plot(dd,X_mean),xlabel('distance from spinneret
[cm]'),ylabel('Crystallisation mean [%]')
subplot(3,2,2)
plot(dd,T_mean),xlabel('distance from spinneret
[cm]'),ylabel('Temperature mean [^oC]')
subplot(3,2,3)
```

```
plot(dd,F_mean),xlabel('distance from spinneret [cm]'),ylabel('Force
mean [dyne]')
subplot(3,2,4)
plot(dd,V_mean),xlabel('distance from spinneret
[cm]'),ylabel('Velocity mean [m/s]')
subplot(3,2,5)
plot(dd,d_mean),xlabel('distance from spinneret
[cm]'),ylabel('Diameter mean [microns]')
subplot(3,2,6)
plot(dd,fa_mean),xlabel('distance from spinneret
[cm]'),ylabel('Orientation mean [microns]')

%coding to save data and figures
automatically_________________________________________________________
W1 = W*100;
s = [dir 'T' int2str(Ta1-273) 'V' int2str(Va) 'W' int2str(W1)];
save(s)
toc/3600
```

C.3 Monofilament model – Iteration approach

The sub-files used in this simulation are identical to those used in the monofilament model. These can be viewed in Appendix C.1.

C.3.1 Main file

```
%multi filament code
clc;close all;clear all;
tic
global type;type = 2;
dir = 'C:\Documents and Settings\HGHALI004\My Documents\Ty\Iteration
model 285 W3\';
%Constants____________________________________________
global W; W = 0.03;% mass flow rate (g/s)
global Va; Va = input('Quench air speed (cm/s):'); %velocity of
cooling medium cm/s
global Ta1;Ta1 = input('Quench air temp in (^oC):') + 273; %Cooling
medium temp (oC)
global g, g = 9.81*100; %gravitational constant (cm/s^2)
global dh, dh = 1.237*10^2/4.184;%(J/g --> cal/g) Heat of
crystallisation (erg/g*10^-7= J/g)
global ps; ps = 1.2022/1000;% density of air (g/cm^3)
global n; n = 4;%Avrami exponent
global Tg; Tg = 70 + 273; %Glass transition temp for PET (343 K)
global Tmax; Tmax = 190 + 273; %Temp corresponding to Kmax for PET
(463 K)
global Km; Km = 0.016; %Max crystallisation rate for PET (1/s)
global Tm; Tm = 280 + 273; %Melting temp for PET (553 K)
global Dh; Dh = 32; %half width of K(T) curve
global A; A = 500; % stress induced crystallisation factor (DKW-ave)
global Co; Co = 5.0*10^(-10); %stress optical co-efficient
(cm^2/dyne*10=m^2/N)
global dn; dn = 0.275; % amorphous birefringence (-)
global Th; Th = 150 + 273; %degrees C
global Eak; Eak = 6923.7; %(K)
global alpha; alpha = 1; %unity for low molecular weights
global X_s; X_s = 0.1; %critical crystallinity
global IV; IV = 0.6;%Intrinsic viscosity

Cp_air = 1.012/4.318; %cal/g deg
```

```
%Initial
conditions_____________________________________________________
Xi= 0.01;%Initial guess (-)
Ti= 285 + 273.15;%K
di = 300*10^(-4);% (m)
Vi = (4*W)/(pi*di^2*density(Ti));%cm/s

%System
Dimensions______________________________________________________
fila_length = 300; %cm
num_filaments = 10; %filaments in R direction
nu_modules = 300; %in z direction
mod_length = (fila_length)/(nu_modules); %length of a cell (cm)
Spinspace = 0.325; %distance between filaments (cm)
hl = round(100/mod_length);%dummy variable

V1 = 2000*100/60;
V2 = 3000*100/60;
V3 = 4000*100/60;
V4 = 5000*100/60;

%Initial force
ranges__________________________________________________
F_d1 = 57.99;
F_d2 = F_d1-2.51;
F_d3 = F_d2-2.41;
F_d4 = F_d3-2.32;
F_d5 = F_d4-2.20;
F_d6 = F_d5-2.10;
F_d7 = F_d6-1.99;
F_d8 = F_d7-1.90;
F_d9 = F_d8-1.79;
F_d10 = F_d9-1.71;
diffF_d = 7;
delta = 0.0075;
na = 1;

F_do = zeros(diffF_d/delta+1,num_filaments);
F_do(1,:) = [F_d1 F_d2 F_d3 F_d4 F_d5 F_d6 F_d7 F_d8 F_d9 F_d10];

for sa = 1:num_filaments%sets up initial force array
    for s = 2:(diffF_d/delta+1)
        F_do(s,sa) = F_do(s-1,sa)+delta;
    end
end

%Air mass flow
rate_____________________________________________________
W_air = ps*Va*Spinspace*mod_length;

%Setting up Ta
matrix___________________________________________________
Ta = zeros(nu_modules+1,num_filaments+1,diffF_d/delta+1);
Taold = zeros(nu_modules+1,num_filaments+1,diffF_d/delta+1);
Tanew = zeros(nu_modules+1,num_filaments+1,diffF_d/delta+1);
Tan = zeros(hl,num_filaments+1,diffF_d/delta+1);

dd = zeros(1,nu_modules);
```

```
for j = 1:nu_modules %space variable
    dd(1) = 0;
    dd(j+1) = (j-1)*mod_length+mod_length;
end

for j = 1:nu_modules+1 %arranging Ta matrix for first filament
    if (((dd(j))<100))
        Ta(j,1,:) = Ta1;
        Tan(j,1,:) = Ta1;
    else
        if (((dd(j))<200)||((dd(j))==200))
            Ta(j,1,:) = Th;

        else if (((dd(j))<300)||((dd(j))==300))
                Ta(j,1,:) = Ta1;
            end
        end
    end
end

%defining place holder to store property values later
X_pp = zeros(nu_modules+1,num_filaments,diffF_d/delta+1); X_pp(1,:,:)
= Xi;
T_pp = zeros(nu_modules+1,num_filaments,diffF_d/delta+1); T_pp(1,:,:)
= Ti;
F_pp = zeros(nu_modules+1,num_filaments,diffF_d/delta+1); %F_pp(1,:)
= Fi id defined below according to take up velocity;
V_pp = zeros(nu_modules+1,num_filaments,diffF_d/delta+1); V_pp(1,:,:)
= Vi;
d_pp = zeros(nu_modules+1,num_filaments,diffF_d/delta+1); d_pp(1,:,:)
= di;

XF = zeros(nu_modules+1,num_filaments,5);
TF = zeros(nu_modules+1,num_filaments,5);
FF = zeros(nu_modules+1,num_filaments,5);
VF = zeros(nu_modules+1,num_filaments,5);
dF = zeros(nu_modules+1,num_filaments,5);
TaF = zeros(nu_modules+1,num_filaments+1,5);

VL_pp = zeros(length(F_d1:delta:F_d1+diffF_d),num_filaments);
DT = zeros(nu_modules+1,num_filaments,diffF_d/delta+1);
As = zeros(nu_modules+1,num_filaments,diffF_d/delta+1);
Q = zeros(nu_modules+1,num_filaments,diffF_d/delta+1);
amax = zeros(1,num_filaments);

%Start of multifilament
coding_____________________________________________
for i = na:num_filaments%:num_filaments

    for m  =1:size(F_do,1) %loop to determine the initial force
required for required take up speed.

        F_pp(1,i,m) = F_do(m,i);

        for j = 1:nu_modules

            Tanew(j,i,m) = Ta(j,i,m); %guess for first value
            Taold(j,i,m) = 2*Tanew(j,i,m); %guess for old value
```

```
            %convergence criteria
            while (abs((Tanew(j,i,m) - Taold(j,i,m))/Taold(j,i,m))>
0.001)

                x0 = [X_pp(j,i,m) T_pp(j,i,m) F_pp(j,i,m)
V_pp(j,i,m)]; %initial condition vector

                global Ta2; Ta2 = Tanew(j,i,m); %sets value for
localAT file
                %ode command statement, build in solver.
                [z,x] = ode23s('M',[(j-1)*(mod_length) (j-
1)*(mod_length)+mod_length],x0,[]);
                %stores calculted values for each cell
                X_pp(j+1,i,m) = x(size(x,1),1);
                T_pp(j+1,i,m) = x(size(x,1),2);
                F_pp(j+1,i,m) = x(size(x,1),3);
                V_pp(j+1,i,m) = x(size(x,1),4);
                d_pp(j+1,i,m) =
sqrt((4*W)/(density(T_pp(j+1,i,m))*V_pp(j+1,i,m)*pi));

                Tavg = (sum(x(:,2)))/size(x(:,2),1);
                DT(j,i,m) = (x(1,2) - x(size(x,1),2));

                %Conditions for calculating change in air temperature
                if (dd(j)<100)||(dd(j)==100) %Ta for zone 1
                    As(j,i,m) =
pi()/4*(d_pp(j,i,m)+d_pp(j+1,i,m))*mod_length;
                    Q(j,i,m) =
al(d_pp(j,i,m),V_pp(j,i,m),Va,z(end))*(Tavg-Ta(j,i,m))*As(j,i,m);

                    Ta(j,i+1,m) = Tanew(j,i,m)
+(Q(j,i,m))/(W_air*Cp_air);

                else if (dd(j)<200)||(dd(j)==200) %Ta for zone 2
                        Ta(j,i+1,m) = Th;
                    else
                        Ta(j,i+1,m) = Ta1; %Ta for zone 3
                    end
                end
                Taold(j,i,m) = Tanew(j,i,m); %sets new Told to Tanew
                Tanew(j,i,m) = (Ta(j,i,m)+Ta(j,i+1,m))/2; %sets
calculated Ta to Tanew
            end

        end
        %dummy variables
        VL_pp(m,i) = V_pp(end,i,m);
        c = V_pp(end,i,m);
        %loop which terminates calculation when final desired
velocity is
        %achieved
        if m < 2
            continue
        else

            if  (VL_pp(m,i)- VL_pp(m-1,i))/(F_do(m,i) - F_do(m-1,i))
< 0 && c<V4
                break
            end
        end
```

```
    end
end

%Coding find elements corresponding to least error with respect to
velocity
V_error = zeros(size(VL_pp,1),num_filaments,4);
a_element = zeros(5,num_filaments);
a_max = zeros(num_filaments,1);

for i = 1:num_filaments
    for m = 1:size(F_do,1)

        a_max(i) = find(VL_pp(:,i) >= max(VL_pp(:,i))); %finding
maximum velocity element

            V_error(m,i,1) = abs(VL_pp(m,i) - V1); %2000 m/min
            V_error(m,i,2) = abs(VL_pp(m,i) - V2); %3000 m/min
            V_error(m,i,3) = abs(VL_pp(m,i) - V3); %4000 m/min
            V_error(m,i,4) = abs(VL_pp(m,i) - V4); %4000 m/min
    end
            a_element(1,i) =find(V_error(1:a_max(i),i,1) <= min(
V_error(1:a_max(i),i,1))); %2000
            a_element(2,i) =find(V_error(1:a_max(i),i,2) <= min(
V_error(1:a_max(i),i,2))); %3000
            a_element(3,i) =find(V_error(1:a_max(i),i,3) <= min(
V_error(1:a_max(i),i,3))); %4000
            a_element(4,i) =find(V_error(1:a_max(i),i,4) <= min(
V_error(1:a_max(i),i,4))); %5000
            a_element(5,i) =a_max(i) + find(V_error(a_max(i):end,i,4)
<= min( V_error(a_max(i):end,i,4)))-1; %5000ph2
end

%coding to store values according to element
for j = 1:size(a_element,1)
    for i = 1:size(a_element,2)
        XF(:,i,j) = X_pp(:,i,a_element(j,i))*100;
        TF(:,i,j) = T_pp(:,i,a_element(j,i))-273.15;
        FF(:,i,j) = F_pp(:,i,a_element(j,i));
        VF(:,i,j) = V_pp(:,i,a_element(j,i))*60/100;
        dF(:,i,j) = d_pp(:,i,a_element(j,i))*10^4;
        TaF(:,i,j) = Ta(:,i,a_element(j,i));
    end
end

for j = 1:size(a_element,1)
    TaF(:,11,j) = Ta(:,11,a_element(j,10));
end

%Coding to calculate orientation
Kpo = zeros(size(XF,1),num_filaments,size(a_element,1));
dp = zeros(size(XF,1),num_filaments,size(a_element,1));
fa = zeros(size(XF,1),num_filaments,size(a_element,1));
K = zeros(size(XF,1),num_filaments,size(a_element,1));
TS = zeros(size(XF,1),num_filaments,size(a_element,1));

for j = 1:size(a_element,1)
    for i = 1:num_filaments
        for m = 1:size(XF,1)
            TS(m,i,j) = FF(m,i,j)/(pi*(dF(m,i,j)/10^4/2)^2);%*10^-5;
            if TF(m,i,j)+273.15 < Tm && TF(m,i,j)+ 273.15 > Tg
```

```
                Kpo(m,i,j) =  Km*exp(-4*log(2)*(((TF(m,i,j)+ 273.15 -
Tmax)^2)/Dh^2));
            else
                Kpo(m,i,j) = 0;
            end

            dp(m,i,j) = (density(TF(m,i,j)+
273.15)*FF(m,i,j)*VF(m,i,j)*100/60)/W;
            B1 = Co/dn;
            B2 = (-3/7)*(Co/dn)^2;
            B3 = (-1/7)*(Co/dn)^3;

            fa(m,i,j) = B1*dp(m,i,j)+B2*dp(m,i,j)^2+B3.*dp(m,i,j)^3;
            K(m,i,j)  = Kpo(m,i,j)*exp(A*(fa(m,i,j))^2);
        end
    end
end

%storing final properties in logical order.
AX1 = XF(:,:,1);AX2 = XF(:,:,2);AX3 = XF(:,:,3);AX4 = XF(:,:,4);AX5 =
XF(:,:,5);
AT1 = TF(:,:,1);AT2 = TF(:,:,2);AT3 = TF(:,:,3);AT4 = TF(:,:,4);AT5 =
TF(:,:,5);
AF1 = FF(:,:,1);AF2 = FF(:,:,2);AF3 = FF(:,:,3);AF4 = FF(:,:,4);AF5 =
FF(:,:,5);
AV1 = VF(:,:,1);AV2 = VF(:,:,2);AV3 = VF(:,:,3);AV4 = VF(:,:,4);AV5 =
VF(:,:,5);
Ad1 = dF(:,:,1);Ad2 = dF(:,:,2);Ad3 = dF(:,:,3);Ad4 = dF(:,:,4);Ad5 =
dF(:,:,5);
Afa1 = fa(:,:,1);Afa2 = fa(:,:,2);Afa3 = fa(:,:,3);Afa4 =
fa(:,:,4);Afa5 = fa(:,:,5);
ATa1 = TaF(:,:,1);ATa2 = TaF(:,:,2);ATa3 = TaF(:,:,3);ATa4 =
TaF(:,:,4);ATa5 = TaF(:,:,5);
ATS1 = TS(:,:,1);ATS2 = TS(:,:,2);ATS3 = TS(:,:,3);ATS4 =
TS(:,:,4);ATS5 = TS(:,:,5);



%Stats
coding______________________________________________________________
num = num_filaments;
X_mean = zeros(nu_modules+1,size(a_element,1));
T_mean = zeros(nu_modules+1,size(a_element,1));
F_mean = zeros(nu_modules+1,size(a_element,1));
V_mean = zeros(nu_modules+1,size(a_element,1));
d_mean = zeros(nu_modules+1,size(a_element,1));
fa_mean = zeros(nu_modules+1,size(a_element,1));

for a = 1:size(a_element,1)
    for j = 1:nu_modules+1 %Calculating the mean for each module
throughout filament bundle

        X_mean(j,a) = mean(XF(j,:,a));
        T_mean(j,a) = mean(TF(j,:,a));
        F_mean(j,a) = mean(FF(j,:,a));
        V_mean(j,a) = mean(VF(j,:,a));
        d_mean(j,a) = mean(dF(j,:,a));
        fa_mean(j,a) = mean(fa(j,:,a));
```

```
    end
end

X_var = zeros(nu_modules+1,size(a_element,1));
T_var = zeros(nu_modules+1,size(a_element,1));
F_var = zeros(nu_modules+1,size(a_element,1));
V_var = zeros(nu_modules+1,size(a_element,1));
d_var = zeros(nu_modules+1,size(a_element,1));
fa_var = zeros(nu_modules+1,size(a_element,1));

for a = 1:size(a_element,1)
        X_var(:,a) = var(XF(:,:,a)')';
        T_var(:,a) = var(TF(:,:,a)')';
        F_var(:,a) = var(FF(:,:,a)')';
        V_var(:,a) = var(VF(:,:,a)')';
        d_var(:,a) = var(dF(:,:,a)')';
        fa_var(:,a) = var(fa(:,:,a)')';
end

X_CV = zeros(nu_modules+1,size(a_element,1));
T_CV = zeros(nu_modules+1,size(a_element,1));
F_CV = zeros(nu_modules+1,size(a_element,1));
V_CV = zeros(nu_modules+1,size(a_element,1));
d_CV = zeros(nu_modules+1,size(a_element,1));
fa_CV = zeros(nu_modules+1,size(a_element,1));

for a = 1:size(a_element,1)
    for j = 1:nu_modules+1 %calculating the std deviation for each
module set.
        X_CV(j,a) = 100*sqrt(X_var(j,a))/X_mean(j,a);
        T_CV(j,a) = 100*sqrt(T_var(j,a))/T_mean(j,a);
        F_CV(j,a) = 100*sqrt(F_var(j,a))/F_mean(j,a);
        V_CV(j,a) = 100*sqrt(V_var(j,a))/V_mean(j,a);
        d_CV(j,a) = 100*sqrt(d_var(j,a))/d_mean(j,a);
        fa_CV(j,a) = 100*sqrt(fa_var(j,a))/fa_mean(j,a);
    end
end

CV_2000 = [X_CV(:,1) T_CV(:,1) F_CV(:,1) V_CV(:,1) d_CV(:,1)
fa_CV(:,1)];
CV_3000 = [X_CV(:,2) T_CV(:,2) F_CV(:,2) V_CV(:,2) d_CV(:,2)
fa_CV(:,2)];
CV_4000 = [X_CV(:,3) T_CV(:,3) F_CV(:,3) V_CV(:,3) d_CV(:,3)
fa_CV(:,3)];
CV_5000ph1 = [X_CV(:,4) T_CV(:,4) F_CV(:,4) V_CV(:,4) d_CV(:,4)
fa_CV(:,4)];
CV_5000ph2 = [X_CV(:,5) T_CV(:,5) F_CV(:,5) V_CV(:,5) d_CV(:,5)
fa_CV(:,5)];

%Integration of dimensionless standard deviation plots
A_int = zeros(6,size(a_element,1));
for a = 1:size(a_element,1)

A_int(1,a) = trapz(dd,X_CV(:,a))/(dd(size(X_CV,1)));
A_int(2,a) = trapz(dd(1:hl),T_CV(1:hl,a))/(dd(hl));
A_int(3,a) = trapz(dd,F_CV(:,a))/(dd(size(F_CV,1)));
A_int(4,a) = trapz(dd,V_CV(:,a))/(dd(size(V_CV,1)));
A_int(5,a) = trapz(dd,d_CV(:,a))/(dd(size(d_CV,1)));
A_int(6,a) = trapz(dd,fa_CV(:,a))/(dd(size(fa_CV,1)));
```

```
end

%Output Coding
figure(2)
subplot(3,2,1),plot(dd,XF(:,:,1)),title('Crystallinity vs
distance'),xlabel('distance [cm]'),ylabel('Crystallinity [%]')
subplot(3,2,2),plot(dd,TF(:,:,1)),title('Temperature vs
distance'),xlabel('distance [cm]'),ylabel('Temprature [^oC]')
subplot(3,2,3),plot(dd,FF(:,:,1)),title('Force vs
distance'),xlabel('distance [cm]'),ylabel('Force [dyne]')
subplot(3,2,4),plot(dd,VF(:,:,1)),title('Velocity vs
distance'),xlabel('distance [cm]'),ylabel('Velocity [m/min]')
subplot(3,2,5),plot(dd,dF(:,:,1)),title('Diameter vs
distance'),xlabel('distance [cm]'),ylabel('Diameter [microns]')
subplot(3,2,6),plot(dd,fa(:,:,1)),title('Orientation vs
distance'),xlabel('distance [cm]'),ylabel('Orientation [-]')

figure(3)
subplot(3,2,1),plot(dd,XF(:,:,2)),title('Crystallinity vs
distance'),xlabel('distance [cm]'),ylabel('Crystallinity [%]')
subplot(3,2,2),plot(dd,TF(:,:,2)),title('Temperature vs
distance'),xlabel('distance [cm]'),ylabel('Temprature [^oC]')
subplot(3,2,3),plot(dd,FF(:,:,2)),title('Force vs
distance'),xlabel('distance [cm]'),ylabel('Force [dyne]')
subplot(3,2,4),plot(dd,VF(:,:,2)),title('Velocity vs
distance'),xlabel('distance [cm]'),ylabel('Velocity [m/min]')
subplot(3,2,5),plot(dd,dF(:,:,2)),title('Diameter vs
distance'),xlabel('distance [cm]'),ylabel('Diameter [microns]')
subplot(3,2,6),plot(dd,fa(:,:,2)),title('Orientation vs
distance'),xlabel('distance [cm]'),ylabel('Orientation [-]')

figure(4)
subplot(3,2,1),plot(dd,XF(:,:,3)),title('Crystallinity vs
distance'),xlabel('distance [cm]'),ylabel('Crystallinity [%]')
subplot(3,2,2),plot(dd,TF(:,:,3)),title('Temperature vs
distance'),xlabel('distance [cm]'),ylabel('Temprature [^oC]')
subplot(3,2,3),plot(dd,FF(:,:,3)),title('Force vs
distance'),xlabel('distance [cm]'),ylabel('Force [dyne]')
subplot(3,2,4),plot(dd,VF(:,:,3)),title('Velocity vs
distance'),xlabel('distance [cm]'),ylabel('Velocity [m/min]')
subplot(3,2,5),plot(dd,dF(:,:,3)),title('Diameter vs
distance'),xlabel('distance [cm]'),ylabel('Diameter [microns]')
subplot(3,2,6),plot(dd,fa(:,:,3)),title('Orientation vs
distance'),xlabel('distance [cm]'),ylabel('Orientation [-]')

figure(5)
subplot(3,2,1),plot(dd,XF(:,:,4)),title('Crystallinity vs
distance'),xlabel('distance [cm]'),ylabel('Crystallinity [%]')
subplot(3,2,2),plot(dd,TF(:,:,4)),title('Temperature vs
distance'),xlabel('distance [cm]'),ylabel('Temprature [^oC]')
subplot(3,2,3),plot(dd,FF(:,:,4)),title('Force vs
distance'),xlabel('distance [cm]'),ylabel('Force [dyne]')
subplot(3,2,4),plot(dd,VF(:,:,4)),title('Velocity vs
distance'),xlabel('distance [cm]'),ylabel('Velocity [m/min]')
subplot(3,2,5),plot(dd,dF(:,:,4)),title('Diameter vs
distance'),xlabel('distance [cm]'),ylabel('Diameter [microns]')
subplot(3,2,6),plot(dd,fa(:,:,4)),title('Orientation vs
distance'),xlabel('distance [cm]'),ylabel('Orientation [-]')

figure(6)
```

```
subplot(3,2,1),plot(dd,XF(:,:,5)),title('Crystallinity vs
distance'),xlabel('distance [cm]'),ylabel('Crystallinity [%]')
subplot(3,2,2),plot(dd,TF(:,:,5)),title('Temperature vs
distance'),xlabel('distance [cm]'),ylabel('Temprature [^oC]')
subplot(3,2,3),plot(dd,FF(:,:,5)),title('Force vs
distance'),xlabel('distance [cm]'),ylabel('Force [dyne]')
subplot(3,2,4),plot(dd,VF(:,:,5)),title('Velocity vs
distance'),xlabel('distance [cm]'),ylabel('Velocity [m/min]')
subplot(3,2,5),plot(dd,dF(:,:,5)),title('Diameter vs
distance'),xlabel('distance [cm]'),ylabel('Diameter [microns]')
subplot(3,2,6),plot(dd,fa(:,:,5)),title('Orientation vs
distance'),xlabel('distance [cm]'),ylabel('Orientation [-]')

figure(7)
subplot(3,2,1),plot(dd,TaF(:,:,1)),title('Quench Temperature vs
distance V_L=2000m/min'),xlabel('distance [cm]'),ylabel('Quench
Temp[^oC]')
axis([0 99 300 max(TaF(:,11,1))])
subplot(3,2,2),plot(dd,TaF(:,:,2)),title('Quench Temperature vs
distance V_L=3000m/min'),xlabel('distance [cm]'),ylabel('Quench
Temp[^oC]')
axis([0 99 300 max(TaF(:,11,2))])
subplot(3,2,3),plot(dd,TaF(:,:,3)),title('Quench Temperature vs
distance V_L=4000m/min'),xlabel('distance [cm]'),ylabel('Quench
Temp[^oC]')
axis([0 99 300 max(TaF(:,11,3))])
subplot(3,2,4),plot(dd,TaF(:,:,4)),title('Quench Temperature vs
distance V_L=4000m/min ph2'),xlabel('distance [cm]'),ylabel('Quench
Temp[^oC]')
axis([0 99 300 max(TaF(:,11,4))])
subplot(3,2,5),plot(dd,TaF(:,:,5)),title('Quench Temperature vs
distance V_L=4000m/min ph2'),xlabel('distance [cm]'),ylabel('Quench
Temp[^oC]')
axis([0 99 300 max(TaF(:,11,5))])

figure(8)
subplot(3,2,1)
plot(dd,X_CV),xlabel('distance from spinneret
[cm]'),ylabel('Crystallisation CV [%]')
subplot(3,2,2)
plot(dd,T_CV),xlabel('distance from spinneret
[cm]'),ylabel('Temperature CV [%]')
axis([0 100 min(T_CV(:,size(a_element,1)))
max(T_CV(:,size(a_element,1)))+1])
subplot(3,2,3)
plot(dd,F_CV),xlabel('distance from spinneret [cm]'),ylabel('Force CV
[%]')
subplot(3,2,4)
plot(dd,V_CV),xlabel('distance from spinneret [cm]'),ylabel('Velocity
CV [%]')
subplot(3,2,5)
plot(dd,d_CV),xlabel('distance from spinneret [cm]'),ylabel('Diameter
CV [%]')
subplot(3,2,6)
plot(dd,fa_CV),xlabel('distance from spinneret
[cm]'),ylabel('Orientation CV [%]')

figure(9)
subplot(3,2,1)
plot(dd,X_mean),xlabel('distance from spinneret
[cm]'),ylabel('Crystallisation mean [%]')
```

```
subplot(3,2,2)
plot(dd,T_mean),xlabel('distance from spinneret
[cm]'),ylabel('Temperature mean [^oC]')
subplot(3,2,3)
plot(dd,F_mean),xlabel('distance from spinneret [cm]'),ylabel('Force
mean [dyne]')
subplot(3,2,4)
plot(dd,V_mean),xlabel('distance from spinneret
[cm]'),ylabel('Velocity mean [m/s]')
subplot(3,2,5)
plot(dd,d_mean),xlabel('distance from spinneret
[cm]'),ylabel('Diameter mean [microns]')
subplot(3,2,6)
plot(dd,fa_mean),xlabel('distance from spinneret
[cm]'),ylabel('Orientation mean [microns]')

%coding to save data and figures
automatically_____________________________________________________
W1 = W*100;
s = [dir 'T' int2str(Ta1-273) 'V' int2str(Va) 'W' int2str(W1)];
save(s)
toc/3600
```